Alla mia famiglia

UNIVERSITA' DEGLI STUDI DI PARMA

Dottorato di ricerca in Scienze Chimiche

Ciclo XXVII (2012-2014)

Model systems for artificial photosynthesis: calix[4]arenes functionalized with chromophoric units for energy and charge transfer

Coordinatore:
Prof. Roberto Cammi

Tutors:
Dr. Laura Baldini
Dr. Francesca Terenziani

Dottoranda: Irene Tosi

2015

Contents

Abstract

The increasing demand for clean and renewable energy sources has promoted many attempts at mimicking natural photosynthesis through the development of artificial systems able to efficiently absorb solar light and transform it into useful forms of energy.

With the aim to elucidate the structure-function relationships in artificial photosynthetic devices and to understand the mechanisms governing the processes of energy transfer and charge separation, in this thesis it is reported the synthesis of calix[4]arenes functionalized with appropriate chromophores, functioning as energy (or electron) donors and acceptors.

Based on their spectral properties, three couples of dyes were selected for the study of energy transfer and one couple to investigate charge transfer. The couples of chromophores were linked at the upper rim of *cone* calix[4]arenes, to obtain bis-chromophoric systems.

In particular, the dyads synthesized with the first two couples were designed to give Förster excitation energy transfer, while the bis-chromophoric compound obtained with the third couple was specifically designed to investigate the occurrence of coherent effects in the energy transfer process. Moreover, the first two couples of chromophores were also linked to *partial cone* calix[4]arenes, in order to study the influence of the chromophore distance and relative orientation on the efficiency of energy transfer.

The obtained compounds were characterized by UV-visible absorption and fluorescence spectroscopies. Some selected systems were also investigated via ultrafast transient absorption techniques. Results confirmed that the synthesized bis-chromophoric calix[4]arenes are good model systems for the investigation of energy transfer and charge separation in different interaction regimes.

Chapter 1

General introduction

1.1. Introduction

One of the big challenges of our century is to replace our reliance on fossil fuels with renewable sources of energy.

By definition, a renewable source is a natural resource, which is replaced and regenerated by a natural process at a rate that is equal to (or faster than) the rate at which that resource is being consumed. In other terms, it is abundant, inexpensive, environmentally clean, and widely distributed in every geographical area (petroleum, for example, is concentrated in a limited number of countries). Only few potential energy sources meet these criteria; among these, sunlight seems to offer the best and most attractive solution. Sun delivers energy to the earth's surface at an average rate of ~120000 TW, which is about 10000 times higher than the current rate of worldwide technological energy used by humans. With the aim to exploit solar energy and convert it to electrical power, photovoltaic devices have been designed and realized since the '50s.

Although every year photovoltaics efficiency is improved,[1] there is a huge gap between our present use of solar energy and its enormous potential,[2,3] and existing practical methods for conversion of sunlight to electricity do not successfully compete with fossil fuels. In addition, for its nature, solar radiation fluctuates in intensity as a function of the season and weather conditions and depends on the location on Earth land. For these reasons, the development of mechanisms for solar energy storage is required.

Organic photovoltaics (OPVs) technology, even if it is in a comparatively early stage of development with respect to inorganic photovoltaics, offers the possibility of obtaining flexible, low-cost devices made from molecular, polymeric, or nanoparticle-based structures.[4,5]

The source of inspiration for efficient solar energy conversion in OPVs is natural photosynthesis, which is able to convert 95% of the energy from sun photons into chemical energy.

Despite much work has been performed, deeper studies on natural photosynthetic systems, in terms of physical and chemical properties, could shed light onto the mechanisms allowing natural photosynthesis to be so highly efficient. At the same time, the knowledge of the natural process could allow to build devices able to artificially emulate it, with the aim to take advantage from sun to produce electrical energy. Potential applications of artificial photosynthesis range from molecular-scale optoelectronics to photonics, sensor design, and other areas of nanotechnology.

1.2. Photosynthesis and synthetic "Antenna-Reaction-Center" mimics

Photosynthesis is a natural process, which efficiently converts solar energy into chemical energy, providing food and oxygen.

The photosynthetic process is initiated by photon absorption, followed by a rapid and efficient energy transfer step that allows the funneling of the excitation energy towards the reaction center, where charge separation occurs.

Photosynthetic systems are constituted by hundreds of pigments, such as chlorophyll b, carotenoids and xantophylls, which are densely embedded (average distance on the order of 10 Å) in special antenna-proteins ("antenna complexes"). Their role is to absorb the solar radiation, store that energy transiently as electronic excited states and transfer those electronic excitations to reaction centers. There, charge separation occurs and an electron is transferred from a donor to a primary electron acceptor, which is the starting point of a sequence of electron transfer reactions, which in turn stabilize a long-living charge-separated state, inducing the generation of an electrochemical gradient able to drive chemical reactions.

The mechanisms regulating excitation energy transfer in natural photosynthetic systems have not been completely understood yet, and a long-standing question concerns the interplay of Förster-type energy transfer (from molecule to molecule) and coherent delocalization of electronic eigenstates (molecular excitons).[6]

The first hypothesis about energy migration in photosynthesis deals with a "normal" FRET (Förster Resonant Energy Transfer) mechanism,[7] which is typically relevant when the coupling between the donor and acceptor is weak and occurs through a transition dipole–transition dipole interaction. The excitation energy is

assumed to be completely on either the donor or the acceptor, and to be transferred via a hopping mechanism. According to the hopping model, each transfer step is independent of the previous one, similar to a random walk.

Early extensions of this dipole-dipole Förster mechanism were developed once it became known that many molecules making up the photosynthetic structures are highly organized and very close together (average distance on the order of 10 Å), so that the point-dipole approximation may not hold. The suggestion, made by Dexter and coworkers,[8,9] involving electron-exchange processes, did not completely clarify the excitation energy transfer mechanisms occurring in photosynthetic systems. New theories of energy transfer were introduced to take into account strong intermolecular couplings. Exciton theory[10] was considered, and the so-called Coherent Resonance Energy Transfer mechanism was coined. Exciton is a quantum mechanical concept, whose formation, structure, dissipation and decoherence kinetics require advanced theoretical descriptions for complex systems, such as photosynthetic structures. A simple explanation can be furnished considering an antenna complex, where each chromophoric unit absorbs and transfers excitation energy. If chromophores are electronically strongly coupled, the excitation can be coherently shared among them (delocalized)[11,12] and the excited state cannot be described by the excitation of a single chromophore. In this sense, the collective excitation, defined exciton, generates a "new chromophore" constituted by the original building blocks (the original single chromophoric units). These new chromophores act as donors and acceptors for energy transfer regulating it through a coherent control, unlike what expected by the excitation hopping mechanism. The excitation travels in a wavelike manner, through interference of multiple pathways,[13,14,15] rather than hopping incoherently from site to site.

All the studies carried on natural photosynthetic systems demonstrate that their specific structural properties, together with the interactions between the molecular pigments and the surrounding proteins, are equally responsible for both the efficiency of energy transfer, in the antennas, and the stabilization of the charge-separated state, in the reaction center.

Recently, research focused on the investigation of the structure-function relationships and on understanding the role of the surrounding medium (the protein in case of natural photosynthetic devices, a solvent or a substrate in case of artificial systems) in promoting an efficient energy transfer and charge separation. It has been confirmed that in photosynthetic complexes, where the chromophores are maintained at relatively fixed distance and orientation, the environment constructively interacts with the photoactive system, originating an excitonic transport called ENAQT (environment-assisted quantum transport). ENAQT acts regulating the efficiency of energy transfer and/or charge separation, both by modulating the electronic and vibrational properties of the chromophores themselves and by promoting specific quantum mechanical effects enhancing the transfer probability.[16,17]

The recent development of an innovative spectroscopic technique, namely two-dimensional (2D) electronic spectroscopy, allows to get a wide range of experimental information on both the site energies and the electronic couplings, in chromophoric aggregates and in photosynthetic antennas. Fleming and coworkers[18,19] reported 2D electronic spectra of a small antenna protein, the water-soluble FMO protein (Fenna-Matthews-Olson pigment protein complex), revealing an interesting and unexpected property: even working at room temperature, long-lived coherences among the electronic excited states of the chlorophylls linked to this antenna were osserved.[20,21]

Following these initial investigations, experiments have been extended to more complex systems, and, recently, electronic coherence has also been observed in the light harvesting complex II (LHC II) of higher plants[22] and purple bacteria.[23,24] Data collected suggest that long-lived coherences, as connotative of all photosynthetic antennas, play a role in determining the high efficiency of energy transfer as observed in those structures. The role of quantum coherence in photosynthetic excitation energy transfer is far to be completely understood, as well as a great challenge is to clarify how to exploit this effect in artificial devices.

1.2.1. Artificial systems to mimic the functions of photosynthesis

While natural light-harvesting systems are extremely efficient in their native conditions, they are not robust enough to be adopted as active components in organic solar cells. A great challenge is therefore represented by the construction of artificial systems capable of efficient light harvesting and fast electron transfer with relatively slow charge recombination. Besides their possible use as functional devices for photovoltaic applications, these systems can provide simple models for the analysis of the factors allowing the artificial photosynthetic systems to function efficiently in absorbing visible light and promoting energy transfer and charge separation.

Inspired by Nature, several research groups have developed multichromphoric systems able to combine the two steps of energy and charge transfer. Among the dyes successfully used for the light-harvesting step are included porphyrins, phthalocyanines, carotenoids and BODIPYs (BF_2-chelated dipyrromethene compounds), while the preferred electron acceptors are fullerenes, and perylenes.[25-33] In these systems, the different dyes can be covalently linked or

assembled through weak, non-covalent interactions (some examples of covalent and supramolecular systems are reported in Figure 1).

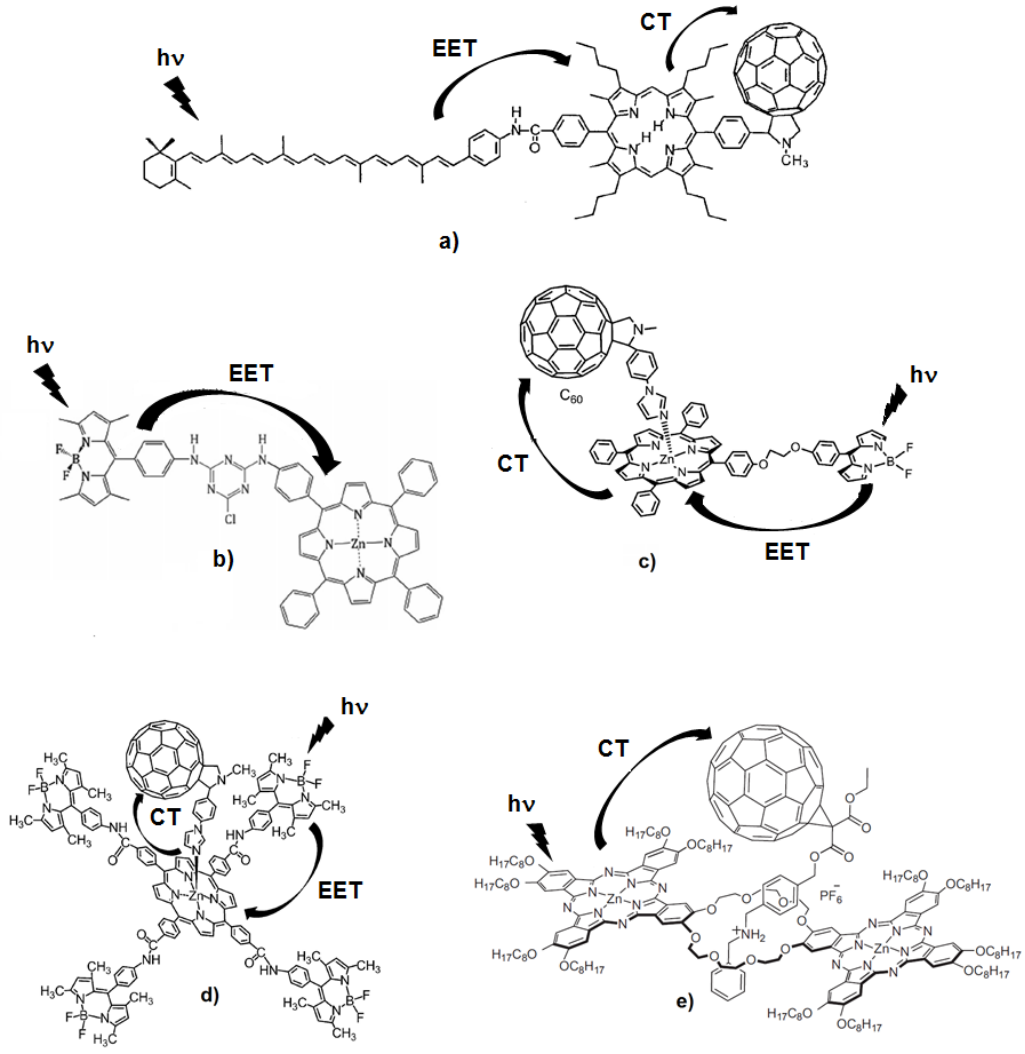

Figure 1. *Examples of covalent and supramolecular systems able to combine energy and electron transfer.*

Very recently and for the first time, it has also been reported a rigid, synthetic dichromophoric system able to reproduce the long-lived quantum coherence phenomenon.[34]

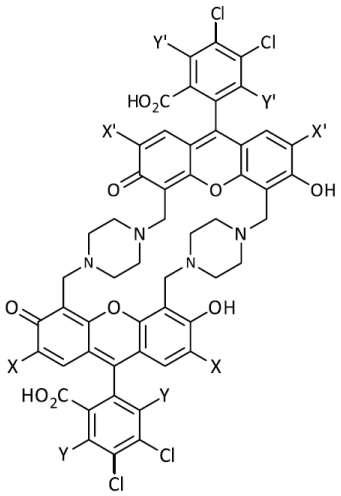

Figure 2. *Rigid synthetic bicromophoric system able to reproduce the long-lived quantum coherence phenomenon from ref. 34*

In this context, interesting results could be obtained through the examination of photoinduced energy and charge transfer occurring between two chromophores linked to an "inert" bridge. A scaffold well fitted for this purpose is the calix[n]arene macrocycle (see paragraph 1.3).

Calix[n]arenes have been widely used as platforms for the linkage of nonlinear optical dyes[35] and fluorophores,[36,37,38] to obtain sensors and probes, nonetheless only few cases where specifically designed calixarene derivatives have been synthesized for energy and charge transfer processes are reported.[32,33,39] Although these compounds (Figure 3) provided interesting results, no systematic studies have been carried out to exploit all the potential offered by calixarenes in terms of rationale and tunable modifications in geometry, orientation, number and reciprocal distance between the photo-active components.

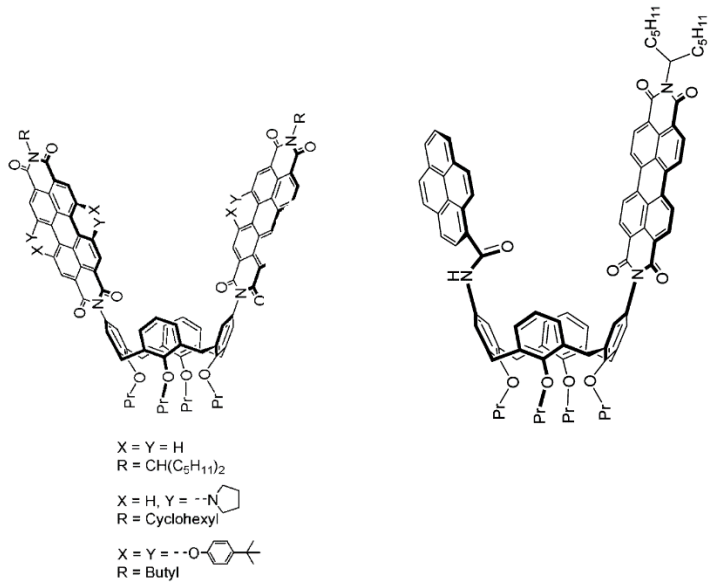

Figure 3. *Examples of bis-chromophoric calix[4]arene for energy (left) and electron transfer(right).*

Moreover, no examples where a single calixarene scaffold bears light-harvesting chromophores and electron acceptor units, are present in the literature, and research focused on multichromophoric calixarenes-based devices for organic photovoltaic applications can be considered at the very early stage. Many important results can be achieved thanks to the design, preparation and spectroscopic characterization of new assemblies.

This thesis is focused on the preparation of calix[4]arenes functionalized with chromophoric units as simple models for the investigation of the dynamics involved in energy and charge transfer mechanisms. These preliminary studies could allow to design artificial systems able to mimic the functions of photosynthesis, to be employed in organic photovoltaics.

1.3. Calix[4]arenes: an overview

Calix[n]arenes[40] belong to the class of [1_n]-metacyclophanes[41] and are cyclic oligomers obtained through the condensation of n units of p-alkyl phenols and formaldehyde in basic conditions. By changing the reaction temperature, the solvent, the ratio of the reactants and the base, the size of the macrocycle can be modulated, promoting the formation of calix[n]arenes having four to eight aromatic units (indicated by the bracketed number "n"). The even numbered cyclic products (n = 4, 6, 8) are obtained in higher yields.[42,43]

Independently of the size, a calix[n]arene is constituted by a hydrophobic core, defined by the aromatic rings linked one to the other by methylene bridges. The phenolic hydroxyl groups are referred to as the "lower rim", while the aromatic p-positions as the "upper rim" (Figure 4).

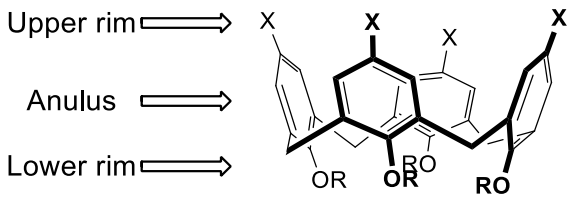

Figure 4. *Representation of the Upper rim, the Annulus and the Lower rim of a generic calix[4]arene.*

A number of consolidated procedures to selectively or exhaustively functionalize the upper and the lower rim are available and allow, for example, the insertion of ancillary binding sites or the extension of the macrocycle aromatic cavity. For this reason, calix[n]arenes can be considered as useful building blocks for the synthesis of new advanced materials.[40]

1.3.1. Conformational properties

Native calix[n]arenes are not rigid compounds and the rotation about the σ-bonds of the Ar-CH_2-Ar groups allows several conformations.[44,45] In particular, calix[4]arenes can exist in four discrete forms, identified as "*cone*", "*partial-cone*", "*1,2-alternate*", and "*1,3-alternate*" conformations (Figure 5).[46]

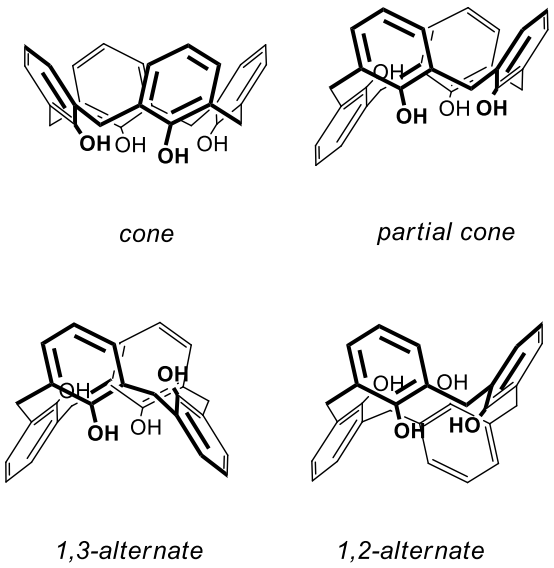

Figure 5. *Cone-, Partial cone, 1,3-Alternate and 1,2-Alternate calix[4]arene conformations.*

The preferred conformation of native calix[4]arenes, both in solution and at the solid state, is the *cone* structure, where all the phenolic nuclei are oriented in the same direction and a π-rich aromatic cavity is well defined, as a result of strong intramolecular hydrogen bonds between the proximal hydroxyl groups (homodromic H-bonds).

It is interesting to observe that the two protons of each methylene "bridge" of calix[4]arenes blocked in *cone* conformation are located in a different position with respect to the aromatic nuclei (Figure 6). The protons that are almost perpendicular to the aromatic nuclei are named equatorials, while the others,

almost parallel, are called axial. At the NMR analysis, such protons experience a different magnetic environment, giving rise to an AX system of two doublets coupled with a typical geminal coupling constant (J) of 13-16 Hz. The equatorial protons are "shielded" by the aromatic rings and thus are upfield shifted with respect to the axial protons.

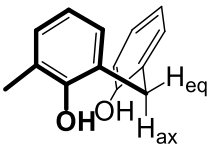

Figure 6. *Axial (H_{ax}) and equatorial (H_{eq}) protons of the methylene "bridge" of calix[4]arenes.*

When the calix[4]arene is substituted at the lower rim with four methyl or ethyl groups, at room temperature, it is conformationally mobile, with the aromatic rings free to rotate. On the contrary, when the substituents are bulkier than ethyl, the rotation of the rings is blocked and the four different conformations can be isolated (depending on the reaction conditions, see below).

In solution, even if the ring inversion process is blocked by the steric hindrance of the lower rim substituents, a residual conformational flexibility remains, due to the wobbling of the aromatic rings around the carbon atoms of the bridge. As a result, calix[4]arenes tetrasubstituted with four identical groups constantly interconvert between two opposite "*flattened" cone* C_{2v} *conformations* equally stable, passing through a C_{4v} structure, which can be considered the transition state for the interconversion (Figure 7).

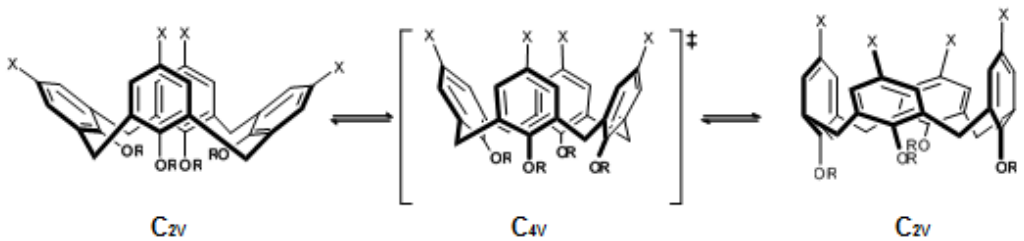

Figure 7. *Equilibrium between the open- (left) and closed-flattened cone conformation (right) through the C_{4v} structure.*

In consequence of this flexibility, the upper rim substituents in 1,3-distal position can get very close together, allowing, for example, the formation of intramolecular hydrogen bonds or the occurrence of intramolecular reactions.
In 1995, Arduini et al.[47] introduced the selective functionalization of the lower rim with short diethylene glycol bridges as a method to inhibit the rapid interconversion between the two flattened cone conformations, donating a greater rigidity to calix[4larenes in solution.

1.3.2. Chemistry of calixarenes

The reactive positions of calixarenes are the phenol OH groups (lower rim) and the aromatic *para* positions (upper rim).
The lower rim modification is the step where a defined conformation of the macrocyclic core can be obtained. The cation of the base employed to deprotonate the hydroxyl groups (and in particular its charge and dimension) plays a key role in determining the structure of the calix[4]arene. For example, Na^+ favors the more polar cone conformation, while Cs^+ and K^+ the *1,3-alternate* and the *partial cone*, respectively.[40,48]
Moreover, appropriate conditions can be chosen to obtain the selective or exhaustive functionalization of the lower rim of calix[4]arenes. A weak base, like carbonate, favors the dialkylation in the 1,3-distal positions, thanks to the greater acidity of the OH groups in opposite positions; on the contrary, a stronger base, like NaH, is able to deprotonate the four hydroxylic groups simultaneously, affording tetra-substituted products.
Concerning the upper rim, several functional groups (such as halogen, cyano, nitro, formyl, ketones)[40] can be introduced and subsequently modified by

functional group interconversion reactions, allowing for the further functionalization of the calixarene.

Procedures to introduce on the calix[4]arene upper rim two, three or four identical groups are well established in the literature.[49,50,51] On the contrary, the functionalization of the upper rim with two, three or four different substituents is not so frequent and it represents a more challenging task.[52]

Three main synthetic approaches can be used. The first is a stepwise approach, consisting in the introduction of the different functional groups in consecutive, non-selective steps. This procedure entails one synthetic and one purification step for each substituent and is intrinsically characterized by a low overall yield. The purification of each intermediate, in particular, can be particularly tedious, due to the possible formation of polysubstituted products or unwanted regioisomers. The advantage of this strategy, however, is the possibility of introducing a vast number of functional groups combinations since each functionalization step is independent of the previous ones.[53] Regioselectivity, moreover, can be improved by the partial functionalization of the lower rim, thus making the non-substituted aromatic rings more reactive. An example of this strategy is reported in Scheme 1. The first reaction, conducted on a 1,3-dialkylated derivative, will lead to a mixture of two products, the mono- and the di-substituted, while the second stage will produce only the desired product.

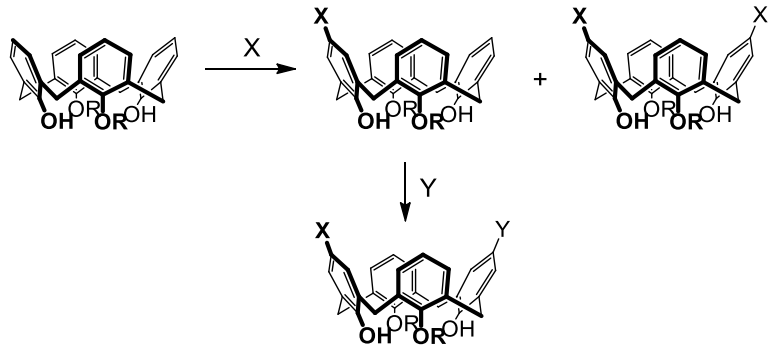

Scheme 1. *Schematic representation of the stepwise upper rim substitution with different functional groups.*

The second strategy consists in the introduction of the different substituents in a single step, by reacting the calix[4]arene with a mixture of different compounds (Scheme 2). The resulting crude will be a mixture of several products with a statistical distribution, from which the desired compound must be isolated. The advantage of this procedure is given by the low number of steps, while the drawback is the low yield and the tricky purification of the product from a mixture of many compounds. This approach has been used in this theses for the synthesis of bichromophoric calix[4]arenes.

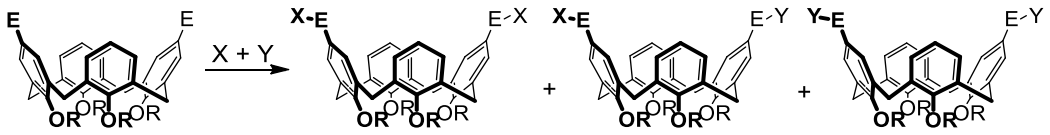

Scheme 2. *Schematic representation of the statistical approach employed in this thesis.*

The third procedure exploits the intramolecular reactivity which can exist (in some cases) between the upper rim functional groups. In a recent paper[52] the 1,3-distal diformylated calix[4]arene undergoes intramolecular Cannizzaro disproportionation in the presence of a strong base, yielding a calixarene bearing an alchol and a carboxylic acid (or ester) functionality (Scheme 3a).

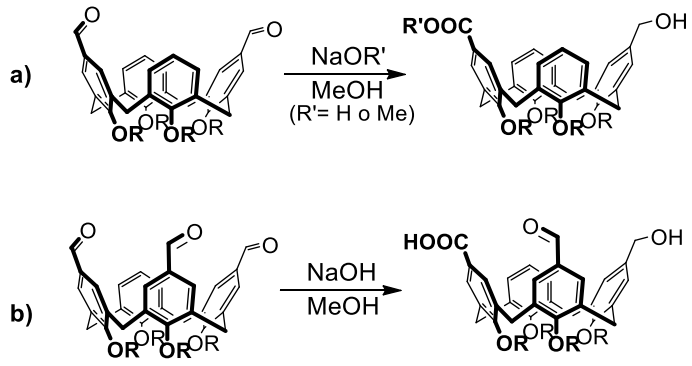

Scheme 3*. Intramolecular Cannizzaro disproportionation on (a) a diformyl and (b) a triformyl calix[4]arene derivative.*

The same intramolecular Cannizzaro reaction on a triformyl derivative yields the inherently chiral ABCH-substituted calix[4]arene in a convenient one-step procedure.[54] This is possible because this intramolecular reaction takes place only between the formyl groups in 1,3-distal position (Scheme 3b).

Despite the synthetic challenges related to the preparation of asymmetrically substituted calix[4]arenes, succeeding in this attempt will widen the scope of calixarene-based systems allowing the synthesis of complex multifunctional derivatives.

1.4. Transient absorption spectroscopy

As previously introduced, this thesis aims to elucidate the structure-function relationships in artificial photosynthetic devices and to understand the mechanisms influencing the efficiency of excitation energy transfer and charge separation.

Linear UV-visible and fluorescence spectroscopies give basic characterization of these mechanisms. To study the kinetics of energy transfer, electron transfer, and solvent dynamics, fast time resolution is required. This is not possible via the NMR technique, due to its intrinsic slow timescale resolution.

Ultrafast transient electronic spectroscopy can instead follow sub-picosecond dynamics. Unfortunately, the timescale advantage entails a loss of structural resolution.

One of the optical pump-probe techniques based on ultrashort laser pulses is Transient Absorption Spectroscopy (TAS). Consider a system at the equilibrium. When the system is excited by a first short laser pulse (pump), a non-equilibrium state is generated and this starts evolving as a function of time. After a certain delay, another broader pulse (called probe) interacts with the sample, reporting on the properties of the system at that particular time delay.

The physical quantity measured in the pump-probe experiment is the change in differential absorbance, ΔA, obtained from the differential transmittance of the sample.

The probe pulse can induce three different mechanisms, inducing a change in the sample absorbance (ΔA, Figure 8):

- The probe pulse can promote absorption from the excited state to a more energetic excited state (excited state absorption, ESA), contributing positively to ΔA,

- The probe can induce absorption from the depleted ground state to the excited state (bleaching, B). Because the ground state has been depopulated by the pump pulse, the sample is more transparent and the transmittance is increased (absorbance is reduced);
- The interaction between the electromagnetic pulse and the excited state of the molecule can induce a radiative decay to the ground state (stimulated emission, SE). SE gives a negative ΔA signal.

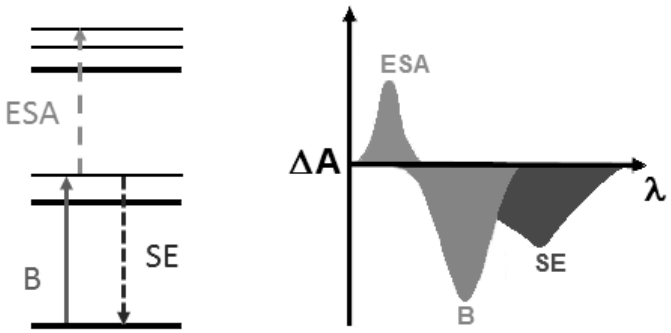

Figure 8. *Excited State Absorption, Bleaching and Stimulated Emission representation in energetic levels (left) and in difference spectra (right) depiction.*

The pump-probe experiment can be repeated for different pump-probe delays, providing the dynamical evolution (kinetics) of the transient absorption signal. The obtained ΔA value is therefore a function of the wavelength and the delay time between the pump and the probe pulse: ΔA(λ, t).

The overlap between opposite sign features promotes a lineshape distortion: if spectra are sufficiently resolved, a careful fitting to find peak centers and widths let to characterize transient peaks.[55] On the contrary, this operation becomes more complicated and often worthless, due to additional peaks and broadening in the region under study.[56]

With the aim to solve these difficulties, multidimensional spectroscopies have been designed and much work to optimize the instrumentation and its assembly is in progress.

1.5. Aim of the work

Calixarenes, thanks to their ease of functionalization and their particular shape, are very useful and adaptable scaffolds, which can be used to achieve molecular structures and supramolecular complexes, devices and materials for a vast range of applications, ranging from the field of nanotechnology, to catalysis, to biochemistry.

Recently, they have been studied also as platforms for the linkage of chromophores and fluorophores to obtain probes and sensors,[35,38] but despite the interesting results provided by Würthner,[33,39] the potential offered by calixarenes in the organic photovoltaics has not been fully exploited yet. For example, a single calixarene scaffold could bear several chromophores, able to harvest solar light and produce the electrons responsible for the electric current generation. In addition, the opportunity to rationally tune the geometry, the orientation and the number and reciprocal distance between the photo-active components makes calixarenes versatile tools and, in this sense, a single functionalized calixarene could be a potential material for new photovoltaic devices.

Since the research focused on multichromophoric calixarene-based devices for organic photovoltaic applications is at the very early stage, many important results could be achieved thanks to the design, preparation and spectroscopic characterization of new assemblies.

The main aim of this work is the realization of simple models as starting point towards more complex structures and, in a near future, working devices.

In this regard, in order to investigate the earliest processes occurring in the photovoltaic mechanism, it is here reported the synthesis of some “ad-hoc” devices, based on the upper rim functionalization of a calix[4]arene with two appropriate chromophores capable of energy transfer and/or charge separation.

The employment of a calix[4]arene as scaffold (see paragraph 1.3) allows to achieve simple and versatile systems where the mutual orientation and the relative distances between the chromophores can be manipulated, thus also influencing the nature of the energy transfer, which is a function of the chromophores features and spectroscopic properties.

The next chapters will examine, in turn, one of the different steps occurring during the early stages of the natural photosynthetic process. Before discussing the choice of the chromophores, the synthesis of the bichromophoric calix[4]arenes and the spectroscopic results, a brief introduction about the inherent energy or electron transfer mechanism will be given.

Chapters 2 and 3 deal with the excitation energy transfer mechanism: since it has been supposed that the pigments of the light-harvesting complex transfer the excitation energy by way of a hopping mechanism and/or a coherence quantum mechanism, different couples of dyes have been selected. Depending on the energetic properties of the chromophores, in fact, the two mechanisms of energy transfer can be studied: non-degenerate energetic levels are required for semi-classical excitation energy transfer (couples 1 and 2), while quasi-degenerate energetic levels for the quantum-mechanical mechanism (couple 3).

We selected, as energy donor and energy acceptor, the following couples of dyes:

1. Coumarin 343 and 7-nitrobenzo furazan (NBD);
2. NBD and 2-hydroxy-9-diethylamino-5H-benzo[a]phenoxazin-5-one (hydroxy Nile red);
3. Two 4,4-difluoro-1,3,5,7-tetramethyl-bora-3a,4a-diaaza-s-indacene (BODIPY) derivatives.

After being functionalized with a proper spacer, all the chromophores have been linked at the 1,3-distal positions of the upper rim of a tetrapropoxy calix[4]arene.

For couples 1 and 2, both the models in *cone*- and *partial cone*-conformation have been synthesized (Figure 9), to clarify if the distance of the two dyes or the interactions of the bi-chromophore units with the medium (solvent) can influence the kinetics of excitation energy transfer (EET).

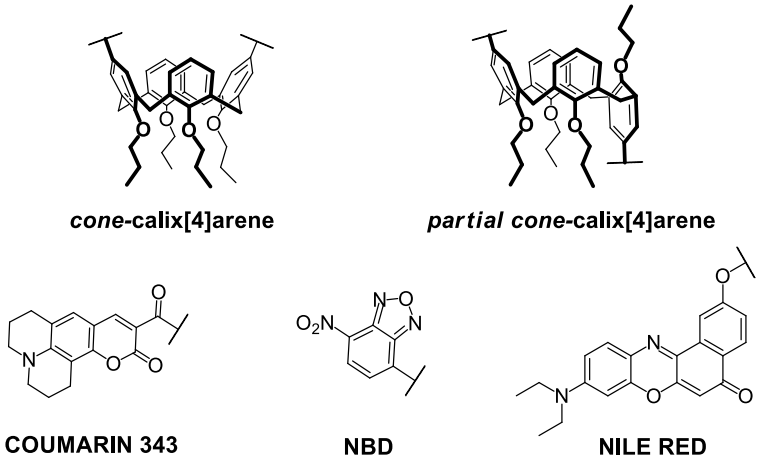

Figure 9. *Calix[4]arene scaffolds and chromophores for hopping EET mechanism studies (Chapter 2).*

The two BODIPY dyes of couple 3 have been linked at the upper rim of a *cone* calix[4]arene (Figure 10), after considerable synthetic effort.

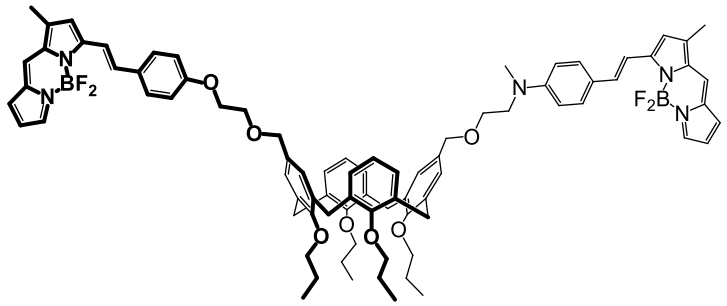

Figure 10. *Bichromophoric calix[4]arene for quantum coherence excitation energy transfer studies (Chapter 3).*

After the excitation energy has been funneled to the reaction center, both the natural photosynthetic and the photovoltaic processes carry on the donation of an electron from the "last energy acceptor dye" to the "first electron acceptor

species". In order to reproduce the charge separation step, a derivative of hydroxy Nile red (electron donor) and fullerene C_{60} (electron acceptor) have been chosen, and the synthesis of the Nile red-C_{60} dyad (Figure 11) is reported in Chapter 4, together with a simpler model. The questions we wanted to answer regard the role of the bridge: does the calix[4]arene core assist the charge dissociation? Does it actively participate?

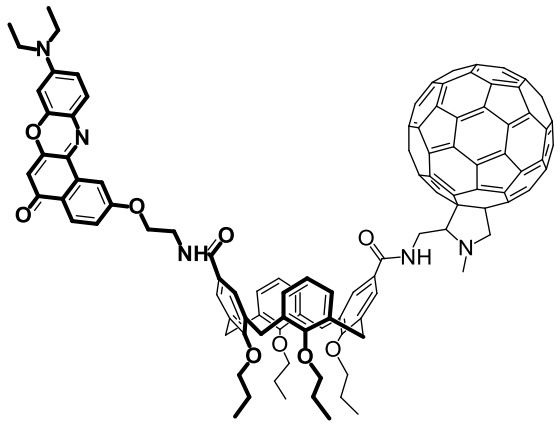

Figure 11. *Bichromophoric calix[4]arene for electron transfer studies (Chapter 4)*

All the bichromophoric calix[4]arene systems have been characterized via NMR spectroscopy (^{1}H, ^{13}C and ^{19}F when opportune) to study their conformational behavior.

Absorption and fluorescence spectra confirmed the observations gained by NMR spectroscopy, and added further information about the occurring of excitation energy transfer or charge separation.

Thanks to the collaboration with LENS (European Laboratory for Non Linear Spectroscopy) in Florence, the synthesized species were also studied via transient pump-probe techniques.

1.6. References

1. REN21, **2014**, "Renewables 2014 global status report";
2. N. S. Lewis, *MRS Bull.*, **2007**, 32, 808-820;
3. N. S. Lewis, *Science*, **2007**, 315 (5813), 798-801;
4. B. Kippelen, J.-L. Brédas., *Energy Environ. Sci.*, **2009**, 2, 251-261;
5. J.-L Brédas, J. E. Norton, J. Cornil, V. Coropceanu, *Acc. Chem. Res.*, **2009**, 42, 1691-1699;
6. A. Olaya-Castro, G. D. Scholes, *Int. Rev. Phys. Chem.*, **2011**, 30, 49–77;
7. T. Förster, *Ann. Phys*., **1948**, 2, 55–75;
8. D. L. Dexter, *J. Chem. Phys.*, **1953**, 21, 836-850;
9. D. L. Dexter, J. H. Schulman, *J. Chem.Phys.*, **1954**, 22 (6), 1063-1070;
10. T. Förster, *Modern Quantum Chemistry; Part III,* Action of Light and Organic Molecules, O. Sunanoglu (eds), Academic, New York, **1965**, 93-137;
11. M. Kasha, *Radiat. Res.*, **1963**, 20, 55–71;
12. G. D. Scholes, G. Rumbles, *Nat. Mater.*, 2006, 5, 683–696;
13. G. D. Scholes, G. R. Fleming, J. *Phys. Chem. B*, **2000**, 104, 1854–1868;
14. H. Sumi, *Chem. Rec.*, **2001**, 1, 480–493;
15. S. Jang, M. D. Newton, R. J. Silbey, *Phys. Rev. Lett.*, **2004**, 92, 218301(1-4);
16. A. Shabani, M. Mohseni, H. Rabitz, S. Lloyd, *Phys. Rev E*, **2014**, 89, 042706 (1-7);
17. R. de J. Leon-Montiel, Ivan Kassal, J. P. Torres, *J. Phys. Chem. B*, **2014**, 118, 10588-10594;
18. T. Brixner, J. Stenger, H. M. Vaswani, M. Cho, R. E. Blankenship, G. R. Fleming, *Nature*, **2005**, 434, 625-628;

19. G. S. Engel, T. R. Calhoun, E. L. Read, T.-K. Ahn, T. Mančal, Y.-C. Cheng, R. E. Blankenship, G. R. Fleming, *Nature*, **2007**, 446, 782-786;
20. E. Collini, *Chem. Soc. Rev.*, **2013**, 42, 4932-4947;
21. A. Ishizaki, T. R. Calhoun, G. S. Schlau-Cohenab, G. R. Fleming, *Phys. Chem. Chem. Phys.*, **2010**, 12, 7319–7337;
22. T.R Calhoun, Naomi S. Ginsberg, G. S. Schlau-Cohen, Y.-C. Cheng, M. Ballottari, R. Bassi, G. R. Fleming*., J. Phys. Chem. B,* **2009**, 113, 16291-16295;
23. R. J. Cogdell, A. Gall, J. Köhler, *Q. Rev. Biophys.*, **2006**, 39, 227– 324;
24. A. M. Van Oijen, M. Ketelaars, J. Kohler, T. J. Aartsma, J. Schmidt, *Science*, **1999**, 285, 400-402;
25. S.-H. Lee, A. G. Larsen, K. Ohkubo, Z.-L. Cai, J. R. Reimers, S. Fukuzumi,M. J. Crossley, *Chem. Sci.*, **2012**, 3, 257 –269;
26. D. Gust, T. A. Moore, A. L. Moore, *Acc. Chem. Res.,* **2001**, 34 (1), 40-48;
27. N. Aratani, D. Kim, A. Osuka, *Acc. Chem. Res.*, **2009**, 42, 1922 –1934;
28. G. Bottari, O. Trukhina, M. Ince, T. Torres, *Coord. Chem. Rev.*, **2012**, 256, 2453 –2477;
29. M. E. El-Khouly, S. Fukuzumi, F. D'Souza, *ChemPhysChem*, **2014**, 15, 30–47;
30. K. R. Justin Thomas, A. L. Thompson, A. V. Sivakumar, C. J. Bardeen, S. Thayumanavan, *J. Am. Chem. Soc.*, **2005**, 127 (1), 373-383;
31. M. –S. Choi, T. Aida, H. Luo, Y. Araki, O. Ito, Angew. Chem. Int. Ed., **2003**, 42, 4060–4063;
32. Vân Anh et al., *J. Phys. Chem. C*, **2009**, 113, 18358–18368;
33. C. Hippius, F. Schlosser, M. O. Vysotsky, V. Böhmer, F. Würthner, *J. Am. Chem. Soc.*, **2006**, 128, 3870-3871;
34. D. Hayes, G. B. Griffin, G. S. Engel, *Science*, **2013**, 340, 1431-1434;
35. P. J. A. Kenis et al., *J. Am. Chem. Soc.*, **1998**, 120, 7875-7883;

36. S. K. Kim, S. Ho Lee, J. Yeon Lee, J Yong Lee,R. A. Bartsch, J. S. Kim, *J. Am. Chem. Soc.*, **2004**, 126, 16499-16506;
37. N. J. Jeon, B. Ju Ryu, K. C. Nam, *Bull. Korean Chem. Soc.*, **2012**, 33 (9), 3129-3132;
38. I. Leray, B. Valeur, *Eur. J. Inorg. Chem.*, **2009**, 3525–3535;
39. C. Hippius, I. H. M. van Stokkum, M. Gsänger, M. M. Groeneveld, R. M. Williams, F. Würthner, *J. Phys. Chem. C*, **2008**, 112, 2476-2486;
40. (a) C. D. Gutsche, Calixarenes, *Monographs in Supramolecular Chemistry*, Ed.: J. F. Stoddart, Royal Society of Chemistry: Cambridge, U.K., **1989**; (b) C. D. Gutsche, Calixarenes Revisited, *Monographs in Supramolecular Chemistry*, Ed.: J. F. Stoddart, Royal Society of Chemistry: Cambridge, U.K., **1998**; (c) L. Mandolini, R. Ungaro, *Calixarenes in Action*, Eds.:, Imperial College Press: London, **2000**; (d) Z. Asfari, V. Böhmer, J. Harrowfield, J. Vicens, *Calixarenes 2001*, Kluwer Academic: Dordrecht, **2001**; (e) C. D. Gutsche, *Calixarenes, An Introduction, Monographs in Supramolecular Chemistry*, Ed.: J. F. Stoddart, Royal Society of Chemistry: Cambridge, U.K., **2008**;
41. See e. g. F. Diederich, *Cyclophanes, Monographs in Supramolecular Chemistry*, Ed.: J. F. Stoddart, *Royal Society of Chemistry: Cambridge*, U.K., **1991**;
42. Calixarenes in the Nanoworld, *Springer*, **2007**;
43. C. D. Gutsche, Calixarenes, Monographs in Supramolecular Chemistry, Ed.: J. F. Stoddart, *Royal Society of Chemistry: Cambridge*, U.K., **1989**;
44. N. R. L. Megson, *Oesterr. Chem. Z.*, **1953**, 54, 317-324;
45. R. Ott, A. Zinke, *Oesterr. Chem. Z.*, **1954**, 55, 156-157;
46. J. W. Cornforth, P. D'Arcy Hart, G. A. Nicholls, R. J. W. Rees, J. A. Stock, *Brit. J. Pharmacol.*, **1955**, 10, 73-86;

47. A. Arduini, M. Fabbi, M. Mantovani, L. Mirone, A. Pochini, A. Secchi, R. Ungaro, *J. Org. Chem*., **1995**, *60*, 1454-1457;
48. J. D. Van Loon, A. Arduini, L. Coppi, W. Verboom, A. Pochini, R. Ungaro , S. Harkema , D. N. Reinhoudt, *J. Org. Chem.*, **1990**, 55 (21), 5639–5646;
49. M. Conner, V. Janout, S. L. Regen, *J. Am. Chem. Soc.*, **1991**, 113, 9670-9671;
50. For a recent review of multifunctionalization of calixarenes, see: W. Sliwa, M. Deska, *ARKIVOC*, **2011**, 496–551;
51. A. Sartori, A. Casnati, L. Mandolini, F. Sansone,D. N. Reinhoudt, R. Ungaro, *Tetrahedron*, **2003**, 59, 5539–5544;
52. M. Galli, J. A. Berrocal, S. Di Stefano, R. Cacciapaglia, L. Mandolini, L. Baldini, A. Casnati and F. Ugozzoli, Org. Biomol. Chem., 2012, 10, 5109–5112;
53. L. Baldini, F. Sansone, G. Faimani, C. Massera, A. Casnati, R. Ungaro, *Eur. J. Org. Chem*., **2008**, 869-886;
54. M. Ciaccia, I. Tosi, R. Cacciapaglia, A. Casnati, L. Baldini, S. Di Stefano, *Org. Biomol. Chem*, **2013**, 11, 3642-3648;
55. C. R. Baiz, R. McCanne, M. J. Nee, K. J. Kubarych, *The Journal of Physical Chemistry A*, **2009**, 113, 8907-8916 (2009);
56. J. C. Owrutsky, A. P. Baronavski, *J. Chem. Phys.*, **1996**, 105, 9864-9873.

Chapter 2

Synthesis of bichromophoric calix[4]arenes for Excitation Energy Transfer

2.1 Introduction

The first step of natural photosynthesis consists of light absorption by pigments embedded in antenna complexes, which funnel the excitation energy towards the reaction center. As described in Chapter 1, two mechanisms have been proposed to explain how the excitation energy is transferred among the dyes towards the reaction center, one based on the hopping mechanism (described in the semi-classical theory), the other based on a coherent mechanism (described in purely quantum-mechanical terms). The current chapter focuses on the first mechanism.

Excitation energy transfer is the physical process by which energy is transferred from an excited molecular chromophore (the energy donor, D) to another chromophore (the energy acceptor, A) according to the following transformation:

$$D^* + A \longrightarrow D + A^* \qquad [* \text{ labels the excited species}]$$

This means that, by exciting D with an appropriate light source, the electronic excitation is initially and unambiguously associated to D, while at some later time the electronic excitation is unambiguously associated to A.[1]

The de-excitation of the species D and the excitation of the species A can occur simultaneously or in two steps; in particular, we can distinguish between two different mechanisms, a radiative and a radiationless excitation energy transfer.

The radiative excitation energy transfer mechanism is a type of transfer that does not require any interaction between the partners involved and it is often named as "trivial" because of the simplicity of the physical processes it is based on.[2]

The radiative energy transfer from D* to A occurs sequentially, as shown:

$$D^* \longrightarrow D + h\nu_D$$

$$A + h\nu_D \longrightarrow A^*$$

The global transfer consists of two steps: the emission and the reabsorption step. In other terms, the excited donor decays by emitting photons and acting as a light source for A, which in turn can absorb this emitted radiation.
This type of energy transfer is of no particular interest and, usually, conditions are chosen as to prevent it (for example, very low concentration in the measurement of fluorescence spectra).

Relevant to the purpose of this work, is the radiationless mechanism, which occurs when the excitation energy moves from D to A without involving the emission and re-absorption of any real photon. This phenomenon takes place when the distance between D and A is much shorter than the wavelength of the corresponding photon (typically, < 10 nm). This “near-field” condition is often referred to as the exchange of a “virtual” photon.
Non-radiative transfer requires an interaction between the donor and the acceptor species, which can be strong (short-range interactions: coulomb, exchange and charge resonance interactions), weak (coulomb long-range interactions) or very weak.
When the intermolecular interaction energy is larger than the interaction between the electronic and nuclear motions within the individual molecules, the coupling is defined “strong”. Therefore, absorption spectra of strongly coupled systems are very different from single spectra of their separated components. In the strong coupling case, the transfer of excitation energy is faster than nuclear vibrations and vibrational relaxation; the excitation is not localized on one of the two molecules, but is delocalized over both the components (Figure 1).

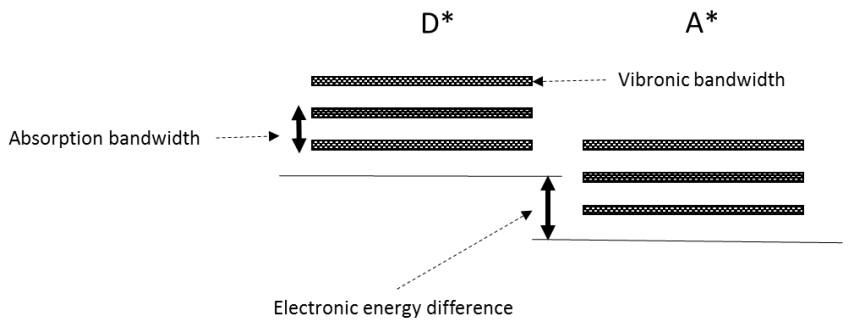

Figure 1. *Schematic representation of the three parameters (Electronic energy difference, Absorption bandwidth and Vibronic bandwidth) allowing classification of the donor-acceptor coupling type.*

In this case, the excitation transfer is a coherent process where the excitation oscillates back and forth between D and A, and is never more than instantaneously localized on either molecule. Such a delocalization is described in the frame of the exciton theory.

The coupling is defined "weak" if the interaction energy is much lower than the absorption bandwidth (Figure 1), but larger than the width of an isolated vibronic level. The vibronic excitation can be considered as delocalized, while the electronic excitation is more localized than under strong coupling; in this sense the system can be described in terms of stationary vibronic exciton states. Consequently, weak coupling leads to minor alterations of the absorption spectrum.

The third kind of intermolecular coupling, the "very weak" case, is the one relevant to this chapter (Chapter 3 will focus on the strong coupling regime).

In the very weak coupling regime the interaction energy between D and A is lower than the width of an isolated vibronic level, ensuring a localization of the electronic excitation ("incoherent" transfer). Accordingly, vibrational relaxation of the donor occurs faster than the energy transfer (this condition is usually satisfied because internal conversion is as fast as 10^{-12} s, while the time scale for energy transfer is typically nanoseconds, i.e. 10^{-9} s).

When two or more chromophoric units are “very weakly” coupled, the spectroscopic characteristics of the interacting molecules are almost unaffected with respect to the isolated molecules.[3] In this regime, the excitation energy transfer process can be described via the perturbation theory, as originally proposed by Förster.

2.1.1 Förster theory for donor-acceptor pairs

In 1959 Förster derived the expression for the excitation resonance energy transfer (RET) rate constant in the very weak coupling regime.[1,2] Thanks to Förster's contribution, RET is often called FRET, which is the acronym for Förster/Fluorescence Resonance Energy Transfer.

The rate (K_{RET}) of the energy-transfer reaction

$$D^* + A \rightarrow D + A^*$$

in the weak-coupling limit, can be expressed through the Fermi golden rule:

$$k_{RET} = \frac{1}{\hbar^2} \left| \langle \phi_{D^*}(1)\phi_A(2) \left| H' \right| \phi_D(1)\phi_{A^*}(2) \rangle \right|^2 \delta(\nu_D - \nu_A) = \frac{1}{\hbar^2} V^2 \delta(\nu_D - \nu_A) \qquad \text{Eq. 1}$$

where $\varphi_{D^*}(1)\varphi_A(2)$ is the initial wavefunction of the coupled system, $\varphi_D(1)\varphi_{A^*}(2)$ the final state, and $\delta(\nu_D - \nu_A)$ is the energy conservation term.

Note that each electron remains on the molecule it was originally located on: electron 1 moves from the LUMO to the HOMO of the donor (de-excitation of D* to D), while electron 2 from the HOMO to the LUMO of the acceptor (excitation of A to A*). The Förster mechanism, in fact, does not account for any electron exchange between the two species.

The interaction Hamiltonian H' can be expressed as follows:

$$H' = \frac{1}{4\pi\varepsilon_0\eta^2} \frac{e^2}{r_{DA}} \qquad \text{Eq. 2}$$

where η is the refractive index of the medium.

The matrix element

$$V = \frac{e^2}{4\pi\varepsilon_0\eta^2} \langle \phi_{D^*}(1)\phi_A(2) \left| \frac{1}{r_{DA}} \right| \phi_D(1)\phi_{A^*}(2) \rangle \qquad \text{Eq. 3}$$

represents the interaction energy between two transition charge densities (that of D and that of A).

When the donor-acceptor separation (R_{DA}) is much larger than the molecular dimensions (as it is typically the case in the very-weak coupling regime), the dipolar

approximation can be adopted, so that V is given by Eq. 4, representing the interaction between the transition dipole moments, μ_D and μ_A, of the D* → D and A → A* transitions:

$$V= \frac{e^2}{4\pi\varepsilon_0\eta^2}\frac{|\overrightarrow{\mu_D}||\overrightarrow{\mu_A}|}{R_{DA}^3}(\cos\theta_T - 3\cos\theta_D\cos\theta_A) = \frac{e^2}{4\pi\varepsilon_0\eta^2}\frac{|\overrightarrow{\mu_D}||\overrightarrow{\mu_A}|}{R_{DA}^3}\kappa \quad \text{Eq. 4}$$

κ is called "orientational factor" and only depends on the orientations of the dipoles with respect to each other and with respect to the vector R connecting them (Figure 2). When the molecules are free to rotate much faster than the de-excitation rate of the donor, the average value of κ^2 is 2/3.

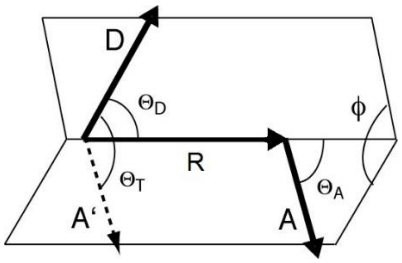

Figure 2. *Visualization of the angles used to define the relative orientations of the donor and acceptor transition dipole moments and the separation vector.*

Considering Eq. 1 and 4, it is possible to conclude that

$$k_{RET} \propto \frac{|\overrightarrow{\mu_D}|^2|\overrightarrow{\mu_A}|^2}{\eta^2 R_{DA}^6}\kappa^2\delta(\nu_D-\nu_A) \quad \text{Eq. 5}$$

Förster related the quantities appearing in this expression (Eq. 5) to spectroscopically available data. In particular, the product of the donor and acceptor squared transition dipole moments (relevant to the emission and absorption process, respectively) and the energy-conservation term (represented by the Dirac delta) is related to the integral (extended to the whole frequency range) of the product between the fluorescence spectrum of the donor and the absorption spectrum of the acceptor, to give the Förster expression for the rate of the FRET process (Eq. 6).

$$k_{RET} \propto \frac{\kappa^2}{\eta^4 R_{DA}^6}\frac{\Phi_D}{\tau_D}\int d\tilde{\nu}\frac{\bar{F}_D(\tilde{\nu})\varepsilon_A(\tilde{\nu})}{\tilde{\nu}^4} \quad \text{Eq. 6}$$

In Eq. 6, κ^2 is the orientational factor; η is the refractive index of the medium; R_{DA} is the effective distance between the donor and acceptor dipoles; τ_D and ϕ_D are the fluorescence lifetime and quantum yield of the donor (in the absence of the acceptor), respectively; $\bar{F}_D(\tilde{\nu})$ is the fluorescence spectrum of the donor, normalized to unit area; $\varepsilon_A(\tilde{\nu})$ is the absorption spectrum of the acceptor, expressed as molar extinction coefficient.

The mechanism can be described in a classical way: the oscillating electric field associated to the oscillating dipole of D induces oscillations in the dipole of A, provided that the two dipoles have common oscillation frequencies (resonance). This last requirement implies that the emission spectrum of D must overlap with the absorption spectrum of A (as described by the integral in Eq. 6).

In particular, the integral assuring for energy conservation is often called overlap integral J (Eq. 7, Figure 3):

$$J = \int d\tilde{\nu} \frac{\bar{F}_D(\tilde{\nu})\varepsilon_A(\tilde{\nu})}{\tilde{\nu}^4} \quad \text{Eq. 7}$$

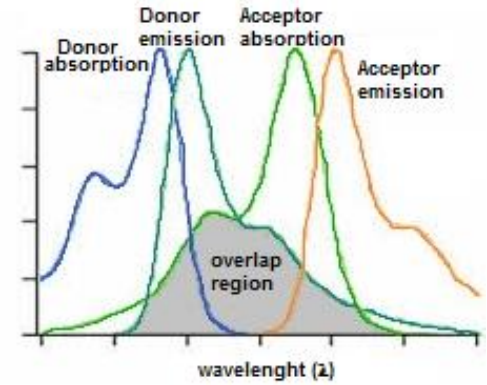

Figure 3. *Illustration of the overlap between the fluorescence spectrum of the donor and the absorption spectrum of the acceptor.*

The quantities ϕ_D, τ_D and J can be accessed through standard spectroscopic analysis of the donor (emission) and of the acceptor (absorption).

On the contrary, the distance between the oscillating dipoles, R_{DA}, is often unknown and the rate of FRET (Fluorescence Resonance Energy Transfer), k_{RET}, is not directly accessible. To fill this gap, Förster introduced the critical distance (also called "Förster radius"), R_0, at which transfer and spontaneous decay of the excited donor are equally probable ($1/\tau_D = k_{RET}$); in other words, R_0 is the distance at which FRET is 50% efficient:[1,3]

$$R_0 \propto \sqrt[6]{\frac{\kappa^2 \varphi_D J}{n^4}} \qquad \text{Eq. 8}$$

According to this equation (Eq. 8), the Förster radius, R_0, can be estimated from easily-accessible spectroscopic properties related to the isolated donor and acceptor and the rate of energy transfer can be expressed as:

$$k_{RET} = \frac{1}{\tau_D}\left(\frac{R_0}{R_{DA}}\right)^6 \qquad \text{Eq. 9}$$

The transfer mechanism is competitive with the spontaneous decay of the donor, according to the ratio between the Förster distance and the effective distance between the two species (Eq. 9).

Another important quantity in describing energy transfer is the quantum efficiency of the process, defined in Eq. 10:

$$E = \frac{k_{RET}}{\tau_D^{-1} + k_{RET}} \qquad \text{Eq. 10}$$

Because of the dependence of k_{RET} on the sixth power of the ratio between the Förster distance R_0 and the effective D-A distance R_{DA} (Eq. 9), the transfer efficiency is strongly dependent on the distance when $R_{DA} \approx R_0$. Conversely, the transfer efficiency quickly decreases to zero if $R_{DA} > R_0$.

Once R_0 is known and the transfer efficiency has been evaluated, the distance R_{DA} between the transition dipoles of the donor and of the acceptor (i.e. roughly the distance between the two species) can be calculated.

Because the efficiency strongly depends on the distance, measurements of the distance are only reliable when R_{DA} is within a factor of 2 of R_0.

- Measurement of the transfer efficiency

There are four methods to measure the efficiency of energy transfer.

1. *Measurement of the enhancement of the acceptor fluorescence in the presence of the donor*.
2. *Comparison between the absorption spectrum and the excitation spectrum, through the observation of the acceptor fluorescence.*

The excitation profiles obtained by detecting the acceptor fluorescence exactly reproduce the sum of the absorption spectrum of the acceptor itself and of the donor if 100% energy transfer occurs. In the case of deviations, the relative intensity of the two bands allows to quantify the efficiency of energy transfer.

These two methods are less direct than the following two:

3. *Decrease of the donor lifetime in the presence of the acceptor.*

When the excited donor is in presence of the acceptor, not only it can decay through its standard (radiative and non-radiative) de-excitation mechanisms, but also transfer its excitation energy to the acceptor. So the lifetime of the donor in the presence of the acceptor, $\tau_{D(A)}$, is shorter that the natural lifetime of the donor in the absence of the acceptor (Eq. 11):

$$\tau_{D(A)}^{-1} = \tau_D^{-1} + k_{RET} \qquad \text{Eq. 11}$$

Substituting k_{RET} in Eq. 5

$$E = \frac{k_{RET}}{\tau_D^{-1}+k_{RET}} = 1 - \frac{\tau_{D(A)}}{\tau_D^{-1}} \qquad \text{Eq. 12}$$

The efficiency of energy transfer can be obtained by measuring the fluorescence lifetime of the donor in the presence and in the absence of the acceptor (Eq. 12).

4. *Decrease of the fluorescence intensity of the donor in the presence of the acceptor.*

The efficiency of energy transfer can be expressed through the ratio of the fluorescence intensity (or quantum yield) of the donor in the presence and in the absence of the acceptor, as follows in Eq. 13:

$$E = 1 - \frac{F_{D(A)}}{F_D} = 1 - \frac{\varphi_{D(A)}}{\varphi_D} \qquad \text{Eq. 13}$$

In a very intuitive and simple way, we can consider the energy transfer process as a quenching mechanism of the fluorescence of the donor, in favor of the excitation of the acceptor.

2.2 Aim of the chapter

Here is reported the synthesis and spectroscopic characterization of simple and versatile bi-chromophore dyads able to efficiently perform intramolecular energy transfer from the donor to the acceptor chromophore. Two different couples of dyes were selected: 7-nitrobenz-2-oxa-1,3-diazol-4-yl (NBD) and Nile red (respectively as energy donor and energy acceptor), and Coumarin 343 and NBD (respectively as energy donor and energy acceptor, Figure 4). The extended spectral overlap between the luminescence spectrum of NBD and the absorption spectrum of Nile red (and similarly of Coumarin 343 and NBD)[4] is a good prerequisite for a highly efficient energy transfer, and allows the investigation of how different factors, such as the mutual orientation of the two dyes, or the interactions of the bi-chromophore units with the medium (solvent) influence the kinetics of excitation energy transfer.

The two couples of dyes were linked at the 1,3-distal positions of the upper rim of a *cone* or *partial cone*- calix[4]arene (Figure 4) through a short spacer. The possibility of linking the dyes to different conformations of the calixarene scaffold allowed to obtain three similar dyads for each couple, in which the donor and the acceptor are kept at different distances.

In addition, mono-chromophoric calixarene derivatives have been synthesized as reference compounds, to take into account the possible influence of the calixarene on the photophysical properties of the dye.

The choice of studying two different couples was dictated by the possibility of eventually combining the three chromophores on a single antenna system that could perform two sequential energy transfer steps (from Coumarin 343 to NBD to Nile red).

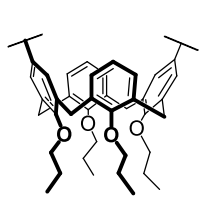

***cone*-calix[4]arene**

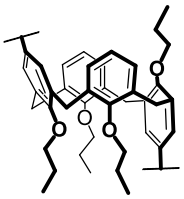

***partial cone*-calix[4]arene**

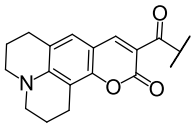

COUMARIN 343

λ_{max}^{abs} (EtOH) ~ 440nm;
λ_{max}^{em} (EtOH) ~ 460 nm

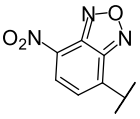

NBD

λ_{max}^{abs} (CH_3OH) ~ 460, 335nm;
λ_{max}^{em} (CH_3OH) ~ 540 nm

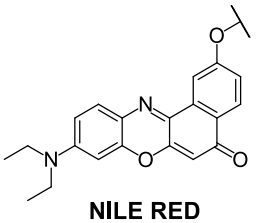

NILE RED

λ_{max}^{abs} (CH_3OH) ~ 550 nm;
λ_{max}^{em} (CH_3OH) ~ 630 nm

Figure 4. *Chosen cone- and partial cone calix[4]arene scaffolds and NBD, Nile red and Coumarin 343 chromophoric units.*

Throughout the discussion, the following nomenclature will be adopted: **NR** = Nile red, **NBD** = 7-nitrobenzo furazan, **Coum** = Coumarin 343.

2.3 Synthesis

2.3.1 *Cone*- NBD-Nile red calix[4]arene, 8a

To anchor NBD and Nile red at the upper rim of the *cone*-calix[4]arene, the synthetic pathway reported in Scheme 1 was designed. This reaction scheme is based on the sequential introduction of the chromophores on the 1,3-distal positions of the calix[4]arene.

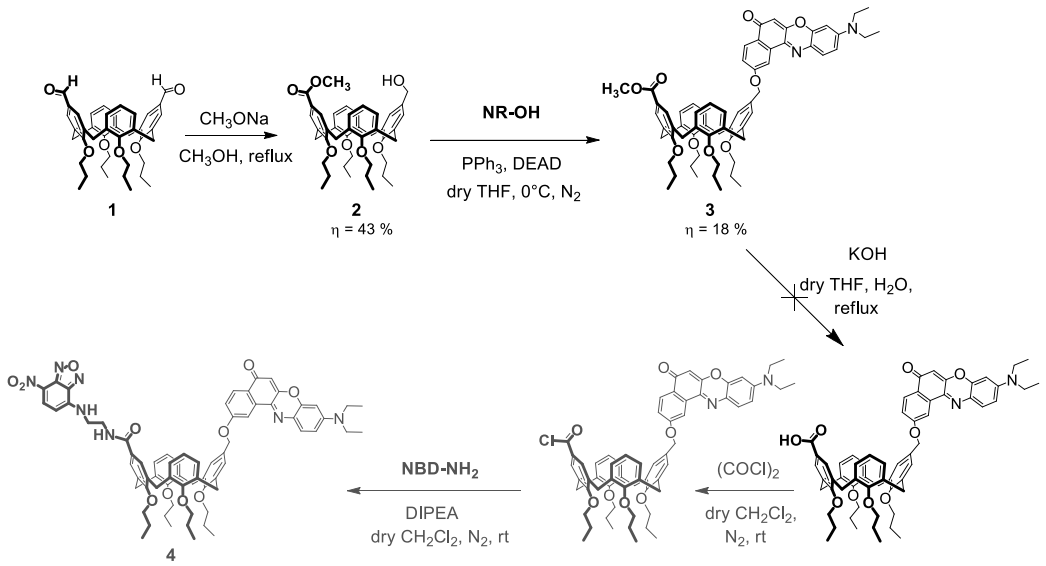

Scheme 1. *Designed synthesis of bichromophoric target **4**.*

The first step, which is the intramolecular Cannizzaro reaction[5] performed on diformyl tetrapropoxycalix[4]arene **1**, would have allowed the generation of two different reacting groups, i.e. an alcoholic and a methyl ester functionality, that could be further and selectively functionalized with the chromophores. It was initially planned to react the alcohol with hydroxy Nile red (**NR-OH**) through a Mitsunobu reaction, then hydrolyze the ester and finally condense the carboxylic acid with an amine derivative of NBD (see Scheme 4 for the synthesis of **NBD-NH_2**).

Reaction of compound **1** with sodium methoxide yielded the dismutation product **2** in satisfactory yield. The use of sodium methoxide as a base is advantageous since it affords the carboxylic acid group protected as a methyl ester.

NR-OH was prepared in 21% overall yield from a Diels-Alder reaction between the commercially available 1,6-dihydroxynaphthalene and 5-diethylamino-2-nitrosophenol hydrochloride **5**,[6] previously obtained by nitrosylation of *m*-diethylaminophenol[7] (Scheme 2).

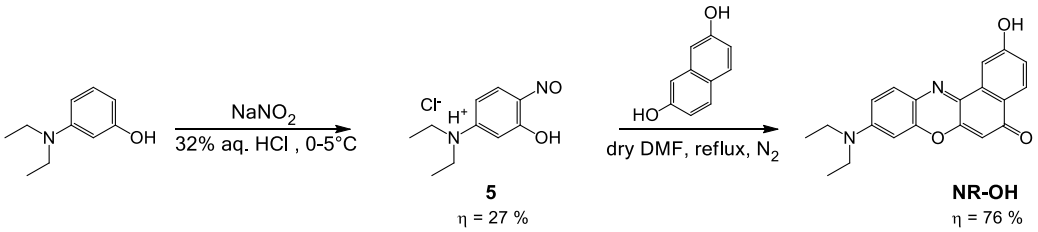

Scheme 2. *Synthesis of **NR-OH**.*

NR-OH was then linked to the hydroxymethylene function of compound **2** through a Mitsounobu reaction[8] carried out with diethyl azodicarboxylate and triphenylphospine in dry tetrahydrofuran. Compound **3** (Scheme 1) was isolated as violet powder in low yield (18%), due to a difficult purification. To obtain pure **3**, in fact, a flash column chromatography had to be followed by preparative TLC.

Compound **3** was then refluxed with potassium hydroxide in a mixture of tetrahydrofuran and water to hydrolize the ester group. Unexpectedly, however, the crude obtained was indeed a mixture of different products, as showed by TLC and NMR analysis, none of which corresponded to the desired compound. A careful literature search allowed to find a paper[9] where the instability of Nile red in aqueous alkali conditions was reported, and enzymatic hydrolysis or the use of potassium trimethylsilanolate as alternative methods for the hydrolysis of alkyl esters in presence of Nile red was recommended. However, also due to the low yield and difficult purification of the product of the Mitsunobu reaction (**3**), this synthetic pathway was discarded.

A new synthetic pathway was designed (Scheme 3), which is based on the reaction of the dicarboxylic acid of the calixarene, activated as acyl chloride, with a mixture of the amine derivatized chromophores. This statistical approach allows the introduction on the calixarene substrate of both the chromophores in a single step; the drawback, on the other hand, is the purification of the crude mixture that can be tedious, due to the presence of at least three compounds.

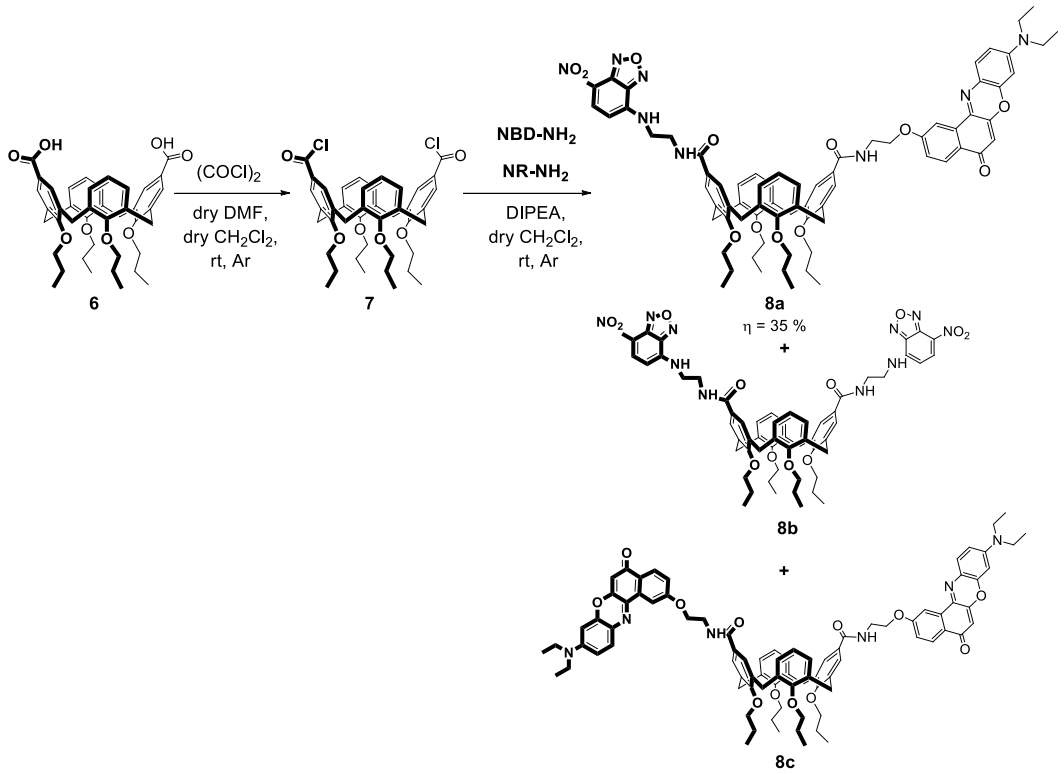

Scheme 3. *Synthesis of hetero-bichromophoric product **8a**.*

The functionalization of both the chromophores with an ethylene amine spacer (Scheme 4) was required in order to make them equally reactive and thus optimize the yield of the desired product, the hetero-bichromophoric compound **8a**, and minimize the formation of the homo-byproducts.

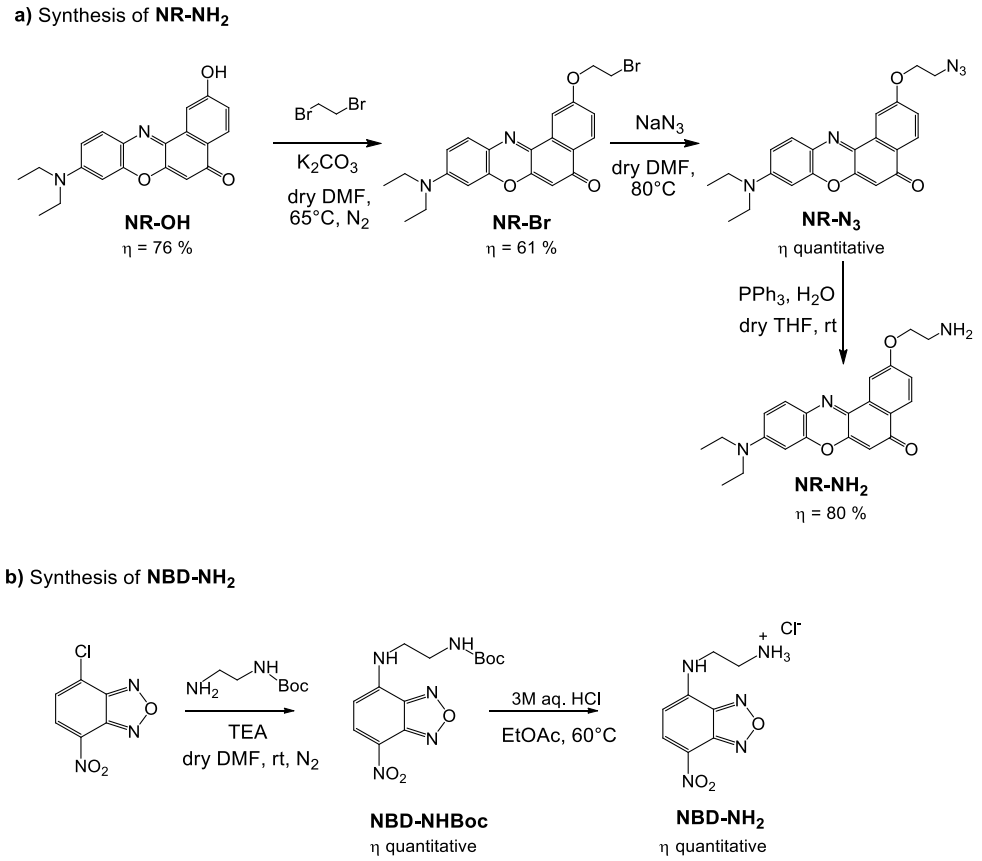

Scheme 4. *Synthesis of a)* ***NR-NH₂*** *and b)* ***NBD-NH₂****.*

Following a literature procedure,[10] **NR-OH** was reacted with 1,2-dibromoethane to obtain **NR-Br** (Scheme 4a). The bromide was then substituted with an azido group[10] that was subsequently converted to amine via the Staudinger reaction. This reduction, carried out with triphenylphospine and water, was chosen because of the mild conditions that did not damage the Nile red structure.

According to the procedure reported by Taliani *et al.*,[11] **NBD-NH₂** (Scheme 4b) was synthesized from commercial NBD via a nucleophilic substitution of the chlorine with N-tert-butoxycarbonyl-1,2-diaminoethane. The resulting **NBD-NHBoc**, was deprotected with a 3M HCl aqueous solution affording pure **NBD-NH₂** hydrochloride salt in 93% yield over two stages.

Diacid tetrapropoxycalix[4]arene **6**[12] was activated as acyl chloride upon treatment with oxalylchloride and was reacted with an equimolar mixture of **NBD-NH_2** and **NR-NH_2**, in methylene chloride in presence of DIPEA. This reaction yielded the desired product, the hetero-bichromophoric calix[4]arene **8a**, together with the two homo-bichromophoric calix[4]arenes **8b** and **8c**. Compound **8a** was isolated as a purple powder in 36% yield by column chromatography and fully characterized by ^{1}H and ^{13}C NMR and ESI mass spectrometry.

2.3.2 *Partial cone* NBD-Nile red calix[4]arenes, 13a and 13b

The positive results obtained with the statistical approach used to synthesize **8a** encouraged us to adopt the same strategy for the preparation of the analogous compounds blocked in the *partial cone (paco)* conformation. In this case, however, also the synthesis of the starting reagent, the *paco*-diacid tetrapropoxycalix[4]arene **11**, had to be optimized, because not known in the literature. The chosen synthetic pathway (Scheme 5) consisted of the alkylation of diformyl dipropoxycalix[4]arene **9**[13] in appropriate conditions to obtain the tetraalkylated derivative in partial cone structure, followed by the oxidation of the aldehyde groups. Since no procedure to selectively obtain the partial cone structure of the diformyl derivative is reported in the literature (depending on the upper rim substituents, the partial cone structure is usually obtained mixed with the cone and/or 1,2- or 1,3-alternate isomers), three different reaction conditions (*Routes A*, *B* and *C* in Scheme 5) were tested and the resulting product mixtures were analyzed by TLC. In particular, the effect of the strength of the base and the polarity of the solvent were examined, while potassium was chosen as the base counterion in the three routes because it is reported that its template effect can favor the partial cone structure.[14]

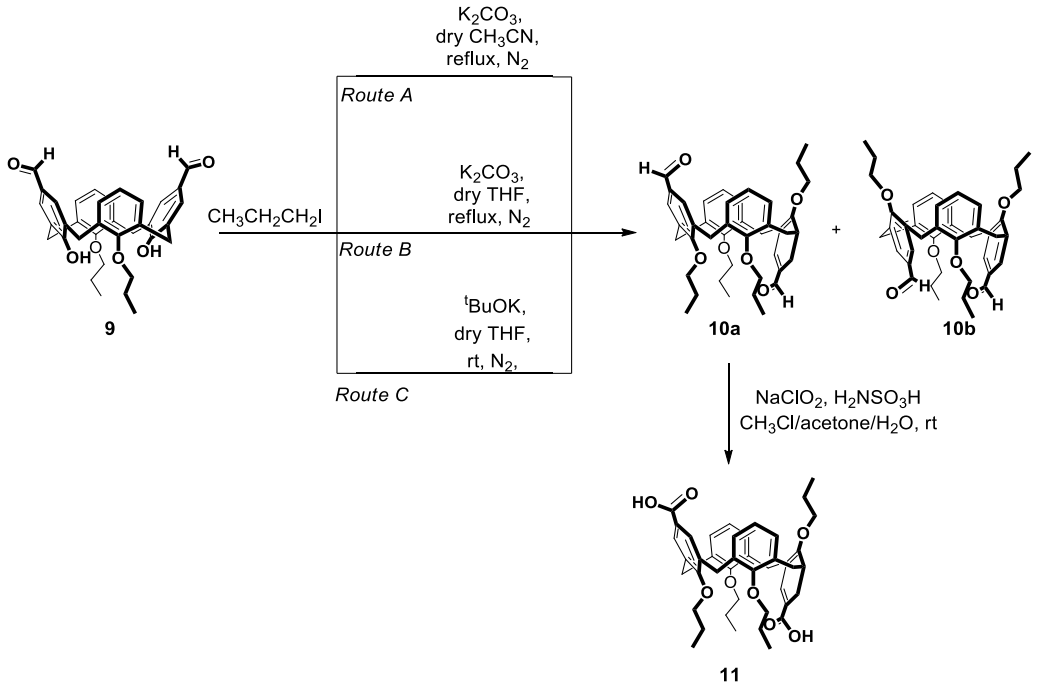

Scheme 5. *The three synthetic strategies for **10a** and its oxidation to **11**.*

To avoid the occurring of an intramolecular Cannizzaro reaction,[5] it was decided to use a weak base as potassium carbonate (Routes A and B) or the strong, but sterically hindered, potassium *tert*-butoxide (*Route C*).

The effect of a polar solvent such as acetonitrile (*Route A*) has been compared with the less polar tetrahydrofuran (*Routes B* and *C*).

The experimental results revealed that all the three routes yielded a mixture of partial cone and 1,3-alternate derivatives and that no dismutation was observed with the use of potassium *tert*-butoxide. However, the higher yield of the partial cone with respect to the 1,3-alternate and the shorter reaction times were obtained in the *Route A* conditions.

^{1}H-NMR analysis (Figure 5) of compound **10a** confirmed its partial cone structure: the methylene bridge protons give two doublets at 4.10 and 3.17 ppm for the axial and equatorial protons, respectively, of the methylene groups between two *syn* aromatic rings, and two other doublets in the range 3.87-3.60 ppm for the protons

of the methylene groups between two *anti* aromatic rings. In addition, the signals of the two formyl groups (9.97 and 9.94 ppm) and of the *m*-aromatic protons of the *p*-formyl rings (7.80 and 7.65 ppm) are displayed as separate signals, due to the different orientation of the two rings. For the same reason, a remarkable difference in terms of chemical shift is shown by the two *m*-aromatic protons within the *p*-H rings, which give rise to two doublets at 6.94 ppm and 6.24 ppm. Moreover, the protons of the propyl chain belonging to the inverted aromatic ring resonate at higher fields than the corresponding protons of the other three propyl chains, because they experience the shielding cone of the three *syn* aromatic rings.

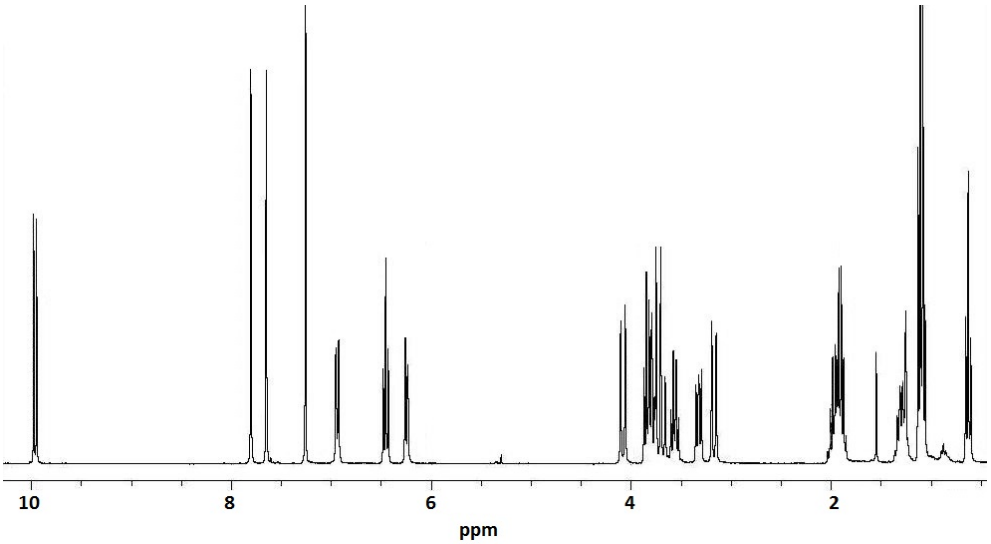

Figure 5. *^{1}H-NMR ($CDCl_3$, 300 MHz) of **10a**.*

Compound **10a** was subsequently oxidized to the dicarboxylic acid derivative **11** with sodium chlorite in presence of sulfamic acid as chlorine scavenger (Pinnick oxidation[15]), a reaction well consolidated in calixarene chemistry.[12]

Then, bis-carboxylic acid **11** was activated as acyl chloride upon treatment with oxalylchloride and reacted with an equimolar mixture of **NBD-NH_2** and **NR-NH_2**, in dichloromethane in presence of DIPEA (Scheme 6).

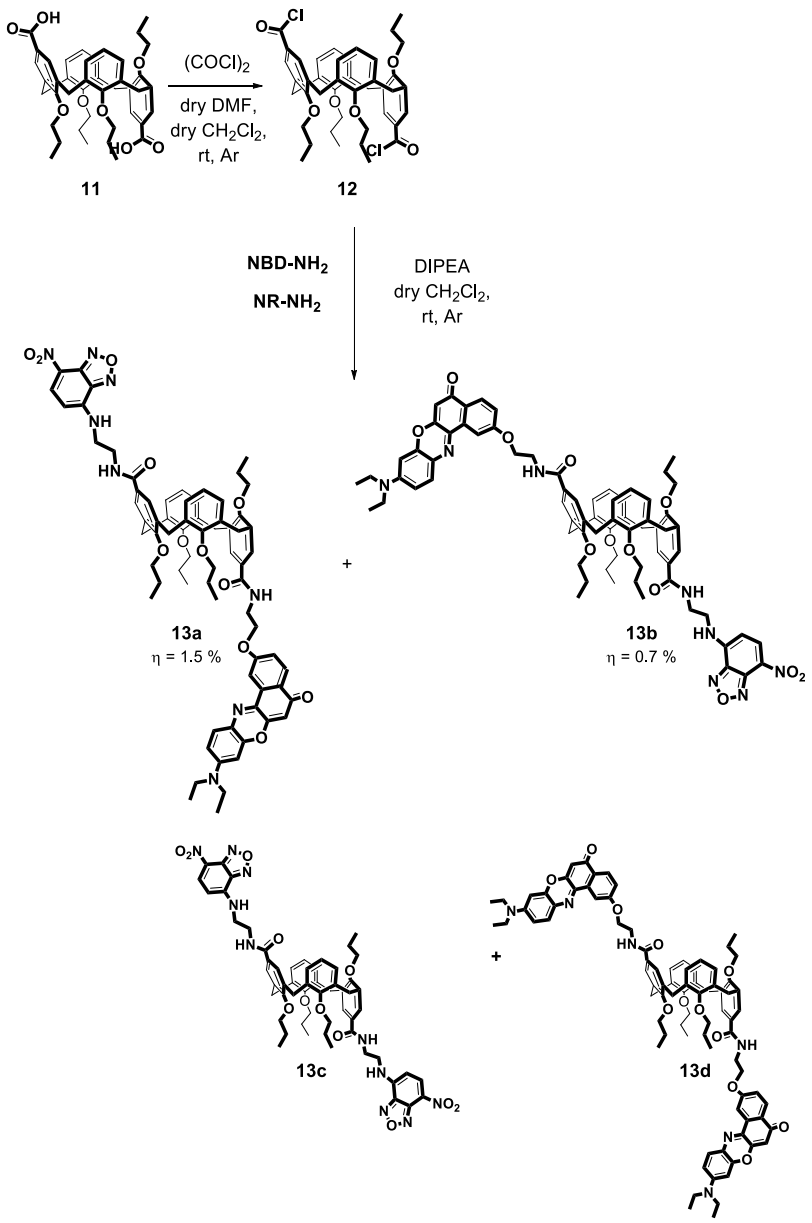

Scheme 6. *Statistical approach to synthesize **13a** and **13b**.*

The two hetero-bichromophoric systems (**13a** and **13b**) were isolated in very low yields (1.5% and 0.7% respectively), because each compound required one flash column chromatography and two preparative TLC purification steps.

The two products were fully characterized by ^{1}H, ^{13}C-NMR, ESI mass spectrometry and unequivocally assigned to their structure by 2D ^{1}H-NMR spectroscopy. In

particular, the through-space coupling between the *m*-aromatic protons of the inverted ring and the NH proton of the amide group linked to the same ring was diagnostic and it was observed in a 2D-NOESY experiment for compound **13a**, and in a 2D-ROESY spectrum for **13b** (Figure 6).

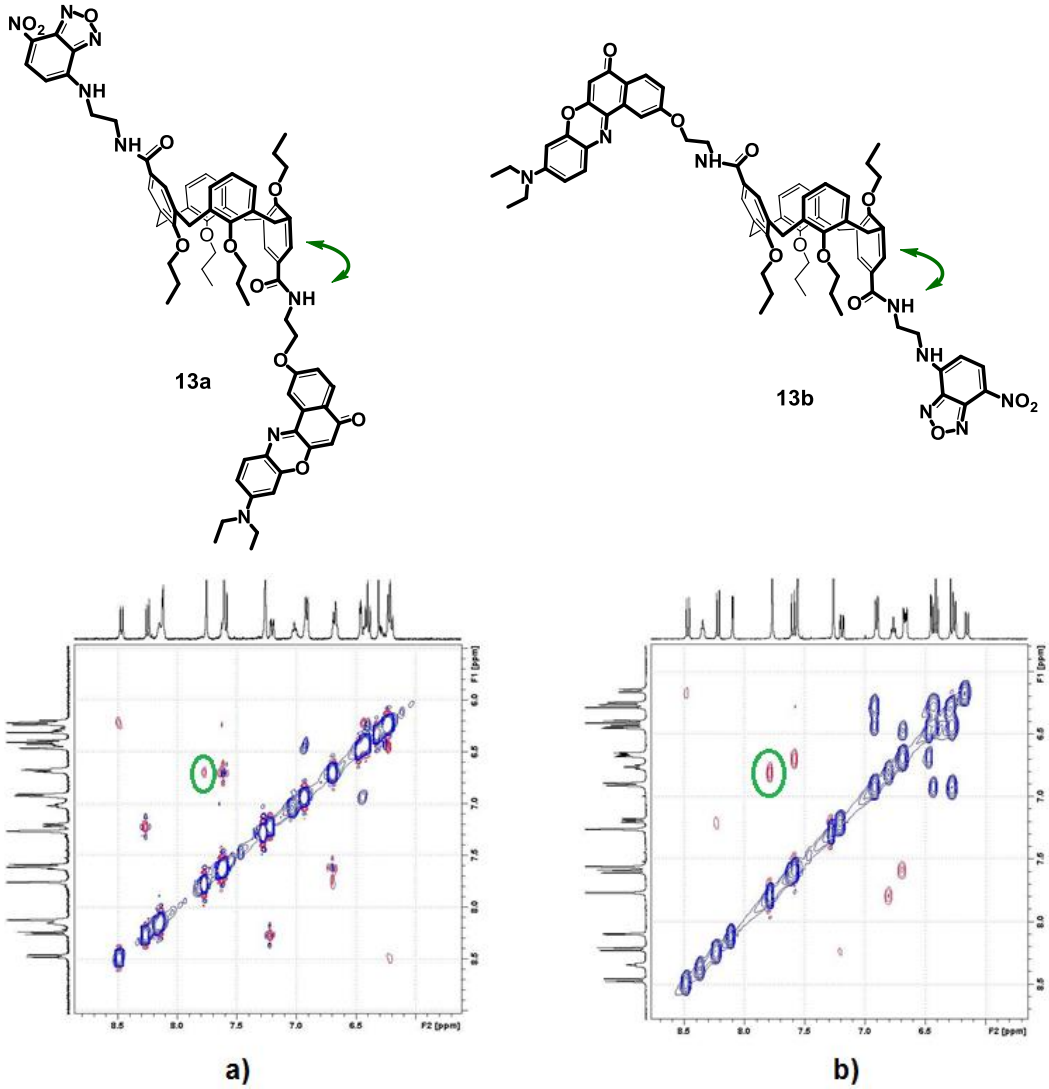

Figure 6. *2D ^{1}H-NMR (CD_3Cl, 400 MHz) a) NOESY spectrum of **13a** and b) ROESY spectrum of **13b**. The diagnostic correlations are circled in green.*

2.3.3 C*one*- and *partial cone* Coumarin 343-NBD calix[4]arenes, 14a, 15a and 15b

The statistical approach was also adopted to attach the second couple of chromophores, Coumarin 343 and NBD, on the *cone*- and *partial cone* diacid calix[4]arenes (Scheme 8 and Scheme 9). Also in this case, the ethylene amine derivatives of the chromophores were used.

To synthesize **Coum-NH₂** (Scheme 7), Coumarin 343 was first activated as acyl chloride by oxalyl chloride and then reacted with N-tert-butoxycarbonyl-1,2-diaminoethane. The subsequent deprotection with trifluoroacetic acid in presence of triethylsilane, as a scavenger, produced the desired compound in 83% overall yield.

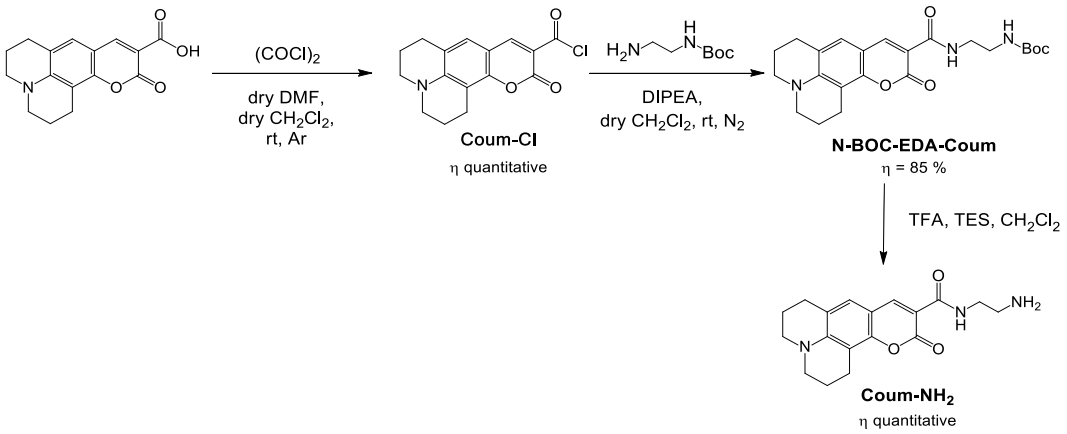

Scheme 7. *Synthesis of* ***Coum-NH₂.***

Compounds **14a**, **15a** and **15b** were synthesized in the same conditions as **8a**, **13a** and **13b** (Scheme 8 and Scheme 9), and isolated in 24%, 6% and 10% yield, respectively; also in this case, the purification of the partial cone derivatives proved difficult and required multiple steps of column and thin layer chromatography.

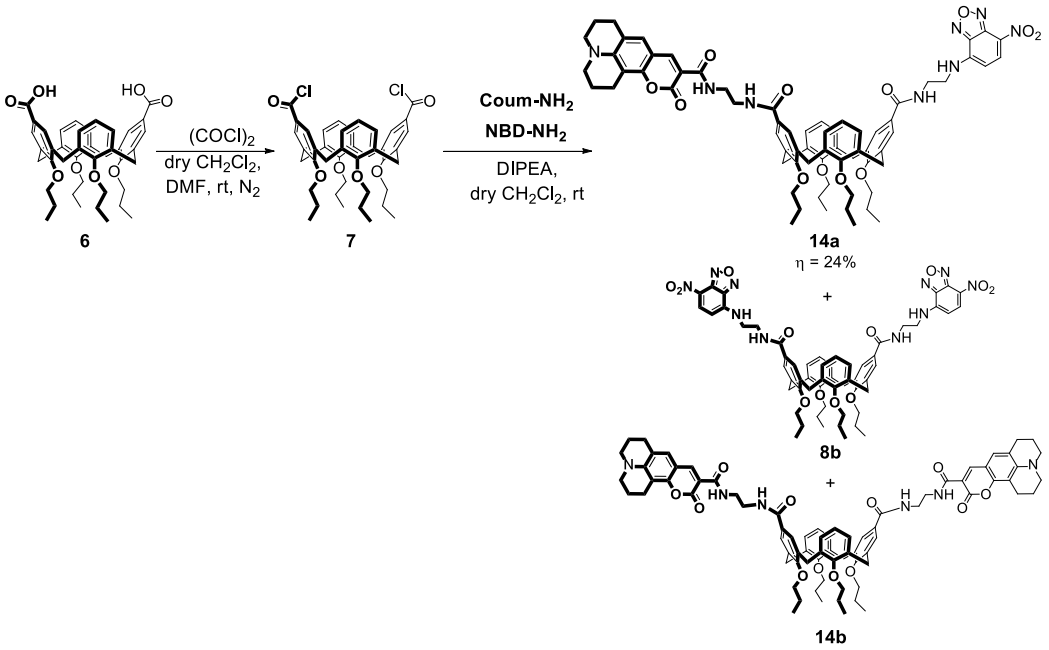

Scheme 8. *Statistical approach to synthesize **14a**.*

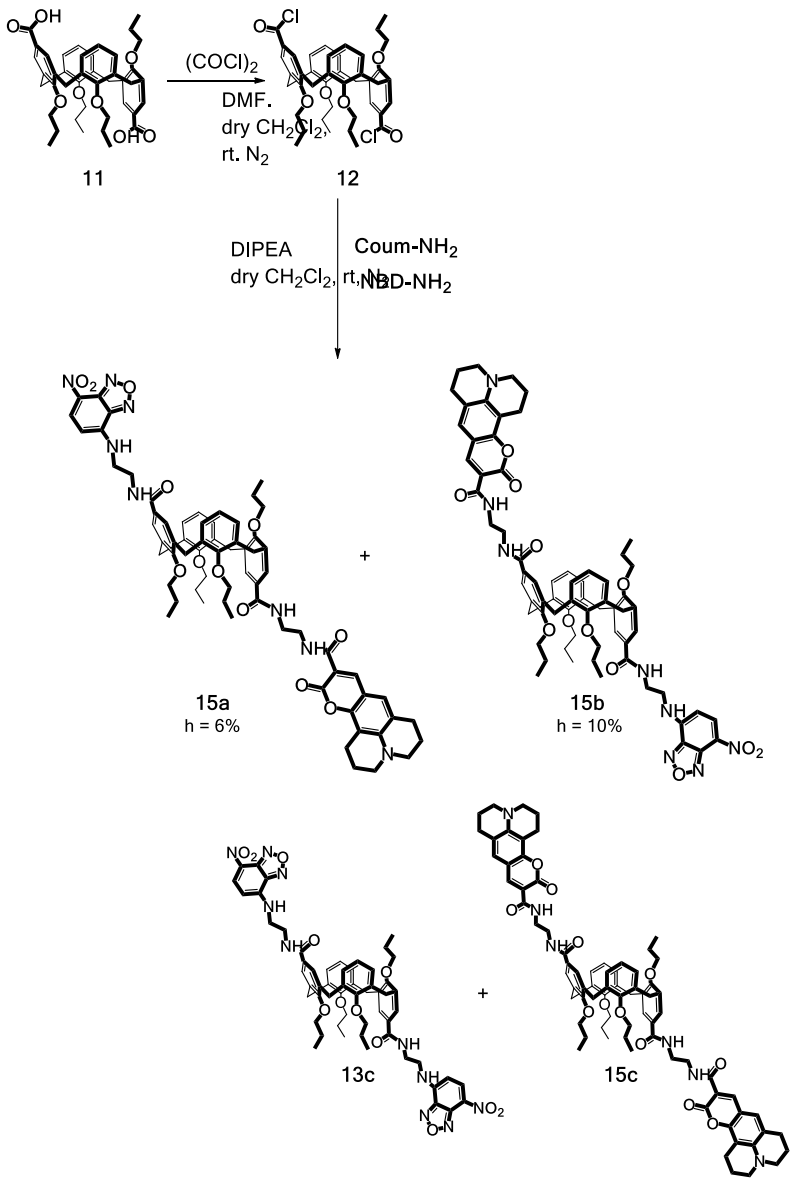

Scheme 9. *Statistical approach to synthesize **15a** and **15b**.*

The three compounds were fully characterized by ^{1}H and ^{13}C NMR and ESI mass spectrometry, and the structures of compounds **15a** and **15b** were assigned by 2D-NOESY and ROESY NMR spectroscopies (Figure 7), in a similar way as for derivatives **13a** and **13b**.

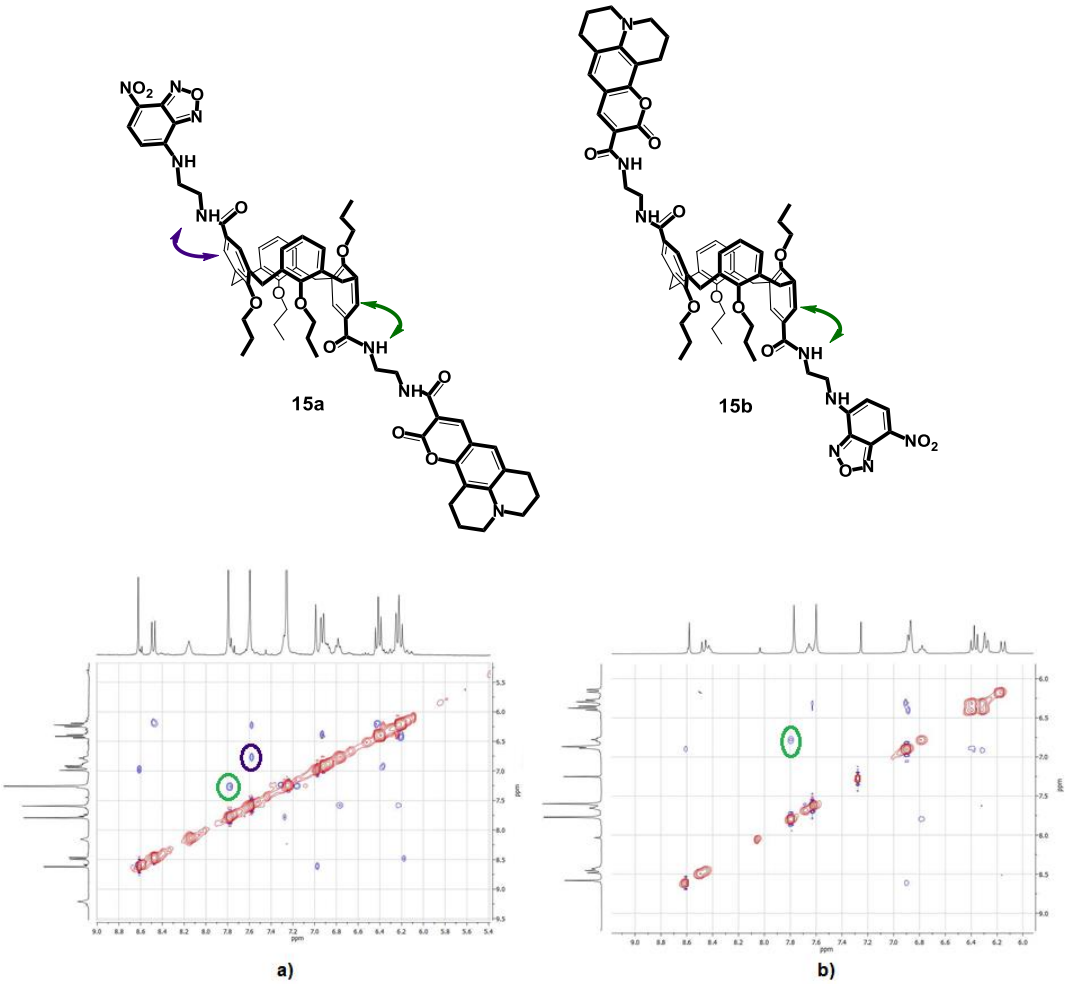

Figure 7. *2D ^{1}H-NMR (CD_3Cl, 400 MHz) a) NOESY spectrum of **15a** and b) ROESY spectrum of **15b.** The diagnostic correlations are circled in green and violet.*

2.3.4 Monochromophoric calix[4]arenes, 18, 19 and 22

Monochromophoric calix[4]arene derivatives were synthesized as reference compounds for the spectroscopic studies.

The preparation of Nile red-calix[4]arene **18** and Coumarin 343-calix[4]arene **19** were carried out according to a reaction pathway similar to the one followed for the synthesis of the hetero-bichromophoric products (Scheme 10). The monoacid tetrapropoxycalix[4]arene **16**[16] was activated with oxalyl chloride and the resulting acyl chloride was reacted with the amine-functionalized chromophore (**NR-NH$_2$** or **Coum-NH$_2$**), affording the desired monochromophoric calixarenes **18** and **19** in 46 and 25% yield, respectively.

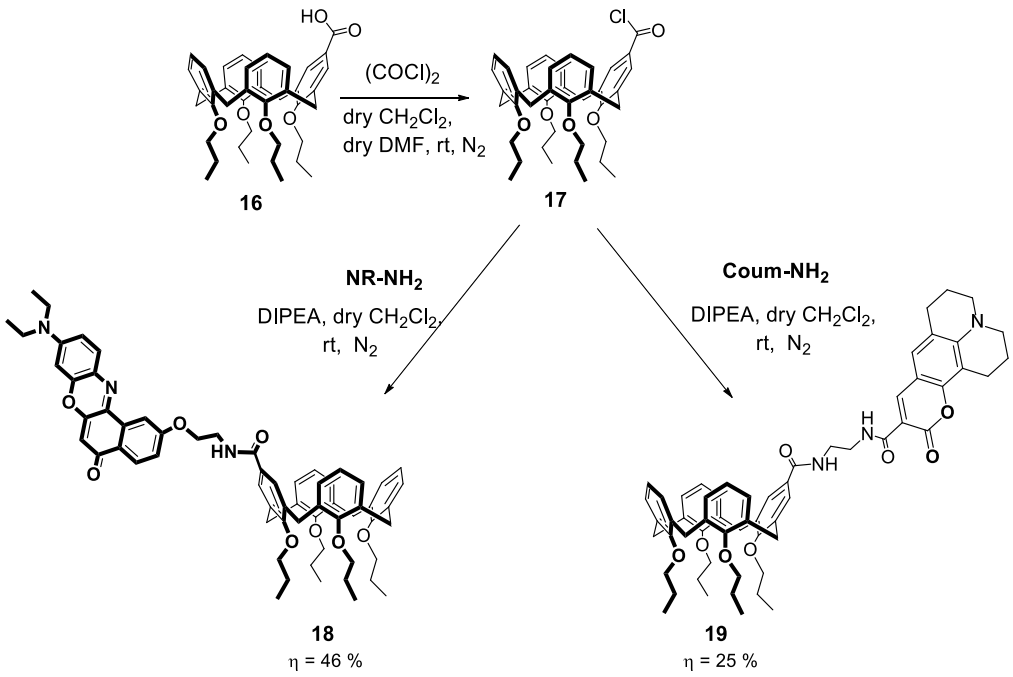

Scheme 10. *Synthesis of reference compounds **18** and **19**.*

NBD-calix[4]arene **22** was obtained from intermediate **2**, following the reaction pathway reported in Scheme 11. First, the hydroxyl group of **2** was protected as methyl ether (**20**), then the methyl ester was hydrolyzed using potassium hydroxide in a mixture of tetrahydrofuran and water at reflux and the resulting carboxylic acid

derivative (**21**) was activated as acyl chloride and coupled with **NBD-NH_2** to obtain **22** in 31% yield .

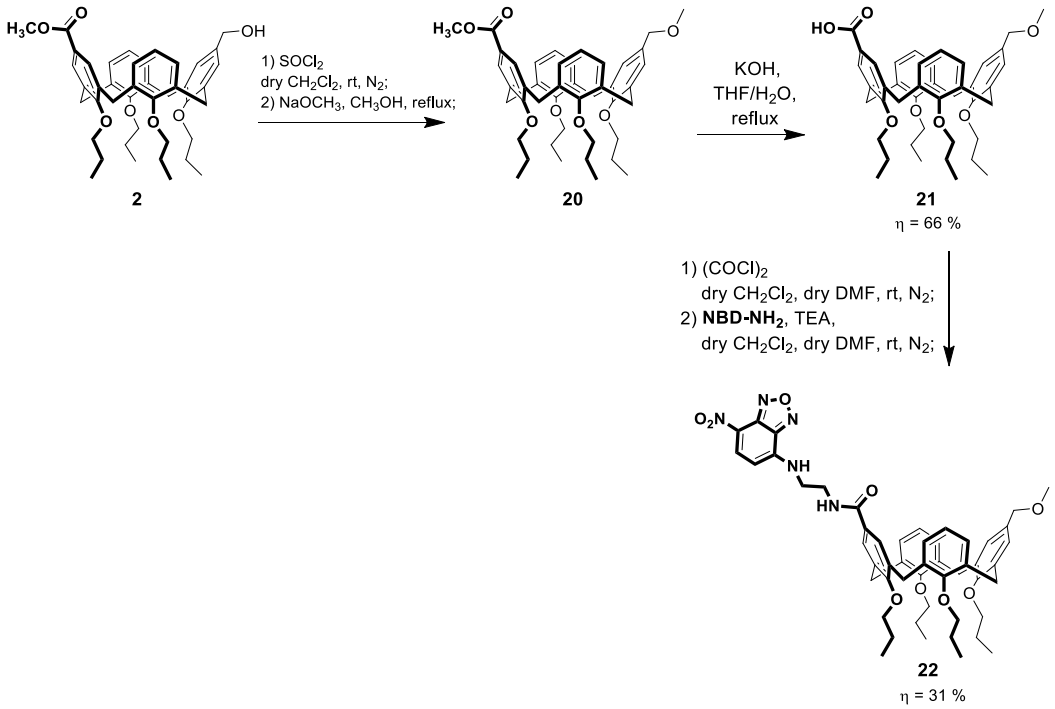

Scheme 11. *Synthesis of reference compound **22**.*

2.3.5 Conformational studies via ^{1}H-NMR

Even if a calix[4]arene is blocked in the *cone* conformation by alkylation of the lower rim with four groups bulkier than ethyl, a residual conformational mobility at room temperature is still present and it results in the calixarene skeleton continuously interchanging between two limiting "flattened" cone conformations having C_{2v} symmetry.[13] In these structures, two opposite aromatic rings are parallel to each other, while the remaining two are tilted outward. Since the interchange movement is fast on the NMR timescale, the NMR spectrum of calix[4]arenes functionalized at the upper rim with four identical groups reflects the C_{4v} symmetrical cone structure of the scaffold (i.e. the signals of the aromatic protons of the four rings are isochronous), which is the average between two equivalent C_{2v} "*flattened*" conformation. On the contrary, when two functional groups are linked at the upper rim in 1,3-position,[17] the two "flattened" cone conformations do not have the same energy and the NMR spectrum is indicative of the more stable structure. Usually, this is the conformation having the substituted aromatic rings pointing outwards *("open" flattened cone* conformation, structure (a) in Figure 8) because the steric repulsions are minimized. However, in case of attractive interactions between the substituents (such as hydrogen bonding or electrostatic interactions), the macrocycle can prefer the opposite *"closed" flattened cone* conformation (structure (b) in Figure 8). In this case, the solvent, and in particular its polarity and ability to form hydrogen bonds, plays a fundamental role in shifting the equilibrium towards one or the other flattened cone conformation.

By ^{1}H NMR spectroscopy it is possible to distinguish the two flattened cone conformations, observing the reciprocal positions of the signals of the aromatic protons of the substituted and the unsubstituted rings. The aromatic protons of the rings that are parallel to each other, in fact, experience the shielding cone of the outward-oriented rings and resonate, therefore, at higher fields.

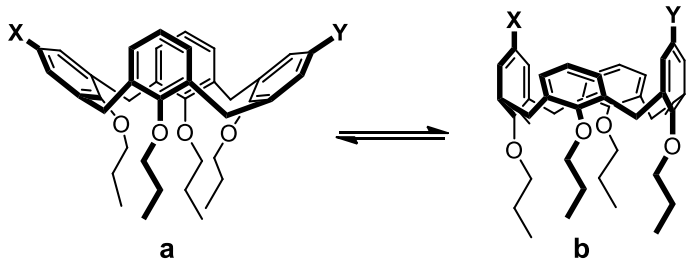

Figure 8. *Equilibrium between the two limiting flattened cone conformations for calix[4]arenes functionalized in the 1,3-distal positions: the open (a) and the closed (b) conformation.*

Compounds **8a** and **14a** have been studied by ^{1}H-NMR to understand their behavior in different solvents and at different concentrations. As shown in Figure 9, the ^{1}H NMR signals of the calixarene aromatic protons of compound **8a** strongly depend on the solvent, thus reflecting a modification of the calixarene conformation according to the medium. In chloroform (Figure 9d), the protons *ortho* to the amide groups are upfield shifted (6.71 and 6.59 ppm), indicating a *"closed" flattened cone* conformation, with the two upper rim substituents brought closer, possibly by attractive hydrogen bonding and/or π-stacking interactions. By increasing the ability of the solvent to break the attractive intramolecular interactions, the structure of compound **8a** becomes an almost regular *cone* conformation (C_{4v}), as demonstrated by the proximity of all the aromatic signals observed in acetonitrile (Figure 9c). In acetone-d_6 (Figure 9b), a solvent able to accept hydrogen bonding, the average conformation is shifted towards a more "*open*" structure, as indicated by the resonances of the aromatic protons (singlets at 7.40 and 7.34 ppm for the protons *ortho* to the amide groups and multiplet at 6.48-6.32 ppm for the protons of the unsubstituted rings). Finally, in dimethyl sulfoxide-d_6 (Figure 9a), compound **8a** displays a fully *"open" flattened cone* conformation, as evinced by the relative position of the calixarene aromatic protons (7.56 and 7.61 ppm for the protons *ortho* to the amide groups and 6.17-6.26 ppm for the protons of the *p*-H rings).

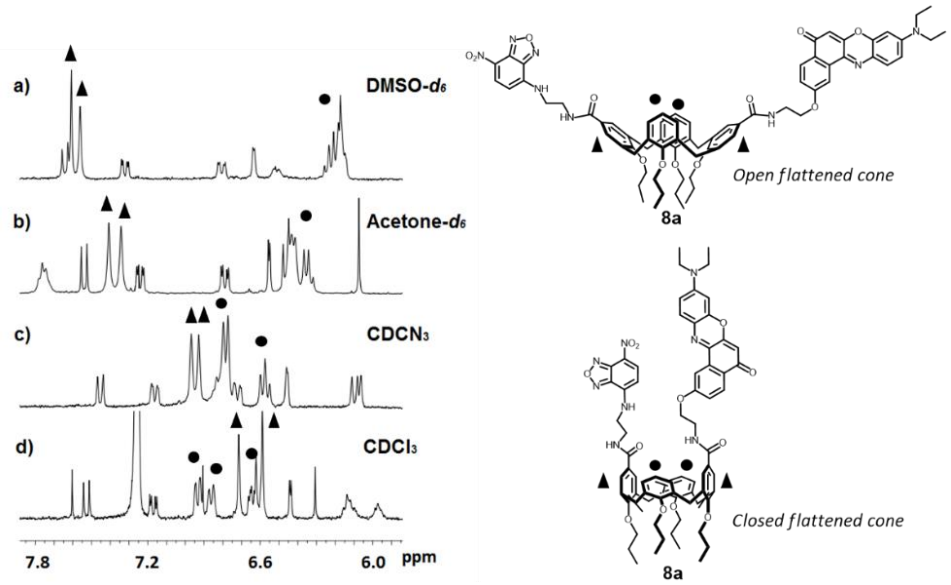

Figure 9. *Portions of ^{1}H-NMR spectra of compound **8a** in a) DMSO-d_6, b) acetone-d_6, c) CD_3CN, d) $CDCl_3$.*

This change between the two *flattened cone* conformations for upper rim 1,3-disubstituted cone calix[4]arenes depending on the polarity of the solvent has been observed before for calix[4]arenes having amide groups at the upper rim[17,18] and had been attributed, in those cases, to the formation of intramolecular hydrogen bonds between the CO and NH groups of the amide moieties on the distal aromatic rings. Molecular modelling calculations on compound **8a** in vacuum revealed as one of the more stable conformers the structure reported in Figure 10, where both an hydrogen bond between the amide NH of the NBD chain and the carbonyl group of the Nile red chain and π-stacking interactions between the chromophores induce the calixarene *"closed" flattened cone* conformation.

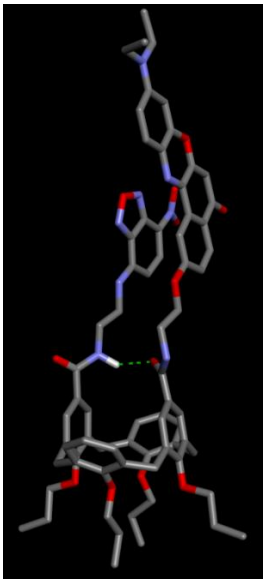

Figure 10*Molecular model (MMFF) of the "closed" flattened cone conformation of compound **8a**. The hydrogen atoms except the one involved in hydrogen bonding have been omitted for clarity.*

These results are supported by the values of the temperature coefficients of the amide NH protons NMR chemical shift ($\Delta\delta/\Delta T$, Figure 11). The less negative temperature coefficient measured for the amide NH of the NBD chain (-5.2 ppb K^{-1}), with respect to the amide NH of the Nile red chain (-21.4 ppb K^{-1}) is diagnostic of its involvement in intramolecular hydrogen bonds.[19]

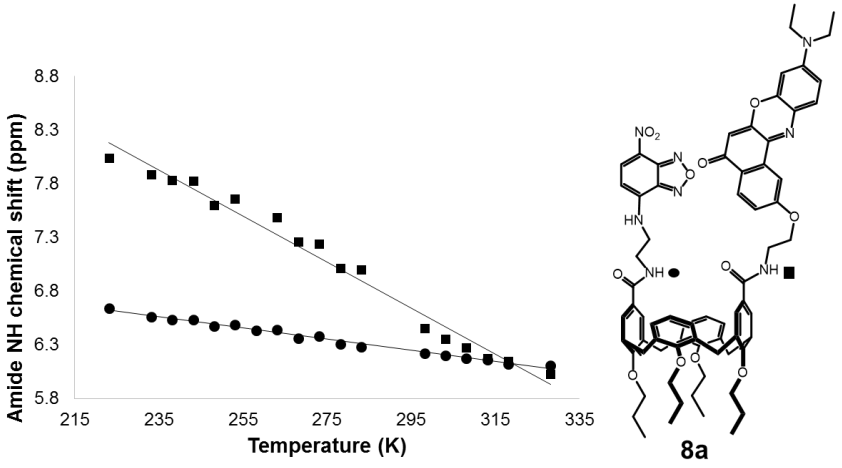

Figure 11. *Amide proton chemical shift of compound **8a** in $CDCl_3$ as a function of temperature.*

Besides intramolecular interactions between the upper rim substituents, when the sample concentration of **8a** in $CDCl_3$ is higher than ~ $5 \cdot 10^{-4}$ M, intermolecular interactions are also observed, as indicated by the presence of an additional set of broad peaks in the ^{1}H NMR spectrum (Figure 12). The low concentrations (below $1 \cdot 10^{-5}$ M) used for the spectroscopic studies, however, rule out the possibility of intermolecular aggregation.

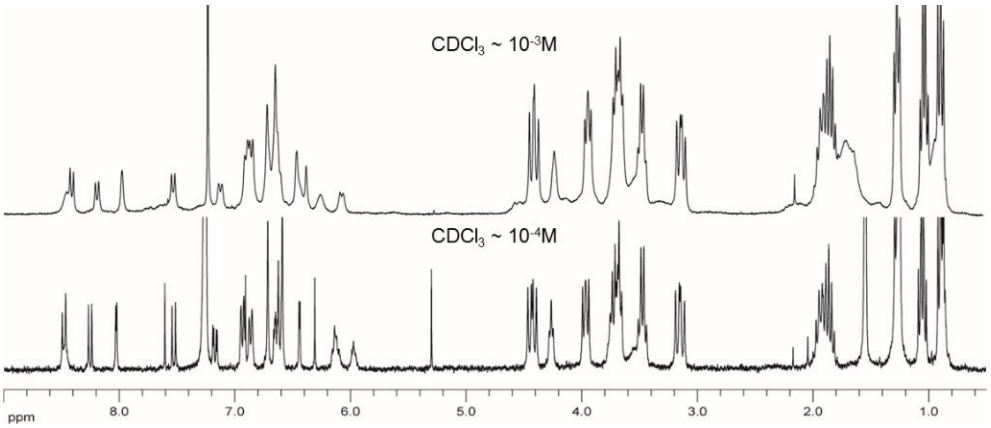

Figure 12. *^{1}H-NMR spectra of compound **8a** in $CDCl_3$ at higher (top) and lower (bottom) concentrations.*

Analogous results have been observed for Coumarin 343-NBD *cone* calixarene **14a** (Figure 13), whose conformation depends on the solvent (*closed* in chloroform and *open* in dimethyl sulfoxide, as showed by ^{1}H NMR spectroscopy).

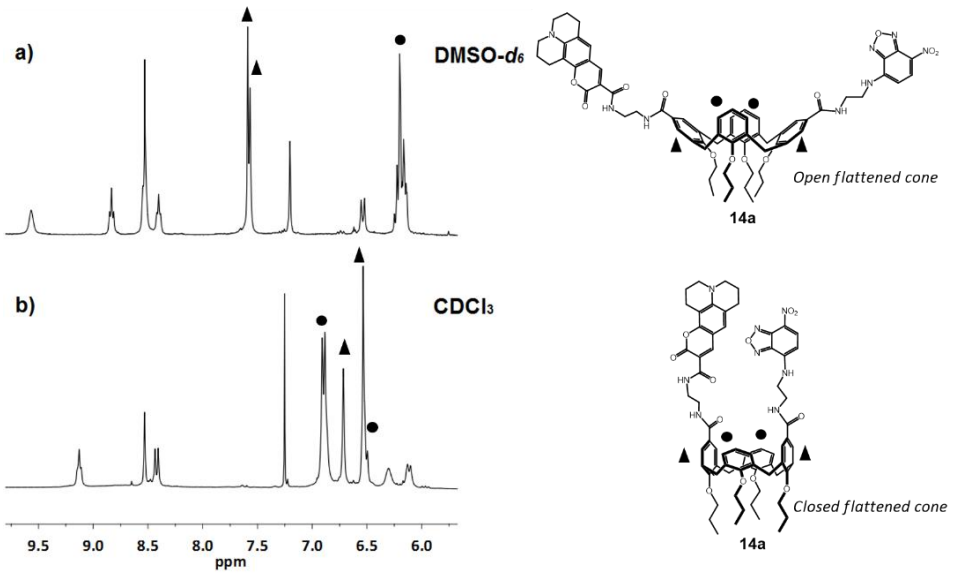

Figure 13. *Portions of ^{1}H-NMR spectra of compound **14a** in a) DMSO-d_6, b) $CDCl_3$. Blue signals belong to the non-substituted aromatic rings, red signals to the functionalized ones.*

The value of the temperature coefficient of the amide group linked to Coumarin (-4.4 ppb K^{-1}) is indicative of an intramolecular hydrogen bond. (Figure 14) On the other hand, the chemical shifts of the amide protons close to the calixarene scaffold show a non linear dependence on the temperature. In particular, for each proton two linear regimes can be recognized, one above and the other below ~ 15°C. More studies are in progress to better understand this unusual behavior.

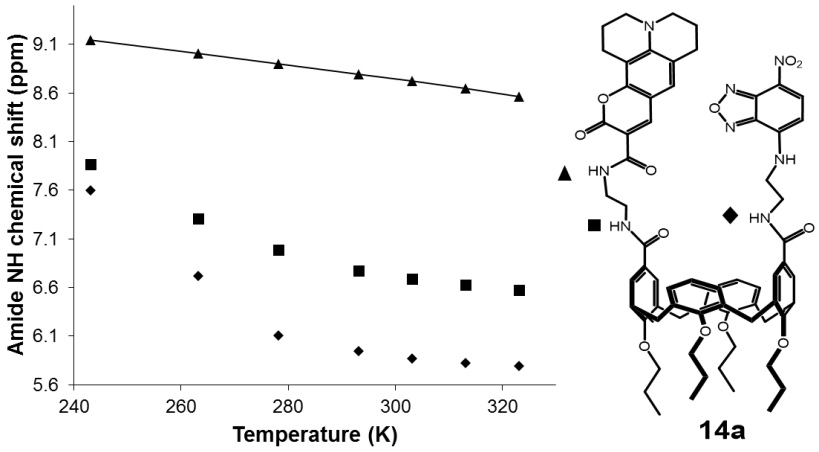

Figure 14. *Amide proton chemical shift of compound **14a** in $CDCl_3$ as a function of temperature.*

2.4 Spectroscopic studies

2.4.1 *Cone*- and *partial cone* NBD-Nile red calix[4]arenes, 8a, 13a and 13b

- Absorption and fluorescence studies

The emission spectrum of reference compound **22** (functionalized with **NBD**) and the absorption spectrum of reference compound **18** (functionalized with **NR**) in chloroform are reported in Figure 15. The good overlap between the spectra confirms that the bichromophoric calixarenes **8a**, **13a** and **13b** satisfy the prerequisite for efficient intramolecular energy transfer.

The Förster radius amounts to ~ 47 Å in all of the three solvents that were investigated. This means that a 50% efficient energy transfer would be obtained if the two chromophores were put at that distance. Any shorter distance will give rise to a more efficient excitation energy transfer process. Since the chromophores are for sure much closer than 47 Å in all the bichromophoric calixarene structures, an extremely efficient EET process is expected.

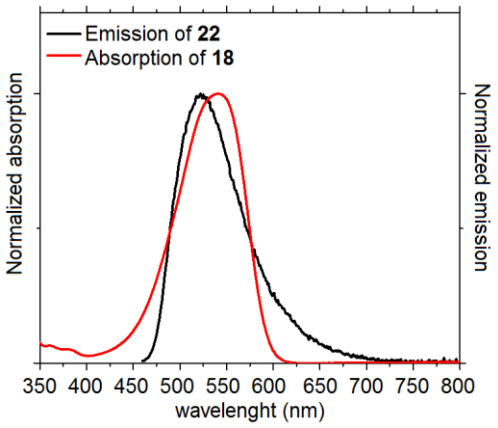

Figure 15. *Overlap between the emission spectrum of **22** and the absorption spectrum of **18** in chloroform.*

Absorption spectra of compounds **8a**, **13a** and **13b**, collected in chloroform, acetonitrile and dimetilsulfoxyde, are shown in Figure 16a. The molar extinction coefficient of **13b** could not be estimated due to the insufficient amount of product, so the reported spectra is normalized to that of **13b**.

As shown, the relative absorbance of the two chromophores in the hetero-bichromophoric calixarenes is comparable to the relative absorbance of the reference compounds **18** and **22**. On the contrary, the molar extinction coefficient of each hetero-bichromophoric system is about 50% higher than what expected from the sum of the molar extinction coefficients of the two reference chromophores, in both chloroform and acetonitrile. In dimethyl sulfoxide, an analogous hyperchromic effect was observed only for **8**, while a much lower molar extinction coefficient was found for **13a** and **13b**. Anyway, the poor solubility of the compounds in acetonitrile and dimethyl sulfoxide possibly hindered the correct estimation of the molar absorptivity. The observed hyperchromic effect has not been satisfactorily explained yet, even if it is quite unavoidably due to intramolecular interactions occurring between the chromophores. In fact, not only the intensity, but also the shape of the spectra is affected, with some deviations of the absorption spectrum of the bichromophoric compound with respect to the sum of the absorption spectra of the isolated chromophores **18** and **22**.

Indeed only **13a** and **13b** behave in the additive way in all the three solvents, while compound **8a** has an additive spectrum only in dimethyl sulfoxide. As shown in Figure 16, the shape of its absorption spectrum is strongly and slightly affected in chloroform and acetonitrile, respectively. This is consistent with the observation by ^{1}H-NMR of a *closed flattened cone* conformation in low-polarity solvents, due to quite strong intramolecular attractive interactions occurring between the chromophoric substituents.

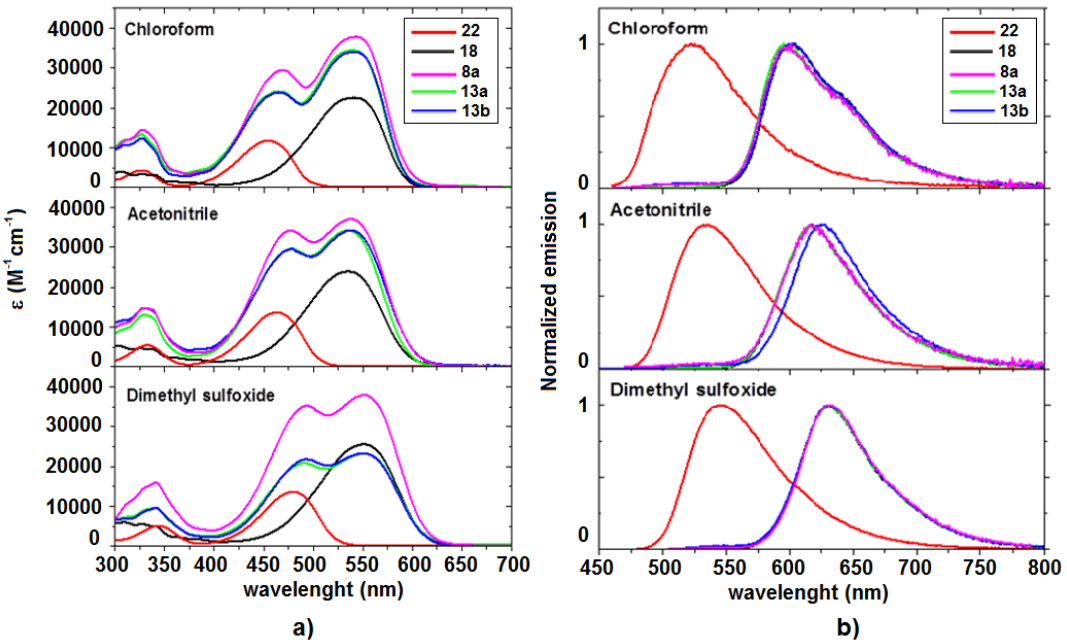

Figure 16. *a) Absorption spectra (molar extinction coefficient) and b) normalized emission spectra of the investigated compounds in chloroform (top), acetonitrile (middle) and dimethyl sulfoxide (bottom). The molar extinction coefficient of **13a** has been normalized to that of **13b**.*

Figure 16b reports the normalized fluorescence spectra of compounds **8a**, **13a** and **13b** in the three different solvents.

From the decrease of the donor emission in the bichromophoric systems with respect to its fluorescence when isolated (compound **22**), it is possible to conclude that energy transfer occurs very efficiently from NBD (energy donor) to Nile red (energy acceptor) in all the compounds, quite independently of the solvent. In particular, the excitation energy transfer is estimated to be quantitative for **13a** and **13b**, and about 98% for **8a**.

A quantitative excitation energy transfer can be also confirmed by the independence of the fluorescence quantum yield (Table 1) of the bichromophoric compounds on the excitation wavelength: spanning all the range from the maximum absorption of the donor to the maximum emission of the acceptor, the fluorescence quantum yield did not change significantly.

In addition, the evaluation of Nile red fluorescence quantum yield when isolated (reference compound **18**) and when in bichromophoric systems, highlights its different behavior depending on the *cone* or *partial cone* conformation of the calixarene scaffold and on the solvent. In particular, strong decreases are observed for the *cone* bichromophore (**8a**) in chloroform and acetonitrile, while in dimenthyl sulfoxide the quantum yield is basically constant (Table 1), confirming the occurrence of strong intramolecular interactions in the *cone* bichromophoric system (as observed by ^{1}H-NMR).

Another proof of energy transfer is typically given by the decrease of the donor fluorescence lifetime when interacting with the acceptor (Table 2); in our case, the residual donor emission was too weak to allow for reliable measurement of the lifetime. On the other hand, the acceptor lifetime in **8a**, **13a** and **13b** significantly decreases in chloroform and acetonitrile with respect to the reference acceptor compound **18**, while it is weakly modified in dimethyl sulfoxide. A bi-exponential decay of the acceptor emission is observed for **8a** in chloroform and acetonitrile, confirming one more time that quite strong attractive interchromophoric interactions are established in these solvents.

	Compound	λ_{abs}^{max} [nm]	ε [$M^{-1}cm^{-1}$] @ λ_{abs}^{max}	λ_{em}^{max} [nm]	Φ
Chloroform	**22**	454	11700	522	0.62
	18	540	22560	601	0.78
	8a	469; 543	29520; 37840	600	0.35; 0.36
	13a	465; 540	-	601	0.71; 0.71
	13b	465; 538	24100; 34380	596	0.68; 0.67
Acetonitrile	**22**	463	13600	535	0.53
	18	534	23900	617	0.73
	8a	477; 538	34170; 37060	617	0.23; 0.26
	13a	479; 538	-	626	0.60; 0.63
	13b	478; 535	29520; 34220	616	0.52; 0.55
Dimethyl sulfoxide	**22**	479	13600	546	0.65
	18	550	23900	631	0.75
	8a	492; 552	35170; 37850	631	0.71; 0.69
	13a	493; 551	-	630	0.72; 0.71
	13b	491; 550	20750; 23230	630	0.74; 0.71

Table 1. *Absorption and emission properties of the investigated compounds in chloroform, acetonitrile and dimethyl sulfoxide. The reported quantum yields were obtained exciting the samples at the λ_{abs}^{max} reported in the second column. Fluorescein in 0.1 M NaOH was used as the standard ($\Phi = 0.9$) for the determination of fluorescence quantum yields.*

		λ_{ex} = 460 nm		λ_{ex} = 560 nm
	Compound	**λ_{em} = 530 nm**	**λ_{em} = 630 nm**	**λ_{em} = 630 nm**
Chloroform	**22**	7.0 (93%) 2.7 (7%)	-	-
	18	-	4.4	4.4
	8a	-	3.5 (45%) 2.0 (55%)	3.6 (40%) 2.0 (60%)
	13a	-	3.9	3.7
	13b	-	3.8	3.8
Acetonitrile	**22**	10.3	-	-
	18	-	4.8	4.8
	8a	-	3.3 (83%) 1.0 (17%)	3.6 (73%) 1.6 (27%)
	13a	-	4.1	4.0
	13b	-	4.2	4.2
Dimethyl sulfoxide	**22**	3.1 (13%) 9.0 (87%)	-	-
	18	-	4.3	4.3
	8a	-	4.0	4.1
	13a	-	4.1	4.1
	13b	-	4.2	4.2

Table 2. *Fluorescence lifetimes (ns) and corresponding relative amplitudes (in parentheses) for the studied compounds in the three solvents, for excitation/detection on the donor and acceptor absorption/emission maxima.*

- Transient absorption measurements

With the aim to investigate the dynamics of the photoinduced excitation energy transfer, transient absorption measurements have been performed.

For a better comparison, compounds **8a**, **13a**, **13b**, **18** and **22** were studied in the three solvents employed for ^{1}H-NMR, absorption and steady-state fluorescence characterizations: chloroform, acetonitrile and dimethyl sulfoxide.

- *Reference compounds **22** and **18***

In order to identify the characteristic transient absorption bands of the NBD-based donor and Nile red-based acceptor chromophores, transient spectra of the reference compounds **22** and **18** were first measured. The excitation wavelength was fixed at 470 nm for compound **22** while compound **18** was excited both at 470 and 530 nm. The time-resolved spectra and the kinetic analysis for compounds **22** and **18** suggested that the covalent linkage of the NBD and Nile red dyes to the calixarene scaffold does not significantly affect the dynamics of their relaxation upon visible excitation, and that the molecules behave similarly to what previously reported for the isolated dyes.[20,21,22]

To extract information about the dynamic evolution of the systems, we globally analyzed the transient data recorded for these two compounds in all the three solvents. The analysis was performed by applying a combined approach, consisting of singular values decomposition (SVD)[23,24] and of simultaneous fitting of all the collected kinetic traces (global analysis),[25] employing a linear decay scheme. In all cases, three kinetic components were necessary to satisfactory fit the data. The EADS (Evolution Associated Decay Spectra) obtained by global analysis are shown in Figure 17 and Figure 18, and lifetimes estimated by global analysis for compounds **22** and **18** are summarized in each panel.

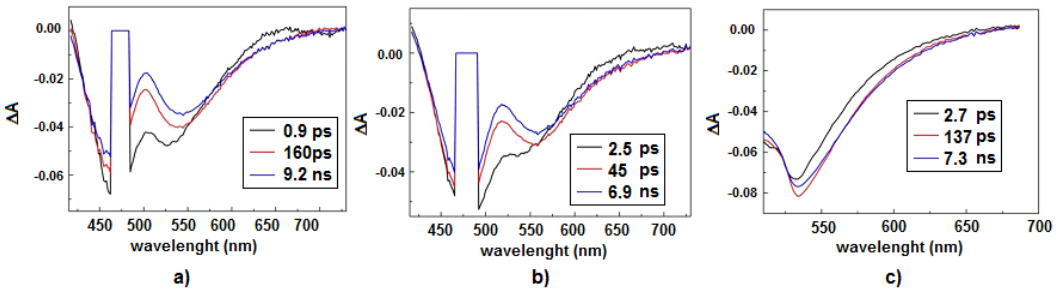

Figure 17. *Evolution associated decay spectra (EADS) obtained by the simultaneous fit of all the kinetic traces recorded for compound **22** in: a) acetonitrile, b) dimethyl sulfoxide, c) chloroform.*

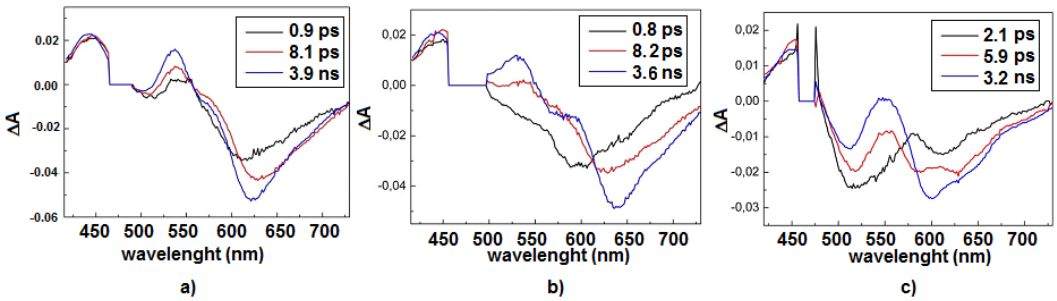

Figure 18. *Evolution associated decay spectra (EADS) obtained by the simultaneous fit of all the kinetic traces recorded for compound **18** in: a) acetonitrile, b) dimethyl sulfoxide, b) chloroform.*

○ *Compound **8a***

Transient absorption spectra of compounds **8a**, **13a** and **13b** have been recorded by exciting the samples in the donor absorption region, at 470 nm. As estimated by the steady-state fluorescence spectra of compounds **22** and **18**, at this excitation wavelength at least 25-30 % of direct Nile red excitation contributes. Figure 19 reports the transient spectra registered for compound **8a** in the three analyzed solvents. The transient spectra of compounds **13a** and **13b** appear qualitatively very similar to those of compound **8a**, although the relaxation dynamics is affected by the fact that in those systems the donor and acceptor molecules are kept at higher distance, being linked on the opposite side of the calixarene scaffold.

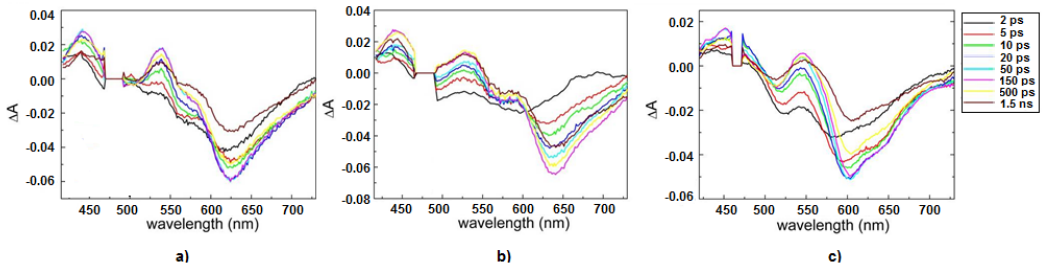

Figure 19. *Selected transient absorption spectra of compound **8a** measured in a) acetonitrile, b) dimethyl sulfoxide, c) chloroform upon excitation at 470 nm.*

At early time delays, the transient spectra of bi-chromophore **8a** show characteristic features of the donor moiety, both in the bleaching (450-480nm) and stimulated emission (530-570nm) regions. In the 450-550 nm spectral range, multiple contributions from both the donor and the acceptor units appear, namely the donor stimulated emission and the acceptor excited-state absorption.

The stimulated emission of the acceptor moiety, peaked between 600 and 630 nm depending on the solvent, is visible already at early time delays: this is in part due to direct excitation of the Nile red chromophore (*ca* 25-30 %) which has a non-negligible absorption at 470 nm. This band gains intensity as energy transfer proceeds, as can be clearly observed by comparing the kinetic trace measured at the maximum of the stimulated emission of the Nile red chromophore in compounds **18** and **8a,** reported in Figure 20. In dimethyl sulfoxide (Figure 20b) a notably different rise time is observed on the short time scale, when the Nile red chromophore is directly excited (in compound **18**) with respect to the situation in which its excitation is the result of energy transfer from the donor (in compound **8a**). In the other two solvents (Figure 20a), traces are more similar on the short time scale (up to *ca* 10 ps), but differ on the long time scale, where a slower rise component, due to energy transfer, is observed for compound **8a**.

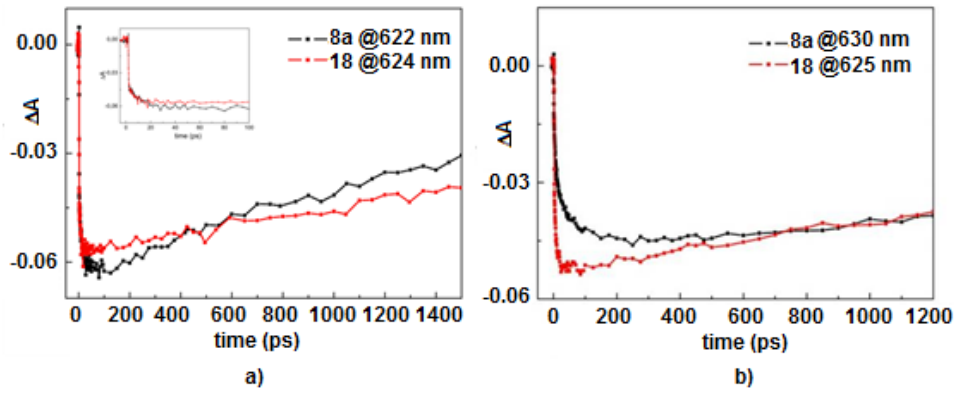

Figure 20. *Kinetic traces measured at the maximum of stimulated emission for compound **18** (red line) and compound **8a** (black line) obtained by exciting the sample at 470 nm in a) acetonitrile and b) dimethyl sulfoxide. The short time delay region (0-100 ps) of the traces measured in acetonitrile is magnified in the inset of panel a).*

The comparison of the transient spectra measured in different solvents demonstrates that the solvent can modulate the kinetics of energy transfer in the bichromophoric system **8a**. In all cases, however, energy transfer appears to be nearly quantitative, as demonstrated by the fact that at long time delays the transient spectra of compound **18** and **8a** are basically the same. The transient data were analyzed with a global analysis procedure, applying a sequential decay scheme. The EADS obtained by global analysis are reported in Figure 21.

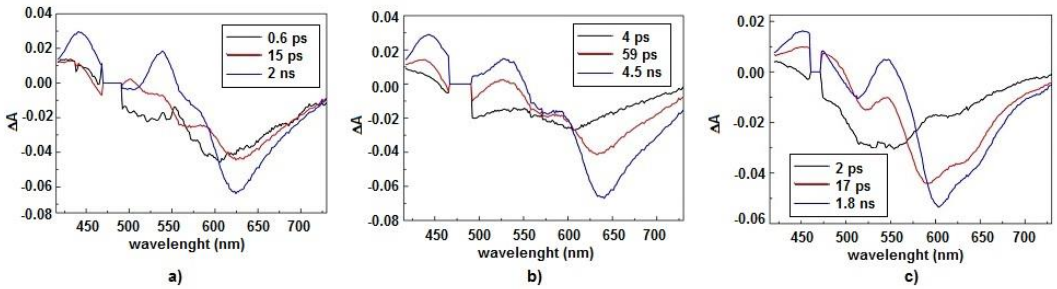

Figure 21. *Evolution associated decay spectra (EADS) obtained by the simultaneous fit of all the kinetic traces recorded for the compound **8a** in: a) acetonitrile, b) dimethyl sulfoxide, c) chloroform.*

In all the analyzed solvents, three kinetic components are necessary to satisfactory fit the data. The first EADS (black line) contains features pertaining both to the

donor (negative band <530 nm) and the acceptor chromophores. The fastest kinetics is observed in acetonitrile where, at 0.6 ps delay, there is a substantial signal due to the acceptor stimulated emission/excited-state absorption, indicating fast energy transfer (besides direct excitation). In order to better evaluate if the fast kinetic component is also ascribable to energy transfer or it is only due to direct excitation of the acceptor, the measurements were repeated exciting the system at 400 nm, where the acceptor dye does not significantly absorb and direct Nile red excitation is not possible. Also in this case a fast sub-picosecond kinetic component is observed, attributing this kinetic component to energy transfer.

In all the analyzed cases the dynamics of energy transfer are multi-exponential, and a marked Stokes shift is observed on a few picosecond timescale on the Nile red stimulated emission band (black to red EADS evolution), as already observed for the isolated acceptor. The multi-exponential nature of the process can be ascribed to the presence of a distribution of conformers in solution, with different donor-acceptor distances due to *open* and *closed* calixarene arrangement. In chloroform and acetonitrile *closed* conformations are the most abundant, while in dimethyl sulfoxide *open* conformers are prevalent. In fact, in dimethyl sulfoxide the energy transfer process occurs with time constants about two times slower than in the two other solvents. This finding also nicely agrees with the NMR data (par. 2.3.5), confirming that in dimethyl sulfoxide the chromophores are more far apart than in chloroform and acetonitrile, because an *open* calixarene conformation with no inter-chromophore hydrogen bonds is predominant.

Steady-state fluorescence measurements reported in the previous section revealed that the yield of energy transfer in all the bi-chromophore systems analyzed is almost quantitative. This implies that at long time delays the donor should not contribute any more to the transient spectrum, and the longer lifetime measured

for the bi-chromophore should correspond to the lifetime of the isolated acceptor molecule. This is verified in dimethyl sulfoxide, while in both acetonitrile and chloroform we observe a shortening of the system lifetime, which in these cases results *ca* 2 ns (compared with almost 4 ns in **18**). Figure 22 shows the comparison between the kinetic traces measured at the maximum of the acceptor stimulated emission in the three analyzed solvents, highlighting the solvent dependence of the relaxation dynamics of the system.

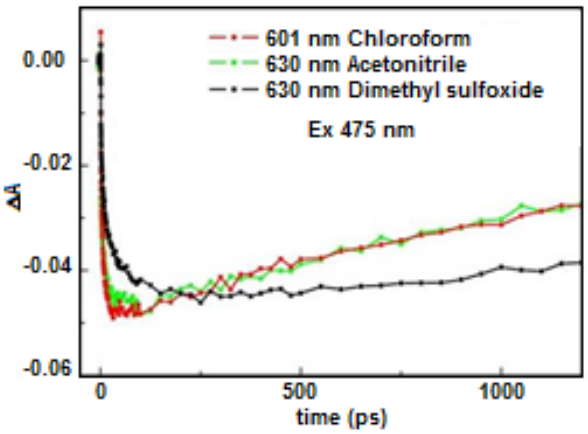

Figure 22. *Kinetic trace measured at the maximum of the acceptor stimulated emission band in acetonitrile (green line), chloroform (red line) and dimethyl sulfoxide (black line) for compound **8a** excited at 475 nm.*

This finding, together with the results of fluorescence quantum yields (see par. 2.4.1) and the observation of a higher molar extinction coefficient measured for the heterodimers compared with what expected from the sum of the molar extinction coefficients of the two reference chromophores, suggests the occurrence of specific interactions between the chromophores, modulated by the solvent properties. In order to investigate how the presence of the donor modifies the relaxation dynamics of the acceptor in the different solvents, transient spectra of compound **8a** were measured directly and selectively exciting the Nile red chromophore at 570 nm (where the donor has vanishing absorbance). The results were compared with those obtained for compound **18** excited at 560 nm,

indicating that the behavior of **8a** and **18** is very similar in dimethyl sulfoxide. In acetonitrile, as reported in Figure 23a, the Nile red stimulated emission band is initially much broader than what observed when both compound **18** and **22** are excited at 470 nm, or when compound **18** is excited at 560 nm. In case of the measurements reported in Figure 23, the stimulated emission band shows a fast decaying component, not observed with different excitation wavelength. Figure 23a shows the raise of two positive bands at shorter wavelengths, respectively peaked at 440 and 560 nm associated to excited-state absorption features of the Nile red. A third positive feature at 500 nm is not observed either in compound **8a** and **18**, when excited at 470 nm, or in compound **18**, if excited at 560nm.

On the long timescale, the transient spectra measured at 560 nm become similar to those measured for compound **18** and **8a** upon excitation at 470 nm, i.e. the acceptor dynamics is regained. By applying global analysis to these transient data, three kinetics components with lifetimes of 0.8 ps, 18 ps and 2.0 ns were obtained. The stimulated emission band, initially peaked at *ca* 600 nm, substantially decreases in intensity on the blue side in less than 1 ps, resulting in a sharper band peaked at 620 nm (black to red evolution Figure 23b). On the same timescale, a positive feature at 500 nm develops. The final spectral component, living 2 ns, coincides with that obtained by exciting compound **8a** at 470 nm, which in turn corresponds to the long timescale spectrum of the isolated acceptor.

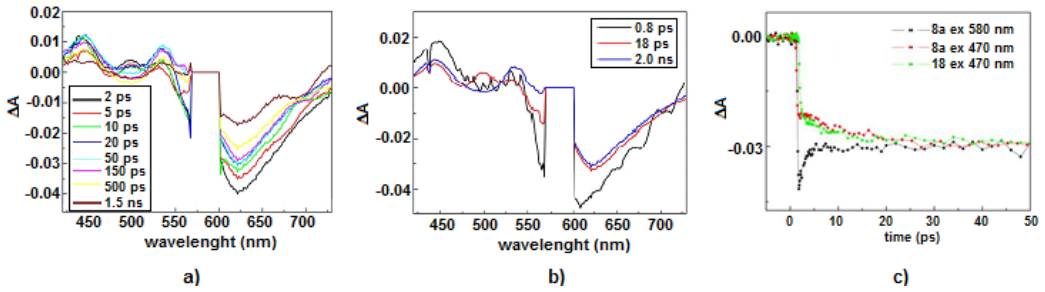

Figure 23. *a) Transient spectra recorded at selected time delay obtained by exciting compound **8a** with a 580 nm pulse in acetonitrile. b) EADS obtained by global analysis of the kinetic traces recorded by exciting compound **8a** at 580 nm; c) Comparison of the kinetic trace at 620 nm measured for compound **8a** excited at 580 (black line) and at 470 nm (red line); compound **18** excited at 470 nm (green line).*

A similar measurement has been repeated also in the other two examined solvents. While in chloroform we see analogies with what observed in acetonitrile, indicating a stronger excited state electronic coupling between donor and acceptor, the spectra registered in dimethyl sulfoxide upon 570 nm excitation are very similar to those measured for the isolated acceptor, indicating a weaker interaction between the chromophores linked to the calixarene scaffold. Based on these results, we suppose that, when exciting the bichromophore on the acceptor side, donor features could be present in the transient spectra, according to the occurrence of electron transfer. The hypothesis is confirmed considering the resulting spectrum obtained by the subtraction of the normalized second EADS component for compound **8a** and **18**, respectively excited at 560 and 570 nm. Comparing the result of this spectral difference with the EADS of the isolated compound **22** (excited at 470 nm), it is clear a strong similarity (Figure 24) in their shapes, thus confirming a strong excitonic coupling in the system. The occurrence of charge transfer from Nile red to NBD explains the presence of donor features in the transient spectra of the bi-chromophore when selectively excited on the acceptor side. Based on these considerations, the 0.8 ps component resulting from global analysis of **18** upon excitation at 570 nm has been considered indicative of

charge transfer from Nile red to NBD. The charge separated state successively relax, populating an excited state only localized on Nile red, which recovers to the ground state in *ca* 2 ns.

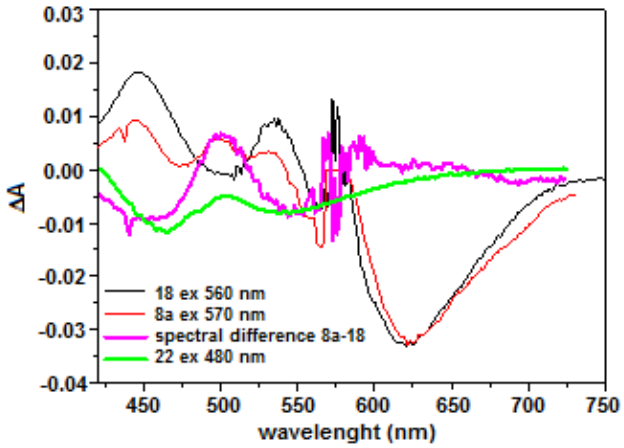

Figure 24. *Second EADS component obtained for compound **18** upon 560 nm excitation (black line), for **8a** upon 570 nm excitation (red line) and their difference (magenta line), for compound **22** upon 480 nm excitation (green line).*

- *Compounds **13a** and **13b***

The comparison between the kinetic traces measured at the maximum of the acceptor stimulated emission band in compounds **13a** and **13b** in the three solvents is reported in Figure 25. The two bichromophoric systems behave similarly to one another and quite independently of the solvent, with results similar to what observed for the bichromophoric compound **8a** in dimethyl sulfoxide. The kinetic parameters obtained for compound **8a**, **13a** and **13b** by global analysis are summarized in Table 3.

While system **8a** can assume configurations where the two chromophores are close one another and can thus strongly interact, this is not the case for compounds **13a** and **13b**, where the chromophores are quite far apart because linked to the two opposite sides of the calix scaffold. This is the reason why the transient behavior of **13a** and **13b** is independent of the solvent, while that of **8a**

is not. The behavior of **8a** becomes similar to **13a** and **13b** only in dimethyl sulfoxide just because this solvent is able to destroy the strong inter-chromophore interactions such as hydrogen-bonding and π-π stacking, as discussed earlier.

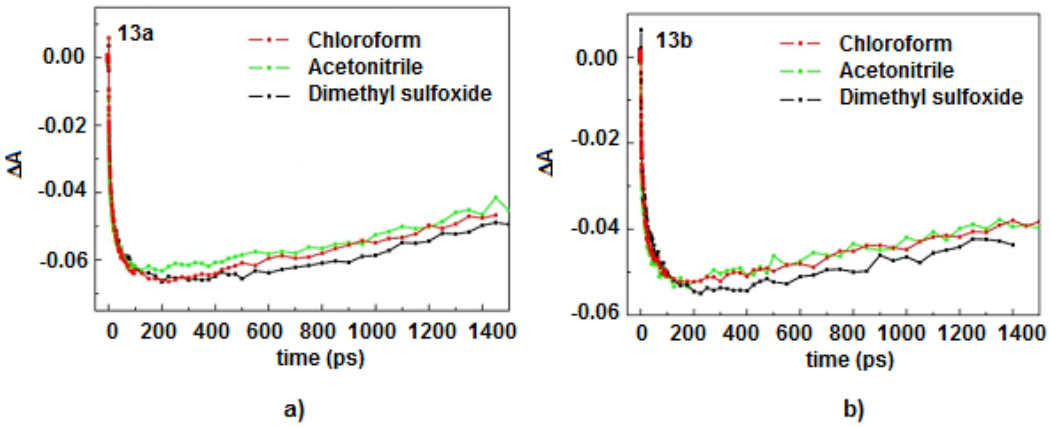

Figure 25. *Kinetic traces measured at the maximum of the acceptor stimulated emission band in the three solvents for a) compound **13a** and b) compound **13b**.*

A summary of all the kinetic parameters extracted from global analysis for **8a**, **13a** and **13b** is reported in Table 3.

Compound 8a	**t1**	**t2**	**t3**
Acetonitrile	0.6 ps	15 ps	2 ns
Chloroform	2.0 ps	17 ps	1.8 ns
Dimethyl sulfoxide	4.0 ps	59 ps	4.5 ns
Compound 13a	**t1**	**t2**	**t3**
Acetonitrile	1.5 ps	29 ps	4.5 ns
Chloroform	2.3 ps	27 ps	4.5 ns
Dimethyl sulfoxide	2.9 ps	57 ps	4.6 ns
Compound 13b	**t1**	**t2**	**t3**
Acetonitrile	1.4 ps	29 ps	4.2 ns
Chloroform	2.3 ps	35 ps	4.1 ns
Dimethyl sulfoxide	2.6 ps	52 ps	4.8 ns

Table 3. *Kinetic parameters extracted from global analysis for compounds **8, 13a** and **13b**.*

2.4.2 *Cone*- and *partial cone* Coumarin 343-NBD calix[4]arenes, 14a, 15a and 15b

Concerning the couple Coumarin 343-NBD, only static absorption and steady-state fluorescence measurements have been performed on compounds **14a**, **15a** and **15b** due to their lower stability and solubility, which, in some cases, affected the experiments.

Repeated absorption measurements revealed the degradation of Coumarin 343 (Figure 26) not only when irradiated with the light beam from the source lamp, but also when the samples were exposed to the light from a neon lamp or to sunlight. Coumarin 343 lost its spectroscopic properties becoming non-fluorescent.

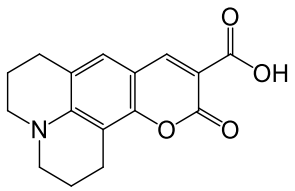

Figure 26. *Structure of commercial Coumarin 343.*

A sample of commercially available Coumarin 343 in $CDCl_3$ was prepared in the dark and analyzed by ^{1}H-NMR (Figure 27). After 3 h exposition to sunlight, the sample degradation was visible also to naked eye, because a pale yellow solid precipitated and the solution lost its brilliant color.

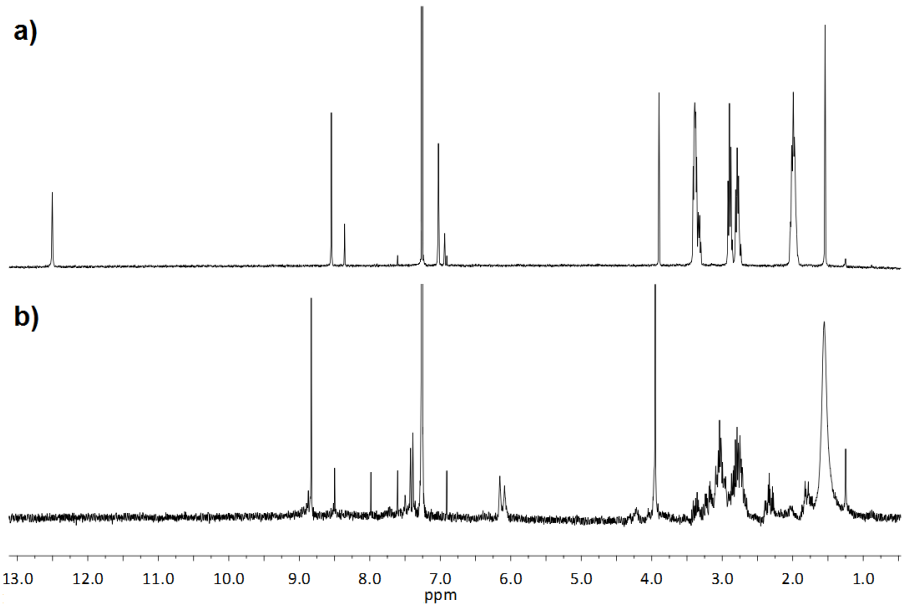

Figure 27. *^{1}H-NMR spectrum in $CDCl_3$ of commercial Coumarin 343 a) before sunlight exposure, b) after sunlight exposure.*

However, some interesting results concerning the spectroscopic behavior of Coumarin 343 and the couple Coumarin 343-NBD have been collected.

Commercially available Coumarin 343 absorption spectra were recorded at different sample concentration in chloroform and the experimental molar extinction coefficient was found to be 44700 ($\pm$ 1100) $M^{-1}cm^{-1}$, in agreement with literature data.[4]

Independently of the concentration of the solution, when the sample was exposed to sunlight, the absorption spectrum showed an absorbance decrease and a slight bathochromic effect, as well as a change in the shape (Figure 28).

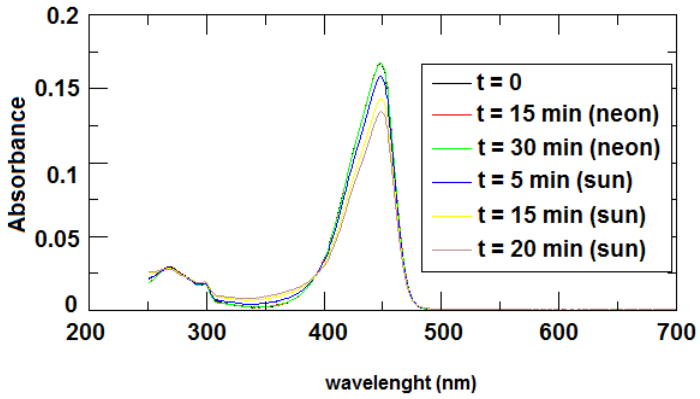

Figure 28. *Absorption spectra in chloroform of commercially available Coumarin 343 when exposed to artificial and solar light.*

On the contrary, Coumarin 343 was stable in standard laboratory working conditions (about 30 minutes and neon lamp irradiation).

On this basis, absorption measurements were performed in chloroform and in acetonitrile on compounds **19**, **14a**, **15a** and **15b**, and their behavior towards light exposure was carefully investigated.

- Compound 19: stability and absorption spectra

The molar extinction coefficient measured for **19** in chloroform and acetonitrile (Figure 29) is about 1/3 of the one measured for isolated Coumarin 343; moreover, measurements repeated on the same samples after evaporation of the solvent and subsequent redissolution of the solid showed that the molar extinction coefficient value decreased (Table 4).

Solvent	ε (M^{-1} cm^{-1})	λ_{abs}^{max} (nm)
Acetonitrile	18970 ± 120	434
Chloroform[a]	17510 ± 220	438
Chloroform[b]	15060	438

Table 4. *Molar extinction coefficient measured for **19** in acetonitrile and chloroform. [a] Analysis performed before light exposure, [b] repeated analysis after light exposure and sample recuperation.*

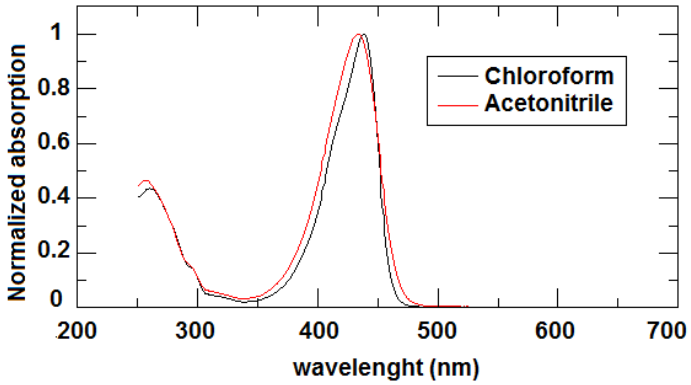

Figure 29. *Normalized absorption spectra of **19** in acetonitrile and chloroform.*

On the other hand, repeated experiments in standard working condition on the same sample showed its stability (Figure 30), indicating quantitative measurements can be performed on freshly prepared samples.

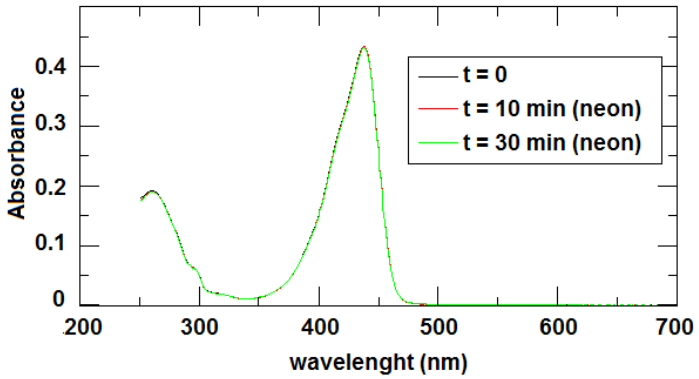

Figure 30. *Absorption spectra of **19** in chloroform.*

- Compound 14a: stability and absorption spectra

Also compound **14a**, when dissolved in chlorinated solvents and exposed to light for long times, was irreversibly damaged and its molar extinction coefficient decreased (Table 5).

Solvent	ε (M^{-1} cm^{-1})	λ_{abs}^{max} (nm)
Acetonitrile	37800±300	430
Chloroform [a]	40700±800	438
Chloroform [b]	28500±1100	438
Methylene chloride [b]	28000±1700	438

Table 5. *Experimental molar extinction coefficient measured for **14a** in different solvents. [a] analysis performed on a freshly prepared new sample, [b] analysis performed on the same sample as (a) after evaporation of the solvent and redissolution of the solid.*

Fortunately, degradation did not occur during the short time required for standard experiment execution. In these conditions, **14a** did not show a marked light sensitivity and repeated analysis at different times revealed only a slight decrease of the absorbance after 30 min, as shown in Figure 31.

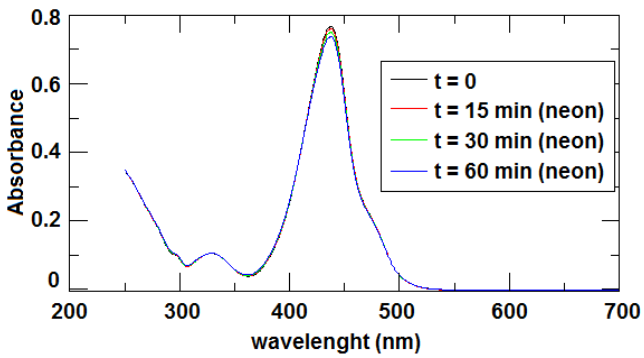

Figure 31. *Absorption spectra in chloroform of **14a** showing the light exposure degradation at different times.*

A comparison between absorption spectra collected in acetonitrile of compounds **14a**, **22** and **19** (Figure 32) revealed that neither the shape of the spectrum nor the molar extinction coefficient match with the spectrum obtained as the sum of the two monochromophoric calixarenes **22** and **19**.

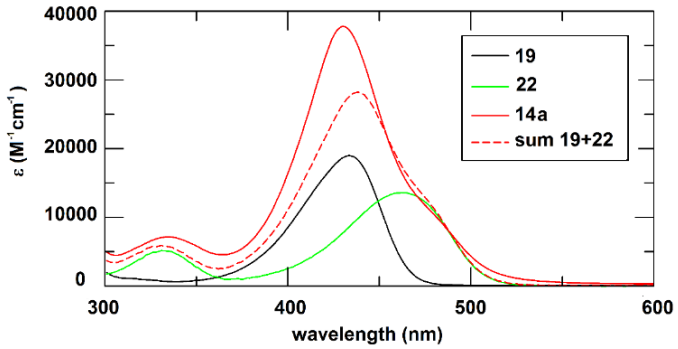

Figure 32. *Absorption spectra of bichromophoric **14a** in acetonitrile (red line) and comparison with reference compounds **19** (black line) and **22** (green line) and the sum spectrum (dashed line).*

The difference can probably be ascribed to the poor solubility of **19** in acetonitrile. It is interesting to note that the molar absorption coefficient measured for **14a** at 430 nm is more similar to the isolated Coumarin 343 in chloroform, than to the molar extinction coefficient of **19** either in chloroform or in acetonitrile.

On the contrary, absorption spectra in chloroform revealed a good match between the absorption spectrum of the bichromophoric system and the sum of the two references compounds **22** and **19** (Figure 33).

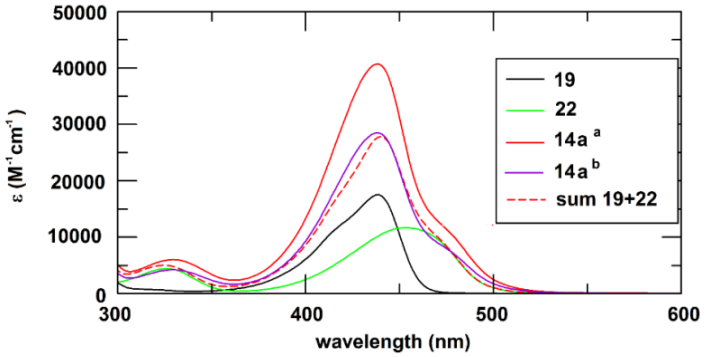

Figure 33. *Absorption spectra of bichromophoric **14a** in chloroform (red and violet lines) and comparison with reference compounds **19** (black line) and **22** (green line) and the sum spectrum (red dashed line).[a]before light exposure, [b]after light exposure, evaporation of the solvent and redissolution of the solid.*

It can be assumed that the higher stability of Coumarin 343 in bichromophoric **14a** compared to monochromophoric **19** observed in chloroform can be due to the occurrence of strong attractive intramolecular interactions between the chromophores which, as observed by ^{1}H NMR, force the calixarene to assume a *closed flattened cone* conformation. In this geometry, the proximity of the chromophores represents a sort of shield, which protects Coumarin 343 towards degradation.

Emission spectra of **14a** in chloroform, measured by exciting at different wavelengths (405, 438 and 460 nm), reveal the presence of two fluorescence bands corresponding to the donor and the acceptor emission, respectively (Figure 34). Due to the occurrence of energy transfer, the acceptor emission band is more intense than the one of the donor.

The fluorescence quantum yield is around 20-25% depending on the excitation wavelength (a dependence on the excitation wavelength is always expected whenever a non-quantitative excitation energy transfer process occurs).

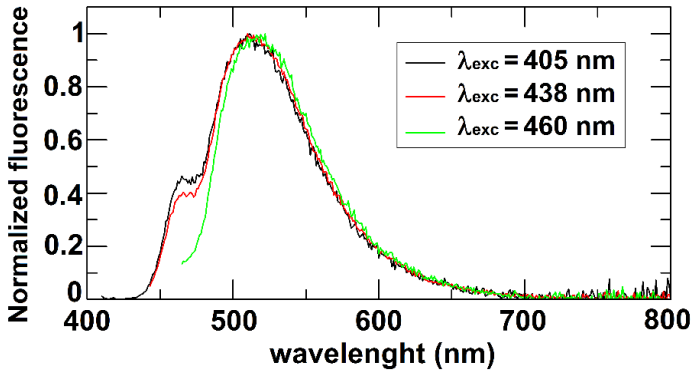

Figure 34. *Emission spectra in Chloroform of compound **14a** at different excitation wavelengths.*

- Energy transfer considerations

Efficient energy transfer is expected to occur from Coumarin 343 to NBD in compound **14a**, as demonstrated by the strong spectral overlap between the donor (reference compound **19**) fluorescence and the acceptor (reference compound **22**) absorption spectra (Figure 35, top).

The Förster radius amounts to ~ 41 Å in in chloroform. This value is slightly shorter than the Förster radius estimated for the couple of dyes in **8a** (NBD and Nile Red). This means that Coumarin 343 and NBD need to be closer to reach the same efficiency than the couple NBD-Nile red. However, as it was the case for compound **8a**, the distance between the chromophores in compound **14a** is for sure much shorter than 41 Å, so a very efficient EET process is expected.

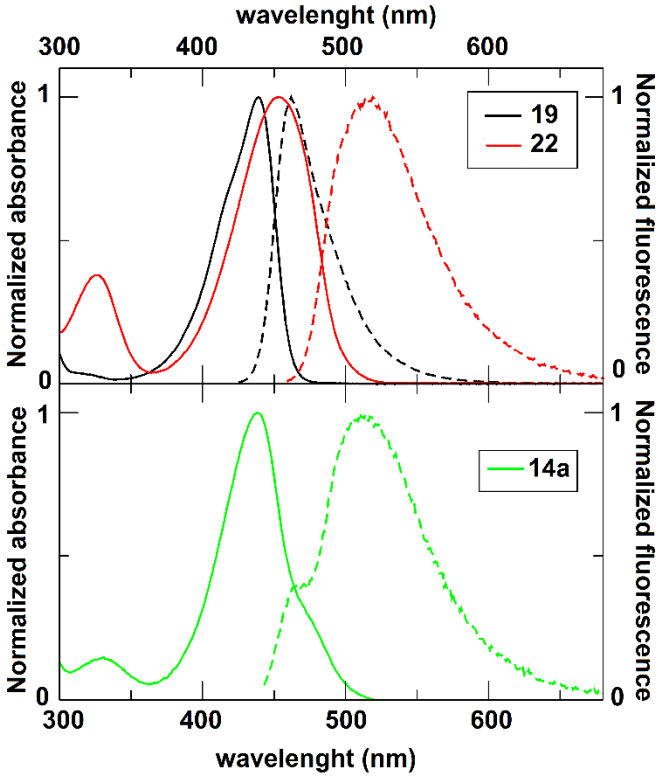

Figure 35. *Absorbance (continuous line) and emission spectra (dashed line) of reference compounds **19** and **22** (black and red line respectively, top), and **14a** (green line, bottom) in chloroform.*

To evaluate the rate of the energy transfer from Coumarin 343 to NBD in compound **14a**, excitation and absorption spectra in chloroform of the bichromophoric system are compared (Figure 36). The excitation spectrum has been recorded in the range 550-600 nm, where only acceptor fluorescence is present. The energy transfer efficiency is on the order of 90%, calculated on the ratio between the spectral intensities in the range 405-460 nm.

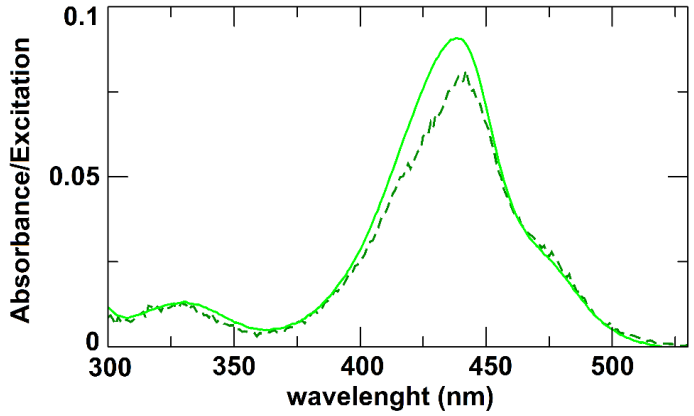

Figure 36. *Absorption (continuous line) and excitation spectra (dashed line) of **14a** in chloroform.*

- Compounds 15a and 15b: stability and absorption spectra

Compound **15a** was studied only in chloroform, because it was not soluble in acetonitrile. Analysis in this solvent revealed time-dependent changes in the absorption spectrum (Figure 37) also when the sample was irradiated with the neon lamp light. This behavior is qualitatively similar to what observed for the isolated Coumarin 343 in the sunlight.

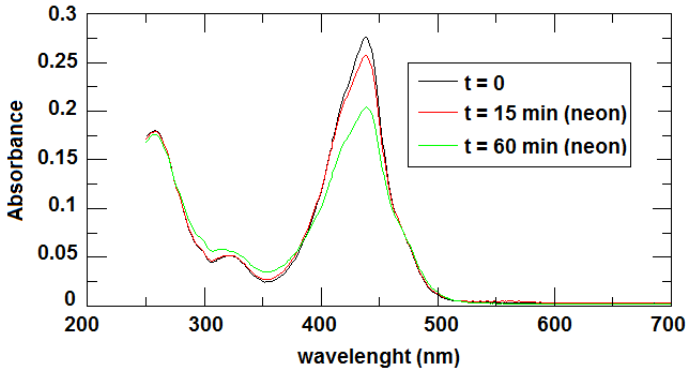

Figure 37. *Absorption spectra of **15a** in chloroform showing light exposure degradation at different times.*

Same conclusions can be drawn for **15b**, whose spectra were recorded only in chloroform due to its poor solubility in other solvents (Figure 38).

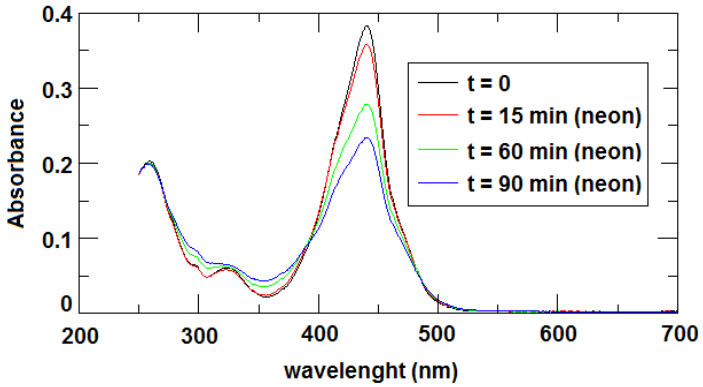

Figure 38. *Absorption spectra of **15b** in chloroform showing the light exposure degradation at different times.*

Energy transfer on compounds **15a** and **15b** has not been investigated, due to the strong light sensitivity of these compounds, which hinders the collection of reliable results.

2.5 Concluding remarks

In this chapter it is reported the synthesis and the spectroscopic characterization of six covalent dyads of two different chromophores. These systems have been obtained by functionalizing the *cone* and *partial cone* calix[4]arene scaffolds with the couples of dyes Coumarin 343-NBD and NBD-Nile red. The synthetic strategy adopted is based on a statistical approach, which consists of the reaction of the bis-acyl chloride of the calixarene with a mixture of the amine derivatives of the two chromophores.

Conformational studies by ^{1}H-NMR in solutions showed that the *cone* derivatives (**8a** and **14a**) display a "*closed*" *flattened cone* conformation in chloroform, due to the occurrence of strong attractive intramolecular interactions, such as hydrogen bonds and/or π-π interactions between the chromophores, and an "*open*" *flattened cone* conformation in solvents able to disrupt the intramolecular interactions such as acetone and dimethyl sulfoxide. The existence of strong attractive intramolecular forces was also confirmed by UV-vis spectroscopy studies.

Concerning the Coumarin 343-NBD bichromophoric compounds (**14a**, **15a** and **15b**), unexpected degradation of the Coumarin 343 dye within the dyad when exposed to both solar and artificial irradiation for long and repeated times, made the quantitative spectroscopic characterization impossible. Fluorescence measurements, however, revealed an efficient energy transfer occurring from Coumarin 343 to NBD, which was estimated to be about 90% for *cone* **14a**, while for *partial cones* **15a** and **15b** it was not estimated because of the light degradation of the compounds not allowing to obtain reliable results.

For NBD-Nile red compounds **8a**, **13a** and **13b**, energy transfer is quantitative quite independently of the solvent (chloroform, acetonitrile and dimethyl sulfoxide). For these compounds, the dynamics of energy transfer have been investigated with

transient absorption spectroscopy. Besides having high energy transfer yields, the classes of compounds presented in this study have interesting characteristics, which make them promising systems to be used in future applications. These NBD and Nile red functionalized systems are in fact highly flexible, due to the possibility of linking the dye molecules to both the rims of the calixarene scaffold, which allows a careful control of the inter-chromophore distances. As shown by all these results, the system performances can be further regulated by the appropriate choice of the external medium, which determines the particular conformation adopted in solution. As demonstrated, the choice of the solvent can highly influence the excitonic coupling between the donor and acceptor dyes, up to promote the stabilization of a charge transfer state where the electron density moves from the energy acceptor to the energy donor chromophore. Furthermore, the simple architecture of the systems presented in this study could be extended to more complicated structures, where an increased number of chromophores could be linked to the same scaffold. This would lead to build a library of easily tunable compounds with improved functionalities (more extended spectral range, possibility of electron transfer capabilities) to be used as starting material for organic photovoltaic devices.

2.6 Experimental Section

General methods

All moisture sensitive reactions were carried out under Nitrogen or Argon atmosphere, using previously oven-dried glassware. Dry solvents were prepared according to standard procedures, distilled before use and stored over 3 or 4 Å molecular sieves. Most of the solvents and reagents were obtained from commercial sources and used without further purification. Analytical TLC were performed using prepared plates of silica gel (Merck 60 F-254 on aluminium) and then, according to the functional groups present on the molecules, revealed with UV light. Merck silica gel 60 (70-230 mesh) was used for flash chromatography and for preparative TLC plates. ^{1}H NMR and ^{13}C spectra were recorded on Bruker AV300 and Bruker AV400 spectrometers (observation of ^{1}H nucleus at 300 MHz and 400 MHz respectively, and of ^{13}C nucleus at 75 MHz and 100 MHz respectively). All chemical shifts are reported in part per million (ppm) using the residual peak of the deuterated solvent, whose values are referred to tetramethylsilane (TMS, δ_{TMS}= 0), as internal standard. All ^{13}C NMR spectra were performed with proton decoupling. Mass spectra were recorded in ESI mode on a single quadrupole instrument SQ Detector, Waters (capillary voltage 3.7 kV, cone voltage 30-160 eV, extractor voltage 3 eV, source block temperature 80 °C, desolvation temperature 150 °C, cone and desolvation gas (N_2) flow rates 1.6 and 8 L/min, respectively). High resolution mass spectra were recorded on a LTQ Orbitrap XL instrument in positive mode using CH_3CN or CH_3OH as solvents. Melting points were determined on an Electrothermal apparatus in closed capillaries. UV-vis absorption spectra were recorded on a Perkin Elmer Lambda 650 spectrometer. Steady-state fluorescence spectra and fluorescence decays were carried out on a Fluoromax-3 Horiba Jobin Yvon spectrofluorometer. Fluorescence decays were measured in a TCSPC (time-correlated single-photon counting) configuration, under excitation from selected nanoLED or laser-diode sources; fluorescence lifetimes were obtained from the reconvolution fit analysis of the decay profiles; the quality of the fits was judged by the reduced χ^2 value (fits are retained for $\chi^2 < 1.1$).

5,17-Diformyl-25,26,27,28-tetrapoxycalix[4]arene **1**,[13] 5,17-dihydroxycarbonyl-25,26,27,28-tetrapropoxycalix[4]arene **6**,[12] 5,17-Diformyl-25,27-

dipropoxycalix[4]arene **9**,[12] 5-hydroxycarbonyl-25,26,27,28-tetrapropoxycalix[4]arene **16**,[16] **NR-OH**,[6,7] **NR-Br**,[10] **NR-N_3**[10] and **NBD-NH_2**[11] were synthesized according to literature procedures.

2-(2-Aminoethoxy)-9-diethylamino-5*H*-benzo[α]phenoxazin-5-one (NR-NH_2)

A mixture of **NR-N_3** (120 mg, 0.29 mmol) and PPh_3 (110 mg, 0.42 mmol) in anhydrous THF (8 mL) was stirred at rt for 1 h, then 5 drops of H_2O were added. The reaction was allowed to proceed for 22 hours at rt and then quenched by evaporation of the solvent at reduced pressure. Pure **NR-NH_2** was isolated by flash column chromatography (CH_2Cl_2/MeOH 90/10) in 80% yield (89 mg, 0.23 mmol). It showed the same spectroscopic data previously reported.[26]

N-Boc-EDA-Coum 343

To a stirring solution of Coumarin 343 (100 mg, 0.35 mmol) in dry CH_2Cl_2 (18 mL), $(COCl)_2$ (460 µL, 5.26 mmol) and dry DMF (10 µL), were slowly dripped and the color of the solution became immediately red. The reaction mixture was stirred for 3 h at rt, then it was concentrated under reduced pressure obtaining a red solid (**Coum-Cl**),[27] which was redissolved in dry CH_2Cl_2 (10 mL). To this solution, a solution of N-*tert*-butoxycarbamoilethylendiamine (191 mg, 1.23 mmol) and DIPEA (54 µL, 3.08 mmol) in dry CH_2Cl_2 (5 mL) was added dropwise. The resulting red mixture was stirred at rt for 48 h, then the reaction was monitored by TLC (CH_2Cl_2/CH_3OH 98/2) and quenched with H_2O (15 mL). The organic layer was washed with 1N NaOH (1x10 mL) and then with H_2O till neutral pH, dried over Na_2SO_4 and concentrated under reduced pressure obtaining a purple solid. Pure **N-Boc-EDA-Coum 343** was isolated as a yellow powder by flash column chromatography (CH_2Cl_2/CH_3OH 98/2) in 56% yield (84 mg, 0.19 mmol).

The product showed the same spectroscopic properties previously reported.[28]

Coum-NH_2

N-Boc-EDA-Coum 343 (84 mg, 0.19 mmol) was dissolved in a mixture of CH_2Cl_2/TFA/TES/H_2O (47.5/47.5/2.5/2.5, v:v, 5 mL), the reaction was allowed to proceed at rt and was monitored by TLC (CH_2Cl_2/CH_3OH 98/2). After 2 h the reaction mixture was concentrated under reduced pressure, the brown crude was dissolved

in CH_2Cl_2 and concentrated again (3 times), then it was redissolved in CH_2Cl_2 (15 mL) and washed with 5% aqueous $NaHCO_3$ (15 mL) and H_2O (15 mL). Pure **Coum-NH_2** was isolated as an orange powder in quantitative yield (60 mg, 0.19 mmol) by evaporating the solvent under vacuum.
The product showed the same spectroscopic properties previously reported.[28]

5-Hydroxymethylen-17-methoxycarbonyl-25,26,27,28-tetrapropoxycalix[4]arene (2)

A solution of $NaOCH_3$ (670 mg, 12.40 mmol) in CH_3OH (43 mL) was added to a solution of 5,17-diformyl-25,26,27,28-tetrapropoxycalix[4]arene **1** (400 mg, 0.62 mmol) in CH_3OH (18 mL). The reaction was refluxed for three days, cooled to room temperature and concentrated under reduced pressure. The crude mixture was dissolved in CH_2Cl_2 (40 mL) and the solution was washed with H_2O till neutral pH and dried over anhydrous Na_2SO_4. The solvent was evaporated under reduced pressure to obtain a yellow solid, which was purified by column chromatography (hexane/ethyl acetate 40/10) affording pure **2** in 43% yield (180 mg, 0.27 mmol). ^{1}H-NMR ($CDCl_3$, 300MHz): δ (ppm) 7.22 (s, 2H, ArH); 6.75-6.64 (m, 6H, ArH); 6.47 (s, 2H, ArH); 4.46 (d, J = 13.2 Hz, 2H, ArC*H*HAr); 4.44 (d, J = 13.2 Hz, 2H, ArC*H*HAr); 4.19 (s, 2H, ArCH_2OH); 3.97-3.78 (m, 11H, O$CH_2CH_2CH_3$ and OCH_3); 3.19 (d, J = 13.2 Hz, 2H, ArCH*H*Ar); 3.15 (d, J = 13.2 Hz, 2H, ArCH*H*Ar); 1.98-1.85 (m, 8H, CH_2); 1.05-0.95 (m, 12H, $OCH_2CH_2CH_3$). ^{13}C-NMR ($CDCl_3$, 75MHz): δ (ppm) 167.6; 160.8; 156.7; 155.9; 135.4; 135.2; 134.79; 134.75; 134.5; 129.6; 128.7; 128.4; 126.3; 123.3; 122.3; 76.9; 76.8; 76.7; 64.7; 51.8; 31.0; 23.3; 10.4. ESI-MS: m/z calcd for $C_{43}H_{52}O_7$+Na^+ 703.4, found 703.3 (100%); m/z calcd for $C_{43}H_{52}O_7$+K^+ 719.5, found 719.4 (33%).

Compound 3

To a stirred solution of **2** (147 mg, 0.22 mmol), PPh_3 (88 mg, 0.34 mmol) and **NR-OH** (73 mg, 0.22 mmol) in dry toluene (4.5 mL), a solution of 40% (v/v) DEAD (140 µL, 0.31 mmol) in toluene was added. The reaction was allowed to proceed at 70 °C for 3.5 h, then additional PPh_3 (28 mg, 0.11 mmol) and 40% DEAD (45 µL, 0.09 mmol) in toluene were added. The mixture was stirred at 70 °C for 3 h, when TLC monitoring (hexane/ethyl acetate 70/30) indicated the complete consumption of the starting materials. The solvent was removed under reduced pressure and the violet crude was first purified by flash column chromatography (hexane/ethyl acetate 70/30). The fractions containing the desired product were then further

purified by two subsequent preparative TLCs (first CH_2Cl_2/CH_3OH 94/6, then hexane/ethyl acetate 60/40), isolating pure **3** in 18% yield (44 mg, 0.04 mmol).

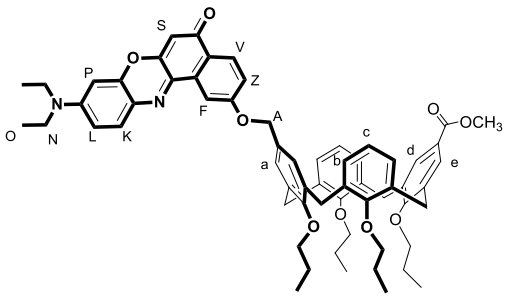

3

M.p.: 134-135 °C. ^{1}H-NMR ($CDCl_3$, 400MHz): δ (ppm) 8.20 (d, J = 8.4 Hz, 1H, H_V); 8.12 (s, 1H, H_F); 7.65 ppm (d, J = 8.8 Hz, 1H, H_K); 7.34 (s, 2H, H_e); 7.18 (d, J = 8,4 Hz, 1H, H_Z); 6.67-6.58 (m, 8H, H_a, H_b, H_c and H_d); 6.46 (bs, 1H, H_L); 6.30 (s, 1H, H_S); 4.76 (s, 2H, H_A); 4.46 (d, J = 13.4 Hz, 4H, ArC*H*HAr); 3.89-3.86 (m, 8H, OC*H*$_2$CH$_2$CH$_3$); 3.83 (s, 3H, OCH_3); 3.46 (q, J = 6.9 Hz, 4H, H_N); 3.20 (d, J = 13.4 Hz, 2H, ArCH*H*Ar); 3.18 (d, J = 13.4 Hz, 2H, ArCH*H*Ar); 1.91-1.93 (m, 8H, OCH_2C*H*$_2$CH$_3$); 1.26 (t, J = 7.3 Hz, 6H, H_O); 0.99 (t, J = 7.6 Hz, 12H, OCH_2CH_2C*H*$_3$). ^{13}C-NMR ($CDCl_3$, 100MHz): δ (ppm) 183.3; 167.2; 161.7; 160.9; 156.7; 156.5; 152.1; 150.7; 146.9; 140.1; 135.32; 135.29; 135.1; 134.5; 134.1; 131.1; 129.8; 129.5; 128.6; 128.4; 128.3; 127.7; 125.7; 124.8; 123.5; 122.3; 118.8; 109.5; 106.9; 105.3; 96,4; 77.2; 76.9; 70.5; 51.9; 45.1; 30.9; 23.2; 12.6; 10.4. HR-MS: m/z calcd for $C_{63}H_{68}N_2O_9$+H^+ 997.4985, found 997.5014 (100%).

Compound 8a

$(COCl)_2$ (550 µL, 6.31 mmol) and dry DMF (30 µL) were added to a solution of 5,17-dihydroxycarbonyl-25,26,27,28-tetrapropoxycalix[4]arene **6** (140 mg, 0.21 mmol) in dry CH_2Cl_2 (21 mL), and the mixture was stirred at rt for 21 h. After removing the solvent under reduced pressure, the acyl chloride thus obtained **7**, was dried for 5 h under vacuum (0.1-0.5 mm Hg). Without further purification, it was redissolved, in dry CH_2Cl_2 (10 mL) and added to a stirred solution of **NR-NH$_2$** (91 mg, 0.24 mmol), **NBD-NH$_2$** (58 mg, 0.24 mmol) and DIPEA (480 µL, 2.77 mmol) in dry CH_2Cl_2 (40 mL). The reaction was allowed to proceed for 3.5 h, then the mixture was washed twice with H_2O and evaporated to dryness under reduced pressure, obtaining a violet residue, from which pure **8a** was isolated as a purple solid in 35% yield (91 mg, 0.07 mmol) after flash column chromatography (CH_2Cl_2/Acetone 87/13).

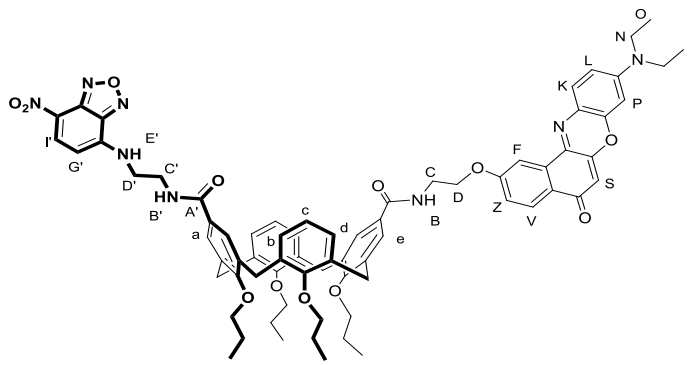

8a

M.p: 194-196°C. UV-vis: λ_{max} ($CHCl_3$): 469 nm (m), ε: 29520 $M^{-1}cm^{-1}$; 543 nm (s), ε: 37840 $M^{-1}cm^{-1}$. ^{1}H-NMR (Acetone-d_6, 300 MHz): δ (ppm) 8.69 (bs, 1H, $H_{E'}$); 8.47 (d, J = 8.8 Hz, 1H, $H_{I'}$); 8.08 (d, J = 8.7 Hz, 1H, H_V); 8.02 (d, J = 2.5 Hz, 1H, H_F); 7.69-7.82 (m, 2H, H_B and $H_{B'}$); 7.54 (d, J = 9.1 Hz, 1H, H_K); 7.41 (bs, 2H, H_a); 7.34 (bs, 2H, H_e); 7.24 (dd, J_1 = 8.8 Hz, J_2 = 2.6 Hz, 1H, H_Z); 6.79 (dd, J_1 = 9.3 Hz, J_2 = 2.8 Hz, 1H, H_L); 6.55 (d, J = 2.7 Hz, 1H, H_P); 6.48-6.34 (m, 7H, H_b, H_c, H_d and $H_{G'}$); 6.07 (s, 1H, H_S); 4.47 (d, J = 13.2 Hz, 4H, ArC*H*HAr); 4.37 (t, J = 5.4 Hz, 2H, H_D); 3.97 (t, J = 7.4 Hz, 4H, OC*H*$_2$$CH_2CH_3$); 3.83-3.77 (m, 10H, OC*H*$_2$$CH_2CH_3$, H_C, $H_{D'}$ and $H_{C'}$); 3.57 (q, J = 6.9 Hz, 4H, H_N); 3.18 (d, J = 13.2 Hz, 2H, ArCH*H*Ar); 3.19 (d, J = 13.2 Hz, 2H, ArCH*H*Ar); 1.98-1.91 (m, 8H, OCH_2C*H*$_2$$CH_3$); 1.29-1.24 (m, 6H, H_O); 1.07-0.96 (m, 12H, OCH_2CH_2C*H*$_3$). ^{1}H-NMR ($CDCl_3$, 300 MHz): δ (ppm) 8.49 (bs, 1H, $H_{E'}$); 8.46 (s, 1H, $H_{I'}$); 8.25 (d, J = 8.7 Hz, 1H, H_V); 8.02 (d, J = 2.5 Hz, 1H, H_F); 7.53 (d, J = 9.1 Hz, 1H, H_K); 7.17 (dd, J_1 = 8.7 Hz, J_2 = 2.6 Hz, 1H, H_Z); 6.94-6.45 (m, 4H, H_b and H_d); 6.71 (s, 2H, H_a); 6.66-6.62 (m, 3H, H_c and H_L) 6.59 (s, 2H, H_e); 6.44 (d, J = 2.6 Hz, 1H, H_P); 6.31 (s, 1H, H_S); 6.15-6.09 (m, 2H, H_B and $H_{G'}$); 5.97 (bs, 1H, $H_{B'}$); 4.44 (d, J = 13.2 Hz, 4H, ArC*H*HAr); 4.41 (d, J = 13.2 Hz, 4H, ArC*H*HAr); 4.27 (t, J = 5.6 Hz, 2H, H_D); 3.99-3.94 (m, 4H, OC*H*$_2$$CH_2CH_3$); 3.73-3.65 (m, 10H, OC*H*$_2$$CH_2CH_3$, H_C, $H_{D'}$ and $H_{C'}$); 3.47 (q, J = 7.0 Hz, 4H, H_N); 3.17 (d, J = 13.2 Hz, 2H, ArCH*H*Ar); 3.13 (d, J = 13.2 Hz, 2H, ArCH*H*Ar); 1.97-1.91 (m, 8H, OCH_2C*H*$_2$$CH_3$); 1.29-1.25 (m, 6H, H_O); 1.09-1.02 (m, 6H, OCH_2CH_2C*H*$_3$); 0.92-0.87 (m, 6H, OCH_2CH_2C*H*$_3$). ^{1}H-NMR (CD_3CN, 300 MHz): δ (ppm) 8.30 (d, J = 8.8 Hz, 1H, $H_{I'}$); 8.19 (bs, 1H, $H_{E'}$); 8.03 (d, J = 8.8 Hz, 1H, H_V); 7.91 (d, J = 2.6 Hz, 1H, H_F); 7.45 (d, J = 9.1 Hz, 1H, H_K); 7.16 (dd, J_1 = 8.8 Hz, J_2 = 2.9 Hz, 1H, H_Z); 6.97 (s, 2H, H_a); 6.93 (s, 2H, H_e); 6.85-6.77 (m, 6H, H_B, $H_{B'}$, H_b and H_d); 6.72 (dd, J_1 = 9.0 Hz, J_2 = 2.7 Hz, 1H, H_L); 6.57 (t, J = 7.4 Hz, 2H, H_c); 6.46 (d, J = 2.7 Hz, 1H, H_P); 6.09 (d, J =8.8 Hz, 1H, $H_{G'}$); 6.06 (s, 1H, H_S); 5.97 (bs, 1H, $H_{B'}$); 4.43 (d, J = 13.2 Hz, 4H, ArC*H*HAr); 4.28 (t, J = 5.6 Hz, 2H, H_D); 3.89 (t, J = 7.6 Hz, 4H, OC*H*$_2$$CH_2CH_3$); 3.81 (t, J = 7.1 Hz, 2H, OC*H*$_2$$CH_2CH_3$);

3.79 (t, J = 7.1 Hz, 2H, OC*H*$_2$CH$_2$CH$_3$); 3.69-3.64 (m, 2H, HC); 3.52-3.45 (m, 8H, $H_{D'}$, $H_{C'}$ and H_N); 3.19 (d, J = 13.2 Hz, 2H, ArCH*H*Ar); 3.18 (d, J = 13.2 Hz, 2H, ArCH*H*Ar); 1.95-1.86 (m, 8H, OCH$_2$C*H*$_2$CH$_3$); 1.22 (t, J = 7.1 Hz, 6H, H_O); 1.05-0.92 (m, 12H, OCH$_2$CH$_2$C*H*$_3$). ^{13}C-NMR (Acetone-d$_6$, 100 MHz): δ (ppm) 182.9; 169.3; 169.2; 162.6; 160.9; 160.8; 157.0; 153.1; 152.2; 147.9; 146.2; 145.8; 145.4; 140.3; 136.5; 134.6; 131.9; 129.1; 129.0; 124.9; 128.6; 128.5; 128.4; 123.0; 105.5; 118.7; 110.7; 108.1; 105.5; 97.1; 77.73; 77.68; 69.3; 45.7; 40.5; 39.5; 32.7; 31.6; 24.13; 24.09; 12.9; 10.9; 10.6. HR-MS: m/z calcd for $C_{72}H_{76}N_8O_{12}$+H^+ 1245.5642, found 1245.5654 (100%); m/z calcd for $C_{72}H_{76}N_8O_{12}$+Na^+ 1267.5462, found 1267.5466 (8%).

A little amount of homo-bichromphoric products was also isolated by chromatography for a partial characterization.

Compound 8b

^{1}H-NMR (Acetone-d$_6$, 400 MHz): δ (ppm) 8.75 (bs, 2H, $H_{B'}$); 8.48 (d, J = 8.8 Hz, 2H, $H_{I'}$); 7.99 (bs, 2H, $H_{E'}$); 7.40 (s, 4H, H_a); 6.52 (d, J = 8.8 Hz, 2H, $H_{G'}$); 6.39 (d, J = 7.2 Hz, 4H, H_b); 6.28 (t, J = 7.4 Hz, 2H, H_c); 4.46 (d, J = 13.3 Hz, 4H, ArC*H*HAr); 3.97 (t, J = 7.5 Hz, 4H, OC*H*$_2$CH$_2$CH$_3$); 3.81-3.77 (m, 12H, OC*H*$_2$CH$_2$CH$_3$, $H_{C'}$ and $H_{D'}$); 3.19 (d, 4H, J = 13.3 Hz, ArCH*H*Ar); 1.97-1.92 (m, 8H, OCH$_2$C*H*$_2$CH$_3$); 1.04 (t, J = 7.4 Hz, 6H, OCH$_2$CH$_2$C*H*$_3$); 0.98 (t, J = 7.5 Hz, 6H, OCH$_2$CH$_2$C*H*$_3$). ^{13}C-NMR (Acetone-d$_6$, 75 MHz): δ (ppm) 183.3; 168.3; 161.4; 159.9; 156.4; 152.2; 150.9; 147.0; 139.8; 135.8; 134.5; 134.2; 131.3; 128.6; 128.3; 127.9; 127.8; 127.3; 126.0; 124.9; 122.7; 118.3; 109.8; 106.9; 105.4; 96.3;77.1; 76.9; 67.4; 45.3; 39.6; 31.13; 23.4; 12.8; 10.49; 10.45. ESI-MS: m/z calcd for $C_{58}H_{62}N_{10}O_{12}$+Na^+ 1113.4, found 1113.9 (100%).

Compound 8c

^{1}H-NMR ($CDCl_3$, 300 MHz): δ (ppm) 8.19 (d, J = 8.73 Hz, 2H, H_V); 8.02 (d, J = 3.0 Hz, 2H, H_F); 7.54 (d, J = 9.1 Hz, 2H, H_K); 7.16 (dd, J_1 = 8.8 Hz, J_2 = 2.5 Hz, 2H, H_Z); 7.14 (s, 4H, H_a); 6.62 (d, J = 2.5 Hz, 2H, H_L); 6.59-6.47 (m, 8H, H_b, H_c and H_B); 6.40 (d, J = 2.5 Hz, 2H, H_P); 6.25 (s, 2H, H_S); 4.42 (d, J = 13.4 Hz, 4H, ArC*H*HAr); 4.29 (t, J = 4.3 Hz, 4H, H_D); 3.87-3.79 (m, 12H, OC*H*$_2$CH$_2$CH$_3$, H_C); 3.44 (q, J = 7.1 Hz, 8H, H_N); 3.17 (d, J = 13.4 Hz, 4H, ArCH*H*Ar); 1.94-1.84 (m, 8H, OCH$_2$C*H*$_2$CH$_3$); 1.27-1.22 (m, 12H, H_O); 0.99-0.93 (m, 12H, OCH$_2$CH$_2$C*H*$_3$). ^{13}C-NMR ($CDCl_3$, 75 MHz): δ (ppm) 178.9; 160.8; 157.0; 146.2; 145.5; 145.2; 137.9; 136.5; 134.9; 129.1; 128.9; 128.6; 99.9; 77.72; 77.66; 45.4; 39.2; 31.6; 24.1; 10.9; 10.6. ESI-MS: m/z calcd for $C_{86}H_{90}N_6O_{12}$+Na^+

1421.7, found 1423.3 (27%); m/z calcd for $C_{86}H_{90}N_6O_{12}$+2Na^+ 722.3, found 722.7 (100%).

Partial cone 5,17-diformyl-25,26,27,28-tetrapropoxycalix[4]arene (10a)

To a solution of 5,17-diformyl-25,27-dipropoxycalix[4]arene **9** (1.5 g, 2.66 mmol) and K_2CO_3 (10.29 g, 74.45 mmol,) in CH_3CN (100 mL), $CH_3CH_2CH_2I$ (7.8 mL, 79.98 mmol,) was added and the mixture was refluxed for 3 h. The reaction was monitored by TLC (hexane/ethyl acetate 7/3). After removing the solvent in vacuo, the crude was dissolved in CH_2Cl_2 (50 mL), then washed with HCl 10% (50 mL), H_2O (2x50 mL), 0.5 M $Na_2S_2O_3$ (1x50 mL), and H_2O till neutral pH, and dried over anhydrous Na_2SO_4. The product was isolated by column chromatography (CH_2Cl_2) in 13% yield (231 mg, 0.22 mmol), separating it from the 1,3-alternate isomer (22%, 423 mg, 0.37 mmol). Mp: 104-106 °C. ^{1}H NMR (300 MHz, $CDCl_3$): δ (ppm) 9.97 (s, 1H, CHO); 9.94 (s, 1H, CHO); 7.80 (s, 2H, ArH*); 7.65 (s, 2H, ArH); 6.94 (dd, J_1 = 7.5 Hz, J_2 = 1.5 Hz, 2H, ArH); 6.45 (t, J = 7.5 Hz, 2H, ArH); 6.24 (d, J = 7.5 Hz, 2H, ArH); 4.1 (d, J = 13.5 Hz, 2H, ArC*H*HAr); 3.87-3.60 (m, 8H, OC*H*$_2$$CH_2CH_3$ and ArC*H*$_2$Ar*); 3.58-3.55 (m, 2H, OC*H*$_2$$CH_2CH_3$); 3.35-3.29 (m, 2H, OC*H*$_2$$CH_2CH_3$*); 3.17 (d, J = 13.5 Hz, 2H, ArCH*H*Ar); 2.00-1.87 (m, 6H, OCH_2C*H*$_2$$CH_3$); 1.34-1.25 (m, 2H, OCH_2C*H*$_2$$CH_3$*); 1.28-1.06 (m, 9H, OCH_2CH_2C*H*$_3$); 0.63 (t, J = 7.8 Hz, 3H, OCH_2CH_2C*H*$_3$*). ^{13}C NMR (75 MHz, $CDCl_3$): δ (ppm) 191.9; 191.7; 163.3; 162.9; 155.5; 134.9; 132.5; 131.4; 131.1; 130.8; 129.5; 128.7; 121.9; 76.3; 75.9; 75.2; 35.6; 30.4; 24.1; 23.8; 22.3; 10.9; 10.6; 9.3. ESI-MS: m/z calcd for $C_{42}H_{48}O_6$+Na^+ 671.3, found 671.1 (100%).

*referred to the inverted aromatic ring

Partial cone 5,17-dihydroxycarbonyl-25,26,27,28-tetrapropoxycalix[4]arene (11)

A freshly prepared aqueous solution of H_2NSO_3H (140 mg, 1.44 mmol) and $NaClO_2$ (112 mg, 1.24 mmol) was rapidly added to a solution of **5** (230 mg, 0.35 mmol) in $CHCl_3$/Acetone (1:1, v/v, 50 mL) cooled in an ice bath. After ten minutes the cooling bath was removed and the reaction was stirred at rt for 16 h and monitored by TLC (hexane/ethyl acetate 70/30). The organic solvents were removed under reduced pressure and the reaction was quenched by addition of 1N HCl (50 mL). The precipitate was collected on a Buchner and washed with cold H_2O to obtain

compound **11** as a white solid in 99% yield (240 mg, 0.347 mmol). M.p.: 200 °C dec. ^{1}H NMR (300 MHz, $CDCl_3$): δ (ppm) 8.05 (s, 2H, ArH*); 7.87 (s, 2H, ArH); 6.93 (d, J = 7.5 Hz, 2H, ArH); 6.45 (t, J = 7.5 Hz, 2H, ArH); 6.28 (d, J = 7.2 Hz, 2H, ArH); 4.07 (d, J = 13.2, 2H, ArC*H*HAr); 3.82-3.53 (m, 10H, OC*H*$_2$CH$_2$CH$_3$ and ArC*H*$_2$Ar*); 3.34 (t, J = 6.9 Hz, 2H, OC*H*$_2$CH$_2$CH$_3$*); 3.14 (d, J = 13.2 Hz, 2H, ArCH*H*Ar); 1.97-1.89 (m, 6H, OCH$_2$C*H*$_2$CH$_3$); 1.13-1.05 (m, 8H, OCH$_2$C*H*$_2$CH$_3$*, OCH$_2$CH$_2$C*H*$_3$); 0.87-0.84 (m, 3H, OCH$_2$CH$_2$C*H*$_3$); 0.66 (t, J = 8.1 Hz, 3H, OCH$_2$CH$_2$C*H*$_3$*). ^{13}C NMR (75 MHz, $CDCl_3$/CD_3OD 95/5 v/v): δ (ppm) 169.7; 169.4; 162.1; 161.8; 155.5; 137.1; 134.0; 132.9; 132.8; 131.6; 130.9; 129.4; 128.7; 123.7; 123.0; 121.7; 76.3; 75.8; 74.9; 35.7; 30.3; 24.1; 23.7, 22.1; 10.8, 10.5; 9.0. HR-MS: m/z calcd for $C_{42}H_{47}O_8$-H^- 679.3258, found 679.3271 (100%).

*referred to the inverted aromatic ring

Compounds 13a and 13b

$(COCl)_2$ (920 µL, 10.55 mmol) and dry DMF (30 µL) were added to a solution of **11** (240 mg, 0.35 mmol) in dry CH_2Cl_2 (36 mL), and the mixture was stirred for 5 h. The solvent was evaporated, the resulting solid **12** was dried for 5 h at reduced pressure (0.1-0.5 mm Hg), dissolved in dry CH_2Cl_2 (30 mL) and added to a stirred solution of **NBD-NH$_2$** (90 mg, 0.34mmol), **NR-NH$_2$** (130 mg, 0.34 mmol,) and DIPEA (790 µL, 4.58 mmol,) in dry CH_2Cl_2 (26 mL). The reaction was allowed to proceed for 24 h, then the mixture was washed with H_2O (2x50 mL) and the solvent was removed in vacuo. The violet crude was first purified by flash column chromatography (gradient CH_2Cl_2/Acetone 90/10 - CH_2Cl_2/Acetone 85/15) obtaining two fractions, each of which contained one of the two conformers. Pure products **13a** and **13b** were isolated as purple powders by preparative TLCs (**13a**: CH_2Cl_2/Acetone/Hexane 9/1.5/1.5; **13b**: CH_2Cl_2/Acetone/TEA 9/0.5/1.5) in 0.2% (1 mg, 0.80 µmol) and 0.7% (3 mg, 2.41 µmol) yield, respectively.

13a

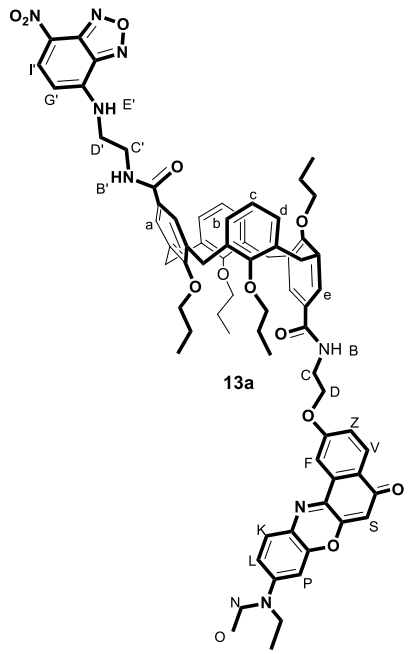

M.p.: 170 °C dec. λ_{max} ($CHCl_3$): 465 nm (s), 540 nm (s). ^{1}H NMR (400 MHz, $CDCl_3$): δ (ppm) 8.46 (d, J = 8.4 Hz, 1H, $H_{I'}$); 8.24 (d, J = 8.8 Hz, 1H, H_V); 8.15 (bs, 1H, $H_{E'}$); 8.11 (d, J = 2.8 Hz, 1H, H_F); 7.74 (s, 2H, H_e); 7.60 (s, 2H, H_a); 7.58 (s, 1H, H_K); 7.20 (dd, J_1 = 8.8 Hz, J_2 = 2.4 Hz, 1H, H_Z); 7.01 (t, J = 6 Hz, 1H, $H_{B'}$); 6.91 (d, J = 6.8 Hz, 2H, H_d); 6.70-6.67 (m, 2H, H_B, H_L); 6.46 (d, J = 2.4 Hz, 1H, H_P); 6.40 (t, J = 7.6 Hz, 2H, H_c); 6.31 (s, 1H, H_S); 6.23-6.19 (m, 3H, $H_{G'}$, H_b); 4.40 (t, J = 4.8 Hz, 2H, H_D); 4.08-3.93 (m, 6H, ArC*H*HAr, H_C, $H_{C'}$); 3.79-3.62 (m, 10H, OC*H*$_2$CH$_2$CH$_3$, $H_{D'}$ and ArC*H*$_2$Ar*); 3.56-3.45 (m, 6H, H_N, OC*H*$_2$CH$_2$CH$_3$); 3.26 (t, J = 8.4 Hz, 2H, OC*H*$_2$CH$_2$CH$_3$*); 3.16-3.06 (m, 2H, ArCH*H*Ar); 1.97-1.83 (m, 6H, OCH$_2$C*H*$_2$CH$_3$); 1.29-1.25 (m, 8H, H_o, OCH$_2$C*H*$_2$CH$_3$*); 1.07-0.99 (m, 9H, OCH$_2$CH$_2$C*H*$_3$); 0.61 (t, J = 7.6 Hz, 3H, OCH$_2$CH$_2$C*H*$_3$*). ^{13}C NMR (100 MHz, $CDCl_3$): δ (ppm) 183.4; 170.2; 167.3; 161.3; 160.8; 160.7; 155.5; 152.2; 150.9; 144.5; 144.4; 144.3; 143.9; 137.5; 136.4; 131.6; 129.5; 129.47; 128.6; 128.0; 127.9; 126.9; 126.8; 126.0; 124.8; 121.7; 118.1; 109.7; 106.6; 105.2; 98.1; 96.3; 76.3; 75.7; 74.9; 67.7; 46.1; 45.1; 39.0; 35.8; 30.5; 23.8; 12.6; 10.9; 8.6. HR-MS: m/z calcd for $C_{72}H_{76}N_8O_{12}$+H^+ 1245.5642, found 1245.5649 (100%); m/z calcd for $C_{72}H_{76}N_8O_{12}$+Na^+ 1267.5462, found 1267.5468 (40%).

*referred to the inverted aromatic ring.

13b

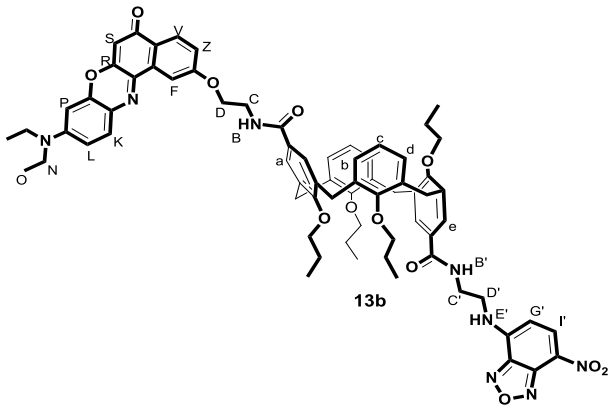

M.p.: 200 °C dec. λ_{max} ($CHCl_3$): 465 nm (s), ε: 24100 $M^{-1}cm^{-1}$; 538 nm (s), ε: 34380 $M^{-1}cm^{-1}$. ^{1}H NMR (400 MHz, $CDCl_3$): δ (ppm) 8.46 (d, J = 8.8 Hz, 1H, $H_{I'}$); 8.35 (bs, 1H, $H_{E'}$); 8.21 (d, J = 8.4 Hz, 1H, H_V); 8.09 (d, J = 2.4 Hz, 1H, H_F); 7.76 (s, 2H, H_e); 7.59 (d, J = 6.9 Hz, 1H, H_K); 7.56 (s, 2H, H_a); 7.19 (dd, J_1 = 2.4 Hz, J_2 = 8.4 Hz, 1H, H_Z); 6.90 (d, J = 6 Hz, 2H, H_d); 6.76 (t, J = 6.4 Hz, 1H, $H_{B'}$); 6.67-6.64 (m, 2H, H_L, H_B); 6.45 (d, J = 2.8 Hz, 1H, H_P); 6.41 (t, J = 7.6 Hz, 2H, H_c); 6.28 (s, 1H, H_S); 6.25 (d, J = 6.8 Hz, 2H, H_b); 6.15 (d, J = 8.4 Hz, 1H, $H_{G'}$); 4.41 (t, J = 4.9 Hz, 2H, H_D); 4.01-3.93 (m, 6H, ArC*H*HAr, H_C and $H_{C'}$); 3.79-3.62 (m, 10H, OC*H*$_2$CH$_2$CH$_3$, $H_{D'}$ and ArC*H*$_2$Ar*); 3.54-3.44 (m, 6H, H_N, OC*H*$_2$CH$_2$CH$_3$); 3.22 (t, J = 8.4 Hz, 2H, OC*H*$_2$CH$_2$CH$_3$*); 3.09 (d, J = 13.2 Hz, 2H, ArCH*H*Ar); 1.93-1.86 (m, 6H, OCH$_2$C*H*$_2$CH$_3$); 1.30-1.25 (m, 8H, OCH$_2$C*H*$_2$CH$_3$* and H_O); 1.11-1.03 (m, 9H, OCH$_2$CH$_2$C*H*$_3$); 0.46 (t, J = 7.2 Hz, 3H, OCH$_2$CH$_2$C*H*$_3$*). ^{13}C NMR (100 MHz, $CDCl_3$): δ (ppm) 183.2; 169.8; 167.8; 161.5; 161.4; 160.1; 155.4; 152.1; 146.9; 144.4; 144.3; 144.0; 143.9; 139.7; 136.4; 134.6; 131.2; 129.6; 129.4; 128.9; 128.1; 127.9; 126.0; 125.5; 121.8; 118.3; 109.7; 106.6; 105.2; 98.1; 96.3; 76.2; 75.4; 75.0; 67.3; 39.2; 30.5; 29.7; 23.9; 12.6; 10.9; 9.1. HR-MS: m/z calcd for $C_{72}H_{76}N_8O_{12}$+H^+ 1245.5642, found 1245.5652 (100%); m/z calcd for $C_{72}H_{76}N_8O_{12}$+Na^+ 1267.5462, found 1267.5471 (42%).
*referred to the inverted aromatic ring

A little amount of homo-bichromphoric products was also isolated by chromatography for a partial characterization:

Compound 13c

^{1}H-NMR ($CDCl_3$, 300 MHz): δ (ppm) 8.49 (d, J = 9.7 Hz, 2H, $H_{I'}$); 8.15 (bs, 2H, $H_{B'}$); 8.04 (s, 4H, H_a); 7.59 (s, 1H, H_e); 6.92 (d, J = 6.2 Hz, 2H, H_d); 6.78 (bs, 2H, $H_{E'}$); 6.42

(t, J = 7.5 Hz, 2H, H_c); 6.26-6.20 (m, 42H, H_b and $H_{G'}$); 4.07 (d, J = 13.3 Hz, 2H, ArC*H*HAr); 3.96-3.91 (m, 2H, $H_{C'}$); 3.84-3.49 (m, 10H, OC*H*$_2$CH$_2$CH$_3$, $H_{C'}$ and ArCH*H*Ar); 3.28 (t, J = 6.5 Hz, 2H, OC*H*$_2$CH$_2$CH$_3$*); 3.13-3.04 (m, 6H, ArCH*H*Ar and H_D); 1.98-1.89 (m, 6H, OCH$_2$C*H*$_2$CH$_3$); 1.13-1.03 (m, 8H, OCH$_2$C*H*$_2$CH$_3$* and OCH$_2$CH$_2$C*H*$_3$); 0.87 (t, J = 6.9 Hz, 3H, OCH$_2$CH$_2$C*H*$_3$); 0.65 (t, J = 7.5 Hz, 6H, OCH$_2$CH$_2$C*H*$_3$*). ESI-MS: m/z calcd for $C_{58}H_{62}N_{10}O_{12}$+Na^+ 1113.4, found 1113.6 (12%); m/z calcd for $C_{58}H_{62}N_{10}O_{12}$+K^+ 1129.6, found 1129.6 (65%).

Compound 13d

^{1}H-NMR ($CDCl_3$, 400 MHz): δ (ppm) 8.24 (d, J = 8.4 Hz, 1H, H_V); 8.19 (d, J = 8.0 Hz, 1H, H_V); 8.13 (d, J = 2.4 Hz, 1H, H_F); 8.12 (d, J = 2.4 Hz, 1H, H_F); 7.75 (s, 2H, H_e); 7.61 (d, J = 9.6 Hz, 1H, H_K); 7.59 (d, J = 8.8 Hz, 1H, H_K); 7.54 (s, 2H, H_a); 7.22 (dd, J_1 = 2.4 Hz, J_2 = 8.4 Hz, 2H, H_Z); 6.91 (d, J = 6.8 Hz, 2H, H_d); 6.67 (d, J = 9.2 Hz, 2H, H_L); 6.02 (bs, 2H, H_B); 6.46 (s, 2H, H_P); 6.41 (t, J = 7.6 Hz, 2H, H_c); 6.31 (s, 1H, H_S); 6.29 (s, 1H, H_S); 6.24 (d, J = 7.6 Hz, 2H, H_b); 4.42-4.41 (m, 4H, H_D); 4.04 (d, J = 13.4 Hz, 2H, Ar*CH*HAr); 4.00-3.98 (m, 4H, H_C); 3.79-3.62 (m, 10H, OC*H*$_2$CH$_2$CH$_3$ and ArC*H*$_2$Ar*); 3.47 (q, J = 7.2 Hz, 8H, H_N); 3.28 (t, J = 7.6 Hz, OC*H*$_2$CH$_2$CH$_3$*); 3.09 (d, J = 13.4 Hz, 2H, ArCH*H*Ar); 1.94-1.86 (m, 6H, OCH$_2$C*H*$_2$CH$_3$); 1.37-1.26 (m, 12H, H_O and OCH$_2$C*H*$_2$CH$_3$*); 1.07-1.02 (m, 9H, OCH$_2$CH$_2$C*H*$_3$); 0.63 (t, J = 7.4 Hz, 3H, OCH$_2$CH$_2$C*H*$_3$*). ESI-MS: m/z calcd for $C_{86}H_{90}N_6O_{12}$+Na^+ 1421.7, found 1422.2 (100%); m/z calcd for $C_{86}H_{90}N_6O_{12}$+K^+ 1437.8, found 1438.2 (20%).

Compound 14a

$(COCl)_2$ (450 µL, 5.11 mmol) and dry DMF (20 µL) were added to a solution of **6** (120 mg, 0.17 mmol) in dry CH_2Cl_2 (18 mL), and the mixture was stirred at rt for 3 h. After removing the solvent under reduced pressure, the acyl chloride thus obtained **7** was dried for 5 h under vacuum (0.1-0.5 mm Hg). Without further purification, it was redissolved, in dry CH_2Cl_2 (15 mL) and added to a stirred solution of **Coum-NH$_2$** (64 mg, 0.19 mmol), **NBD-NH$_2$** (49 mg, 0.19 mmol) and DIPEA (150 µL, 0.85 mmol) in dry CH_2Cl_2 (15 mL). Then, to this brown solution, DIPEA (75 µL, 0.43 mmol) was added. The reaction proceeded at rt for 19 h and was monitored by TLC (CH_2Cl_2/CH_3OH 98/2).

The reaction was quenched with H_2O; the organic layer was washed with H_2O (2x50 mL) and dried over anhydrous Na_2SO_4 and concentrated under reduced pressure. The red crude was purified by flash column chromatography (gradient

CH_2Cl_2/Acetone 90/10, Acetone) to afford **14a** as a dark orange-red powder in 24% yield (50 mg, 0.04 mmol).

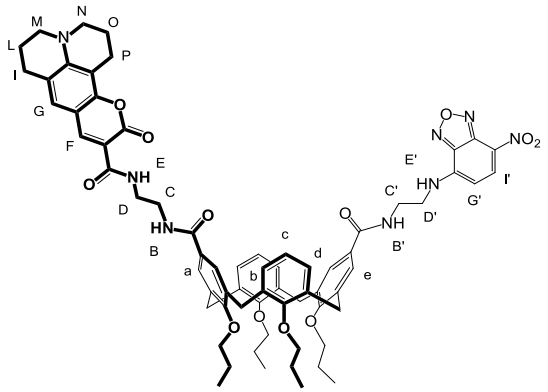

14a

M.p.: decomposition over 196°C. ^{1}H NMR (400 MHz, $CDCl_3$) δ (ppm): 9.14 (bs, 1H, H_E); 8.72 (s, 1H, $H_{E'}$); 8.55 (s, 1H, H_F); 8.42 (d, J = 7.2 Hz, 1H, $H_{I'}$); 6.94-6.89 (m, 6H, H_b, H_d, H_B, H_G); 6.70 (s, 2H, H_e), 6.59-6.53 (m, 4H, H_c and H_a); 6.42 (bs, 1H, $H_{B'}$); 6.13 (d, J = 7.2 Hz, 1H, $H_{G'}$); 4.45 (d, J = 13.6 Hz, 2H, ArC*H*HAr); 4.40 (d, J = 13.2 Hz, 2H, ArC*H*HAr); 3.99 (t, 4H, J = 7.6 Hz, O*CH*$_2$CH$_2$CH$_3$); 3.73-3.63 (m, 8H, O*CH*$_2$CH$_2$CH$_3$, $H_{C'}$ and $H_{D'}$); 3.51 (bs, 2H, H_D); 3.46 (bs, 2H, H_C); 3.34 (t, J = 5.2 Hz, 4H, H_M, H_N); 3.20 (d, J = 13.2 Hz, 2H, ArCH*H*Ar); 3.11 (d, J = 13.6 Hz, 2H, ArCH*H*Ar); 2.85 (t, J = 6.0 Hz, 2H, H_P); 2.72 (t, J = 6.0 Hz, 2H, H_I); 1.98-1.83 (m, 12H, H_O, H_L, OCH$_2$*CH*$_2$CH$_3$); 1.09 (t, J = 7.2 Hz, 3H, OCH$_2$CH$_2$C*H*$_3$); 1.04 (t, J = 7.6 Hz, 3H, OCH$_2$CH$_2$C*H*$_3$); 0.89 (t, J = 7.6 Hz, 6H, OCH$_2$CH$_2$C*H*$_3$). ^{1}H NMR (300 MHz, DMSO-d_6) δ (ppm): 9.56 (bs, 1H, H_E); 8.83 (t, J = 5.5 Hz, 1H, $H_{E'}$); 8.55-8.51 (m, 3H, $H_{I'}$, H_F and H_B); 7.59 (s, 2H, H_e); 7.57 (s, 2H, H_a); 7.20 (s, 1H, H_G); 6.54 (d, J = 9.0 Hz, 1H, $H_{G'}$); 6.25-6.13 (m, 6H, H_b, H_d and H_c); 4.36 (d, J = 13.2 Hz, 2H, ArC*H*HAr); 4.02 (t, 4H, J = 7.8 Hz, O*CH*$_2$CH$_2$CH$_3$); 3.66-3.57 (m, 4H, O*CH*$_2$CH$_2$CH$_3$); 3.55-3.41 (m, 8H, H_C, H_D, $H_{C'}$ and $H_{D'}$); 3.35-3.29 (m, 4H, H_M and H_N); 3.21 (d, J = 13.2 Hz, 2H, ArCH*H*Ar); 3.19 (d, J = 13.2 Hz, 2H, ArCH*H*Ar); 2.73-2.66 (m, 4H, H_P and H_I); 1.96-1.78 (m, 12H, H_O, H_L and OCH$_2$*CH*$_2$CH$_3$); 1.07 (t, J = 7.4 Hz, 6H, OCH$_2$CH$_2$C*H*$_3$); 0.89 (t, J = 7.4 Hz, 6H, OCH$_2$CH$_2$C*H*$_3$). ^{13}C NMR (100 MHz, $CDCl_3$): δ (ppm): 170.1; 168.3; 165.1; 162.8; 158.5; 158.1; 157.3; 152.5; 148.4; 147.6; 144.0; 144.3; 136.5; 136.0; 134.1; 133.9; 129.0; 128.0; 126.9; 126.6; 126.5; 122.9; 122.2; 119.8; 108.3; 107.8; 105.7; 97.9; 77.2; 76.6; 50.2; 49.9; 45.0; 41.4; 39.7; 37.9; 31.0; 29.7; 27.4; 23.4; 23.0; 22.7; 21.0; 20.1; 10.7; 9.8. HR-MS: m/z calculated for $C_{68}H_{74}N_8O_{12}$+H^+ 1217.5324, found 1217.5491 (100%).

A little amount of homo-bichromphoric products was also isolated by chromatography for a partial characterization.

Compound 14b

M.p. decomposition over 204°C. UV-vis: λ_{max} ($CHCl_3$): 438 nm, ε: 40700 $M^{-1}cm^{-1}$. ^1H NMR (300 MHz, $CDCl_3$) δ(ppm): 9.18 (t, J = 8.0 Hz, 2H, H_E); 8.38 (s, 2H, H_F); 7.84 (bs, 2H, H_B); 7.56 (s, 4H, H_a); 6.60 (s, 2H, H_G); 6.25 (d, J = 7.7 Hz, 4H, H_d); 6.01 (t, J = 7.7 Hz, 2H, H_c); 4.45 (d, J = 13.2, 4H, ArC*H*HAr); 4.04 (t, J = 8.1 Hz, 4H, OC*H*$_2$$CH_2CH_3$); 3.75-3.62 (m, 12H, H_C, H_D, OC*H*$_2$$CH_2CH_3$); 3.31-3.21(m, 12H, H_M, H_N, ArCH*H*Ar); 2.78 (t, J = 6.2 Hz, 4H, H_P); 2.52 (t, J = 6.2 Hz, 4H, H_I); 2.02-1.86 (m, 16H, $OCH_2CH_2CH_3$, H_O, H_L); 1.08 (t, J = 7.2 Hz, 6H, $OCH_2CH_2CH_3$); 0.91 (t, J = 7.5 Hz, 6H, $OCH_2CH_2CH_3$). ^{13}C NMR (75 MHz, $CDCl_3$): δ(ppm) 168.2; 166.2; 162.8; 160.4; 155.2; 152.6; 148.4; 147.9; 136.6; 132.8; 128.2; 127.8; 127.7; 127.2; 122.4; 119.7; 107.9; 107.8; 105.3; 77.2; 76.6; 50.3; 49.8; 43.1; 38.6; 30.9; 29.7; 27.2; 23.5; 23.1; 20.9; 20.0; 10.7; 9.9. ESI-MS: m/z calculated for $C_{78}H_{86}N_6O_{12}$+Na^+ 1321.6, found 1321.8 (100%).

Compounds 15a and 15b

$(COCl)_2$ (40 µL, 0.46 mmol) and dry DMF (20 µL) were added to a solution of **11** (105 mg, 0.15 mmol) in dry CH_2Cl_2 (16 mL), and the mixture was stirred for 4 h. The solvent was evaporated and the resulting solid **12** was dried for 5 h at reduced pressure (0.1-0.5 mm Hg). Then it was dissolved in dry CH_2Cl_2 (5 mL) and added to a stirred solution of **Coum-NH_2** (56 mg, 0.17 mmol), **NBD-NH_2** (44 mg, 0.17 mmol) and DIPEA (130 µL, 0.77 mmol) in dry CH_2Cl_2 (15 mL) and dry DMF (1 mL). The reaction mixture was stirred at rt overnight. The reaction was quenched by addition of aqueous HCl (pH=5, 20 mL), then the organic layer was washed with H_2O till neutral pH and the solvent was evaporated under reduced pressure. The yellow crude material was first purified by flash column chromatography (CH_2Cl_2/Acetone 87/13) and the two isolated products were further purified by preparative TLCs (CH_2Cl_2/Acetone 86/14 for **15a**, and CH_2Cl_2/CH_3OH 95/5 for **15b**) giving the two conformers as yellow solids respectively in 6% (10.9 mg, 9.00 µmol) and 11% (20.4 mg 16.5 µmol) yield.

15a

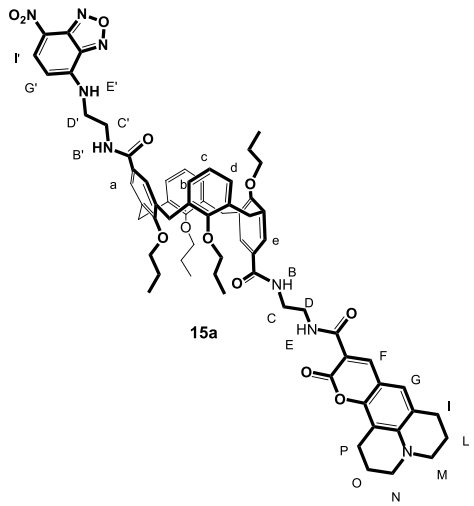

M.p.: 156°C, decomposition over 200°C. UV-vis: λ_{max} ($CHCl_3$): 465 nm (m), ε: 29520 $M^{-1}cm^{-1}$; 540 nm (s), ε: 37840 $M^{-1}cm^{-1}$. ^1H NMR (300 MHz, $CDCl_3$) δ (ppm): 9.20 (bs, 1H, H_E); 8.60 (s, 1H, H_F); 8.46 (d, 1H, J = 8.6 Hz, $H_{I'}$); 8.13 (bs, 1H, $H_{E'}$); 7.79 (s, 2H, H_e); 7.59 (s, 2H, H_a); signal under $CDCl_3$ (H_B); 6.97-6.87 (m, 4H, H_d, $H_{B'}$, H_G); 6.40 (t, J = 7.5 Hz, 2H, H_c); 6.24-6.19 (m, 3H, H_b and $H_{G'}$); 4.06 (d, 2H, J = 13.3 Hz, ArC*H*HAr); 3.91 (bs, 2H, $H_{C'}$); 3.79-3.66 (m, 14H, ArC*H*HAr*, OC*H*$_2$CH$_2$CH$_3$, $H_{D'}$, H_D, H_C); 3.53-3.50 (m, 2H, OC*H*$_2$CH$_2$CH$_3$*); 3.32-3.24 (m, 6H, ArCH*H*Ar*, H_M, H_N); 3.09 (d, 2H, J = 13.3 Hz, ArCH*H*Ar); 2.86-2.84 (m, 2H, H_P); 2.75-2.73 (m, 2H, H_I); 1.95-1.88 (m, 10H, H_O, H_L, OCH$_2$*CH*$_2$CH$_3$); 1.31-1.241 (m, 2H, OCH$_2$*CH*$_2$CH$_3$*); 1.235-1.01 (m, 11H, OCH$_2$*CH*$_2$CH$_3$ and OCH$_2$CH$_2$C*H*$_3$); 0.62 (t, 3H, J= 7.5 Hz, OCH$_2$CH$_2$C*H*$_3$*). ^{13}C NMR (100 MHz, $CDCl_3$): δ (ppm): 169.9; 167.4; 165.2; 163.0; 160.8; 160.5; 155.5; 152.7; 148.4; 148.1; 144.5; 144.3; 143.9; 137.5; 136.4; 133.9; 133.4; 132.6; 131.8; 129.6; 129.55; 128.5; 128.0; 127.1; 127.0; 126.8; 123.5; 121.6; 105.6; 98.3; 77.3; 75.8; 74.8; 50.3; 49.8; 45.8; 45.3; 41.4; 39.6; 39.1; 37.1; 31.74; 27.7; 24.5; 24.1; 22.7; 21.5; 20.1; 10.8; 10.6; 9.3. ESI-MS: m/z calculated for $C_{68}H_{74}N_8O_{12}$+Na^+ 1217.5, found 1218.8 (50%); m/z calculated for $C_{68}H_{74}N_8O_{12}$ K^+ 1233.6, found 1233.7 (100%).

*referred to the inverted aromatic unit

15b

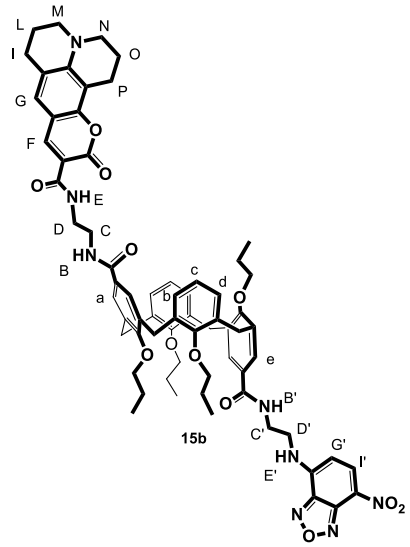

M.p.: decomposition over 200°C. UV-vis: λ_{max} ($CHCl_3$): 465 nm (m), ε: 29520 $M^{-1}cm^{-1}$; 540 nm (s), ε: 37840 $M^{-1}cm^{-1}$. ^{1}H NMR (300 MHz, $CDCl_3$) δ (ppm): 9.25 (t, J = 5.6 Hz, 1H, H_E); 8.58 (s, 1H, H_F); 8.46 (d, 1H, J = 8.6 Hz, $H_{I'}$); 8.39 (bs, 1H, $H_{E'}$); 7.77 (s, 2H, H_e); 7.64-7.59 (m, 3H, H_B and H_a); 6.88-6.87 (m, 3H, H_d, H_G); 6.78 (bs, 1H, $H_{B'}$); 6.38 (t, J = 7.6 Hz, 2H, H_c); 6.28 (d, J = 7.3 Hz, 2H, H_b); 6.16 (d, 1H, J = 8.7 Hz, $H_{G'}$); 4.02-3.94 (m, 4H, ArC*H*HAr and $H_{C'}$); 3.76-3.53 (m, 16H, ArCH*H*Ar*, OC*H*$_2$CH$_2$CH$_3$, OC*H*$_2$CH$_2$CH$_3$*, $H_{D'}$, H_D, H_C); 3.32-3.09 (m, 6H, ArCH*H*Ar*, H_M, H_N); 3.09 (d, 2H, J = 13.3 Hz, ArCH*H*Ar); 2.85 (t, J = 6.8 Hz, 2H, H_P); 2.69 (t, J = 6.1 Hz, 2H, H_I); 1.95-1.88 (m, 10H, H_O, H_L, OCH$_2$*CH*$_2$CH$_3$); 1.37-1.25 (m, 2H, OCH$_2$*CH*$_2$CH$_3$*); 1.12-1.01 (m, 9H, OCH$_2$CH$_2$C*H*$_3$); 0.48 (t, 3H, J = 7.5 Hz, OCH$_2$CH$_2$C*H*$_3$*). ^{13}C NMR (100 MHz, $CDCl_3$): δ (ppm) 170.0; 167.8; 165.8; 162.9; 161.5; 159.7; 155.4; 153.2; 148.5; 148.2; 144.3; 136.8; 136.5; 134.6; 133.0; 131.0; 129.6; 129.2; 129.1; 128.5; 128.0; 127.3; 125.5; 121.8; 119.7; 105.7; 97.9; 77.2; 75.3; 74.9; 50.3; 49.8; 42.5; 39.2; 39.1; 35.9; 30.5; 27.4; 24.1; 23.9; 21.1; 20.1; 10.9; 10.6; 9.1. ESI-MS: m/z calculated for $C_{68}H_{74}N_8O_{12}$+Na^+ 1217.5, found 1217.5 (50%); m/z calculated for $C_{68}H_{74}N_8O_{12}$+K^+ 1233.6, found 1233.6 (100%).

*referred to the inverted aromatic unit

A little amount of homo-bichromophoric products was also isolated by chromatography for a partial characterization.

Compound 15c

^{1}H NMR (300 MHz, $CDCl_3$) δ (ppm): 9.24 (bs, 1H, H_E); 9.19 (bs, 1H, H_E*); 8.63 (s, 1H, H_F); 8.59 (s, 1H, H_F); 7.79 (s, 2H, H_e); 7.60 (s, 2H, H_a); 7.00 (bs, 1H, H_B); 6.87-6.90 (m, 3H, H_B* and H_G); 6.37 (t, J = 7.5 Hz, 2H, H_c); 6.29 (m, 4H, H_b and H_d); 4.05 (d, J = 13.2 Hz, 2H, ArC*H*HAr); 3.76-3.52 (m, 18H, ArCH*H*Ar*, OC*H*$_2$CH$_2$CH$_3$, H_D and H_C); 3.32-3.25 (m, 10H, OC*H*$_2$CH$_2$CH$_3$*, H_M and H_N); 3.12 (d, 2H, J = 13.2 Hz, ArCH*H*Ar); 2.88-2.87 (m, 4H, H_P); 2.76 (t, J = 5.7 Hz, 2H, H_I); 2.69 (t, J = 5.8 Hz, 2H, H_I); 1.96-1.87 (m, 16H, H_O, H_L, OCH$_2$*CH*$_2$CH$_3$ and OCH$_2$*CH*$_2$CH$_3$*); 1.12-1.01 (t, J = 7.2 Hz, 9H, OCH$_2$CH$_2$C*H*$_3$); 0.628 (t, J = 7.2 Hz, 3H,OCH$_2$CH$_2$C*H*$_3$*). ^{13}C NMR (100 MHz, $CDCl_3$): δ (ppm): 167.8; 167.3; 165.8; 165.1; 163.0; 160.5; 159.9; 155.5; 152.8; 148.4; 148.22; 148.16; 136.9; 133.9; 133.1; 131.6; 129.6; 129.2; 128.9; 128.3; 127.9; 127.2; 121.6; 119.73; 119.65; 108.6; 108.2; 105.73; 105.68; 76.3; 75.7; 74.7; 50.9; 49.9; 42.6; 41.5; 39.6; 39.1; 35.9; 30.6;27.5;27.4; 24.1; 23.8; 22.1; 21.1; 20.2; 20.1;10.9; 10.6. ESI-MS: m/z calculated for $C_{78}H_{86}N_6O_{12}$+Na^+ 1321.6, found 1321.9 (40%); m/z calculated for $C_{78}H_{86}N_6O_{12}$+K^+ 1321.7, found 1337.9 (50%)

*referred to the inverted aromatic unit

Compound 18

$(COCl)_2$ (190 µL, 2.17 mmol) and dry DMF (30 µL) were added to a solution of 5-hydroxycarbonyl-25,26,27,28-tetrapropoxycalix[4]arene **16** (68 mg, 0.11 mmol) in dry CH_2Cl_2 (10 mL). The mixture was stirred overnight, then the solvent was removed under vacuum, the resulting acyl chloride **17** was dried for 5 h under vacuum (0.1-0.5 mm Hg) and redissolved in dry CH_2Cl_2 (15 mL). Then DIPEA (75 µL, 0.43 mmol) and **NR-NH$_2$** (50 mg, 0.13 mmol) were added and the solution was stirred at rt for 25 h. The reaction was quenched by addition of H_2O (15 mL); the organic layer was separated and the aqueous layer was extracted with CH_2Cl_2 (3x15 mL). The combined organic layers were washed with H_2O (50 mL) dried over anhydrous Na_2SO_4 and concentrated to dryness. Pure **18** was isolated as a violet solid by preparative TLC plates (2x CH_2Cl_2/ethyl acetate 84/16, 1x THF/cyclohexane 1/1) in 46% yield (50 mg, 0.05 mmol).

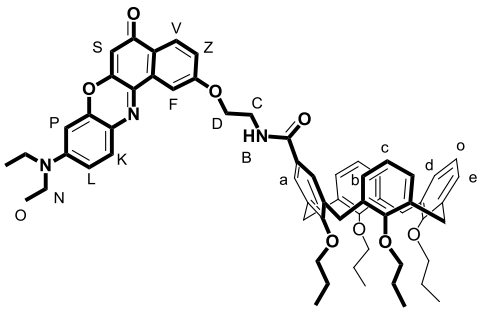

18

M.p: 102-103 °C. UV-vis: λ_{max} ($CHCl_3$): 540 nm, ε: 22560 $M^{-1}cm^{-1}$.^{1}H-NMR (Acetone-d_6, 400MHz): δ (ppm) 8.10 (d, J = 8.4 Hz, 1H, H_V); 8.05 (d, J = 2.8 Hz, 1H, H_F); 7.55 (d, J = 9.2 Hz, 1H, H_K); 7.49 (bs, 1H, NH_B); 7.23-7.26 (m, 3H, H_a and H_Z); 6.79 (dd, J_1 = 9.2 Hz, J_2 = 2.8 Hz, 1H, H_L); 6.48-6.60 (m, 10H, H_P, H_b, H_c, H_d, H_e and H_o); 6.09 (s, 1H, H_S); 4.47 (d, J = 13.6 Hz, 4H, ArC*H*HAr); 4.44 (d, J = 13.2 Hz, 4H, ArC*H*HAr); 4.33 (t, J = 5.6 Hz, 2H, H_D); 3.93 (t, J = 7.2 Hz, 2H, H_C); 3.77-3.88 (m, 8H, OCH_2); 3.57 (q, J = 7.0 Hz, 4H, H_N); 1.25 (t, J = 8.0 Hz, 6H, H_O); 3.19 (d, J = 13.2 Hz, 4H, ArCH*H*Ar); 3.13 (d, J = 13.6 Hz, 4H, ArCH*H*Ar); 1.90-1.98 (m, 8H, CH_2); 0.98-1.03 (m, 12H, CH_3). ^{13}C-NMR (Acetone-d_6, 100MHz): δ (ppm) 182.6; 167.7; 162.5; 157.5; 160.3; 157.3; 152.9; 152.0; 147.7; 140.3; 136.2; 136.1; 135.9; 135.3; 135.0; 131.9; 129.3; 125.2; 129.3; 129.0; 128.3; 122.9; 122.8; 118.4; 110.7; 108.1; 105.5; 97.1; 77.4; 77.6; 68.0; 45.7; 40.1; 31.6; 24.1; 12.9; 10.7. HR-MS: m/z calcd for $C_{63}H_{69}N_3O_8$+Na^+ 1018.4965, found 1018.5022 (100%), m/z calcd for $C_{63}H_{69}N_3O_8$+H^+ 996.5145, found 996.5200 (55%), m/z calcd for $C_{63}H_{69}N_3O_8$+K^+ 1034.6087, found 1034.4758 (30%).

Compound 19

$(COCl)_2$ (190 µL, 2.18 mmol) and dry DMF (30 µL) were added to a solution of 5-hydroxycarbonyl-25,26,27,28-tetrapropoxycalix[4]arene (68 mg, 0.11 mmol) in dry CH_2Cl_2 (7 mL) and the mixture was stirred at rt for 4 h. The solvent was removed under vacuum and the resulting acyl chloride was dryed for 2 h under vacuum (0.1-0.5 mm Hg), then redissolved in dry CH_2Cl_2 (15 mL) and added to a solution of **Coum-NH_2** (43 mg, 0.13 mmol) and DIPEA (100 µL, 0.65 mmol) in dry CH_2Cl_2 (10 mL). The reaction mixture was stirred at rt for 20 h, then the reaction was quenched by adding H_2O (20 mL). The aqueous layer was extracted with CH_2Cl_2 (4x20 mL) and the combined organic layers were dried over Na_2SO_4 and concentrated under vacuum. The pure product was isolated as a yellow solid by preparative TLC plates

(1x CH_2Cl_2/Acetone 80/20, 1x THF/Cyclohexane 50/50, 3x CH_2Cl_2/CH_3CN 80/20) in 25% yield (25 mg, 0.03 mmol).

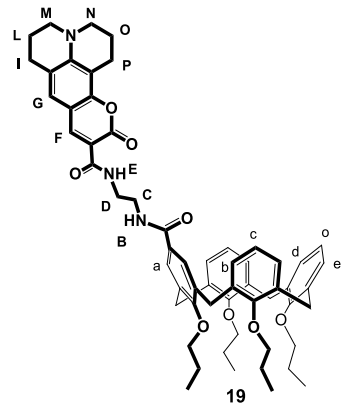

19

M.p: 110 °C. UV-vis: λ_{max} ($CHCl_3$): 438 nm. ^{1}H-NMR (Acetone-d_6, 300MHz): δ (ppm) 8.56 (bs, 1H, NH_E); 7.02 (s, 1H, H_F); 7.73 (bs, 1H, NH_B); 7.41 (s, 2H, H_a); 7.02 (s, 1H, H_G); 6,79 (d, J = 7.4 Hz, 2H, H_e); 6.65 (t, J = 6.99 Hz, 1H, H_f); 6.32-6.42 (m, 6H, Ar H_c, H_b, H_d); 4.49 (d, J = 13.3 Hz, 2H, ArC*H*HAr); 4.47 (d, J = 13.5 Hz, 2H, ArC*H*HAr); 4.02-3.79 (m, 8H, OC*H*$_2$$CH_2CH_3$); 3.64 (t, J = 5.9 Hz, 2H, H_D); 3.55 (t, J = 5.5 Hz, 2H, H_C); 3.36-3.41 (m, 4H, H_N, H_M); 3.21 (d, J = 13.5 Hz, 2H, eq ArCH*H*Ar); 3.15 (d, J = 13.3 Hz, 2H, eq ArCH*H*Ar); 2.71-2.85 (m, 4H, H_I, H_P); 2.06-2.04 and 1.93-1.97 (m, 12H, OCH_2C*H*$_2$$CH_3$, H_L, H_O); 1.06 (t, J = 7.5 Hz, 6H, OCH_2CH_2C*H*$_3$); 0.98 (t, J = 7.5 Hz, 6H, OCH_2CH_2C*H*$_3$). ^{13}C-NMR (Acetone-d_6, 75MHz): δ (ppm) 164.9; 167.6; 163.1; 160.6; 153.7; 156.9; 157.9; 149.2; 148.6; 136.7; 134.4; 134.7; 135.3; 136.6; 128.1; 128.6; 128.85; 128.; 129.4; 129.6; 120.7; 109.6; 106.2; 77.4; 77.5; 77.7; 69.4; 50.4; 50.8; 41.6; 39.7; 30.7; 21.9; 23.4; 20.9; 10.6; 10.9. HR-MS: m/z calcd for $C_{59}H_{67}N_3O_8$+H^+ 946.4989, found 946.5016 (100%), m/z calcd for $C_{59}H_{67}N_3O_8$+Na^+ 968.4809, found 968.4833 (50%).

5-Hydroxycarbonyl-17-methoxymethylen-25,26,27,28-tetrapropoxycalix[4]arene (21)

$SOCl_2$ (70 µL, 0.92 mmol) was added to a solution of **2** (125 mg, 0.18 mmol) in dry CH_2Cl_2 (8 mL), and the reaction stirred at rt for 4 h. The solvent was removed under vacuum, the residue was dried for 1 h under vacuum (0.1-0.5 mm Hg) and then suspended in CH_3OH (5 mL). After the addition of $NaOCH_3$ (40 mg, 0.74 mmol), the mixture was refluxed for 17 h, then cooled to rt and evaporated to dryness. The residue was dissolved in CH_2Cl_2 and the solution was washed with H_2O till neutral pH, dried over anhydrous Na_2SO_4 and evaporated under reduced pressure giving a

yellow oil in 70% yield (89 mg, 0.13 mmol). ^{1}H NMR spectroscopy indicated that this oil was a mixture of the expected 5-methoxycarbonyl-17-methoxymethylen-25,26,27,28-tetrapropoxycalix[4]arene **20** and the corresponding carboxylic acid, the final target of this synthetic procedures. Then, without further treatment and characterization, the oil was suspended in THF/H_2O (4/1, v/v, 3.3 mL) and mixed with a solution of KOH (71 mg, 1.26 mmol) in THF/H_2O (4/1, v/v, 2.2 mL). The reaction was refluxed for 48 h and then, after cooling to rt, quenched by addition of 1N HCl (1.3 mL). The solution was extracted with CH_2Cl_2 (10 mL) and the organic layer was washed with H_2O till neutral pH, dried over anhydrous $MgSO_4$ and concentrated under reduced pressure, giving compound **21** in 66% overall yield (83 mg, 0.12 mmol). ^{1}H-NMR ($CDCl_3$, 300 MHz): δ (ppm) 7.35 (s, 2H, ArH); 6.68-6.55 (m, 6H, ArH); 6.54 (s, 2H, ArH); 4.45 (d, J = 12.6 Hz, 2H, ArC*H*HAr); 4.41 (d, J = 12.6 Hz, 2H, ArC*H*HAr); 4.03 (s, 2H, ArCH_2O); 3.95-3.72 (m, 8H, OCH_2CH$_2$CH$_3$); 3.20 (d, J = 12.6 Hz, 2H, ArCH*H*Ar); 3.14 (d, J = 12.6 Hz, 2H, ArCH*H*Ar); 1.98-1.82 (m, 8H, OCH$_2$CH_2CH$_3$); 1.05-0.90 (m, 12H, OCH$_2$CH$_2$CH_3). ESI-MS: m/z calcd for $C_{43}H_{52}O_7$+Na^+ 703.4, found 703.4.

Compound 22

$(COCl)_2$ (150 µL, 1.72 mmol) and dry DMF (15 µL) were added to a solution of **21** (83 mg, 0.12 mmol) in dry CH_2Cl_2 (20 mL), and the mixture was stirred for 3.5 h at rt. The solvent was removed under vacuum and the acyl chloride product was dried for 3 h under vacuum (0.1-0.5 mm Hg) and redissolved in dry CH_2Cl_2 (4 mL). Then TEA (150 µL, 1.08 mmol) and a solution of **NBD-NH$_2$** (35 mg, 0.14 mmol) in dry CH_2Cl_2 (6 mL) were added, and the reaction mixture was stirred at rt overnight. The reaction was quenched by addition of aqueous HCl (1M, 20 mL); the organic layer was washed with a saturated solution of $NaHCO_3$ and with H_2O till neutral pH, and dried over anhydrous $MgSO_4$. The solvent was evaporated under reduced pressure. The brown crude material was purified by flash column chromatography (hexane/ethyl acetate 50/50) and the desired product was isolated as an orange solid in 31% yield (33 mg, 0.04 mmol).

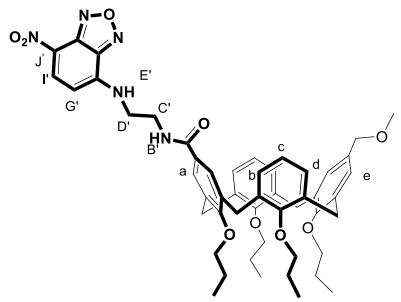

22

M. p.: 128.6-129.7°C. UV-vis: λ_{max} ($CHCl_3$): 454 nm (m), ε: 11700 $M^{-1}cm^{-1}$.^{1}H-NMR ($CDCl_3$, 300MHz): δ (ppm) 8.48 (d, J = 8.7 Hz, 1H, $CH_{I'}$); 8.07 (bs, 1H, $H_{B'}$); 7.09 (s, 2H, H_a); 6.49-6.64 ppm (m, 8H, H_b, H_c, H_d and H_e); 6.33 (bs, 1H, $H_{E'}$); 6.17 (d, J = 8.7 Hz, 1H, $H_{G'}$); 4.45 (d, J = 13.4 Hz, 2H, ArC*H*HAr); 4.42 (d, J = 13.2 Hz, 2H, ArC*H*HAr); 4.06 (s, 2H, ArCH_2OCH_3); 3.76-3.88 (m, 8H, $OCH_2CH_2CH_3$); 3.17 (d, J = 13.4 Hz, 2H, ArCH*H*Ar); 3.14 (d, J = 13.2 Hz, 2H, ArCH*H*Ar); 3.13 (s, 3H, OCH_3); 1.83-1.98 (m, 8H, $OCH_2CH_2CH_3$); 0.98 (t, J = 7.5 Hz, 12H, $OCH_2CH_2CH_3$). ^{13}C-NMR ($CDCl_3$, 100MHz): δ (ppm) 169.5; 160.3; 156.5; 156.2; 144.3; 143.9; 136.4; 135.7; 135.3; 134.9; 134.3; 130.9; 128.6; 128.1; 127.7; 127.2; 126.3; 123.8; 122.2; 98.5; 77.2; 76.9; 76.8; 74.3; 57.5; 38.7; 30.9; 23.3; 23.24; 23.18; 10.34; 10.29; 10.2. HR-MS: m/z calcd for $C_{51}H_{59}N_5O_9$+NH_4^+ 903.4641, found 903.4650 (60%).

Molecular modelling studies

Molecular modelling was carried out at the molecular mechanics level using the MMFF94 force field[43] implemented in SPARTAN '10[44] using a Monte Carlo method for the conformational search.

Transient absorption measurements

Transient measurements were carried out in the LENS laboratories (Florence). The apparatus used for the transient absorption spectroscopy (TAS) measurements has been described in detail in refs.[31,32,33,34] The fs-laser oscillator is a Ti:sapphire laser (Spectra Physics Tsunami) pumped by the second harmonic from a Nd:YVO (Spectra Physics Millennia). The short (≤70 fs) pulses are stretched and amplified at 1 kHz repetition rate by a regenerative amplifier (BMI Alpha 1000). After compression a total average power of 450-500 mW and pulse duration of 100 fs are obtained. The repetition rate of the output beam is reduced to 100 Hz by a mechanical chopper in order to avoid the photodegradation of the sample. Pulses in the UV-Visible

range can be achieved by Second Harmonic Generation (SHG) or by doubling or mixing the output of an optical parametric generator and amplifier (OPG-OPA) based on a BBO crystal (TOPAS by Light Conversion, Vilnius, Lithuania).[35,36] For the current measurements the pump beam polarization was set to magic angle with respect to the probe beam by rotating a $\lambda/2$ plate so as to exclude rotational contributions to the transient signal. The probe pulse was generated by focusing a small portion of the 800 nm radiation on a 3 mm thick CaF_2 window mounted on a motorized translation stage. The continuum light was optimized for the 350-750 nm wavelength range and a moveable delay line made it possible to increase the time-of-arrival-difference of the pump and probe beams up to 2.0 ns. Multichannel detection for transient spectroscopy was achieved by sending the white light continuum after passing through the sample to a flat field monochromator coupled to a home-made CCD detector [http://lens.unifi.it/ew]. TAS measurements were carried out in a static cell (2 mm thick) under magnetic stirring in order to refresh the solution and avoid photo degradation. The integrity of the sample has been checked by visible absorption measurements (Perkin Elmer LAMBDA 950) before and after the time resolved measurements. The OD of the sample at the excitation wavelength was between 0.2 and 0.5 in all the examined solvents (chloroform, acetonitrile and chloroform). Transient spectra have been analysed by applying a combined approach, consisting of singular values decomposition (*SVD*)[25,37] and the simultaneous fitting of all the collected kinetic traces (global analysis). The aim of global analysis is to decompose the two way data matrix into time-independent spectra and wavelength independent kinetics.[38] Once the number of components is identified through the SVD, the second step involves the parameterization of the time evolution of the spectral components. This was accomplished by assuming first-order kinetics, describing the overall temporal evolution as the sum or combination of exponential functions. Global analysis was performed using the GLOTARAN package [http://glotaran.org],[38,39] and employing a linear unidirectional "sequential" model shown in Scheme 12:

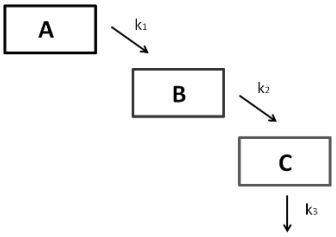

Scheme 12. *Sequential kinetic model applied for global analysis.*

2.7 References

1 N. J. Turro, *Pure & Appl. Chem.*, **1977**, 49, 405-409;

2 T. Forster, *Disc. Faraday Soc.*, **1959** , 27, 7-17;

3 B. Valeur, *Molecular Fluorescence: Principles and Applications*, **2001**,Wiley, 247-272;

4 http://www.fluorophores.tugraz.at/substance/;

5 M. Galli, J. A. Berrocal, S. Di Stefano, R. Cacciapaglia, L. Mandolini, L. Baldini, A. Casnati and F. Ugozzoli, *Org. Biomol. Chem*., **2012**, 10, 5109–5112;

6 H. Lee, M.G. Choi, H.-Y. Yu, S. Ahn, S.-K. Chang, *Bull. Korean Chem. Soc.*, **2010**, 31 (12), 3539-3542;

7 E. F. Elslager, D. Worth, *J. Med. Chem.*, **1970**, 13 (3), 370-376;

8 O. Mitsunobu And Masaaki Yamada, *Bulletin Of The Chemical Society Of Japan*, **1967**, 40, 2380-2382;

9 M. S. J. Briggs, I. Bruce, J. N. Miller, C. J. Moody, A. C. Simmonds, E. Swann, *J. Chem. Soc., Perkin Trans.*, **1997**, 1, 1051-1058;

10 G. Ghini, L. Lascialfari, C. Vinattieri, S. Cicchi, A. Brandi, D. Berti, F. Betti, P. Baglioni, M. Mannini, *Soft Matter*, **2009**, *5*, 1863–1869;

11 S. Taliani, F. Simorini, V. Sergianni, C. La Motta, F. Da Settimo, B. Cosimelli, G. Greco, E. Novellino, L. Rossi, V. Gremigni, F. Spinetti, B. Chelli, C. Martini, *J. Med. Chem.*, **2007**, 50, 404-407;

12 F. Sansone, S. Barboso, A. Casnati, M. Fabbi, A. Pochini, F. Ugozzoli, R. Ungaro, *Eur. J. Org. Chem.*, **1998**, 897-905;

13 A. Arduini, M. Fabbi, M. Mantovani, L. Mirone, A. Pochini, A. Secchi, R. Ungaro, *J. Org. Chem.*, **1995**, 60, 1454-1457;

14 L. C. Groenen, B.H. M. Ruël, A. Casnati, P. Timmerman, W. Verboom, S. Harkema, A. Pochini, R. Ungaro, D. N. Reinhoudt, *Tetrahedron Lett*., **1991**, *32,* 2675-2678;

15 B. O. Lindgren, T. Nilsson, *Acta Chemica Scandinavica*, **1973**, 27, 888-890;

16 S. A. Herbert, G. E. Arnott, *Org. Lett.,* **2010**, 12 (20), 4600-4603;

17 M. Lazzarotto, F. Sansone, L. Baldini, A. Casnati, P. Cozzini, R. Ungaro, *Eur. J. Org. Chem.,* **2001,** 595-602;

18 L. Baldini, F. Sansone, G. Faimani, C. Massera, A. Casnati, R. Ungaro, *Eur.J.Org.Chem*., **2008**, 869-886;

19 B. Dolenský, R. Konvalinka, M. Jakubek, V. Král, **2013**, *Journal of Molecular Structure*, 1035, 124–128;

20 A. Cser, K. Nagy, L. Biczék, *Chem. Phys. Lett*, **2002,** *360*, 473-478;

21 S. Lin, W. S. Struve, *Photochemistry and Photobiology*, **1991,** *54* (3), 361-365;

22 J. Jose, Y. Ueno, J. C. Castro, L. Li, K. Burgess, *Tetrahedron Lett.*, **2009**, 50, 6442-6445;

23 R. W. Hendler, R. I. Shrager, *Journal of Biochemical and Biophysical Methods*, **1994**, 28 (1), 1-33;

24 E. R. Henry, J. Hofrichter, Singular value decomposition: Application to analysis of experimental data. In *Methods in Enzymology*, Ludwig Brand, M. L. J., Ed. Academic Press, **1992**, 210, 129-192.

25 I. H. M. van Stokkum, D. S. Larsen, R. van Grondelle, *Biochimica et Biophysica Acta (BBA) – Bioenergetics*, **2004**; 1657 (2–3), 82-104;

26 D. B. Sherman, J. B. Pitner, A. Ambroise, K. J. Thomas, *Bioconjugate Chem.*, **2006**, 17, 387-392;

27 J. Van Gompel, G. B. Schuster, *J. Org. Chem.*,**1987**,*52*, 1465-1468;

28 R. P. Briñas, T. Troxler, R. M. Hochstrasser, S. A. Vinogradov, *J. Am. Chem. Soc.*, **2005**, 127, 11851;

29 T. A. Halgren, *J. Comput. Chem.* **1996**, *17*, 490–519;

30 SPARTAN '10, Release 1.0.1, Wavefunction, Inc., Irvine, CA, **2011**; http://www.wavefun.com;

31 P. L. Gentili, M. Mugnai, L. Bussotti, R. Righini, P. Foggi, S. Cicchi, G. Ghini, S. Viviani, A. Brandi, *Journal of Photochemistry and Photobiology A: Chemistry*, **2007**, 187, 209-221;

32 A.Marcelli, P. Foggi, L. Moroni, C. Gellini, P. R Salvi, *J. Phys. Chem. A*, **2008**, 112 (9), 1864-1872;

33 L. Moroni, C. Gellini, P. R. Salvi, A. Marcelli, P. Foggi, *J. Phys. Chem. A,* **2008,** *112* (44), 11044-11051;

34 P. L. Gentili, L. Bussotti, R. Ruzziconi, S Spizzichino, P Foggi, *J. of Phys. Chem. A*, **2009**, 113 (52), 14650-14656;

35 I. M. Bayanov, R. Danielius, P. Heinz, A. Seilmeier, *Optics Communications*, **1994**, 113, 99-104;

36 R. Danielius, A. Piskarskas, P. Di Trapani, A. Andreoni, C. Solcia, P. Foggi, *Applied Optics*, **1996**, 35 (27), 5336-5339;

37 E. R. Henry, *Biophysical journal*, **1997**, *72* (2), 652-673

38 J. J. Snellenburg, S. P. Laptenok, R. Seger, K. M. Mullen, I. H. M. van Stokkum, *Journal Of Statistical Software,* **2012**, 49 (3), 1-22;

39 Mullen, K. M.; van Stokkum, I. H. M., An Introduction to the Special Volume "Spectroscopy and Chemometrics in R". *Journal Of Statistical Software* **2007,** *18* (1), 1-5.

Chapter 3

Synthesis of bichromophoric calix[4]arenes for Quantum Coherence Energy Transfer

3.1 Introduction

Förster's theory describes the rate of energy transfer between weakly interacting chromophores adopting the dipolar approximation, which only holds when donor and acceptor are relatively far apart.

In the case of strong coupling, the excitation can be delocalized over several molecules and can travel through the system in a coherent, wavelike manner until dephasing destroys the coherence. In the strong coupling regime, the time it takes an excitation to travel to the next molecule is shorter than the time it takes for intramolecular vibrational relaxation to occur. Hence, energy transfer occurs between non-equilibrated exciton states. This is for example the case of molecular aggregates.

In this regime, neither Förster's nor Dexter's theory suitably describe energy transfer. Coherent, wavelike energy transfer needs to be taken into account.

Most photosynthetic species share, as a common feature, a photosynthetic unit (PSU) containing peripheral pigment-protein (antenna) complexes surrounding the reaction centers. Initial absorption of sunlight in peripheral pigments creates excitons, electronic excitations spread over several neighboring pigments exhibiting strong quantum mechanical coherence. Efficient harvesting of light energy demands transfer of excitons to the reaction centers well within the decay time of excitons (approximately a nanosecond), typically within tens of picoseconds.

Photosynthesis is a very efficient process and this seems to be strictly related to the coherent excitation energy transfer (maybe simultaneously to the hopping mechanism).

Thanks to recent 2D optical spectroscopy techniques,[1,2] Fleming and co-workers observed the existence of long-lived coherences at high temperature in

photosynthetic light-harvesting complexes (in the FMO pigment-protein complex isolated from *Chlorobaculum tepidum*[3,4]).

Engel and coworkers[5] provided evidence that a synthetic small molecule could reproduce the long-lived quantum coherence phenomenon observed in photosynthetic light-harvesting systems. Since the models they introduced were chromophoric units anchored to a *rigid* scaffold, the challenge is the investigation of the possible occurrence of quantum coherence energy transfer in relatively small and *flexible* artificial systems. With this aim, the second part of this thesis is focused on the synthesis of a calix[4]arene derivative functionalized at the upper rim with two different fluorophores, properly chosen according to their spectroscopic characteristics, that shall strongly interact as to give rise to coherent phenomena. The transient spectral properties of the system have been measured thanks to the collaboration with the European Laboratory for Non-Linear Spectroscopy (LENS) in Florence.

In order to induce strong coupling effects between the chromophores without reducing their distance, their absorption bands have to be very close in energy (max a few tens of nm). Moreover, in order to allow for their investigation via 2D-electronic spectroscopy, the photo-active units are required to absorb in the red spectral region of the visible spectrum (because of experimental setup requirements). Finally, narrow absorption and fluorescence bands are envisaged in order to be able to well distinguish the different spectral features in the bichromophoric system.

3.2 BODIPY dyes

The fluorophores chosen to investigate the possible occurrence of quantum coherence energy transfer in a bichromophoric calix[4]arene-based system belong to the family of BF_2-chelated dipyrromethene compounds (BODIPY, Figure 1).

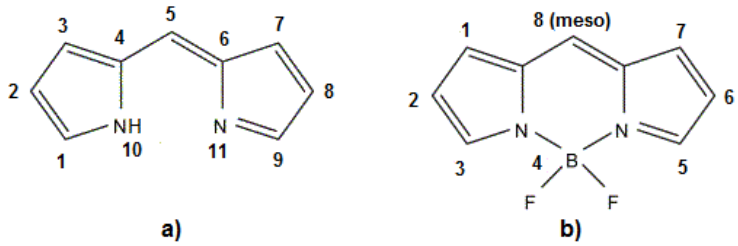

Figure 1. *Unsubstituted dipyrromethene precursor (a) and 4,4-Difluoro-4-bora-3a,4a-diaza-s-indacene(BODIPY) core (b).*

BODIPYs are extremely versatile fluorescent materials that have found numerous applications in biochemistry and molecular biology,[6] and whose popularity has increased in the past twenty years. The first example related to these dyes was reported by Treibs and Kreuzer in 1968,[7] although relatively little attention was given to the discovery until the end of the 80s and 90s, when their potential use for biological labeling and their application in tunable lasers were recognized. As a consequence, BODIPY came to be known to the biochemists and biologists as a photostable substitute for fluorescein, and the number of papers and patents started to escalate in the mid-1990s.[8,9]

BODIPYs are very stable compounds, due to their atomic composition and their geometrical structure. The presence of boron, nitrogen and fluorine atoms allows efficient orbital overlaps promoting delocalization of the π system, which results in red-shifted absorption and fluorescence spectra. Fluorophores with tunable spectral properties can be synthesized by changing the substituents on the BODIPY core, leading to the creation of a series of longer-wavelength BODIPY dyes with spectroscopic properties that span the visible spectrum.[10]

3.2.1. Synthesis and chemistry of BODIPY

- Synthesis of BODIPY core

There are few methods to synthesize the boron dipyrromethene core. The most used approaches are based on the well-known chemistry of porphyrins.[11] The key point is the synthesis of the dipyrromethene (or dipyrrin) core, which is then reacted with boron trifluoride diethyletherate in the presence of a tertiary amine, such as triethylamine, N,N-diisopropylethylamine or 1,8-diazabicyclo[5.4.0]undec-7-ene, to obtain the boron complexation and stabilize the chromophoric core (Scheme 1). Since the unsubstituted dipyrromethene (Figure 1a) is unstable in solution at temperatures above -40° C and it undergoes nucleophilic attack on 3 and 5 positions,[12] the fully unsubstituted BODIPY (Figure 1b) has not been prepared until 2009, when three independent research groups reported different syntheses.[13,14,15]

A first method to obtain the BODIPY core is the acidic-catalyzed condensation of two pyrrole derivatives with an aldehyde (Scheme 1a). The reaction leads to the formation of a first symmetric intermediate, a dipyrromethane compound, which is a rather unstable compound (sensitive to light, air and acid) and requires an oxidation step to be converted in dipyrromethene. The use of oxidizing agents (such as chloranil or 2,3-dichloro-5,6-dicyano-1,4-benzoquinone) causes the formation of byproducts, which are removed after the final boron complexation. To the best of our knowledge, when the aldehyde is not aromatic, oxidation tends to fail.[16,17]

8-Substituted BODIPY dyes (i.e. with substituents in the *meso* position) can be also synthesized by reaction of pyrroles with an acylium equivalent (acyl chlorides or acid anhydrides or orthoesters, Scheme 1b). The unstable intermediate dipyrromethene is immediately reacted with boron trifluoride diethyletherate to complete the synthesis of BODIPY. A recent strategy involving cyclic anhydrides

leads to a product bearing a free carboxylic acid, useful for further functionalization.[18]

The main advantage of these two procedures is the possibility of obtaining BODIPYs with different *meso*-substituents.

A third approach is represented by the convenient method developed by Wu and Burgess (Scheme 1c),[19] who prepared the symmetric dipyrromethene by direct condensation of two units of the same pyrrole-2-carbaldehyde in presence of an excess of phosphorus oxychloride.

Asymmetric dipyrrins can be obtained by the reaction of 2-acylpyrrole with a second pyrrole, not substituted on the 2-position, in acidic condition (Scheme 1d).

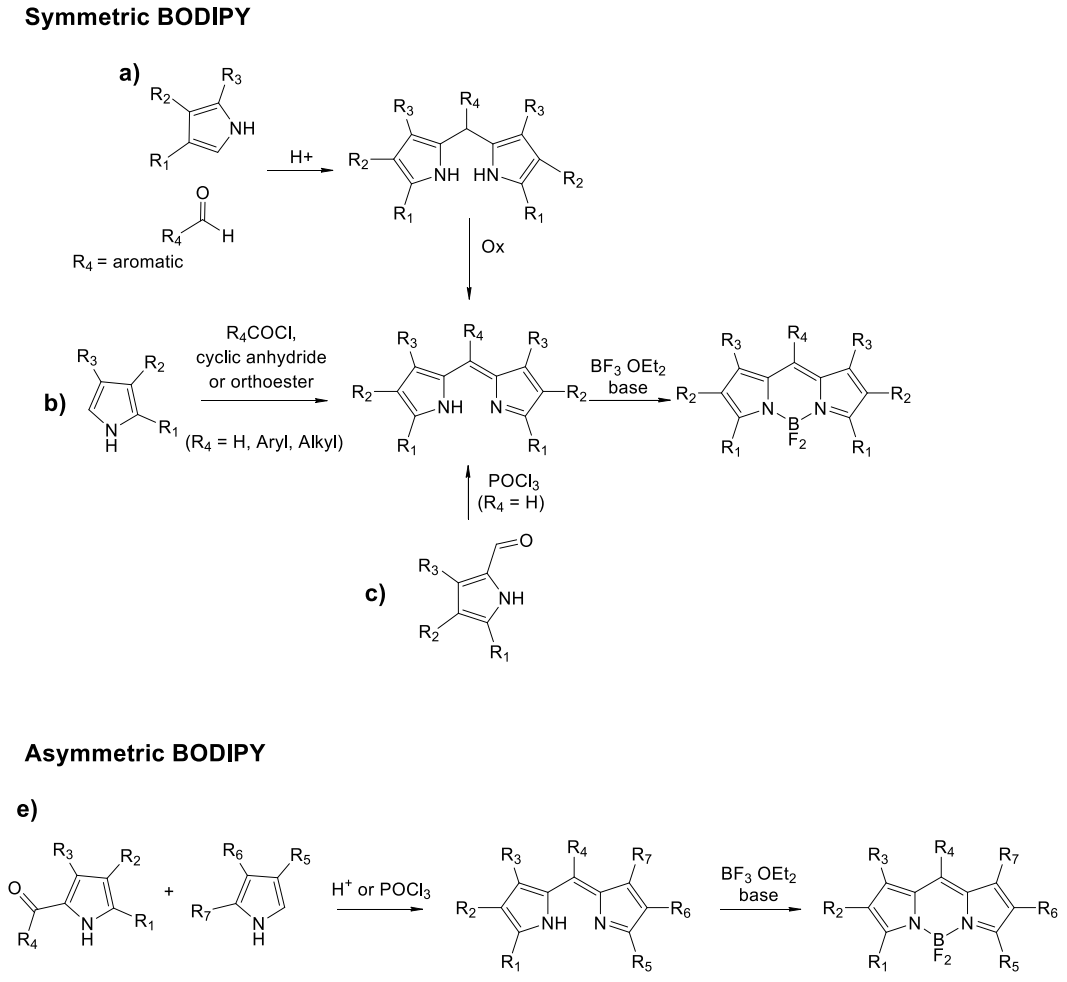

Scheme 1. *Different approaches for the synthesis of BODIPY core.*

- Peripheral modification of BODIPYs

The most straightforward way of preparing functional BODIPYs is the introduction of the desired functional groups on the building blocks (pyrroles, aldehyde or acyl chloride, Scheme 1), but it is also possible to functionalize the dye in a second time following longer and generally lower yielding routes.[10]

The functionalization of the *meso*-position does not affect the spectroscopic properties of the core. On the contrary, the substitution or the modification of

functional groups either on the pyrrolic rings, or on the boron nucleus, induce strong changes in absorption and emission spectra.

The BODIPY core is robust enough to withstand a range of chemical transformations. Many reviews[8,10] report examples of reactions to modify the BODIPY core by halogenation, metal-catalyzed Cross-Coupling, nucleophilic substitution of leaving groups, Knoevenagel condensation.

3.3 Aim of the chapter

With the aim to investigate if quantum coherence energy transfer can be reproduced in small artificial model systems and, in case of a positive feedback, to examine the dynamics and the mechanisms involved in the process, BODIPY chromophoric units were chosen to be anchored at the upper rim of a *cone* calix[4]arene. Three different couples of dyes based on the BODIPY core were considered and their synthesis was undertaken. The chromophores of the first couple belong to the class of dibenzo-fused BODIPY (compounds **29** and **37**), those of the second consist of BODIPYs functionalized with aliphatic and ester groups (compounds **42** and **43**), and those of the third are characterized by a styryl group linked to the BODIPY core in position 3 (compounds **56** and **VI**). The spectroscopic properties of these compounds make them ideal candidates for the study of coherent excitation energy transfer since they satisfy the following requirements:

- absorption bands very close in energy (max a few tens of nm);
- absorption bands in the red spectral region of the visible spectrum (above 550 nm because of 2D-electronic spectroscopy experimental setup requirements);
- narrow absorption and fluorescence bands (in order to be able to well distinguish the different spectral features in the bichromophoric system).

Unfortunately, due to difficulties in their synthesis, the preparation of the first two couples of chromophores was not completed and only derivatives **56** and **VI** (third couple of dyes) were obtained.

3.4 Synthesis

3.4.1. First couple of BODIPYs: 29 and 37

The first couple of BODIPY dyes that were designed for the study of excitation energy transfer and the possible occurrence of quantum-coherence effects are compounds **29** and **37**, reported in Scheme 2 together with the target bichromophoric calix[4]arene **38**. The aminoethyl chains on the BODIPYs *meso* positions have the function of keeping a short distance between the chromophores and the calixarene without imparting rigidity to the system.

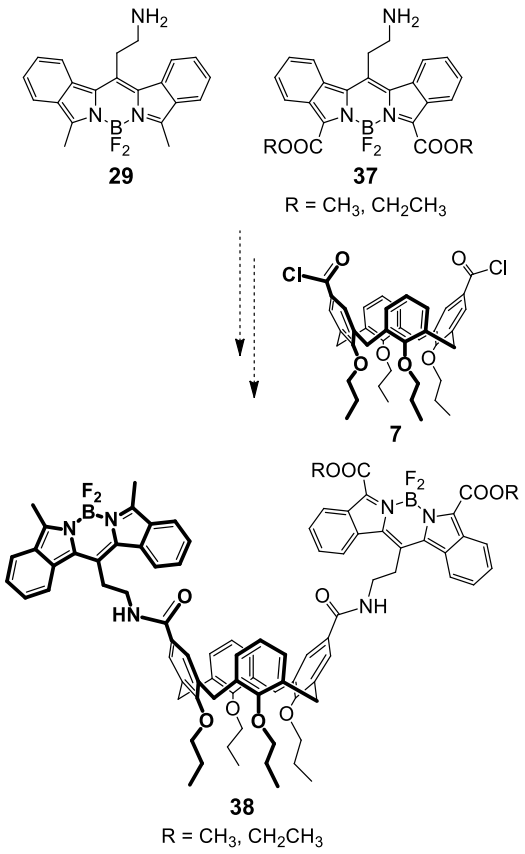

Scheme 2. *First target molecules: dibenzo-fused BODIPYs **29, 37** and bichromophoric system **38**.*

Dyes **29** and **37**, which are BODIPYs with an extended conjugation due to aromatic rings fused to the β-pyrrolic positions, are not present in the literature, but their spectroscopic properties can be assumed to be very similar to those of compounds **I**[10,20] and **II**[21] (Figure 2), from which they differ only for the functionalization on the *meso* position.

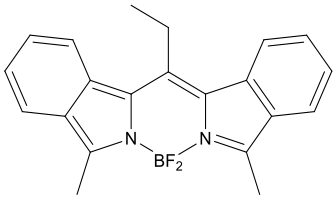

I

λ_{max}^{abs} ($CHCl_3$) = 601 nm; λ_{max}^{em}($CHCl_3$) = 608 nm
λ_{max}^{abs} (EtOH) = 602 nm; λ_{max}^{em}(EtOH) = 608 nm

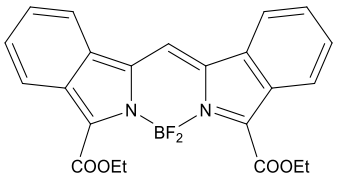

II

λ_{max}^{abs} (CH_2Cl_2) = 642 nm; λ_{max}^{em}(CH_2Cl_2) = 664 nm
λ_{max}^{abs} (CH_3OH) = 635 nm; λ_{max}^{em}(CH_3OH) = 651 nm

Figure 2. *BODIPYs **I** and **II**.*

The *meso*-position can be functionalized with halogenated or nitro-aromatic groups or alkyl chains, but no examples exist regarding a primary amino-chain. In order to allow the linkage of the chromophores to the calixarene scaffold maintaining a certain distance and avoiding the steric hindrance (Scheme 2), the *meso*-position of the BODIPY cores provided an ethyl chain ending with primary amine, as reactive site for further functionalization.

- Synthesis of compound 37

The retrosynthetic approach for the preparation of dye **37** is depicted in Figure 3.

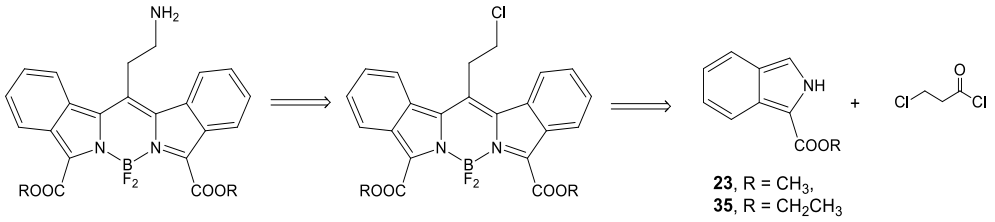

Figure 3. *Retrosynthetic approach for the preparation of dye **37**.*

The synthesis of precursor **23** (Figure 4) is reported in a literature procedure.[22] In the paper, Batra and coworkers exalt the successful assembling of N-heterocycles in mild conditions and in one step, describing the synthesis of 2*H*-isoindole-1-carboxylates through a Cu-catalyzed cascade reaction between a 2-halobenzaldehyde and an α-aminoacid ester. The proposed mechanism is a one-pot domino process involving a condensation between the amino group of the α-amino acid ester and the formyl group of 2-halobenzaldehyde, followed by α-arylation of the α-amino acid ester.

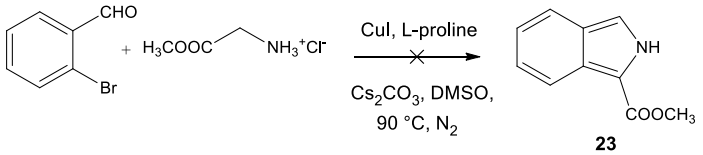

Figure 4. *Copper-catalyzed cascade reaction for the synthesis of compound **23**.*

The reported procedure was meticulously followed. Commercial 2-bromobenzaldehyde and glycine methyl ester hydrochloride were dissolved in dimethyl sulfoxide under nitrogen atmosphere, in presence of a base (Cs_2CO_3), the catalyst (CuI) and the ligand (L-proline). The mixture was heated at 90°C and immediately the white solution became yellow, then green and, at the end, red. When the starting material was completely consumed, the reaction was quenched

and the brown crude oil was purified by flash column chromatography, but none of the collected fractions contained the desired product **23**.

It was then decided to follow a different synthetic pathway (Scheme 3) to obtain the isoindole ethyl ester **35**.

Intermediates **24** and **25** were successfully synthesized according to literature procedures.[23]

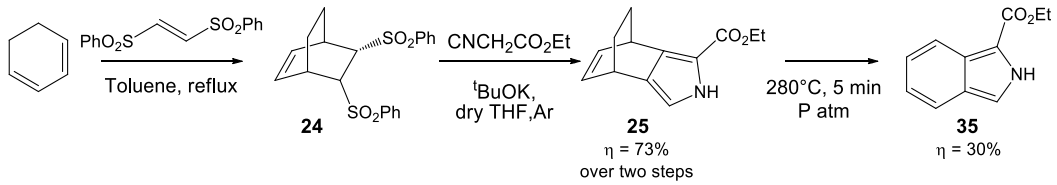

Scheme 3. S*ynthesis of compound **35**.*

Many attempts for the aromatization of precursor **25** by thermal retro-Diels-Alder reaction were required in order to optimize the reaction conditions. When the reaction was performed solvent-free, in the range 200-230°C for several hours (15 h), the starting material decomposed and the desired product was not observed. Although long times were necessary to completely convert the starting material, it was decided to reduce the reaction time from 15 h to 70 minutes. After five minutes heating a sublimation occurred and three kind of products, a green sticky oil, a white powder and colorless crystals were observed. Because the desired product **35** was contained in all the fractions, the crude was purified by column chromatography affording the desired product **35** as a white solid in 30% yield.

In order to force a major conversion of **25** towards the aromatic product **35**, another attempt was performed increasing the temperature (280 °C) and lowering the reaction time to 5 minutes. Pure compound **35** was collected in 30% yield after flash column chromatography. However, since other fractions contained a mixture of the desired target **35** and other byproducts, it is possible to conclude

that these conditions (high temperatures and very short times) allow the highest conversion of the starting material.

As shown in Scheme 4, intermediate **35** was then reacted in a three-steps procedure with 3-chloropropionyl chloride.

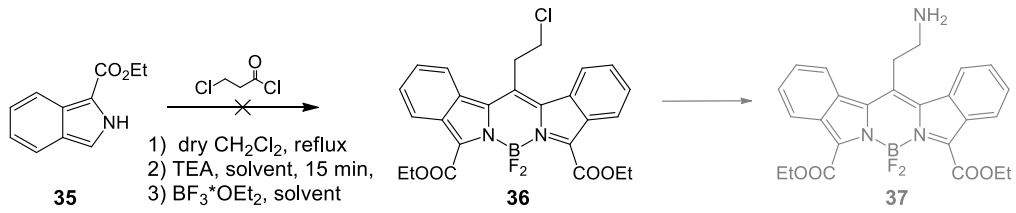

Scheme 4. *Designed synthesis of compound **37**.*

Many attempts to perform this reactions were performed, following literature procedures described for similar systems.[20,24,25] Different solvents (e. g. dry CH_2Cl_2, a mixture of dry CH_2Cl_2 and dry hexane or dry toluene), working temperature and molar ratio among the reagents were employed, but TLC monitoring and ESI-MS analysis always revealed the presence of several products none of which corresponding to the desired compound.

The values of m/z found in the mass spectra suggested the possible elimination of HCl with subsequent formation of the conjugated double bond in *meso*-position, favored by high temperatures (Figure 5).

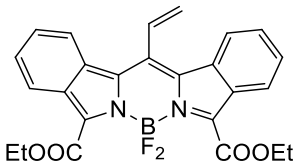

Figure 5. *ESI-MS suggested byproduct formed during the synthesis of **36**.*

The formation of this byproduct was not confirmed by other analytical techniques, but due to these discouraging results the synthesis of BODIPY **36** and of the target dye **37** was abandoned.

- Synthesis of derivative 29

Concurrently to the preparation of compound **37** and its precursors, the synthesis of the second chromophore of the couple, **29**, was performed. The planned synthetic pathway (Figure 6) takes into account the problems observed in the attempted synthesis of **37**. Instead of 3-chloropropionyl chloride, it was decided to use the acyl chloride of β-alanine protected as phthaloyl derivative in the synthesis of the BODIPY core. The phthaloyl protecting group was chosen because it fulfilled the following requirements:

- stability in presence of boron trifluoride diethyletherate employed for the synthesis of the BODIPY;
- deprotection conditions that would not affect the coordination F-B-N, which degrades in strong acidic and basic conditions or is subject to the nucleophilic substitution of the fluorine atoms in a base/alcohol mixture.

Phthalimides are stable to boron trifluoride diethyletherate and are readily deprotected by hydrazinolysis using hydrazine.

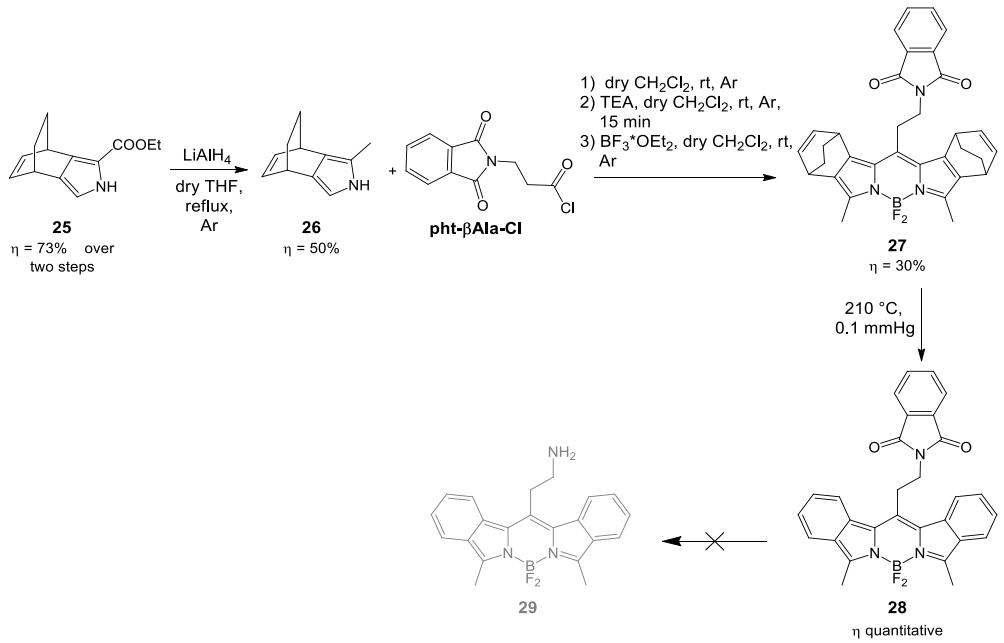

Figure 6. *Designed synthesis of compound **29**.*

2-Methylpyrrole **26** was obtained by reduction of **25** according to the literature.[26] β-alanine protected as phthalimide and activated as acyl chloride[27] was then added to a stirred solution of **26** in dry CH_2Cl_2 and the reaction mixture was refluxed for 3 h under argon atmosphere. When the amino acid starting material was completely consumed, triethylamine was dropped in the solution and 15 minutes later boron trifluoride diethyletherate was added. The reaction was allowed to proceed at round temperature for 15 h, when TLC monitoring revealed the complete reaction of pyrrole **26**. Both the *anti* and *syn* isomers of the desired product **27** were isolated as a shining orange powder by flash column chromatography.

^{1}H- and ^{19}F-NMR spectra confirmed the presence of the two isomers of the product. In the ^{1}H NMR spectrum, two sets of signals for the BODIPY-core protons are present, one of which is sharp and the other broad. The ^{19}F-NMR spectrum (Figure 7) shows a quartet at -146 ppm for the *anti* isomer and two doublets of quartets at -145.9 and -147.2 ppm for the *syn* isomer.

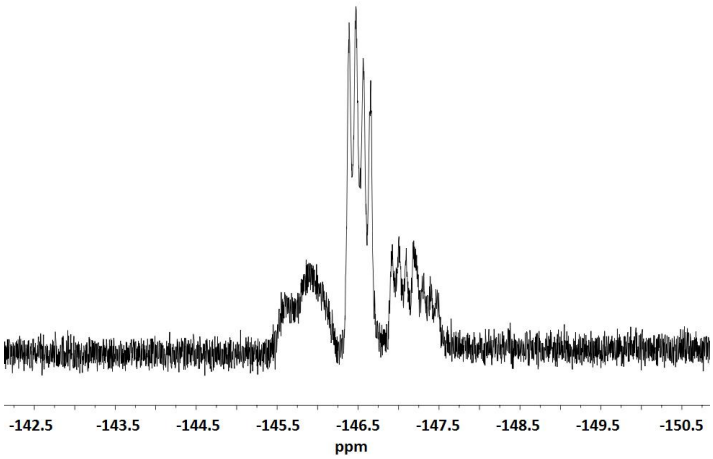

Figure 7. *^{19}F-NMR spectrum ($CDCl_3$, 400 MHz) of compound **27**.*

Compound **27** was then aromatized via a retro Diels-Alder reaction, by heating the sample for 5 h at 210 °C under vacuum (0.1 mmHg) and in a sand bath. After

cooling to room temperature, pure **28** was collected in quantitative yield as a blue/violet solid. ^{1}H-NMR analysis (Figure 8) confirmed the disappearance of the ethylenic bridge, whose signals were in the aliphatic spectral region (in the range 1.72-1.44 ppm), in favor of the appearance of aromatic peaks (two doublets at 8.49 and 7.75 ppm and a triplet at 7.59 ppm). In addition, broad signals changed in narrow signals and this was considered diagnostic for the aromatization, because only one geometry of the aromatic system is possible. The signals of the phthalimide group at 7.96 and 7.79 ppm were not modified, confirming its stability at high temperatures.

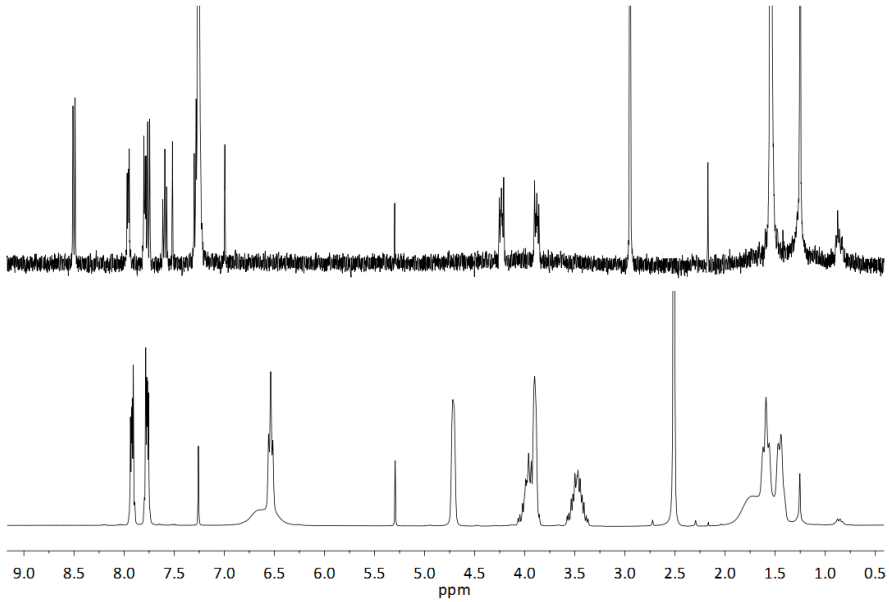

Figure 8. *^{1}H-NMR spectra ($CDCl_3$, 400 MHz) of compound **27** (bottom) and **28** (top).*

Unfortunately, the last step of the synthetic pathway, the removal of the protecting group to obtain the target compound **29**, resulted much more difficult than expected.

Hydrazinolysis in ethanol did not yield the deprotected product, but even after several hours only the starting reagent was present in the reaction mixture. The addition of other solvents such as DMF or toluene had no effect. Only after

refluxing a methanol solution of **28** and hydrazine for 14 days a trace amount of product **29** was detected, together with other byproducts.

A second strategy using $NaBH_4$ in a mixture of 2-propanol and water in acidic condition (acetic acid) was performed. As reported by Osby et al.,[28] this method may be superior in cases where hydrazine proves to be inefficient. However, probably because of the poor solubility of compound **28**, also this attempt failed and only the starting material and some intermediates were observed after 5 days.

Another reported method for the deprotection from phthalimide employs methylamine in aqueous or alcoholic solution. Compound **27** was added to a solution of 33% methylamine in ethanol and the mixture was stirred at rt for 3 days. ^{1}H-NMR and ESI mass spectrometry analysis of the crude revealed the presence of a mixture of several products, including a small amount of the desired product, which nonetheless could not be isolated by chromatography.

It was proposed that these discouraging results could be due to the scarce solubility of the aromatic starting material and/or to the steric hindrance around the phthalimide nitrogen atom given by the BODIPY core. The first hypothesis proved indeed to be the correct one, since the hydrazinolysis of **27**, the non aromatic precursor of **28**, resulted in the deprotection of the phthalimide group.

^{1}H-NMR (Figure 9) and ESI-MS analysis of the product, however, indicated that together with the phthalimide removal, hydrazine had also caused the reduction of the non-conjugated double bonds, yielding compound **30** (Figure 10).

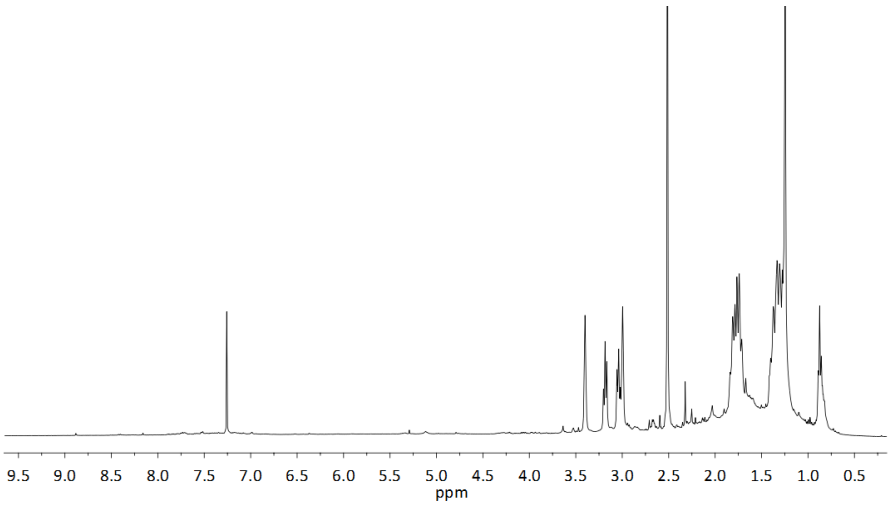

Figure 9. *^{1}H-NMR spectra ($CDCl_3$, 400 MHz) of compound **30**.*

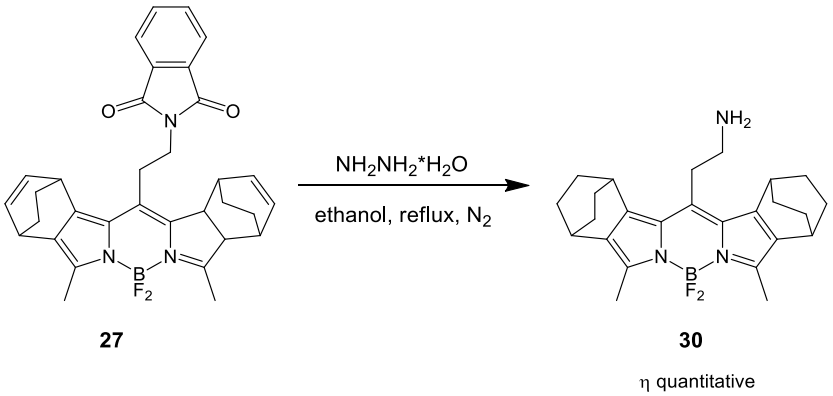

Figure 10. *Phthalimide removal and double bond reduction performed by hydrazine on precursor **27**.*

The UV-vis spectrum of BODIPY **30** in chloroform showed the maximum absorption wavelength at 525 nm. Since the instrumentation used at LENS laboratories adopts a light source whose cut-off is around 550 nm, BODIPY **30** was not considered suitable for our studies.

- A small variation on the structure of target BODIPY 29: compound 34

A new attempt to synthesize dibenzo-fused BODIPY was performed by reacting pyrrole derivative **26** with bromoacetyl chloride (Figure 11). The use of this

reagent instead of chloropropionyl chloride (see above) would have avoided the problems related to the elimination side-reactions occurred during the attempted synthesis of BODIPY **36**. The bromide would have been subsequently converted to amine either before or after the aromatization step, to obtain dye **34**, which differed from the initial target **29** for a shorter chain (one carbon atom instead of two) on the *meso* position.

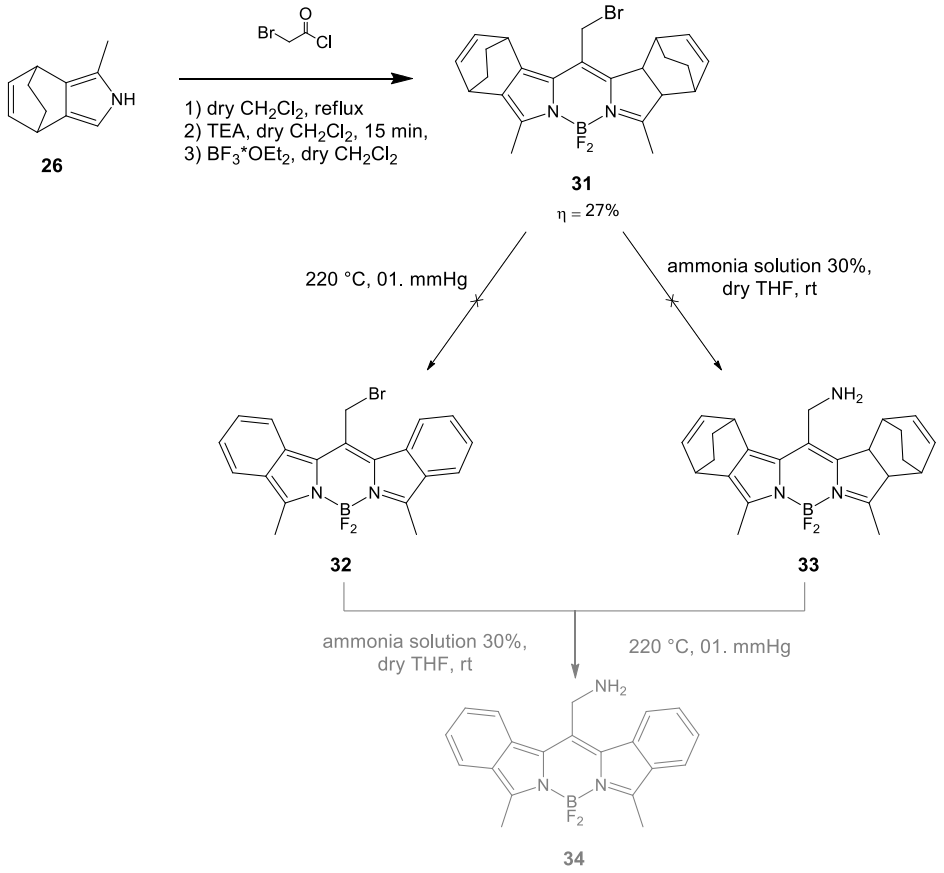

Figure 11. *Planned synthesis of BODIPY **34**.*

Compound **31** was obtained in 27% yield by reaction of compound **26** with bromoacetyl chloride, following a literature procedure reported for similar compounds.[25]

Compound **31** was divided into two portions to test which sequence of reactions (amination-aromatization or aromatization-amination) would give the higher yield.

Unfortunately, none of the two attempts was successful, since the first step failed in both cases: amination led to a mixture of products where desired compound **33** was present only in trace (based on TLC monitoring). The ^{1}H NMR spectrum of the product of the aromatization reaction **32**, even if it showed the presence of the aromatic protons (multiplets at 8.01-7.93 ppm, 7.75-7.72 ppm, 7.44-7.39 ppm and 7.35-7.26 ppm), lacked the signal corresponding to the CH_2Br group (at 4.95 ppm for compound **31**).

Considering all these failures, a new couple of BODIPYs was proposed for the synthesis.

3.4.2. Second couple of BODIPYs: 42 and 43

The second couple of chromophores (dyes **42** and **43**) are inspired to compounds **III** and **IV**[21] (Figure 12), supposing that little changes on non-conjugated substituents linked to the BODIPY core would not significantly affect the spectroscopic properties.

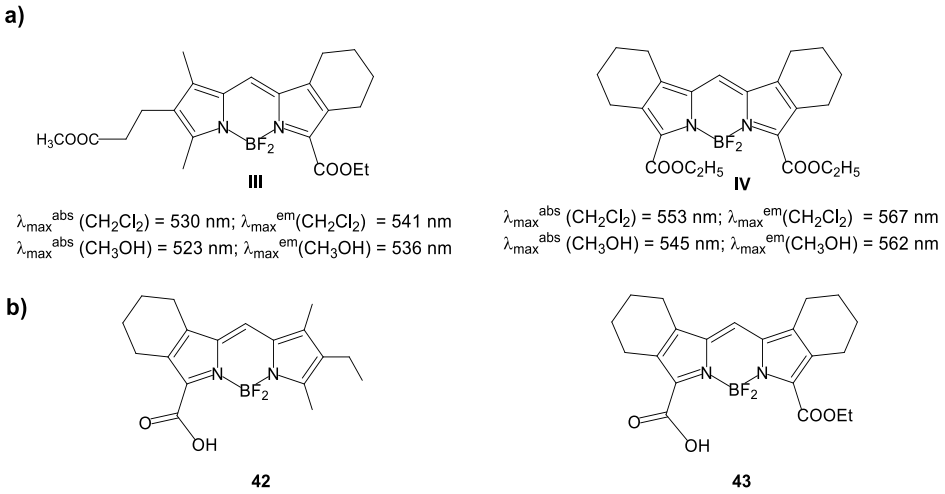

Figure 12. *a) Literature compounds BODIPYs **III** and **IV**, b) designed compounds **42** and **43**.*

These dyes would be condensed to dihydroxymethylencalix[4]arene **44** through their carboxylic acid groups obtaining the bichromophoric target **45** (Figure 13). In this way the ester groups of **III** and **IV** would be maintained.

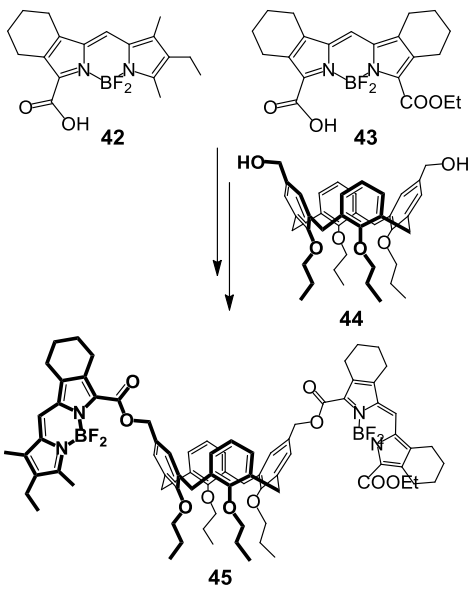

Figure 13. *Proposed coupling for the synthesis of compound **45**.*

A retrosynthetic analysis for compounds **42** and **43** is proposed in Scheme 5.

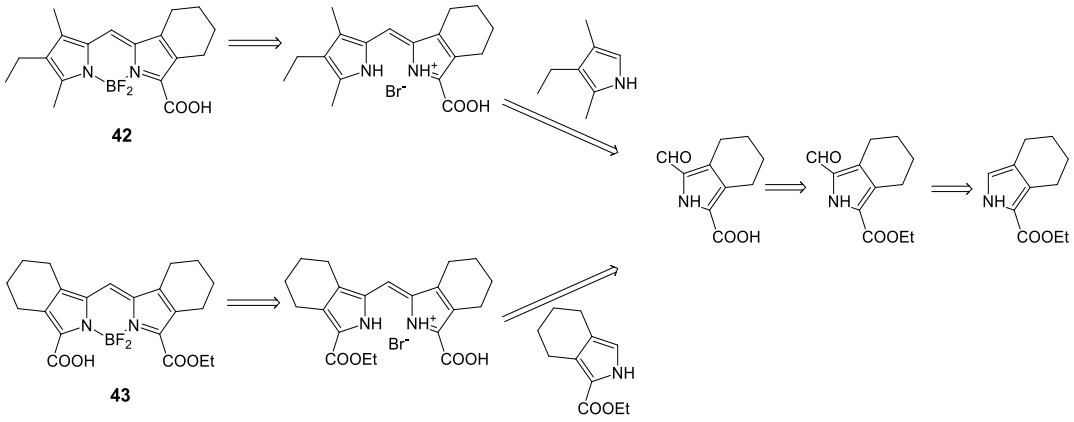

Scheme 5. *Retrosynthetic analysis for compounds **42** and **43**.*

The synthetic pathway planned for the synthesis of BODIPY **42** is reported in Figure 14. The commercially available ethyl-4,5,6,7-tetrahydroisoindole ester was formylated on the free pyrrolic position through the Vilsmeier-Haak reaction and, subsequently, the ethyl ester group of **39** was hydrolyzed to carboxylic acid isolating compound **40** as a brown solid in 90% overall yield.

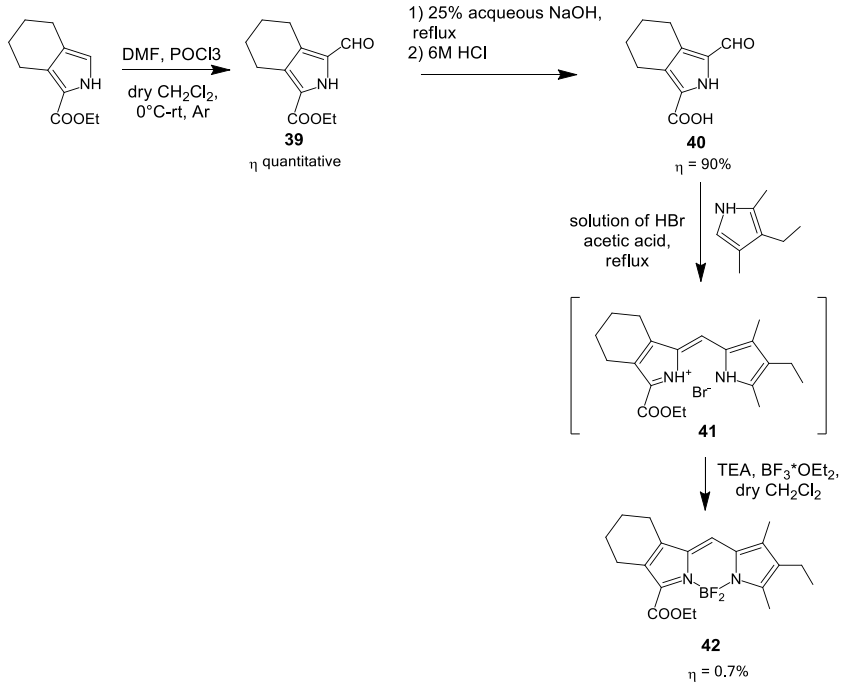

Figure 14. *Synthesis of compound **42**.*

Compound **40** was condensed with commercially available 3-ethyl-2,4-dimethylpyrrole in strong acid conditions following a literature procedure[29] reported for the synthesis of similar compounds, which consisted in the heating of a solution of the reagents and concentrated HBr in acetic acid. The crude mixture was analyzed by ESI mass spectroscopy that showed the presence of compound **41** among other byproducts. However, due to the reported instability of dipyrromethene,[29] the product was used without purification for the next step. The crude mixture containing **41** was then reacted with boron trifluoride diethyletherate in presence of triethylamine. The reaction yielded a complex mixture of several products, from which BODIPY **42** was isolated as an orange/pink solid in 0.7% yield.

Due to the difficulties met with this synthetic procedure and to the very low yield, also this pathway was discarded.

3.4.3. Third couple of BODIPYs: Bistyryl-BODIPYs 56 and VI

The third couple of BODIPYs considered for the synthesis of the bichromophoric system belongs to the family of 3-styryl BODIPYs. These dyes are obtained by the Knoevenagel condensation of 3-methyl pyrroles with aromatic aldehydes (Figure 15).[30]

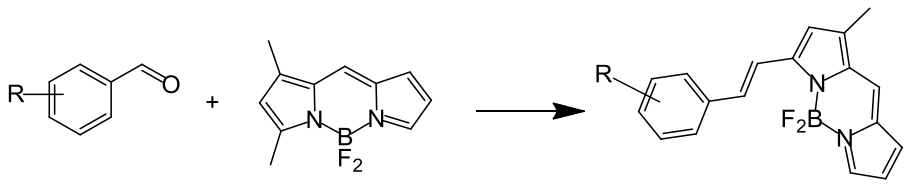

Figure 15. *Reaction scheme for the synthesis of 3-styryl BODIPY.*

Knoevenagel condensation normally takes place under basic conditions or in buffer and requires the removal of water from the mixture by a Dean-Stark apparatus, or by using molecular sieves. Although this reaction is of widespread use, yields are often low, or not reported in literature.

The styryl BODIPYs are particularly interesting for our purposes, because their absorption and emission wavelengths can be tuned according to the aldehyde used in the Knoevenagel condensation. In particular, the presence of electron-donating substituents on the *p*-position of the phenyl ring results in a red-shift of the dye absorption and fluorescence, due to the extended π-conjugation.[31] J.-S. Lee and coworkers[30] reported the synthesis of a 238 members BODIPY library by Knoevenagel condensation in microwave assisted conditions of 1,3-dimethyl BODIPY **48** with 238 different aldehydes. Among these compounds we selected styryl BODIPYs **V** and **VI** (Figure 16), whose spectral properties satisfy all the requirements for the investigation of the possible occurrence of quantum coherence energy transfer (e.g. maximum absorption wavelengths longer than

550 nm, short distance between the absorption maxima, narrow absorption and emission bands).

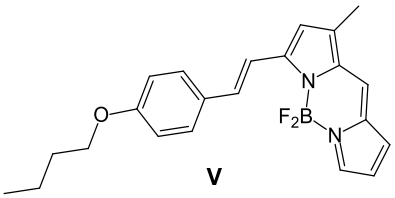

V

λ_{max}^{abs} (EtOH) = 560 nm

λ_{max}^{em} (EtOH) = 580 nm

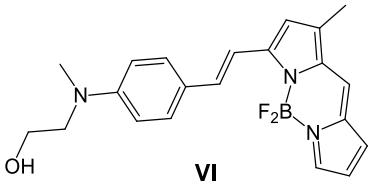

VI

λ_{max}^{abs} (EtOH) = 605 nm

λ_{max}^{em} (EtOH) = 725 nm

Figure 16. *Third couple of BODIPYs selected from ref. 30.*

While dye **VI** presents a terminal hydroxyl group useful for linkage to the calixarene, the same group can be easily inserted in BODIPY **V** using the appropriate benzaldehyde (Figure 15Figure 15), obtaining dye **56** (Figure 17), presumably having the same spectroscopic properties of **V**.

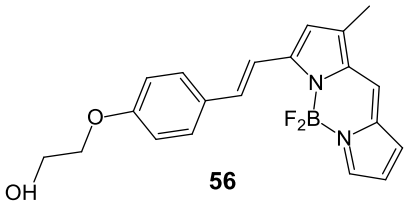

56

Figure 17. *Compound **56**.*

However, instead of preparing the styryl BODIPYs **56** and **VI** and react them with the calixarene derivative, it was decided to first anchor the two different aldehydes on the calixarene through nucleophilic substitution according to a *statistical approach* (see Chapter 2) and, in a second time, condense BODIPY **48** with the aldehydes by Knoevenagel reaction (Figure 18). This sequence was preferred because of the strong basic conditions required in the nucleophylic substitution step, which could affect the BF_2 stability.

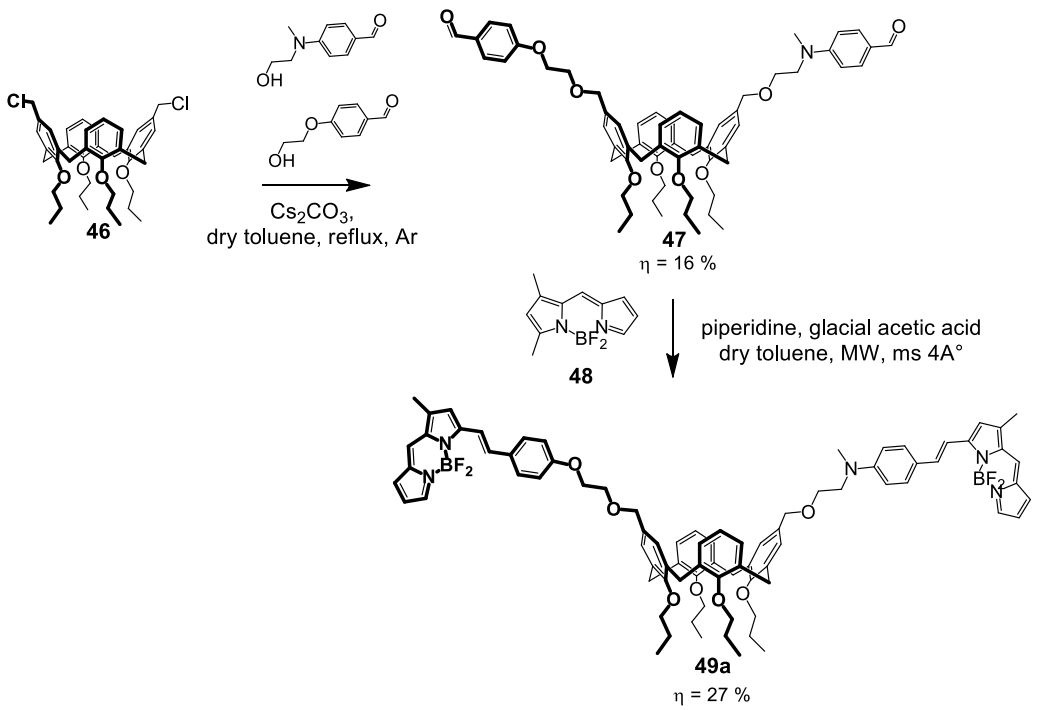

Figure 18. *Synthetic procedure to bichromophoric calix[4]arene **49a**.*

Calix[4]arene **46** was reacted with an equimolar mixture of the two benzaldehyde derivatives in toluene, in presence of cesium carbonate. The reaction mixture was refluxed for four days in order to obtain, on TLC plates, the complete disappearance of reagent **46** and the appearance of three new spots, corresponding to the three statistical products. Purification by flash column chromatography afforded the desired compound **47** in 16% yield.

Calixarene **47** was then reacted with 2 equivalents of 1,3-dimethyl BODIPY **48**, previously prepared according to a literature procedure,[30] in presence of piperidine and acetic acid. Different reaction conditions were tested with the aim to increase the yield of the Knoevenagel reaction:

- microwave assisted reaction with toluene as solvent and some 4 Å molecular sieves (procedure reported in refs 30 and 31a).

The condensation reaction was carried out with consecutive 15-35 min microwave irradiation (200 W) steps maintaining the temperature at 110 °C. After every step, the reaction mixture was cooled to room temperature and monitored by TLC. The reaction was stopped after six steps, when no change from the previous step was observed. From the crude mixture were isolated by preparative TLC the desired product **49a** (21% yield) and the mono-styryl BODIPY derivatives **49b** and **49c** (23% yield for **49b** and 28% yield for **49c**, Figure 19).

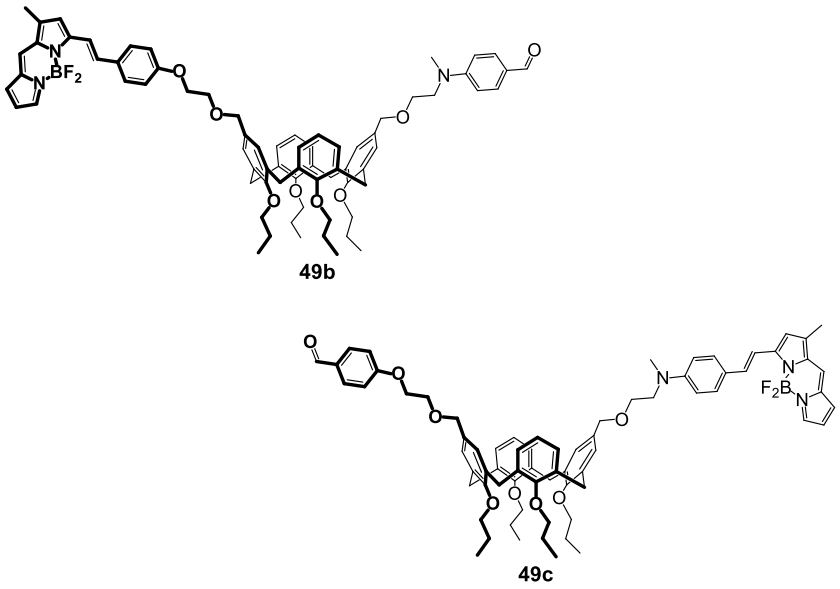

Figure 19. *Mono-styril BODIPY intermediates **49b** and **49c**.*

Compounds **49b** and **49c** were reunited and subjected to the Knoevenagel condensation in the conditions previously described, obtaining product **49a** in 11% yield. The overall yield of the two processes was 27%.

- Ultrasound promoted condensation in toluene at room temperature (procedure reported in refs 32 and 33).

  In these conditions the reaction proceeded very slowly and after 10 h only a small consumption of reagents **47** and **48** was observed.

- Reflux heating in acetonitrile.*

  After 24 h a small amount of **49a** had formed, but no progression of the reaction was observed. The reaction was then quenched and **49a** was isolated by flash column chromatography in 7% yield. Also in this case, an additional aliquot of **49a** was obtained in 23% yield by further reaction of the intermediates **49b** and **49c.** The overall yield for the two steps was 10%.

In light of these results, it has been possible to confirm the better performance provided by the reaction assisted by microwaves both in terms of reaction time and overall yields. A partial degradation of the bichromophoric compound **49a** when heated over 40 °C was observed by UV-vis spectroscopy. The spectra measured before and after the heating process (Figure 20), in fact, show a modification of the absorption band shape, corresponding to a decrease of the band centered at 608 nm (which is related to BODIPY **57**, see below). This may be due to the detachment of the BODIPY core. TLC analysis supports this hypothesis, thanks to the appearance of a yellow spot corresponding to the isolated BODIPY **48**. Without further investigation, it is possible to attribute the very low yields also to a degradation of the desired product under high temperature reaction conditions. The shorter reaction times allowed by the microwave assistance enable to reduce this thermal degradation.

* The reflux heating in toluene was also tested, but with even lower yields

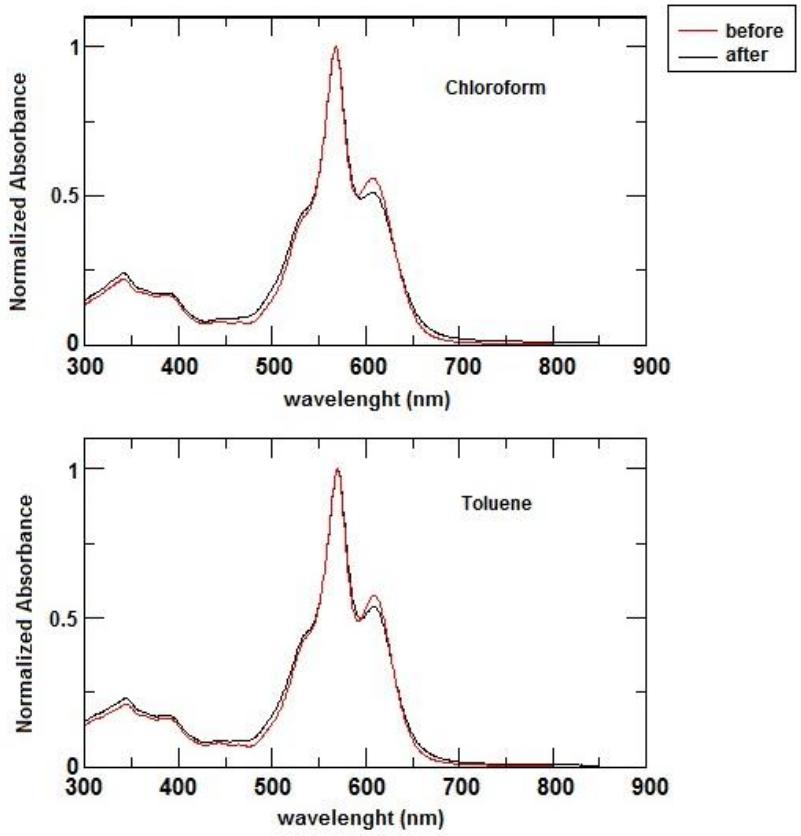

Figure 20. *Changes in the absorption spectra of **49a** after heating the sample at 50°C for 15 min.*

The bichromophoric calixarene **49a** was fully characterized by ^{1}H, ^{13}C and ^{19}F NMR spectroscopy and by High-res ESI-MS. 2D-COSY and NOESY spectra were registered to completely assign the proton resonances. The conformation adopted by **49a** in solution was investigated by ^{1}H-NMR spectroscopy. Spectra were collected in two different solvents, to highlight if significant changes in the chemical shifts of the aromatic protons occurred, depending on the polarity of the medium. Analysis in acetone-d_6 and $CDCl_3$ (Figure 21) indicated, in both solvent, a *regular cone* conformation with C_{4V} symmetry for the calixarene scaffold, as indicated by the isochrony of all the aromatic protons (a multiplet at 6.53-6.72 ppm in $CDCl_3$ and 6.59-6.54 ppm in acetone-d_6). This apparent C_{4v} symmetry is indeed the result of the fast equilibrium between two opposite *flattened cone*

conformations (see Chapter 2, paragraph 2.3.5). In this case, differently from what observed for compounds **8a** and **14a**, the two equilibrating structures have roughly the same stability, due to the absence of attractive intermolecular interactions between the two upper rim substituents and to the flexibility of the -OCH_2CH_2- spacer between the macrocycle and the BODIPYs that prevents strong steric repulsions between the chromophores.

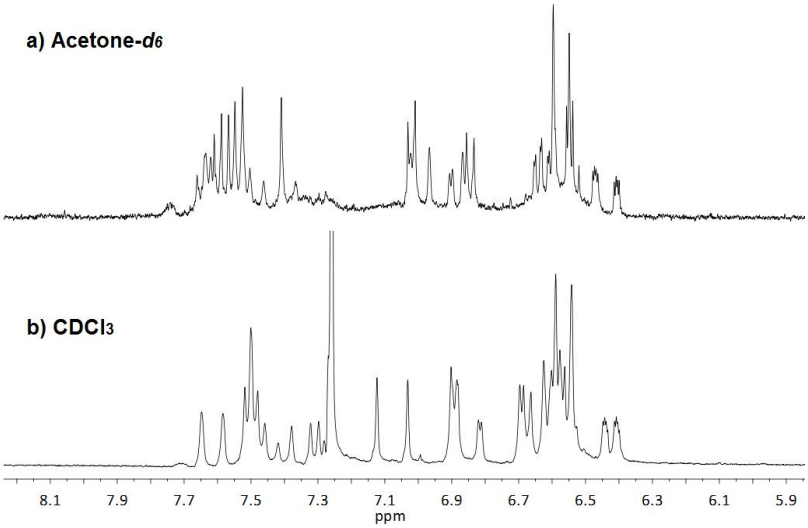

Figure 21. *Portion of ^{1}H-NMR spectra (400 MHz) of compound **49a** in a) Acetone-d_6 and b) $CDCl_3$.*

- Synthesis of monochromophoric compounds 53 and 56

The synthesis of the monochromophoric calix[4]arenes functionalized with only one styryl-BODIPY unit at the upper rim was then undertaken, to obtain the reference compounds for the spectroscopic studies. The synthetic pathway was similar to the one followed for the bichromophoric system **49a** (Figure 22 and Figure 23).

Calixarene **51** was prepared by reaction of hydroxymethyl calixarene **50**[34,35] with thionyl chloride.

Nucleophilic substitution in basic conditions by N-methyl-N-(2-hydroxyethyl)-4-aminobenzaldehyde afforded intermediate **52** in 32% yield, while the subsequent Knoevenagel condensation with BODIPY **48** in refluxing acetonitrile gave the desired compound **53** in 19% yield.

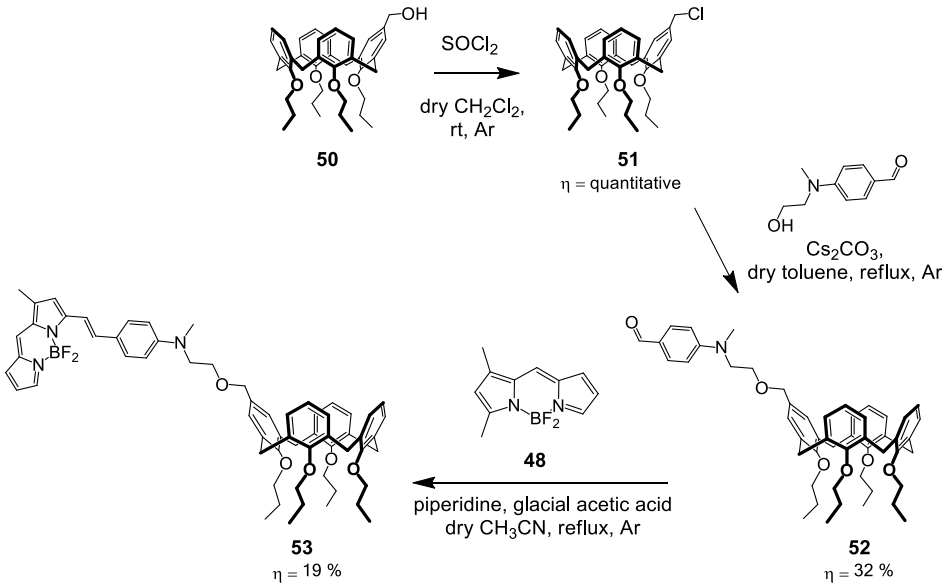

Figure 22. *Synthetic strategy followed for compound **53**.*

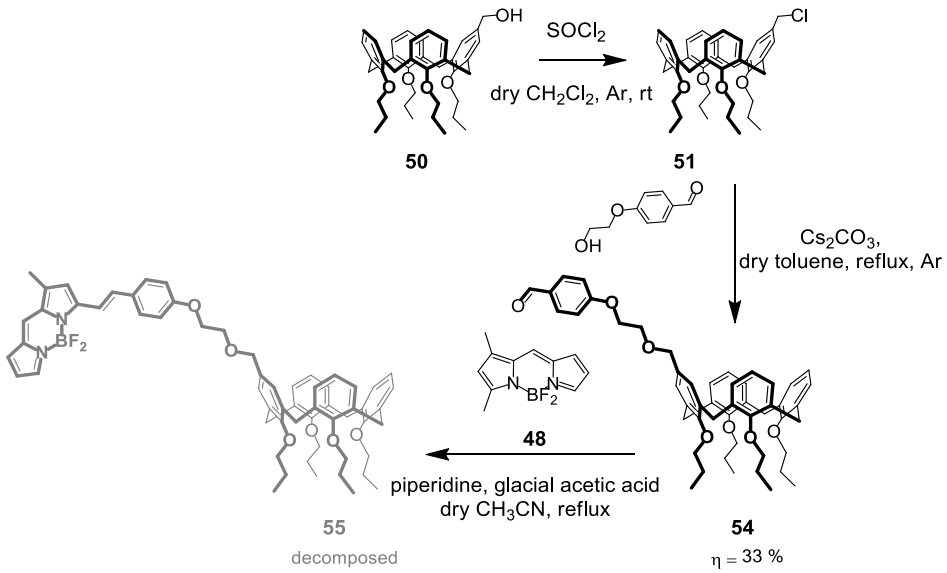

Figure 23. *Designed synthesis of compound **55***

To synthesize the second reference compound **55**, intermediate **54** was obtained in 33% yield by reaction of calixarene **51** with 4-(2-hydroxyethoxy)benzaldehyde. The subsequent Knoevenagel condensation, however, did not afford the target product. Although TLC analysis of the crude mixture indicated the presence of the desired product,[†] no compound was isolated after column chromatography, probably due to a degradation of the product during the chromatographic procedure.

Another attempt was performed by changing the order of the reactions (Figure 24).

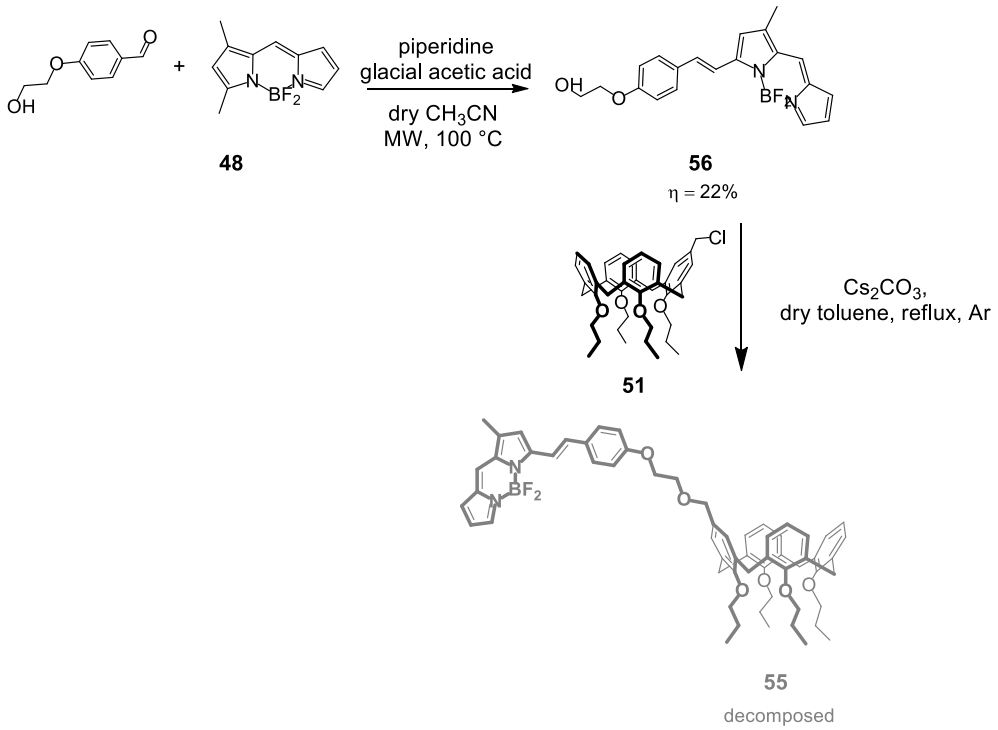

Figure 24. *Designed synthesis of compound **55** through intermediate **56**.*

Knoevenagel condensation between 4-(2-hydroxyethoxy)benzaldehyde and BODIPY **48** in dry CH_3CN and assisted by microwave irradiation afforded **56** as a violet solid in 22% yield. The following coupling with the calix[4]arene **51**,

[†] This assumption was made on the basis of the characteristic pink color of styryl BODIPY **V**.

however, failed. TLC analysis indicated the formation of a mixture of byproducts, none of which corresponded to the desired **55** derivative.

Due to the impossibility to synthesize monochromophoric **55**, intermediate **56** was used as a reference compound for preliminary spectroscopic studies.

3.5 Spectroscopic studies

3.5.1. Absorption and fluorescence studies

As described above (3.4.3), the couple of chromophores was chosen according to their spectroscopic properties,[30] in particular their quasi-degenerate excitations. Compounds **53** and **56** have been employed as references for a correct interpretation of the data collected on product **49a**.

Absorption and fluorescence spectra of **53** and **56** in chloroform are reported in Figure 25.

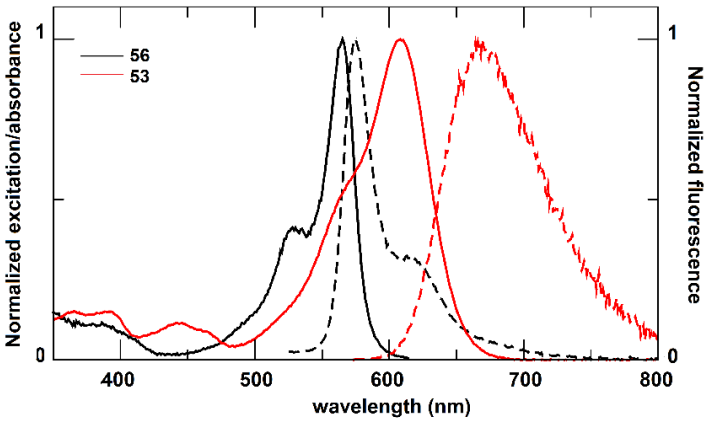

Figure 25. *Absorption (full lines) and fluorescence (dashed lines) spectra of compounds **56** (black lines) and **53** (red lines) in chloroform.*

The molar extinction coefficients of **53** and **56** could not be estimated due to the insufficient amount of product, so collected spectra were normalized.

The good overlap between the emission spectrum of **56** and the absorption spectrum of **53** is a prerequisite for an efficient energy transfer from **56** (that should act as energy donor) to **53** (that should behave as the energy acceptor). Due to the scarce overlap between the emission spectrum of **53** and the absorption spectrum of **56**, only weak back transfer is expected.

The spectroscopic characterization of compound **53** was performed in different solvents (cyclohexane, toluene, chloroform, acetonitrile and dimethyl sulfoxide, Figure 26). The fluorescence band is strongly solvatochromic, while absorption spectra are only marginally affected by the solvent polarity. Moreover, the fluorescence quantum yield decreases with increasing solvent polarity (Table 1), reaching very low values (Φ < 1%) in acetonitrile and dimethyl sulfoxide.

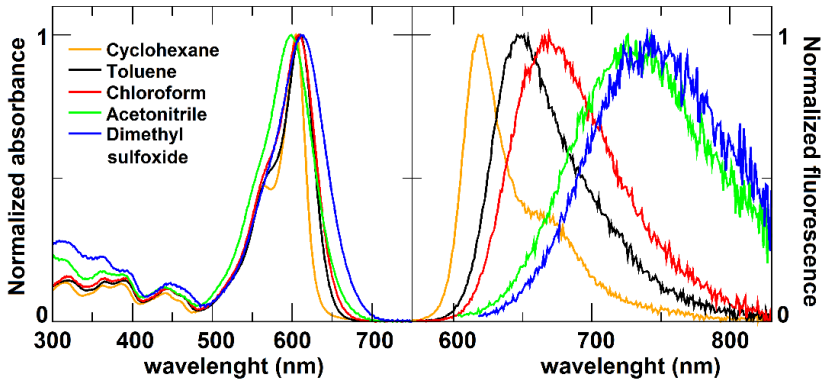

Figure 26. *Absorption and fluorescence spectra of compound **53** in solvents of different polarity.*

The second reference chromophore **56** was only qualitatively studied in chloroform (Figure 25), to give preliminary data to be completed once the envisaged reference (bearing the calixarene moiety) will be available.

Bichromophoric compound **49a** was studied in three different solvents: toluene, chloroform and acetonitrile (Figure 27). Fluorescence spectra reveal an efficient excitation energy transfer, as demonstrated by the strong quenching of the donor emission band, particularly in toluene and chloroform (in these solvents, in fact, the donor-emission/acceptor-absorption spectral overlap is high). Qualitative studies revealed the same solvatochromic fluorescence behavior for the acceptor band as for monomeric compound **53**: the acceptor fluorescence contribution in bichromophoric system **49a** is in the range 600-750 nm depending on the solvent

and its fluorescence quantum yield decreases for increasing solvent polarity (Table 1).

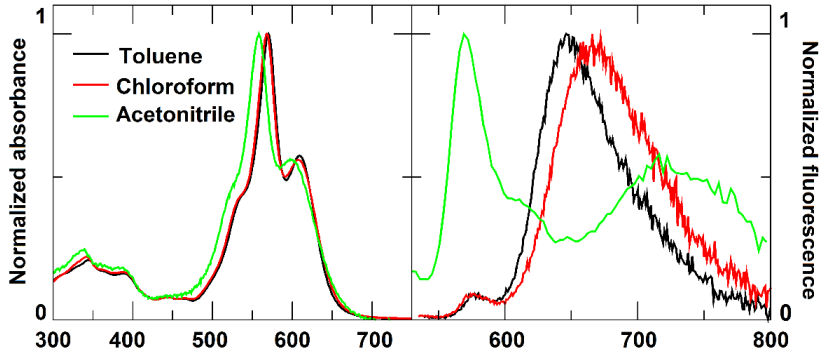

Figure 27. *Absorption and fluorescence spectra of compound **49a** in toluene, chloroform and acetonitrile.*

	Compound	λ_{abs}^{max} [nm]	ε [$M^{-1}cm^{-1}$] @ λ_{abs}^{max}	λ_{em}^{max} [nm]	Φ (λ_{exc})
	56	-	-	-	-
Toluene	**53**	610	-	646	0.71 (570)
	49a	570	57100	646	0.29 (534) 0.30 (570) 0.27 (609)
Chloroform	**56**	574[a]	-	565	-
	53	608	-	669	0.6 (568)
	49a	568	61800	666	0.34 (530) 0.33 (568) 0.28 (607)
Acetonitrile	**56**	-	-	-	-
	53	599	-	726	< 0.01
	49a	-	-	569	< 0.01

Table 1. *Absorption and emission properties of the investigated compounds **53**, **56**, **49a** in toluene, chloroform and acetonitrile. The reported quantum yields were obtained exciting the samples at the λ_{abs}^{max} reported in the second column. Fluorescein in 0.1 M NaOH was used as the standard (Φ = 0.9) for the determination of fluorescence quantum yields.[a] wavelength extracted by excitation spectrum in chloroform.*

3.5.2. Transient absorption measurements

With the aim to investigate the dynamics of the photoinduced excitation energy transfer, preliminary transient absorption measurements on compound **49a** have been performed in chloroform.

Transient absorption spectra of compounds **49a** have been recorded by exciting the samples in the donor absorption region, at 520 nm.

Figure 28 reports the bleaching of the donor species, picked at 565 nm, and a broader band at higher wavelengths, due to the acceptor bleaching and stimulated emission. The co-presence of these signals confirms the occurrence of energy transfer between the two chromophoric units in **49a**.

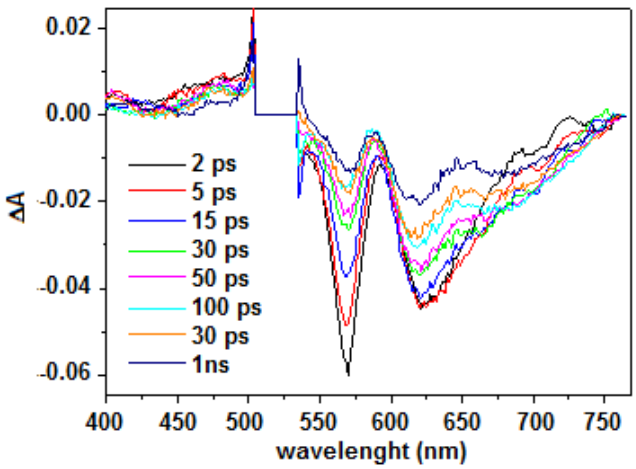

Figure 28. *Selected transient absorption spectra of compound **49a** measured in chloroform upon excitation at 520 nm.*

The donor stimulated emission is hidden by acceptor excited state absorption (picked at 580 nm). At higher delays (>20 ps) the broad bleaching/stimulated emission becomes more structured and two well-defined bands can be distinguished.

The dynamics of the different spectral features is reported in Figure 30.

The transient data were analyzed with a global analysis procedure, applying a sequential decay scheme. The EADS obtained by global analysis are reported in Figure 29 and reveal a multiexponential energy transfer. Two components have been observed, a faster (0.8 ps) and a slower one (26 ps), while the excited state of **49a** lives 1.5 ns.

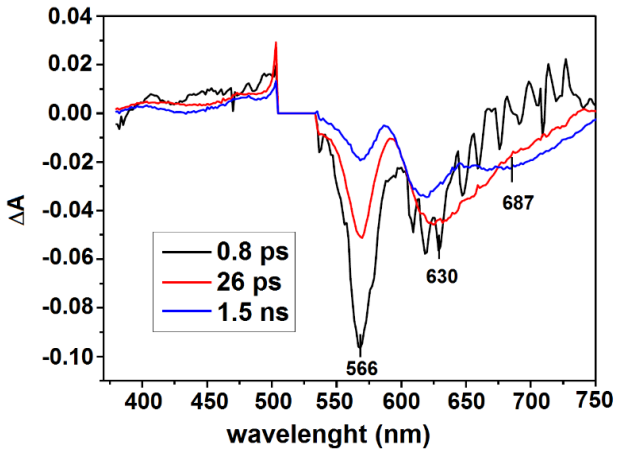

Figure 29. *Extracted EADS from global analysis.*

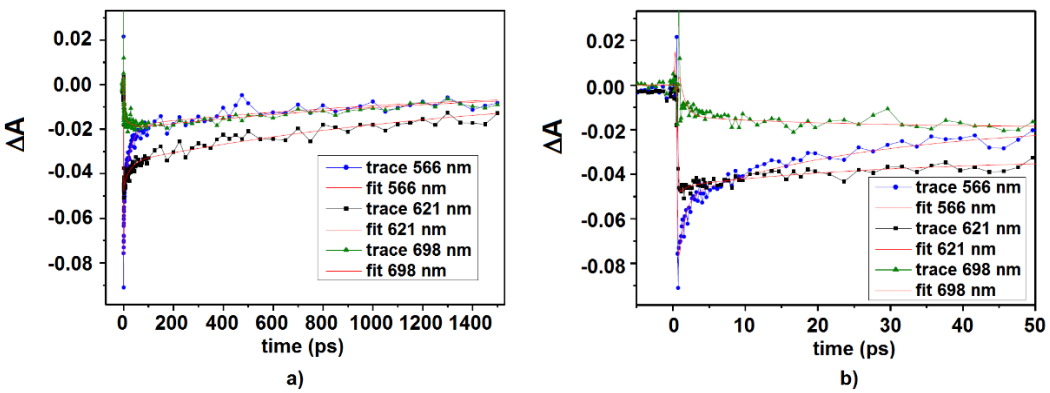

Figure 30. *a) Kinetic traces and corresponding fit at different wavelengths: donor bleaching (566 nm), acceptor bleaching (621 nm) and acceptor stimulated emission (698 nm). Earlier 50 ps are magnified in b).*

Focusing on the intensity of the donor bleaching band from the black to the red line, it is possible to conclude that the faster dynamics corresponds to 40-45% of

the energy transfer, whose yield, calculated on the donor moiety bleaching, has been estimated to amount to 85-90%.

The multiexponential decay can be ascribed to the presence of several conformations, due to the flexible nature of the linkers between the calixarene scaffold and the chromophores. Interconversion among the different conformations is very fast on NMR timescale, in fact this process is not observed via NMR.

When transient spectra are collected for excitation at 620 nm (where the acceptor absorbs, while the donor has negligible absorbance), a broad intense band is observed as due to acceptor bleaching/stimulated emission, but also a feature due to donor bleaching, at 570 nm (Figure 31). This suggests the occurrence of a weak back transfer from the "acceptor" to the "donor".

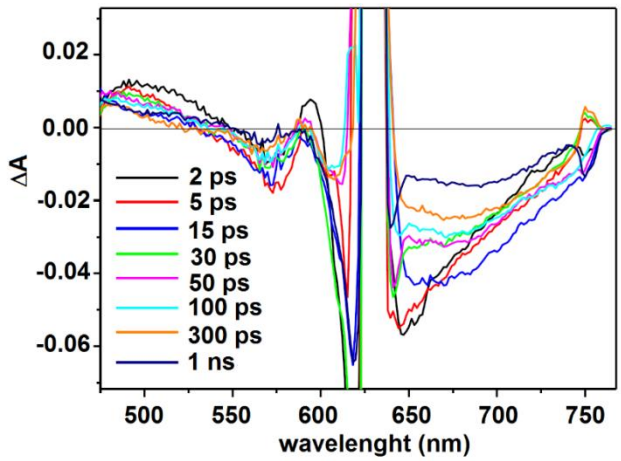

Figure 31. *Transient absorption spectra in chloroform at different delays, selectively exciting compound **49a** on the acceptor maximum absorption wavelength (at 620 nm).*

Also in this case, kinetic traces (Figure 33) depict a multiexponential decay, composed by a faster (2.5 ps) and a slower decay (4.7 ps), while the lifetime is estimated to be about 1.7 ns (Figure 32).

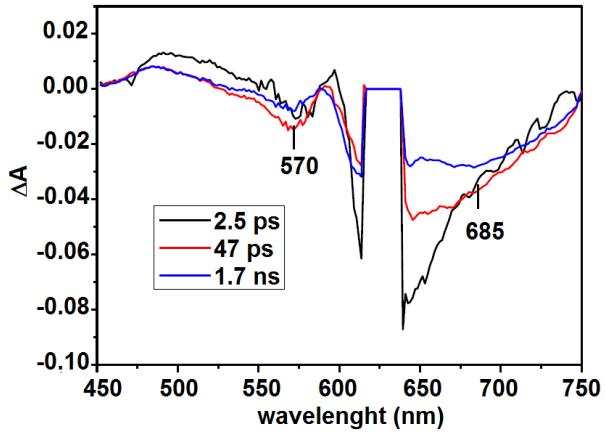

Figure 32. *EADS extracted from global analysis.*

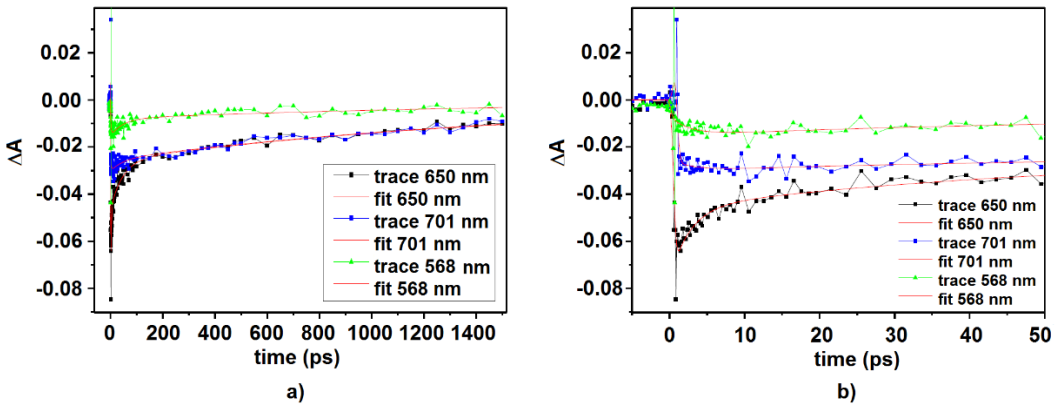

Figure 33. *a) Kinetic traces and corresponding fit at different wavelengths: donor bleaching (568 nm), acceptor bleaching/donor stimulated emission (650 nm) and acceptor stimulated emission (701 nm). Earlier 50 ps are magnified in b).*

Unfortunately, the absence of a considerable amount of monochromophoric derivatives **53** and **55** limits the investigations of the energy transfer dynamics. These preliminary studies, however, suggest compound **49a** as a good candidate for the study of quantum coherence energy transfer by 2D-electronic spectroscopy

3.6 Concluding remarks

In this chapter it is reported the synthesis of a donor-acceptor bichromophoric system potentially suitable to investigate the occurrence of quantum coherence energy transfer. The system is based on the functionalization of a *cone*-calix[4]arene scaffold with two different dyes, whose spectroscopic properties had to fulfill stringent requirements (quasi-degenerate excitations, absorption bands in the red spectral region of the visible spectrum and narrow absorption and fluorescence bands). The choice fell on the BODIPY dyes, a family of highly fluorescent, chemically stable chromophores characterized by narrow bands, whose absorption and emission wavelengths can be tuned according to the peripheral substituents of the BODIPY core.

Three couples of BODIPYs have been selected to be linked to the calixarene, but only one of them was successfully synthesized.

The chromophores of the first couple were dibenzo-fused BODIPYs functionalized with an amino-terminating short alkyl chain for linkage to the calixarene. Their synthesis failed because of problems both in the aromatization step and in the amine protecting group removal.

The second couple of chromophores, characterized by the presence of an ester group, was discarded because the dipyrromethene intermediate could not be synthesized.

The third couple of chromophores is constituted by two styryl BODIPYs. Thanks to a synthetic strategy based on the functionalization of the calix[4]arene upper rim with the two different aromatic aldehydes and their subsequent Knoevenagel condensation with a previously synthesized BODIPY core, the bichromophoric system **49a** has been synthesized, even if in quite low yield.

Dyad **49a** was characterized by absorption and fluorescence spectroscopy, showing the efficient occurrence of energy transfer between the dyes. However, due to the little amount obtained for the reference compounds **56** and **53** quantitative studies could not be performed.

Preliminary transient absorption studies with pump-probe technique performed on **49a**, highlighted multiexponential energy transfer. The fastest dynamics, among the two observed, corresponds to 40-45% of the energy transfer, whose yield, estimated through the donor bleaching, amounts to 85-90%.

A weak back transfer from the acceptor to the donor has also been recognized when exciting the acceptor chromophore.

Further investigations, based on the analysis of monochromophoric references, are required to better understand the dynamics involved in the energy transfer.

Finally, the possible contribution of quantum-coherent effects could be investigated by means of 2D-electronic spectroscopy.

3.7 Experimental Section

General methods

All moisture sensitive reactions were carried out under Nitrogen or Argon atmosphere, using previously oven-dried glassware. Dry solvents were prepared according to standard procedures, distilled before use and stored over 3 or 4 Å molecular sieves. Most of the solvents and reagents were obtained from commercial sources and used without further purification. Analytical TLC was performed using prepared plates of silica gel (Merck 60 F-254 on aluminium) and then, according to the functional groups present on the molecules, revealed with UV light. Merck silica gel 60 (70-230 mesh) was used for flash chromatography and for preparative TLC plates. ^{1}H NMR ^{13}C and ^{19}F spectra were recorded on Bruker AV300 and Bruker AV400 spectrometers (observation of ^{1}H nucleus at 300 MHz and 400 MHz respectively, and of ^{13}C nucleus at 75 MHz and 100 MHz respectively). All chemical shifts are reported in part per million (ppm) using the residual peak of the deuterated solvent, whose values are referred to tetramethylsilane (TMS, δ_{TMS}= 0), as internal standard. All ^{13}C NMR spectra were performed with proton decoupling. Mass spectra were recorded in ESI mode on a single quadrupole instrument SQ Detector, Waters (capillary voltage 3.7 kV, cone voltage 30-160 eV, extractor voltage 3 eV, source block temperature 80 °C, desolvation temperature 150 °C, cone and desolvation gas (N_2) flow rates 1.6 and 8 L/min, respectively). High resolution mass spectra were recorded on a LTQ Orbitrap XL instrument in positive mode using CH_3CN or CH_3OH as solvents. Melting points were determined on an Electrothermal apparatus in closed capillaries.

UV-vis absorption spectra were recorded on a Perkin Elmer Lambda 650 spectrometer. Steady-state fluorescence spectra and fluorescence decays were carried out on a Fluoromax-3 Horiba Jobin Yvon spectrofluorometer. Fluorescence decays were measured in a TCSPC (time-correlated single-photon counting) configuration, under excitation from selected nanoLED or laser-diode sources; fluorescence lifetimes were obtained from the reconvolution fit analysis of the decay profiles; the quality of the fits was judged by the reduced χ^2 value (fits are retained for $\chi^2 < 1.1$).

2-Methyl-4,7-dihydro-4,7-ethano-2*H*-isoindole (**26**),[26] 3-Phthalimidopropionic acid **pht-β-Ala-OH**,[27] 1-(2-Phthalimidopropionyl)chloride **pht-β-Ala-Cl**,[27] 5,17-bis(chloromethyl)-25,26,27,28-tetrapropoxycalix[4]arene (**46**),[36] 4,4-Difluoro-5,7-dimethyl-4-bora-3a,4a-diaza-S-indacene (**48**),[30] and 5-hydroxymethyl-25,26,27,28-tetrapropoxycalix[4]arene (**50**)[34,35] were synthesized according to literature procedures.

2,3-Bis(phenylsulfonyl)bicyclo[2.2.2]oct-5-ene (24) was synthesized according to the literature.[23]

M. p.: 146.5-146.9. ^{1}H-NMR ($CDCl_3$, 300 MHz): δ (ppm) 7.93-7.84 (m, 2H, ArH); 7.76-7.50 (m, 8H, ArH); 6.32 (t, J = 7.2 Hz, 1H, CH vinylic); 6.23 (t, J = 7.2 Hz, 1H, CH vinylic); 3.93-3.91 (m, 2H, CH); 3.76-3.73 (m, 2H, CH); 3.16-3.14 (m, 1H, CH); 3.06-3.04 (m, 1H, CH); 2.24-2.31 (m, 1H, C*H*H); 1.68-1.62 (m, 1H, C*H*H); 1.41-1.35 (m, 1H, CH*H*); 1.13-1.09 (m, 1H, CH*H*). ^{13}C-NMR ($CDCl_3$, 100 MHz): δ (ppm) 139.3; 139.0; 134.2; 134.1; 133.14; 133.13; 129.41; 129.39; 128.8; 128.6; 66.1; 63.5; 31.9; 31.3; 23.4; 20.0.

Ethyl 4,7-dihydro-4,7-ethano-2*H*-isoindole-1-carboxylate (25) was synthesized according to the literature.[23] Pure product was isolated by recrystallization from CH_2Cl_2/hexane in 74% (3.750 g, 17.3 mmol) yield.

It showed the same spectroscopic data previously reported.[37]

Ethyl-2*H*-isoindole-1-carboxylate (35)

Compound **35** was synthesized by heating Ethyl-4,7-dihydro-4,7-ethano-2*H*-isoindole-1-carboxylate (**25**, 410 mg, 1.95 mmol) at 280°C for 5 minutes in a sand bath. Pure product was isolated by chromatography (hexane/ethyl acetate 75/25) in 29% yield (105 mg, 0.56 mmol).

Compound **35** showed the same spectroscopic data previously reported.[22]

Compound 27

To a stirred solution of **26** (689 mg, 4.33 mmol) in dry CH_2Cl_2 (30 mL), a solution of **pht-β-Ala-Cl** (501 mg, 2.11 mmol) in dry CH_2Cl_2 (20 mL) was added. The reaction mixture was refluxed for 3 h, then it was cooled to room temperature and TEA (880 µL, 6.33 mmol) was added. After 30 min, BF_3OEt_2 (1.6 mL, 12.66 mmol) was added, and the violet solution was stirred at rt. After 20 h, TLC (cyclohexane/ethyl

acetate 80/20) indicated the complete consumption of the starting materials. The reaction was then quenched by adding aqueous HCl 1M (50 mL) and the two phases were separated. The aqueous layer was extracted with CH_2Cl_2 (3×40 mL) and the combined organic layers were washed with H_2O till neutral pH, dried over $MgSO_4$ and concentrated under reduced pressure. The violet crude was purified by two subsequent flash column chromatographies (first column: gradient cyclohexane/ethyl acetate 80/20- 70/30, then pure CH_2Cl_2; second column: CH_2Cl_2). Pure product **27** was isolated as an orange/pink powder in 30% (342 mg, 0.62 mmol) yield.

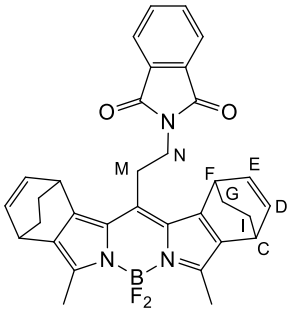

27

M.p.: was not measured because of retro Diels-Alder reaction over 200 °C. ^{1}H-NMR ($CDCl_3$, 400 MHz): δ (ppm) 7.93 (dd, J_1 = 5.5 Hz, J_2 = 2.8 Hz, 2H, H-pht); 7.78 (dd, J_1 = 5.5 Hz, J_2 = 2.8 Hz, 2H, H-pht); 6.67 (bs, 2H, H_E and H_D); 6.56-6.52 (m, 2H, H_E and H_D); 4.71 (bs, 2H, H_C); 4.02-3.91 (m, 4H, H_F and H_N), 3.54-3.41 (m, 2H, H_M); 2.51 (s, 6H, CH_3); 1.75-1.44 (m, 8H, H_I and H_G). ^{13}C-NMR ($CDCl_3$, 75 Hz): δ (ppm) 168.2; 137.6; 136.1; 135.9; 134.6; 134.3; 127.3; 123.5; 82.9; 39.7; 37.9; 32.9; 28.8; 26.4;26.3; 12.48; 12.46. ^{19}F-NMR ($CDCl_3$, 400 MHz): - 145.9 (*syn*-diastereomer, bd, J_{F-F} = 114.3 Hz, 1F); -146.5 (*anti*-diastereomer, q, J_{F-B} = 32.2 Hz, 2F); -147.2 (*syn*-diastereomer, dq, J_{F-F} = 114.3 Hz, J_{F-B} = 34.4 Hz, 1F). ESI-MS: m/z calcd. for $C_{33}H_{30}BF_2N_3O_2$+Na^+ 572.2, found 572.5 (50%).

Compound 28

Compound **27** (41 mg, 0.07 mmol) was heated in a round bottomed flask at 210 °C under vacuum (0.1 mmHg) and in a sand bath. After 5 h, TLC (hexane/ethyl acetate 80/20) and ESI-MS indicated the complete consumption of the starting material. The flask was allowed to cool to rt and product **28** was collected in quantitative yield (35 mg, 0.07 mmol).

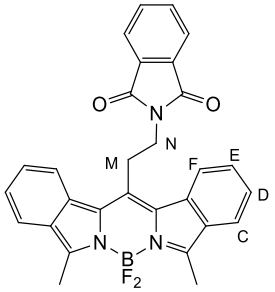

28

^{1}H-NMR ($CDCl_3$, 400 MHz): δ (ppm) 8.49 (d, J = 8.4 Hz, 2H, H_C); 7.96 (dd, J_1 = 5.5 Hz, J_2 = 2.8 Hz, 2H, H-pht); 7.79 (dd, J_1 = 5.5 Hz, J_2 = 2.8 Hz, 2H, H-pht); 7.75 (d, J = 8.0 Hz, 2H, H_F); 7.59 (t, J = 7.2 Hz, 2H, H_E); signal under $CDCl_3$ H_D; 4.25-4.21 (m, 2H, H_N), 3.90-3.86 (m, 2H, H_M); 2.95 (s, 6H, CH_3). ESI-MS: m/z calcd. for $C_{29}H_{22}BF_2N_3O_2$+Na^+ 516.2, found 516.4 (100%).

The scarce solubility of compound **28** did not allow its complete characterization.

Compound 30

$NH_2NH_2{\cdot}H_2O$ (230 µL, 4.75 mmol) was added to a solution of **27** (43 mg, 0.08 mmol) in absolute ethanol (9 mL), and the reaction mixture was heated at 80 °C for 6 h. The reaction was monitored by TLC (cyclohexane/ethyl acetate 80/20), then it was quenched by the addition of aqueous 6mM NaOH (50 mL) and extracted with CH_2Cl_2 (3x50 mL). The combined organic layers were washed with H_2O till neutral pH and concentrated under reduced pressure, affording **30** in 45% (15 mg, 0.04 mmol) yield.

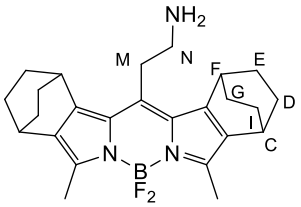

30

^{1}H-NMR ($CDCl_3$, 400 MHz): δ (ppm) 3.40 (bs, 2H, CH); 3.18 (t, J = 7.6 Hz, 2H, CH_2); 3.05 (t, J = 7.2 Hz, 2H, CH_2); 2.99 (bs, 2H, CH); 2.95 (s, 6H, CH_3); 1.81-1.67 (m, 8H, CH_2); 1.37-1.28 (m, 8H, CH_2). ^{19}F-NMR ($CDCl_3$, 400 MHz): δ (ppm) -146.3 (q, $J_{F\text{-}B}$ = 36.1 Hz, 2F). ESI-MS: m/z calcd. for $C_{25}H_{32}BF_2N_3$+Na^+ 446.2, found 446.2 (50%).

Compound 31

Bromoacetyl chloride (71 µL, 0.84 mmol) was added to a stirred solution of **26** (270 mg, 1.69 mmol) in dry CH_2Cl_2 (24 mL) and the reaction was allowed to proceed at rt for 3 h, when TLC monitoring (hexane/CH_2Cl_2 50/50) revealed the total consumption of **26**. TEA (350 µL, 2.51 mmol) and BF_3OEt_2 (1.6 mL, 12.66 mmol) were subsequently added and the violet solution was stirred at rt for 20 h. The reaction was quenched by adding H_2O (20 mL). The yellow aqueous layer was extracted with CH_2Cl_2 (3×40 mL) and the combined organic layers were concentrated under reduced pressure. Pure compound **31** was isolated from the purple crude by flash column chromatography (CH_2Cl_2/hexane 60/40), in 27% (109 mg, 0.23 mmol) yield.

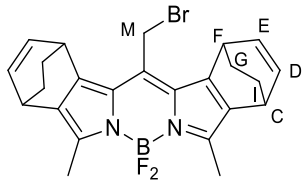

31

M.p. was not measured because of retro Diels-Alder reaction over 200 °C. ^{1}H-NMR ($CDCl_3$, 300 MHz): δ (ppm) 6.56-6.44 (m, 4H, H_E and H_D); 4.95 (s, 2H, H_M); 4.32-4.31 (m, 2H, H_C); 3.92-3.90 (m, 2H, H_F), 3.54-3.41 (m, 2H, H_M); 2.53 (s, 6H, CH_3); 1.69-1.43 (m, 8H, H_I and H_G). ESI-MS: m/z calcd. for $C_{24}H_{24}BBrF_2N_2$+Na^+ 491.1, found 491.5 (20%); m/z calcd. for $C_{24}H_{24}BBrF_2N_2$+K^+ 507.2, found 507.4 (10%).

3-Formyl-4,5,6,7-tetrahydro isoindole-1-carboxylic acid ethyl ester (39)

$POCl_3$ (770 µL, 8.27 mmol) was added dropwise to a solution of DMF (700 µL, 9.04 mmol) in dry CH_2Cl_2 (8 mL) at 0 °C The resulting solution was stirred at 0 °C until the formation of Vilsmeier complex as a solid white material. After the solid was dried in vacuo for 2 h, dry CH_2Cl_2 (1.5 mL) was added to the solid and the mixture was cooled to 0 °C. A solution of Ethyl 4,5,6,7-Tetrahydroisoindole-1-carboxylate (799 mg, 4.14 mmol) in dry CH_2Cl_2 (6.5 mL) was added dropwise, and the mixture was warmed to room temperature and then stirred for 5 h. An aqueous solution of sodium acetate trihydrate 5.5 M (4 mL) was added and the resulting mixture was heated at 40 °C for 15 min. The solution was cooled at rt and the two layers were separated. The aqueous layer was further extracted with CH_2Cl_2 (3x5 mL),

the combined organic layers were washed with a saturated $NaHCO_3$ solution (15 mL), then with H_2O (15 mL), dried over Na_2SO_4 and concentrated under reduced pressure, obtaining a brown solid (915 mg, 4.14 mmol) in quantitative yield.

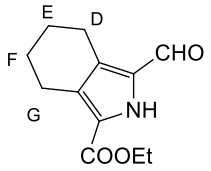

39

^{1}H-NMR (CDCl3, 400 MHz): δ (ppm) 9.71 (s, 1H, CHO); 9.41 (bs, 1H, NH); 4.34 (q, J = 7.2 Hz, 2H, OC*H*$_2$CH$_3$); 2.88-2.79 (m, 4H, H_D and H_G); 1.80-1.79 (bs, 4H, H_E and H_F); 1.37 (t, J = 7.2 Hz, 3H, CH_3). ^{13}C-NMR (CDCl3, 75 MHz): δ (ppm) 178.9; 160.9; 131.9; 128.9; 128.5; 60.9; 22.8; 22.5; 22.4; 20.9; 14.4.

3-Formyl-4,5,6,7-tetrahydro-2H-isoindole-1-carboxylic acid (40)

Compound **39** (915 mg, 4.14 mmol) was suspended in 25% aqueous NaOH (72 mL) preheated at about 80 °C. After heating at reflux for 1 h, the brown solution was cooled to room temperature and carefully acidified with aqueous HCl (6 M, 150 mL) in an ice-salt bath. Upon acidification, a brown precipitate formed. After filtering and washing with H_2O, pure **40** was collected in 90% yield (822 mg, 4.26 mmol).

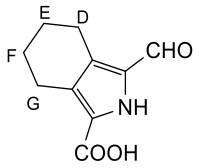

40

^{1}H-NMR (DMSO, 400 MHz): δ (ppm) 13.35 (bs, 1H, OH); 12.81 (s, 1H, NH); 9.70 (s, 1H, CHO); 2.70-2.67 (m, 4H, H_D and H_G); 1.65-1.45 (m, 4H, H_E and H_F). ^{13}C-NMR ($CDCl_3$, 75 MHz): δ (ppm) 181.8; 162.4; 130.1; 128.7; 127.8; 123.9; 22.96; 22.89; 22.7; 20.5. ESI-MS: m/z calcd. for $C_{10}H_{11}N_1O_3$+Na^+ 216.1, found 216.0 (55%).

Compound 41

A 48% solution of HBr in H_2O (650 µL) was added to a solution of **40** (100 mg, 0.52 mmol) and 2,4-dimethyl-3-ethyl-1H-pyrrole (70 µL, 0.52 mmol) in acetic acid (570 µL), and the green mixture was stirred at rt for 1 h. TLC (ethyl acetate/hexane/acetic acid 20/10/0.3) monitoring indicated the complete

consumption of both the reagents. 48% HBr in H_2O (1.4 mL) was added and the solution was cooled to 0 °C. After 4 h, since no precipitation was observed, the mixture was extracted with CH_2Cl_2 (3x10 mL) and the organic layers were washed with H_2O and brine till neutral pH. The green organic solution was concentrated under reduced pressure. The brown/green crude **41** was used without further purification (77% yield, 152 mg, 0.40 mmol).
ESI-MS: m/z calcd. for $C_{18}H_{23}BrN_2O_2$+Na^+ 401.1, found 402.5 (45%).

Compound 42

To a stirred solution of **41** (152 mg, 0.40 mmol) in dry CH_2Cl_2 (10 mL), TEA (500 µL, 3.59 mmol) was added. After 1 h, BF_3OEt_2 (900 µL, 7.17 mmol) was added and the violet solution was stirred at rt for 2 days and monitored by TLC (CH_2Cl_2/CH_3CN 80/20). The reaction was quenched by adding 1M aqueous HCl (10 mL) and the mixture was stirred for 30 min. The aqueous layer was extracted with CH_2Cl_2 (3x10 mL) and the combined organic layers were washed with H_2O till neutral pH, dried over $MgSO_4$ and concentrated under reduced pressure obtaining a violet oil. The crude was purified by flash column chromatography (gradient ethyl acetate/hexane/acetic acid 40/80/1, 60/40/1, ethyl acetate/acetic acid 10/0.1, acetone/acetic acid 10/0.1). Pure product **42** was isolated as an orange/pink solid in 0.7% yield (1 mg, 2.89 µmol).

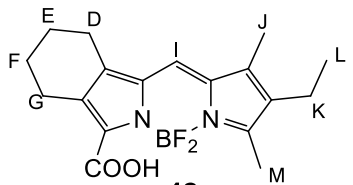

42

^{1}H-NMR (Acetone-d_6, 400MHz): δ (ppm) 7.54 (s, 1H, H_I); 2.57 (bs, 4H, H_D and H_G); 2.49 (q, J = 5.4 Hz, 2H, H_K); 2.28 (s, 3H, H_M); 2.10 (s, 3H, H_J); 1.75 (bs, 4H, H_E and H_F); 1.10 (t, J = 5.4 Hz, H_L). ^{19}F-NMR ($CDCl_3$, 400 MHz): δ (ppm) -141.9 (q, $J_{F\text{-}B}$ = 29.6 Hz, 2F). ESI-MS: m/z calcd. for $C_{18}H_{21}BF_2N_2O_2$+H^+ 347.2, found 349.4 (100%); m/z calcd. for $C_{18}H_{21}BF_2N_2O_2$+Na^+ 369.2, found 369.3 (50%).

Compound 47

A solution of 5,17-bis(chloromethyl)-25,26,27,28-tetrapropoxycalix[4]arene **46** (515 mg, 0.75 mmol) in dry toluene (25 mL) was added to a 40 °C preheated stirred solution of 4-(2-hydroxyethoxy)benzaldehyde (149 mg, 0.89 mmol), N-methyl-N-(2-hydroxyethyl)-4-aminobenzaldehyde (201 mg, 1.12 mmol) and Cs_2CO_3 (97 mg, 0.29 mmol) in dry toluene (25 mL). The reaction was refluxed for 4 days, during which most of the solvent evaporated. This increase in the concentration of the solution improved the kinetics of the reaction, as indicated by TLC analysis (hexane/ethyl acetate 70/30). Then H_2O (50 mL) was added to the pale yellow solution and the two layers were separated. The aqueous layer was extracted with ethyl acetate (50 mL) and the combined organic layers were washed with H_2O till neutral pH. The yellow oil obtained after the evaporation of the solvent under reduced pressure was purified by flash column chromatography (gradient hexane/ethyl acetate 98/2, 94/6). Pure product **47** was isolated as a colorless oil in 16% (116 mg, 0.12 mmol) yield.

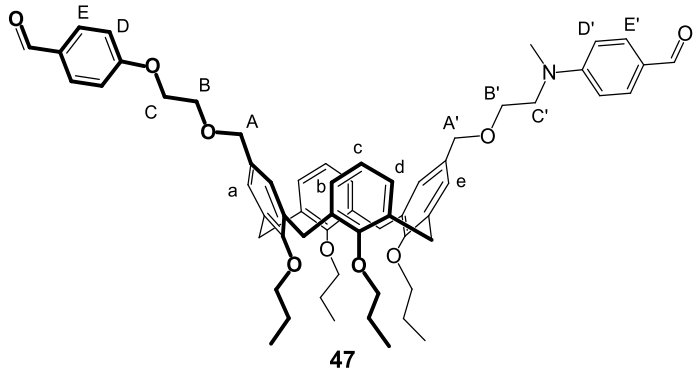

47

^{1}H-NMR ($CDCl_3$, 300MHz): δ (ppm) 9.87 (s, 1H, CHO); 9.71 (s, 1H, CHO), 7.82 (d, J = 8.8 Hz, 2H, H_E); 7.71 (d, J = 8.8 Hz, 2H, $H_{E'}$); 7.01 (d, J = 8.8 Hz, 2H, H_D); 6.71 (d, J = 9.2 Hz, 2H, $H_{D'}$); 6.68 (s, 2H, H_a); 6.63 (s, 2H, H_e); 6.51-6.44 (m, 6H, H_b, H_c and H_d); 4.43 (d, J = 13.2 Hz, 2H, ArC*H*HAr); 4.42 (d, J = 13.2 Hz, 2H, ArC*H*HAr); 4.29 (s, 2H, H_A); 4.22 (s, 2H, $H_{A'}$); 4.16 (t, J = 4.8 Hz, 2H, $H_{C'}$); 3.87-3.79 (m, 8H, OC*H*$_2$CH$_2$CH$_3$); 3.69 (t, J = 4.8 Hz, 4H, H_B); 3.64-3.58 (m, 4H, H_C and $H_{B'}$); 3.12 (d, J = 13.2 Hz, 4H, ArCH*H*Ar); 3.08 (s, 3H, NCH_3); 1.95-1.86 (m, 8H, OCH$_2$C*H*$_2$CH$_3$); 1.01 (t, J = 7.2 Hz, 6H , OCH$_2$CH$_2$C*H*$_3$), 0.94 (t, J = 7.2 Hz, 6H , OCH$_2$CH$_2$C*H*$_3$). ^{13}C-NMR ($CDCl_3$, 100MHz): δ (ppm) 190.8; 190.1; 163.9; 156.7; 156.6; 156.2; 135.5; 135.4; 134.55; 134.60; 132.1; 131.9; 130.8; 130.7; 128.1; 127.98;127.91; 127.7; 125.3; 121.9; 114.9; 111.0; 77.23; 77.7; 73.4; 73.3; 67.79; 67.77; 67.1; 52.1; 39.3; 30.3; 23.3;

23.2; 10.4; 10.2. ESI-MS: m/z calcd for $C_{61}H_{71}NO9+Na^+$ 984.9, found 984.5 (100%); m/z calcd for $C_{61}H_{71}NO_9+K^+$ 1000.6, found 1000.6 (20%).

Compound 49a

To a solution of calixarene **47** (19 mg, 0.02 mmol) and BODIPY **48** (9 mg, 0.04 mmol) in dry toluene (3 mL), piperidine (9.5 µL, 0.09 mmol), acetic acid (5.5 µL, 0.09 mmol) and 4 Å molecular sieves (few beads) were added. The reaction was performed by consecutive 15-35 min-steps of microwave irradiation (200 W) maintaining the temperature at 110 °C. After every step, the reaction mixture was cooled down to rt and monitored by TLC (CH_2Cl_2/ethyl acetate 99/1). The reaction was stopped after 6 cycles, when the bichromophoric compound was when starting compound **47** was consumd. The resulting blue crude mixture was concentrated under vacuum and purified by preparative TLCs (CH_2Cl_2/ethyl acetate 99/1), isolating pure **49a** as a violet solid in 21% yield (6 mg, 0.004 mmol) and mono-styryl BODIPY intermediates **49b** and **49c** in 52% overall yield.

Compounds **49b** and **49c** (11 mg, 0.009 mmol altogether) were then dissolved in dry toluene (1 mL) and **48** (3 mg, 0.01 mmol), piperidine (10 µL, 0.09 mmol), glacial acetic acid (6 µL, 0.09 mmol) and few 4 Å molecular sieves were added. The mixture was subjected to consecutive 30-60 min microwave irradiation (200 W) steps at 110 °C for 6 steps, when the TLC monitoring revealed the complete consumption of the starting materials. The desired product **49a** was isolated from many other byproducts by preparative TLC (CH_2Cl_2/ethyl acetate 99/1) in 11% yield (1 mg, 0.001 mmol).

Overall yield of the two steps: 27% (7 mg, 5 mmol).

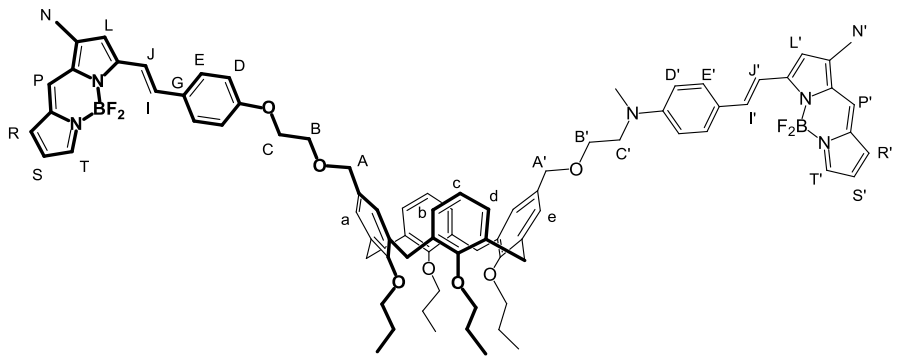

49a

UV-vis: λ_{max} ($CHCl_3$): 568 nm (s), ε: 61800 $M^{-1}cm^{-1}$; 540 nm (s), ε: 37840 $M^{-1}cm^{-1}$ ^{1}H-NMR ($CDCl_3$, 400 MHz): δ (ppm) 7.67 (s, 1H, H_R); 7.61 (s, 1H, $H_{R'}$); 7.54 (d, J = 8.4 H, 2H, H_E); 7.49 (d, J = 8.4 Hz, 2H, $H_{E'}$); 7.50 (d, J = 15.6 Hz, 1H, H_I); 7.42 (d, J = 16.4 Hz, 1H, H_J); 7.33 (d, J = 16.4 Hz, 1H, $H_{J'}$); 7.31 (d, J = 15.6 Hz, 1H, $H_{I'}$); 7.15 (s, 1H, H_P); 7.06 (s, 1H, $H_{P'}$); 6.92 (d, J = 8.4 Hz, 2H, H_D); 6.92 (d, J = 4.0 Hz, 1H, H_T); 6.84 (d, J = 4.0 Hz, 1H, $H_{T'}$); 6.72-6.53 (m, 14H, $H_{D'}$, $H_{L'}$, H_L, H_a, H_e H_b, H_c and H_d); 4.42 (d, J = 13.3 Hz, 4H, ArC*H*HAr); 4.19 (s, 2H, H_A); 4.16 (s, 2H, $H_{A'}$); 4.07-4.05 (m, 2H, H_C); 3.61 (q, J = 7.8 Hz, 8H, OC*H*$_2$$CH_2CH_3$); 3.62-3.59 (m, 6H, H_B, $H_{B'}$ and $H_{C'}$); 3.15 (d, J = 13.3 Hz, 2H, ArCH*H*Ar); 3.13 (d, J = 13.3 Hz, 2H, ArCH*H*Ar); 3.04 (s, 3H, NCH_3); 2.29 (s, 3H, H_N); 2.25 (s, 3H, $H_{N'}$); 1.94-1.87 (m, 8H, OCH_2C*H*$_2$$CH_3$); 0.97 (t, J = 7.2 Hz, 12H , OCH_2CH_2C*H*$_3$). ^{13}C-NMR ($CDCl_3$, 100 MHz): δ (ppm) 160.7; 160.6; 159.7; 156.5; 156.4; 156.3; 150.8; 144.6; 144.3; 141.9; 140.3; 138.0; 136.3; 135.1; 135.0; 134.99; 134.95; 132.9; 132.7; 130.9; 130.8; 130.2; 129.7; 128.7; 128.2; 128.1; 127.9; 127.3; 125.1; 123.8; 123.4; 122.2; 121.9; 120.4; 117.5; 117.3; 116.3; 116.0; 115.2; 115.1; 113.4; 111.8; 77.2; 73.4; 73.2; 67.9; 67.5; 66.8; 52.1; 39.3; 31.9; 30.9; 29.7; 29.4; 23.2; 22.9; 22.7; 11.5; 11.4; 10.3; 10.3. ^{19}F-NMR ($CDCl_3$, 400 MHz): -142.3 (q, J_{F-B} = 37.68 Hz, 2F); - 142.7 (q, J_{F-B} = 37.28 Hz, 2F). HR-MS: m/z calcd for $C_{83}H_{89}B_2F_4N_5O_7$+H^+ 1366.6962, found 1366.6974 (10%); m/z calcd for $C_{83}H_{89}B_2F_4N_5O_7$+Na^+ 1388.6638, found 1388.6788 (15%).

A little amount of partial compounds **49b** and **49c** were isolated for further characterization:

49b

^{1}H-NMR ($CDCl_3$, 400 MHz): δ (ppm) 9.71 (s, 1H, CHO), 7.71 (d, J = 9.1 H, 2H, $H_{E'}$); 7.65 (s, 1H, H_R); 7.53 (d, J = 9.1 Hz, 2H, H_E); 7.55 (d, J = 16.6 Hz, 1H, H_J); 7.51 (d, J = 16.6 Hz, 1H, H_I); 7.14 (s, 1H, $H_{P'}$); 7.07 (dd, J_1 = 8.4 Hz, J_2 = 2.2 Hz, 2H, $H_{D'}$); 6.90 (d, J = 3.3 Hz, 1H, H_T); 6.71 (d, J = 8.4 Hz, 2H, H_D); 6.67-6.47 (m, 12H, H_L, H_a, H_e H_b, H_c, H_d and H_S); 4.42 (d, J = 13.6 Hz, 2H, ArC*H*HAr); 4.41 (d, J = 13.6 Hz, 2H, ArC*H*HAr); 4.29 (s, 2H, H_A); 4.20 (s, 2H, $H_{A'}$); 4.13-4.10 (m, 2H, H_C); 3.86-3.79 (m, 8H, OC*H*$_2$$CH_2CH_3$); 3.69-3.58 (m, 6H, H_B, $H_{B'}$ and $H_{C'}$); 3.13 (d, J = 13.6 Hz, 2H, ArCH*H*Ar); 3.09 (d, J = 13.6 Hz, 2H, ArCH*H*Ar); 3.07 (s, 3H, NCH_3); 2.32 (s, 3H, H_N); 1.94-1.88 (m, 8H, OCH_2C*H*$_2$$CH_3$); 1.02-0.93 (m, 12H, OCH_2CH_2C*H*$_3$). ESI-MS: m/z calcd for $C_{72}H_{80}BF_2N_3O_8$+Na^+ 1186.6, found 1187.0 (50%).

49c

^{1}H-NMR ($CDCl_3$, 400 MHz): δ (ppm) 9.85 (s, 1H, CHO), 7.79 (d, J = 8.4 H, 2H, H_E); 7.58 (s, 1H, $H_{R'}$); 7.50 (d, J = 9.2 Hz, 2H, $H_{E'}$); 7.42 (d, J = 16.0 Hz, 1H, $H_{J'}$); 7.33 (d, J = 16.0 Hz, 1H, $H_{I'}$); 7.04 (s, 1H, $H_{P'}$); 6.98 (d, J = 8.4 Hz, 2H, H_D); 6.83 (d, J = 3.8 Hz, 1H, $H_{T'}$); 6.69 (d, J = 8.8 Hz, 2H, $H_{D'}$); 6.65-6.53 (m, 11H, H_L, H_a, H_e H_b, H_c and H_d); 6.41 (dd, J_1 = 3.8 Hz, J_2 = 2.4 Hz, 1H, $H_{S'}$); 4.421 (d, J = 13.3 Hz, 2H, ArC*H*HAr); 4.418 (d, J = 13.3 Hz, 2H, ArC*H*HAr); 4.21 (s, 2H, H_A); 4.19 (s, 2H, $H_{A'}$); 4.12-4.09 (m, 2H, $H_{C'}$); 3.82 (t, J = 7.9 Hz, 8H, $OCH_2CH_2CH_3$); 3.65-3.58 (m, 6H, H_B, $H_{B'}$ and H_C); 3.13 (d, J = 13.4 Hz, 2H, ArCH*H*Ar); 3.10 (d, J = 13.4 Hz, 2H, ArCH*H*Ar); 3.05 (s, 3H, NCH_3); 2.27 (s, 3H, $H_{N'}$); 1.93-1.86 (m, 8H, $OCH_2CH_2CH_3$); 0.98 (t, J = 7.6 Hz, 12H ,$OCH_2CH_2CH_3$). ESI-MS: m/z calcd for $C_{72}H_{80}BF_2N_3O_8$+Na^+ 1186.6, found 1187.0 (60%).

Compound 51

To a stirred solution of compound **50** (625 mg, 1.00mmol) in dry CH_2Cl_2 (20 mL), thionyl chloride (1.10 mL, 15.16 mmol) was added. The reaction was carried out for 5 h, when TLC monitoring (hexane/ethyl acetate 1/1) indicated the complete consumption of the starting material. The solvent was removed under reduced pressure obtaining compound **51** as a red solid in quantitative yield (640 mg, 1.01 mmol), which was employed in the next step without further purification.

^{1}H-NMR ($CDCl_3$, 300MHz): δ (ppm) 6.76 (m, 6H, ArH); 6.42 (s, 2H, ArH); 6.42-6.40 (m, 3H, ArH); 4.42 (d, J = 13.3 Hz, 2H, ArC*H*HAr); 4.43 (d, J = 13.3 Hz, 2H, ArC*H*HAr); 4.17(s, 2H, CH_2Cl); 3.90-3.75 (m, 8H, $OCH_2CH_2CH_3$); 3.13(d, J = 13.3 Hz, 4H, ArCH*H*Ar); 1.94-1.85 (m, 8H, $OCH_2CH_2CH_3$); 1.01 (t, J = 7.5 Hz, 6H, $OCH_2CH_2CH_3$); 0.94 (t, J=7.5 Hz, 6H, $OCH_2CH_2CH_3$).

Compound 52

To a stirred solution of compound **51** (320 mg, 0.50 mmol) in dry toluene (10 mL), a solution of N-methyl-N-(2-hydroxyethyl)-4-aminobenzaldehyde (102 mg, 0.57 mmol) and Cs_2CO_3 (326 mg, 1.00 mmol) in dry toluene (10 mL) was added and the reaction was refluxed for 5 days, when TLC monitoring (hexane/ethyl acetate 1:1) indicated the complete consumption of the reagent **51**.

The reaction was quenched with H_2O (10 mL) and the aqueous layer was extracted with ethyl acetate (2x10 mL). The combined organic layers were washed with H_2O until neutral pH, and concentrated under reduced pressure. The yellow crude was

purified by flash column chromatography (cyclohexane/ethyl acetate 87/13), isolating pure **52** as yellow oil in 32% yield (125 mg, 0.16 mmol).

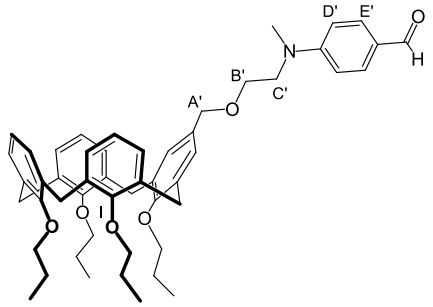

52

^{1}H-NMR ($CDCl_3$, 400 MHz): δ (ppm) 9.72 (s, 1H, CHO), 7.71 (d, J = 9.0 H, 2H, $H_{E'}$); 6.70 (d, J = 9.0 Hz, 2H, $H_{D'}$); 6.68-6.64 (m, 6H, ArH); 6.60-6.41(m, 5H, ArH); 4.44 (d, J = 13.3 Hz, 2H, ArC*H*HAr); 4.43 (d, J = 13.3 Hz, 2H, ArC*H*HAr); 4.13 (s, 2H, $H_{A'}$); 3.87 (t, J = 7.5 Hz, 4H, OC*H*$_2$CH$_2$CH$_3$); 3.81 (t, J = 7.2 Hz, 2H, OC*H*$_2$CH$_2$CH$_3$); 3.79 (t, J = 7.2 Hz, 2H, OC*H*$_2$CH$_2$CH$_3$); 3.59-3.54 (m, 2H, $H_{C'}$); 3.51-3.48 (m, 2H, $H_{B'}$); 3.14 (d, J = 13.4 Hz, 2H, ArCH*H*Ar); 3.10 (d, J = 13.4 Hz, 2H, ArCH*H*Ar); 3.06 (s, 3H, NCH_3); 1.95-1.87 (m, 8H, OCH_2C*H*$_2$$CH_3$); 1.00 (t, J = 7.5 Hz, 6H, OCH_2CH_2C*H*$_3$); 0.97 (t, J = 7.5 Hz, 6H, OCH_2CH_2C*H*$_3$). ^{13}C-NMR ($CDCl_3$, 100 MHz): δ (ppm) 190.2; 156.8; 156.5; 156.1; 153.6; 135.5; 135.3; 134.9; 134.8; 132.1; 130.9; 128.3; 128.2; 127.9; 127.4; 125.2; 121.9; 121.5; 76.7; 66.9; 52.1; 39.3; 30.99; 30.98; 29.7; 23.29; 23.28; 23.2; 10.43; 10.41; 10.2. ESI-MS: m/z calcd for $C_{51}H_{61}N_1O_6$+Na^+ 806.4, found 806.8 (100%); m/z calcd for $C_{51}H_{61}N_1O_6$+K^+ 822.4, found 822.5 (50%);

Compound 53

Compounds **52** (125 mg, 0.16 mmol) and **48** (40 mg, 0.18 mmol) were dissolved in dry CH_3CN (15 mL) and piperidine (47 µL, 0.48 mmol) and acetic acid (27 µL, 0.48 mmol) were added. The black solution was refluxed (85 °C) for 3 h, till TLC monitoring (hexane/ethyl acetate 80/20) indicated the complete consumption of compound **52**. After the solvent was removed under reduced pressure, the crude was redissolved in CH_2Cl_2 and the reaction was quenched with aqueous HCl (0.05M, 2x50 mL), sat. aqueous $NaHCO_3$ (1x20mL) and H_2O (1x20mL). The organic layer was concentrated under reduced pressure and the blue crude was purified by flash column chromatography (gradient CH_2Cl_2/hexane 75/25, 80/20, 90/10, CH_2Cl_2) isolating pure **53** in 19% yield (30 mg, 0.03 mmol).

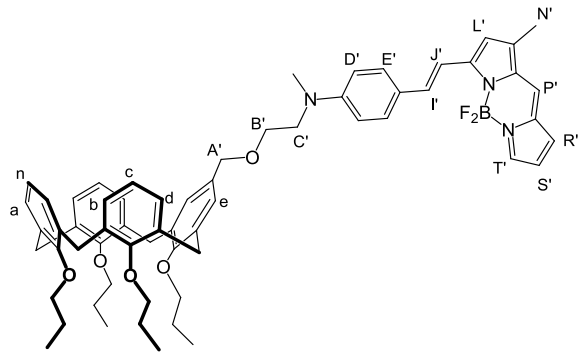

53

^{1}H-NMR ($CDCl_3$, 300 MHz): δ (ppm) 7.59 (s, 1H, $H_{R'}$); 7.51 (d, J = 8.9 H, 2H, $H_{E'}$); 7.44 (d, J = 16.1 Hz, 1H, $H_{J'}$); 7.32 (d, J = 16.1 Hz, 1H, $H_{I'}$); 7.04 (s, 1H, $H_{P'}$); 6.81 (d, J = 4.0 Hz, 1H, $H_{T'}$); 6.71-6.57 (m, 9H, $H_{D'}$, $H_{L'}$, H_b, H_c and H_d); 6.52-6.38 (m, 6H, H_a, H_e, H_n and $H_{S'}$); 4.44 (d, J = 13.3 Hz, 2H, ArC*H*HAr); 4.42 (d, J = 13.3 Hz, 2H, ArC*H*HAr); 4.14 (s, 2H, $H_{A'}$); 3.85-3.77 (m, 8H, $OCH_2CH_2CH_3$); 3.58-3.45 (m, 4H, $H_{C'}$ and $H_{B'}$); 3.13 (d, J = 13.3 Hz, 2H, ArCH*H*Ar); 3.10 (d, J = 13.3 Hz, 2H, ArCH*H*Ar); 3.04 (s, 3H, NCH_3); 2.29 (s, 3H, $H_{N'}$); 1.96-1.87 (m, 8H, $OCH_2CH_2CH_3$); 1.05-0.95 (m, 12H ,$OCH_2CH_2CH_3$). ^{13}C-NMR ($CDCl_3$, 75 MHz): δ (ppm) 160.7; 156.8; 156.5; 156.1; 150.8; 144.3;141.9; 135.4; 135.3; 134.9; 134.8; 132.6; 130.9; 130.2; 128.2; 127.9; 127.4; 127.0; 123.8; 123.4; 121.9; 121.5; 120.4; 117.5; 115.3; 113.4; 111.9; 76.7; 76.6; 73.3; 67.2; 52.1; 39.2; 31.9; 30.9; 30.1; 29.7; 23.3; 23.2; 10.4; 10.2. HR-MS: m/z calcd for $C_{62}H_{70}BF_2N_3O_5$+H^+ 986.5376, found 986.5477 (65%); m/z calcd for $C_{62}H_{70}BF_2N_3O_5$+Na^+ 1008.5196, found 1008.5296 (100%); calcd for $C_{62}H_{70}BF_2N_3O_5$+K^+ 1024.6318, found 1024.5040 (20%).

Compound 54

To a stirred solution of compound **51** (320 mg, 0.50 mmol), in dry toluene (4 mL), a solution of 4-(2-hydroxyethoxy)benzaldehyde (100 mg, 0.60 mmol) and Cs_2CO_3 (326 mg, 1.00 mmol) in dry toluene (4 mL) was added and the reaction was refluxed for 5 days, when TLC monitoring (hexane/ethyl acetate 70/30) indicated the complete consumption of the reagent **51**. The reaction was quenched with H_2O (10 mL) and the aqueous layer was extracted with ethyl acetate (2x10 mL). The combined organic layers were washed with H_2O until neutral pH, and concentrated under reduced pressure. The yellow crude was purified by flash column chromatography (cyclohexane/ethyl acetate 90/10), isolating pure **54** as yellow oil in 33% yield (127 mg, 0.17 mmol)

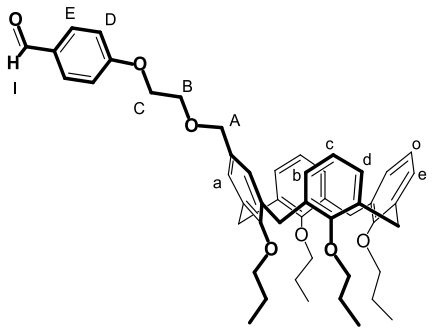

54

^{1}H-NMR ($CDCl_3$, 300 MHz): δ (ppm) 9.89 (s, 1H, CHO), 7.85 (d, J = 8.7 H, 2H, H_E); 7.03 (d, J = 8.7 Hz, 2H, $H_{D'}$); 6.76-6.73 (m, 4H, H_b and H_d); 6.66 (t, J = 7.8 Hz, 2H, H_c); 6.53-6.49 (m, 5H, H_a, H_e and H_o); 4.471 (d, J = 13.3 Hz, 2H, ArC*H*HAr); 4.467 (d, J = 13.3 Hz, 2H, ArC*H*HAr); 4.26 (s, 2H, H_A); 4.14-4.07 (m, 2H, H_C); 3.91 (t, J = 7.4 Hz, 4H, OC*H*$_2$CH$_2$CH$_3$); 3.81 (t, J = 7.4 Hz, 4H, OC*H*$_2$CH$_2$CH$_3$); 3.61-3.53 (m, 2H, H_B); 3.47 (d, J = 13.3 Hz, 2H, ArCH*H*Ar); 3.16 (d, J = 13.3 Hz, 2H, ArCH*H*Ar); 2.01-1.88 (m, 8H, OCH$_2$C*H*$_2$CH$_3$); 1.04 (t, J = 7.1 Hz, 6H ,OCH$_2$CH$_2$C*H*$_3$); 0.99 (t, J = 7.1 Hz, 6H ,OCH$_2$CH$_2$C*H*$_3$). ^{13}C-NMR ($CDCl_3$, 75 MHz): δ (ppm) 190.9; 163.9; 156.9; 156.4; 156.1; 135.6; 135.5; 134.8; 131.9; 130.7; 130.0; 128.3; 127.9; 127.6; 121.9; 114.9; 76.8; 67.8; 67.4; 31.0; 23.3; 23.2; 10.5; 10.2. ESI-MS: m/z calcd for $C_{50}H_{58}O_7$+Na^+ 793.9, found 793.5 (100%); m/z calcd for $C_{50}H_{58}O_7$+K^+ 810.4, found 810.1 (20%).

Compound 56

To a solution of 4-(2-hydroxyethoxy)benzaldehyde (15 mg, 0.09 mmol) and BODIPY **48** (20 mg, 0.09 mmol) in dry CH_3CN (2 mL), piperidine (0.05 mL, 0.55 mmol) and acetic acid (0.03 mL, 0.55 mmol) were added. The condensation reaction was performed by using three consecutive 1 min microwave irradiation (200 W) steps maintaining the temperature at 100 °C, and a fourth step at 150°C. After every cycle, the reaction mixture was cooled down to rt, and then monitored by TLC (CH_2Cl_2/hexane 70/30). The resulting pink crude mixture was concentrated under vacuum and purified by preparative TLCs (CH_2Cl_2/hexane 70/30), isolating pure **56** as violet solid in 22% yield (8 mg, 0.02 mmol).

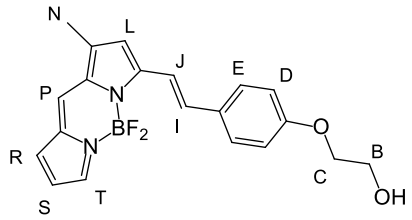

56

^{1}H-NMR ($CDCl_3$, 400 MHz): δ (ppm) 7.65 (s, 1H, H_R); 7.56 (d, J = 8.7 Hz, 2H, H_E); 7.51 (d, J = 16.3 Hz, 1H, H_J); 7.33 (d, J = 16.3 Hz, 1H, H_I); 7.13 (s, 1H, H_P); 6.93 (d, J = 8.7 Hz, 2H, H_D); 6.89 (d, J = 3.8 Hz, 1H, H_T); 6.73 (s, 1H, H_L); 6.44 (dd, J_1 = 3.7 Hz, J_2 = 2.2 Hz, 1H, H_S); 4.12 (m, 2H, H_C); 3.99-3.97 (m, 2H, H_B); 2.29 (s, 3H, H_N).

Transient absorption measurements

Transient measurements were carried out in the LENS laboratories (Florence). The apparatus used for the transient absorption spectroscopy (TAS) measurements has been described in detail in refs.[38,39,40,41] The fs-laser oscillator is a Ti:sapphire laser (Spectra Physics Tsunami) pumped by the second harmonic from a Nd:YVO (Spectra Physics Millennia). The short (≤70 fs) pulses are stretched and amplified at 1 kHz repetition rate by a regenerative amplifier (BMI Alpha 1000). After compression a total average power of 450-500 mW and pulse duration of 100 fs are obtained. The repetition rate of the output beam is reduced to 100 Hz by a mechanical chopper in order to avoid the photodegradation of the sample. Pulses in the UV-Visible range can be achieved by Second Harmonic Generation (SHG) or by doubling or mixing the output of an optical parametric generator and amplifier (OPG-OPA) based on a BBO crystal (TOPAS by Light Conversion, Vilnius, Lithuania).[42, 43] For the current measurements the pump beam polarization was set to magic angle with respect to the probe beam by rotating a $\lambda/2$ plate so as to exclude rotational contributions to the transient signal. The probe pulse was generated by focusing a small portion of the 800 nm radiation on a 3 mm thick CaF_2 window mounted on a motorized translation stage. The continuum light was optimized for the 350-750 nm wavelength range and a moveable delay line made it possible to increase the time-of-arrival-difference of the pump and probe beams up to 2.0 ns. Multichannel detection for transient spectroscopy was achieved by sending the white light continuum after passing through the sample to a flat field monochromator coupled to a home-made CCD detector [http://lens.unifi.it/ew].

TAS measurements were carried out in a static cell (2 mm thick) under magnetic stirring in order to refresh the solution and avoid photo degradation.
The integrity of the sample has been checked by visible absorption measurements (Perkin Elmer LAMBDA 950) before and after the time resolved measurements. The OD of the sample at the excitation wavelength was between 0.2 and 0.5 in all the examined solvents (chloroform, acetonitrile and chloroform). Transient spectra have been analysed by applying a combined approach, consisting of singular values decomposition (*SVD*)[44, 45] and the simultaneous fitting of all the collected kinetic traces (global analysis). The aim of global analysis is to decompose the two way data matrix into time-independent spectra and wavelength independent kinetics.[46] Once the number of components is identified through the SVD, the second step involves the parameterization of the time evolution of the spectral components. This was accomplished by assuming first-order kinetics, describing the overall temporal evolution as the sum or combination of exponential functions. Global analysis was performed using the GLOTARAN package (http://glotaran.org),[46, 47] and employing a linear unidirectional "sequential" model shown in Scheme 6:

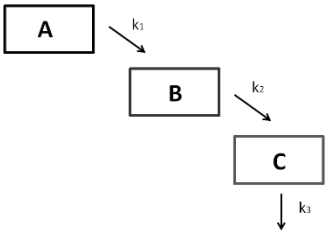

Scheme 6. *Sequential kinetic model applied for global analysis.*

3.8 References

1. T. Brixner, J. Stenger, H. M. Vaswani, M. Cho, R. E. Blankenship, G. R. Fleming, *Nature*, **2005**, 434, 625-628;
2. G. S. Engel, T. R. Calhoun, E. L. Read, T.-K. Ahn, T. Mančal,Y. -C. Cheng, R. E. Blankenship, G. R. Fleming, *Nature*, **2007**, 446, 782-786;
3. R. E. Blankenship, *Molecular Mechanisms of Photosynthesis*, World Scientific, London, **2002**;
4. R. E. Fenna, B. W. Matthews, *Nature*, **1975**, 258, 573-577;
5. D. Hayes, G. B. Griffin, G. S. Engel, *Science*, **2013**, 340, 1431-1434;
6. Wagner, R. W.; Lindsey*, J. S. Pure Appl. Chem.*, **1996**, 68, 1373-1380;
7. A. Treibs, F.H. Kreuzer, *Liebigs Ann. Chem.*, **1968**, 718, 208-223;
8. G. Ulrich, R. Ziessel,A. Harriman, *Angew. Chem. Int. Ed.*, **2008**, 47, 1184 – 1201;
9. M. E. El.Khouly, S. Fukuzumi, F. D'Souza, *ChemPhysChem*, **2014**, 15, 30–47;
10. A. Loudet, K. Burgess, Chem. Rev., **2007**, 107, 4891-4932;
11. T. Wood, A. Thompson, *Chem. Rev.*, **2007**, 107, 1831-1861;
12. J. A. Van Koeveringe, J. Lugtenburg, *Recl. Trav. Chim. Pays-Bas*, **1977**, 96, 55–57;
13. A. Schmitt, B. Hinkeldey, M. Wild, G. Jung, *J. Fluoresc.*, **2009**, 19 (4), 755–759;
14. K. Tram, H. Yan, H. A. Jenkins, S. Vassiliev, D. Bruce, *Dyes and Pigments*, **2009**, 82 (3), 392–395;
15. I. J. Arroyo, R. Hu, G. Merino, B. Z. Tang, E. Peña-Cabrera, *J. Org. Chem.*, **2009**, 74 (15), 5719–5722;
16. N. Boens, V. Leen, W. Dehaen, *Chem. Soc. Rev.*, **2012**, 41, 1130-1172;

17. R. W. Wagner, J. S. Lindsey, *Pure Appl. Chem.*, **1996**, *68*, 1373-1378;
18. D. Wang, J. Fan, X. Gao, B. Wang, S. Sun, X. Peng, *J. Org. Chem.*, **2009**, 74, 7675-7683;
19. L. Wu, K. Burgess, *Chem. Commun.*, **2008**, 4933–4935;
20. M. Wada, S. Ito, H. Uno, T. Murashima, N. Ono, T. Urano, Y. Urano, *Tetrahedron Letters*, **2001**, 42, 6711–6713;
21. T. Uppal, X. Hu, F. R. Fronczek, S. Maschek, P. Bobadova-Parvanova, M. G. H. Vicente, *Chem. Eur. J.*, **2012**, 18, 3893-3905;
22. S. Biswas, M. Nayak, S. Kanojiya, S. Batra, *Adv. Synth. Catal.*, **2011**, 353, 3330 – 3334;
23. T. Okujima, N. Komobuchi, H. Uno, N. Ono, *Heterocycles*, **2006**, 67 (1), 255-267;
24. W.N. Sisk, N. Ono, T. Yano, M. Wada, *Dyes and Pigments*, **2002**, 55, 143–150;
25. B. Guo et al., *Dyes and Pigments*, **2007**,73, 206-210;
26. K. Rurack, N. Ono et al., *Chem. Eur. J.*, **2004**, 10, 4853-4871;
27. S.-L. Deng, I. Baglin, M. Nour, C. Cavé, *Heteroatom Chemistry*, **2008**, 19 (1), 55-65;
28. J. O. Osby, M. G. Martin, B. Ganem, *Tetrahedron Lett.*, **1984**, 25, 2093-2096;
29. J. B. Paine, J. Hiom, D. Dolphin, *J. Org. Chem.*, **1988**, 53, 2796-2802;
30. J.-S. Lee et al., *J. Am. Chem. Soc.*, **2009**, 131 (29), 10077-10081;
31. a) M. Baruah, W. Qin, C. Flors, J. Hofkens, R. A. Vallee, D. Beljonne, M. Van der Auweraer, W. M. De Borggraeve, N. Boens, *J. Phys. Chem. A*, **2006**, 110, 5998–6009; (b) S. Atilgan, T. Ozdemir, E. U. Akkaya, *Org. Lett.*, **2008**, 10, 4065–4067;
32. Y. Peng, G. Song, *Green Chemistry*, **2003**, 5, 704–706;

33. J. McNulty, J. A. Steere, S. Wolf, *Tetrahedron Letters*, **1998**, 39, 8013-8016;
34. A. Casnati, A. Sartori, L. Pirondini, F. Bonetti, N. Pelizzi, F. Sansone, F. Ugozzoli, R. Ungaro, *Supramolecular Chemistry*, **2006**, 18 (3), 199–218;
35. O. Struck, J. P. M. van Duynhoven, W. Verboom, S. Harkema, D. N. Reinhoudt, *Chem. Comm.*, **1996**, 13, 1517-1518;
36. A. Casnati, M. Fochi, P. Minari, A. Pochini, M. Reggiani, R. Ungaro, Gazz. Chim. Ital., **1996**, 126, 99-106;
37. S. Ito, T. Murashima, N. Ono, *J. Chem. Soc.*, *Perkin Trans. 1*, **1997**, 3161-3165;
38. P. L. Gentili, M. Mugnai, L. Bussotti, R. Righini, P. Foggi, S. Cicchi, G. Ghini, S. Viviani, A. Brandi, *Journal of Photochemistry and Photobiology A: Chemistry*, **2007**, 187, 209-221;
39. A.Marcelli, P. Foggi, L. Moroni, C. Gellini, P. R Salvi, *J. Phys. Chem. A*, **2008**, 112 (9), 1864-1872;
40. L. Moroni, C. Gellini, P. R. Salvi, A. Marcelli, P. Foggi, *J. Phys. Chem. A,* **2008,** *112* (44), 11044-11051;
41. P. L. Bussotti, R. Ruzziconi, S Spizzichino, P Foggi, *J. of Phys. Chem. A*, **2009**, 113 (52), 14650-14656;
42. I. M. Bayanov, R. Danielius, P. Heinz, A. Seilmeier, *Optics Communications*, **1994**, 113, 99-104;
43. R. Danielius, A. Piskarskas, P. Di Trapani, A. Andreoni, C. Solcia, P. Foggi, *Applied Optics*, **1996**, 35 (27), 5336-5339;
44. E. R. Henry, *Biophysical journal*, **1997**, *72* (2), 652-673;
45. I. H. M. van Stokkum, D. S. Larsen, R. van Grondelle, *Biochimica et Biophysica Acta (BBA) – Bioenergetics*, **2004**, 1657 (2–3), 82-104;

46. J. J. Snellenburg, S. P. Laptenok, R. Seger, K. M. Mullen, I. H. M. van Stokkum, *Journal Of Statistical Software,* **2012**, 49 (3), 1-22;
47. J. Jose, Y. Ueno, J. C. Castro, L. Li, K. Burgess, *Tetrahedron Lett.*, **2009**, 50, 6442-6445.

Chapter 4

Synthesis of bichromophoric systems for Electron Transfer

4.1 Introduction

Electron transfer processes are ubiquitous in biological, physical, inorganic, and organic chemical systems, such as iron oxidation with rust formation, oxidative phosphorylation and in the respiratory chain.

More relevant for our purpose is their implication in photosynthetic systems: after the absorption of a photon and the excitation energy transfer among the chromophores embedded in the antenna complexes, the excitation energy is funneled to the reaction center, where a charge-separation process occurs, generating an electron transfer cascade chain for the production of chemical energy.[1]

As for many other processes (e.g. excitation energy transfer), nature performs exciton separation in the most efficient way and no electron is dissipated or results useless.

In organic photovoltaic devices, bound electron-hole pairs (or excitons) are created upon light absorption and, as a consequence, the exciton population is directly related to the number of absorbed photons.[2,3] These excitons remain bound in organic electronic materials due to Coulomb attraction and the localized energy nature of organic semiconductors.[4]

Organic semiconductors generally have high absorption coefficients at the peak of their absorption spectrum[5] and, as such, the exciton generation rate can be maximized by increasing the overlap of the absorption profile and AM1.5 solar spectrum.[*] Consequently, substantial efforts have been focused on developing

[*] AM1.5 solar is the acronym for Air Mass coefficient. It is a parameter commonly adopted to indicate the solar irradiation on Earth. The air mass coefficient is used to characterize the solar spectrum after solar radiation has traveled through the atmosphere and it is employed to characterize solar cells performances under standardized conditions. It is often referred to

low band gap polymers[6] to extend the spectral response of organic photovoltaic devices. Once generated, the exciton diffuses through the active layer by a hopping mechanism due to the lack of molecular interactions in the organic conducting material.[4] The charge-separation step in organic photovoltaic devices is critical, because of time-competitive exciton decay and recombination processes. The active layer geometry and the donor-acceptor materials interface are two crucial factors to avoid the exciton recombination.

If an exciton is not separated within its lifetime, the electron-hole pair recombines and is lost. To avoid recombination, organic semiconductors generally exhibit small exciton diffusion lengths, approximately 10 nm.[6,7]

Electron transfer occurs from donor to acceptor at the interface between these two semiconductors (heterointerface) provided that the LUMO offset and/or HOMO offset is favorable, while the hole remains in the hole conducting moiety, thus structurally separating the electron and hole. Hole transfer from the electron acceptor into the electron donor may also occur yielding exciton dissociation. Furthermore, impurities may induce dissociation,[8] but this process often leads to trapped charges instead of free charge carriers and is thus detrimental to device performance.[9] The heterointerface is the main dissociation site in the photoactive layer and dissociation at this interface is often treated as the only light-induced charge generation mechanism.[10]

The exciton dissociation efficiency is also a function of the heterointerface area and the ability of the exciton to diffuse to this interface. Consequently, a phase separated donor-acceptor composite would appear to be an ideal material thanks to the control of the morphology of the phase separation. The aim is to achieve a

---

using the syntax "AM" followed by a number. "AM1.5" is almost universal when characterizing terrestrial power-generating panels.

high interfacial area within a bulk material (the so-called bulk-heterojunction, BHJ) in which any point is within a few nanometers of a donor-acceptor interface.

Before the photovoltaic assembly, the first problem it is necessary to focus on, regards the choice of the electron donor and the electron acceptor. It is obvious that if the charge separation cannot occur, long-living excitons and an ideal active layer interface are useless.

The understanding of the dynamics involved in the charge transfer mechanism is of paramount importance for the optimization of the process itself, which is in turn regulated by the best choice of the chromophoric units.

Since the photovoltaic first step consists in the light harvesting, the most interesting process for the purpose of this work, is the photoinduced electron transfer, whose mechanism can be schematized as follows:

$$D^* + A \rightarrow D^+ + A^-$$

where D* is the excited donor (resulting by a direct photoexcitation or via excitation energy transfer) and D^+ and A^- the charged species originated by the electron transfer.

The donor and the acceptor can belong to the same molecule (intramolecular electron transfer) or to different molecules (intermolecular electron transfer). Since this thesis deals with the study of systems where the donor and the acceptor are anchored on the same scaffold, a brief description of the intramolecular mechanism will follow.

4.1.1 Intramolecular electron transfer

Electron transfer (ET) requires that the reactants approach each other to promote the overlap between their electronic orbitals. At the same time, there must be a variation along the nuclear coordinates: in fact, the change of the electronic

charge distribution during an electron transfer reaction implies new equilibrium positions of the nuclei.

Figure 1 shows the potential energy surfaces (PES) of the reactants (R) and of the products (P) as functions of one of the possible nuclear or solvation coordinates. The reaction proceeds from the equilibrium configuration of the reactants (A) to the one of the products (B).

Electron transfer can only occur at (or close to) the intersection point (C), where the energy of reactants and products is the same (in this way energy is conserved).[11]

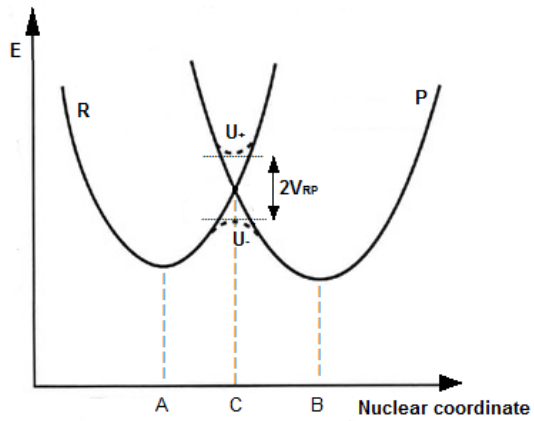

Figure 1. *Simplified representation of the potential energy surfaces (PES) of the reactants (R) and the products (P). Their interaction results in a splitting of the PES (U_+ and U_-), which is most effective at the crossing point.*

When the system reaches the crossing point C, one of the most important factors influencing the transformation from R to P is the extent of coupling of the electronic orbitals, which depends on the distance r between the reactants.

The interaction between donor and acceptor (V_{RP}) causes a mixing of the states of R and P, which results in a splitting of the PES (see U_+ and U_-) whose value is $2V_{RP}$. In particular, the magnitude of V_{RP} is determined by the overlap between the electronic orbitals, i.e. by the distance between donor and acceptor.

In the simple, thermally-activated case, the rate of electron transfer can be expressed by the Arrehenius relation (Eq. 1):

$$k_{ET}=A \exp\left(-\frac{E_{ACT}}{K_B T}\right) \qquad \text{Eq. 1}$$

being related to the crossing of an energy barrier.

Marcus defined the activation energy (E_{ACT}) as a function of two quantities (E_λ and ΔE, Figure 2), suggesting a more refined model for the rate (Eq. 2):

$$k_{ET}=|V_{RP}|^2 \sqrt{\frac{\pi}{\hbar K_B T E_\lambda}} \exp\left(-\frac{(E_\lambda+\Delta E)^2}{4E_\lambda K_B T}\right) \qquad \text{Eq. 2}$$

E_λ is the "*reorganization energy*", the energy spent due to the molecular rearrangement of the donor, the acceptor and the solvent, during the electron transfer process. This parameter depends on the distance between the two minima of the PES (AB distance, Figure 2).

ΔE is the energy difference between the product and reagent, and is called "*driving force*" of the electron transfer reaction (Figure 2).[11]

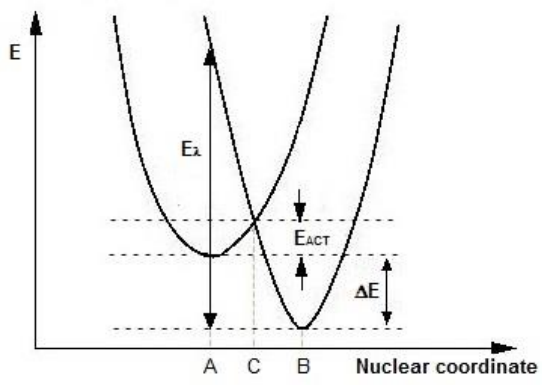

Figure 2. *Graphic representation of Activation energy E_{ACT}, Reorganization energy E_λ and of the driving force ΔE.*

The rate of electron transfer depends on temperature: spontaneous electron transfer typically occurs with thermal activation, which lets the reagents reach the energy barrier at the crossing point. The thermal contribution is the leading one in the so-called "normal region" ($E_\lambda > |\Delta E|$).

On the other hand, at low temperature, electron transfer can proceed via tunneling; this case, called "*nuclear tunneling*" requires quantum mechanical considerations of the vibrational coordinates.[1,11] Nuclear tunneling can be the dominating electron-transfer mechanism in the so-called "inverted region" ($E_\lambda < |\Delta E|$), where the overlap between the vibrational wave functions of the reactants and the products is large.

4.1.2 Photo-induced and bridge-assisted electron transfer

The electron transfer process can proceed directly from the donor to the acceptor, or involve some bridging units. In particular, we can distinguish two cases:

- *Trough-space transfer*: the donor transfers the electron directly to the acceptor. This is possible only when D and A are very close one another (less than 20 Å), as to have a finite overlap between the relevant molecular orbitals;
- *Trough-bond energy transfer*: a bridge, linking the donor with the acceptor, participates in the transfer process.

For the second typology to occur, the energy of the LUMO of the bridge has to meet specific requirements; two different situations can be envisaged:

- If the LUMO of the bridge is energetically higher than the LUMOs of the donor and the acceptor (high ΔE_{DB} in Figure 3a), the system is off-resonant and the electron cannot populate the LUMO of the linker (*superexchange mechanism*). The bridge behaves as a perturbation on the donor and acceptor species.
- If the LUMOs of donor, bridge and the acceptor are close in energy, the transferred electron can hop from the starting orbital to the final one. A number of sequential steps, during which the electron is located on a

precise LUMO for a finite time, describes this process (*hopping mechanism*, Figure 3b). The global rate of the hopping depends on the number of steps constituting the electronic pathway.[12]

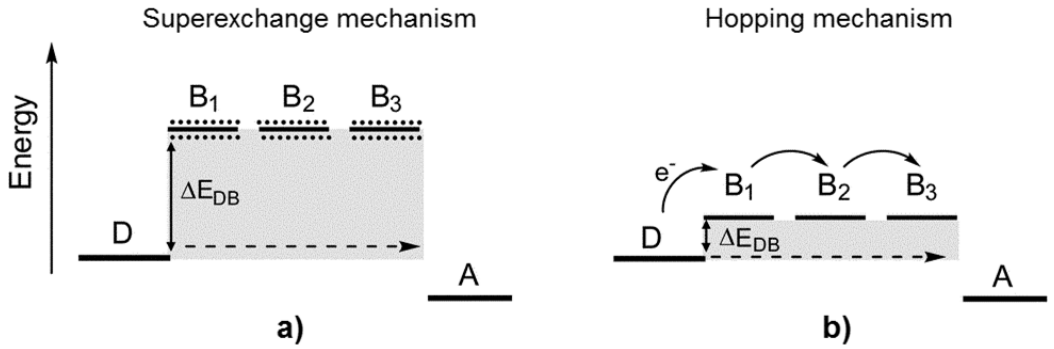

Figure 3. *Superexchange (a) and Hopping (b) mechanisms of bridge assisted electron transfer.*

Independently of the way the electron transfer occurs, it is also important to specify how it is promoted. In this thesis, only the photoinduced electron transfer will be discussed.

According to the photoinduced mechanism, the donor is first promoted to its excited state (no matter the way this is achieved), corresponding to the excitation of one of its electrons from the HOMO to the LUMO and the creation of an exciton (an electron-hole pair). In order to promote the electron transfer to the acceptor species, the energy of the LUMO of the donor must be higher than that of the LUMO of the acceptor, and the same order has to be satisfied by the HOMOs.

The respect of these conditions ensures a net electron transfer from D to A, avoiding a back transfer phenomenon via the HOMOs, that would result in charge recombination and energy transfer (Figure 4).

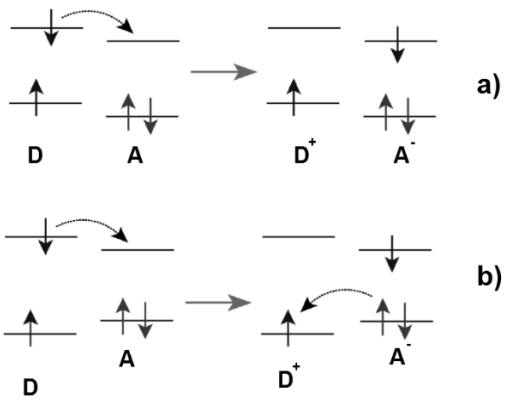

Figure 4. *Donor and Acceptor HOMOs and LUMOs a) in the right geometry for direct ET, b) in the configuration leading to exciton recombination.*

To promote the charge separation, the binding energy of the exciton has to be lower than the energy difference between the LUMOs: only if this condition is respected the charge separation leads to an energy gain.

Electron transfer and exciton recombination are competitive: electron transfer occurs when the exciton lifetime is long enough to let the electron move from the donor to the acceptor.

4.1.3 Chromophores for the electron transfer process

In order photoinduced electron transfer to occur between a donor and an acceptor, two criteria are required:

- Short distance between the species, resulting in the good overlap between their molecular orbitals;
- The energy of the HOMO and LUMO of the donor must be higher than the energy of the HOMO and LUMO of the acceptor, respectively.

Excitation energy- and electron transfer are both excited-state quenching mechanisms. The occurrence of one or the other can however be distinguished on the basis of the acceptor fluorescence, that is expected to increase only in the case of energy transfer.[13]

With the aim to improve organic photovoltaics performances and obtain the most efficient electron transfer, many covalent and non-covalent donor-acceptor systems have been designed and investigated. Porphyrin-fullerene pairs seem to be the most widely studied classes of compounds due to their rich photo- and redox chemical properties.[14,15]

Thanks to their spherical shape, fullerenes are characterized by high electron affinity and require small reorganization energy in the electron-transfer processes,[16,17] which make them ideal candidates as electron-acceptor systems. Fullerenes, in fact, tend to accelerate forward electron transfer and slow down backward electron transfer, promoting long-live charge-separated states.[18, 19, 20]

On the other hand, porphyrins are electron-rich macrocyclic compounds, capable of absorbing light over a wide wavelength spectrum in the visible region and exhibit favorable redox potentials.[15]

Porphyrins are only an example of the numerous chromophores fullerenes can be coupled with; another suitable donor, for example, is Nile red.[21]

Nile red is a well-known and largely employed dye showing high fluorescence efficiency and solvatochromism, applied as luminescent probe in the study of many chemical and biological systems.

Recently, Nile red photoinduced electron transfer studies in presence of TiO_2/Y zeolites or TiO_2 colloidal nanoparticles, have been reported.[22,23] Nile red, chemisorpted on the surface of the semiconductors, was excited by visible light irradiation and injected electrons from its excited state into the conduction band of the semiconductor.

Here it is proposed the coupling between Nile red and fullerene C_{60} as electron donor-electron acceptor pair for the evaluation of the photoinduced charge transfer.

Reported calculations by McGehee and coworkers[21] suggest that the energy of the frontier orbitals are ideally disposed to favor the electron migration, avoiding the back transfer.

Electron transfer also requires a short distance between the chromophores involved, to favor their orbital overlap; this condition can be satisfied by fixing the relative position of the photoactive species on a scaffold. As previously explained, (par. 4.1.2) the bridge can assist the process, according with two mechanisms. With the idea to qualify and quantify the electron transfer, if any, the understanding of the spacer role is a key step.

For all these reasons, two covalent electron donor-acceptor pairs have been synthesized, one of them acting as reference compound.

4.2 Aim of the chapter

With the aim to evaluate the electron transfer occurring from Nile red to fullerene C_{60}, two bichromophoric systems have been synthesized, one acting as reference compound, while the other being the real target of this study (Figure 5).

The first system is based on a linear tri-components structure, composed by Nile red (electron donor) –aromatic spacer (bridge) – fullerene C_{60} (electron acceptor), capable to give information about direct electron transfer between the photoactive units. The selected spacer is a derivative of 3-aminobenzaldehyde, which imposes a short distance and avoids a direct conjugation between the chromophores.

For the second target, the chromophores are both fixed at the upper rim of a *cone*-tetrapropoxy calix[4]arene through short linkers, resulting in a different spatial disposition which could allow the establishment of attractive intramolecular interactions, whose influence on the electron transfer is not known. For these reasons, the reference compound previously introduced is so important.

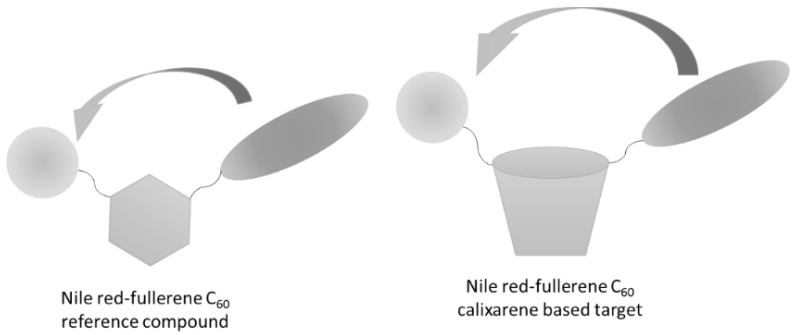

Figure 5. *Simple representation of the two bichromophoric systems for the study of electron transfer.*

4.3 Synthesis

4.3.1 Reference compound, 61

Commercially available 3-aminobenzaldehyde ethylene acetal functionalized with bromoacetyl chloride was chosen as spacer between the two chromophores. This scaffold (**57** in Scheme 1) can be functionalized with hydroxy Nile red (**NR-OH**) by nucleophilic substitution of the bromide and with fullerene C_{60} (**C_{60}**) by condensation on the deprotected aldehyde through the Prato reaction.

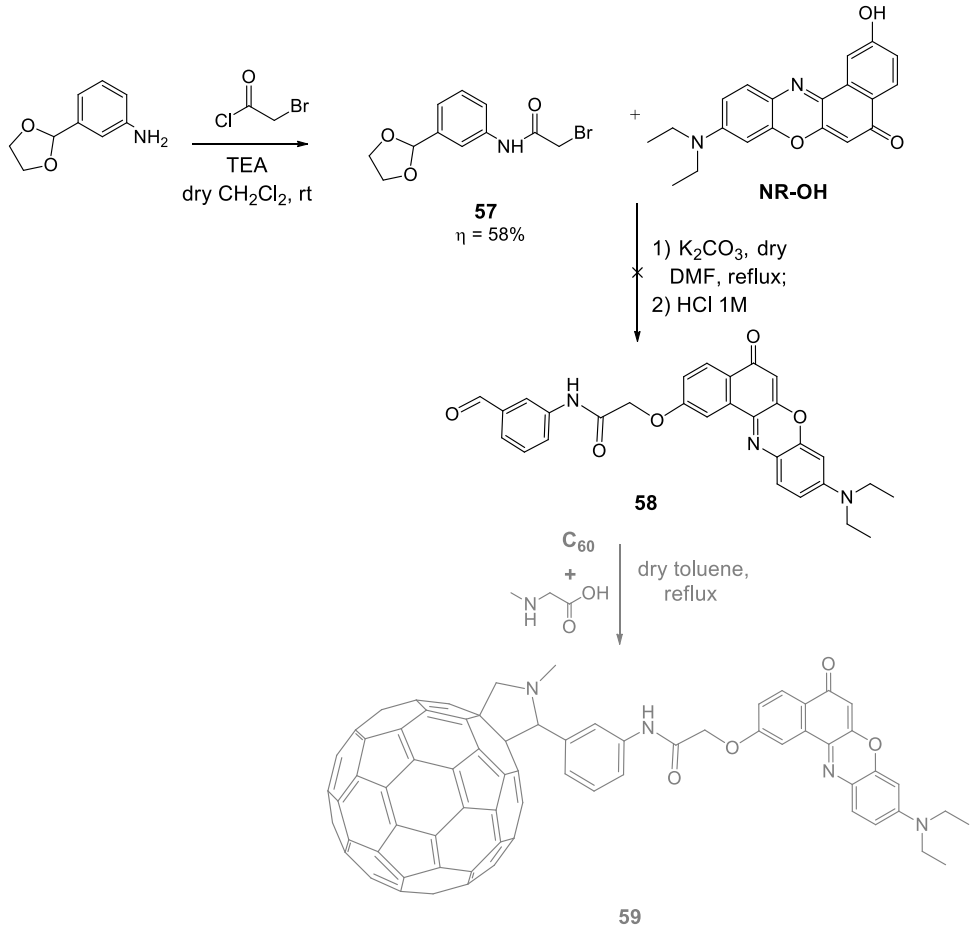

Scheme 1. *Designed synthesis of compound **59**.*

The spacer **57** was thus obtained in good yield from the coupling between 3-aminobenzaldehyde ethylene acetal and bromoacetyl chloride in basic conditions. Nucleophilic substitution of the bromide group of **57** by **NR-OH** was carried out in refluxing dry DMF using potassium carbonate as base to deprotonate the hydroxyl group of Nile red. The violet product obtained after acidic quenching and chromatographic purification, however, showed a ^{1}H NMR spectrum that did not correspond to that of the desired compound **58**. The spectrum, in particular, lacked the signal of the methylene group α to the carbonyl group, which should resonate at 4.6-4.7 ppm (Figure 6). In addition, the ^{13}C-NMR spectrum did not show either the signal corresponding to the methylene carbon and the carbonyl of the amide group.

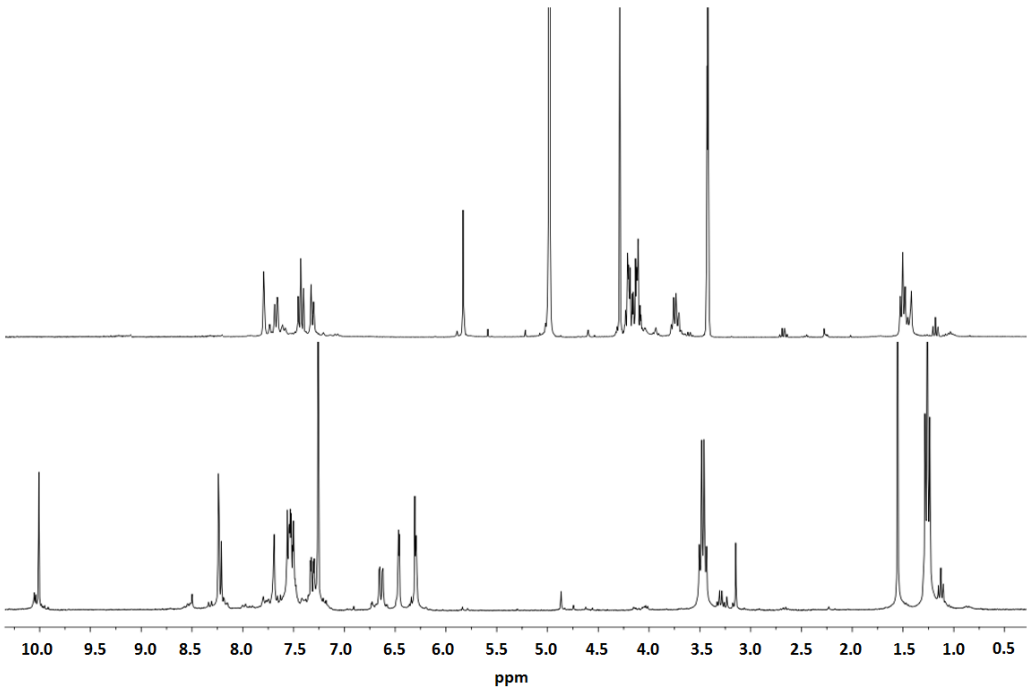

Figure 6. *^{1}H-NMR spectra of **57** in methanol-d_4 (400 MHz, top), and supposed **58** in $CDCl_3$ (300 MHz, bottom).*

ESI mass spectrometry analysis showed, as most intense signals, two peaks (m/z 438.3 and 460.3) corresponding to m/z values lacking 58 mass units with respect

to the desired compound (m/z calculated for [**58**+H^+]: 496.2 and m/z calculated for [**58**+Na^+]: 518.2), suggesting the absence of the -$COCH_2O$- group, as indicated by NMR analysis.

The unambiguous proof of the structure of this product was furnished by X-Ray diffraction of a crystal obtained by slow evaporation of a CH_2Cl_2/methanol solution. Crystallographic analysis yielded the molecular structure shown in Figure 7, where Nile red is linked to the aromatic spacer through a secondary amine.

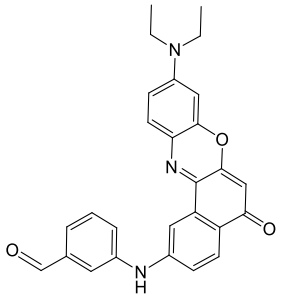

60

Figure 7. *Molecular structure of compound **60**.*

In the solid state (Figure 8, left), compound **60** presents two planar portions constituted by the benzaldehydic ring and the Nile red unit, linked together through an amine group, showing a distorted trigonal planar geometry. This distortion is evidenced by the values of the angles around the nitrogen atom, adding up to 356° (see Table 1). In addition, the dihedral angles between each aromatic portion and the NH group are 166.8(9) and 170.6(9)°, respectively, and the angle between the two least-squares planes passing through the two moieties is 148.6(1)°.

The crystal packing (Figure 8, right) is directed by intermolecular H-bonds between the NH group and the Nile red carbonyl group of two adjacent molecules, which result in the formation of tapes running in the direction of the *b*

axis of the unit cell. These tapes are, in turn, stacked along the *a* axis through π-π and Van der Waals interactions occurring among the aromatic units.

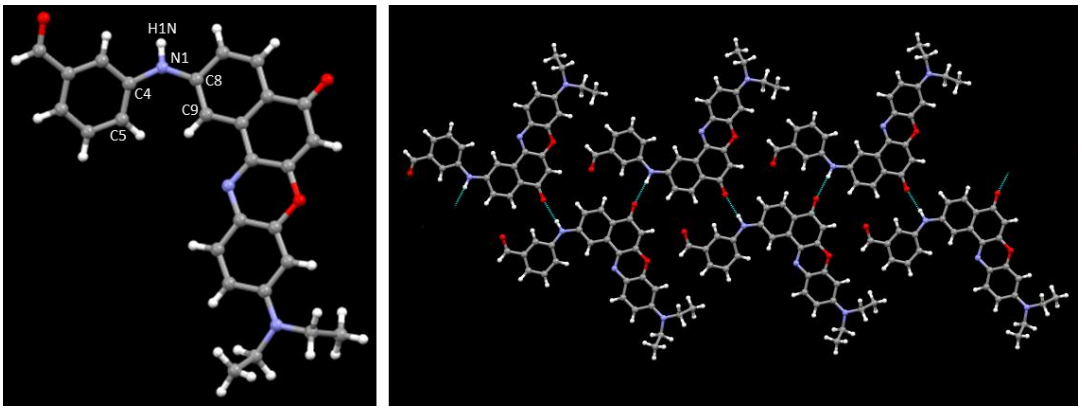

Figure 8. *Molecular structure of compound **60** (left) and crystal packing viewed along the c axis of the unit cell (right). Hydrogen bonds are represented as blue dotted lines.*

C8-N1-H1N	111.7(9)	C9-C8-N1-H1N	170.6(9)
C4-N1-C8	131.2(5)	*Hydrogen bonds*	
C4-N1-H1N	112.9(9)	N1---O2	2.947(6)
C5-C4-N1-H1N	166.8(9)	N1—H1N---O2	175.6(9)

Table 1. *Selected geometrical parameters (Å, °) for **60**.*

A careful literature search highlighted that the obtained compound is indeed the result of a one-pot sequence of three reactions (alkylation - Smiles rearrangement – hydrolysis, Scheme 2), occurring when a phenol is reacted at high temperature with a 2-halogenated acetamide in basic conditions.[24]

In our case, the phenolic unit is **NR-OH**, which is condensed with N-aryl-2-bromo acetamide **57** forming the diarylamine **60**.

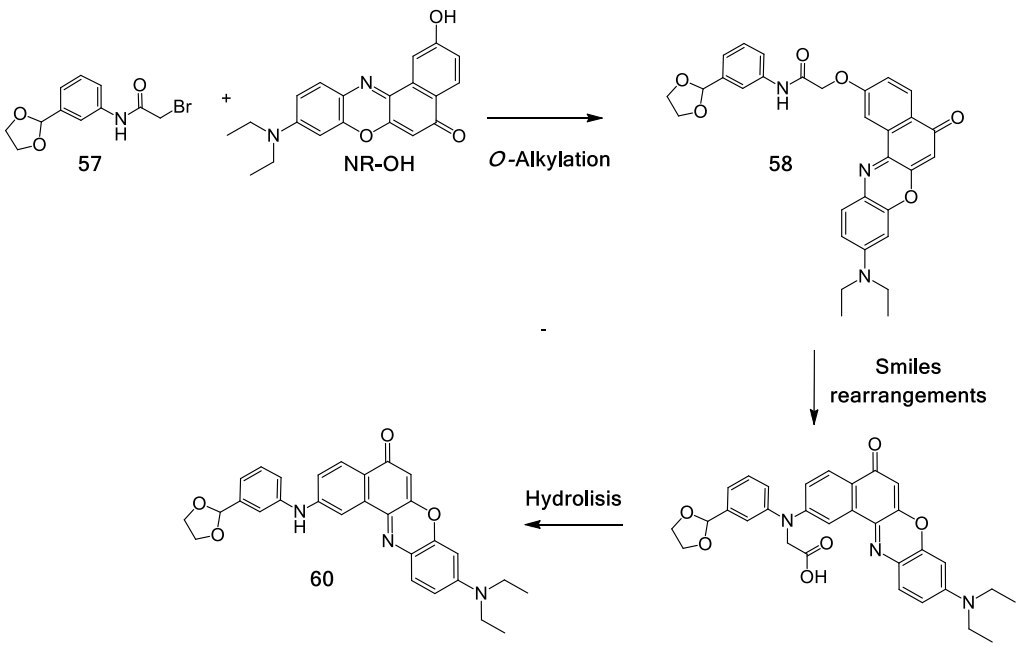

Scheme 2. *One-pot sequence of three reactions for the synthesis of diarylamine **60**.*

The key step of this sequence is the central rearrangement (Smiles rearrangement, Scheme 3), according to which an electron withdrawing group on the aromatic ring promotes the nucleophilic substitution of a heteroatom (i.e. the oxygen) with another one (i.e. the nitrogen).

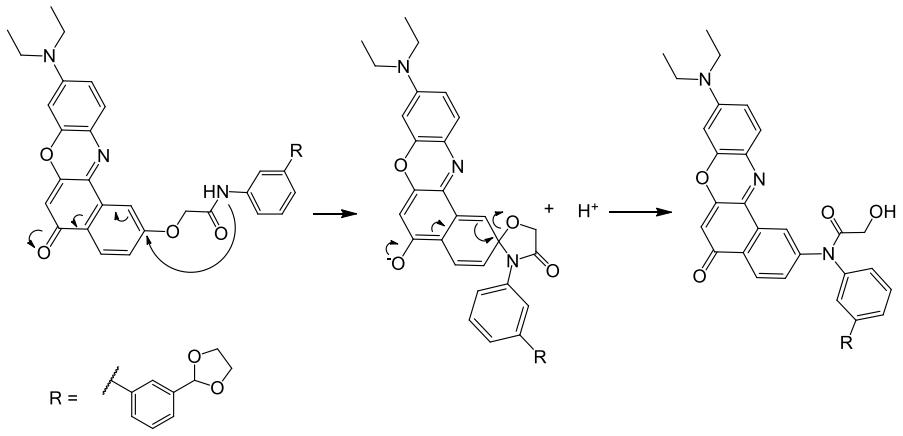

Scheme 3. *Mechanism of the Smiles rearrangement leading to compound **60**.*

Once the real molecular structure of the compound has been ascertained, the planned synthetic pathway (Scheme 4) was carried out, considering that the absence of the methylene-carbonyl unit, getting the two chromophores closer together, could even increase the transfer efficiency. Moreover, the spectroscopic characterization (*vide infra*) indicated that compound **60** basically maintains the original characteristics of Nile red, despite the substitution of the phenol oxygen with an arylamine.

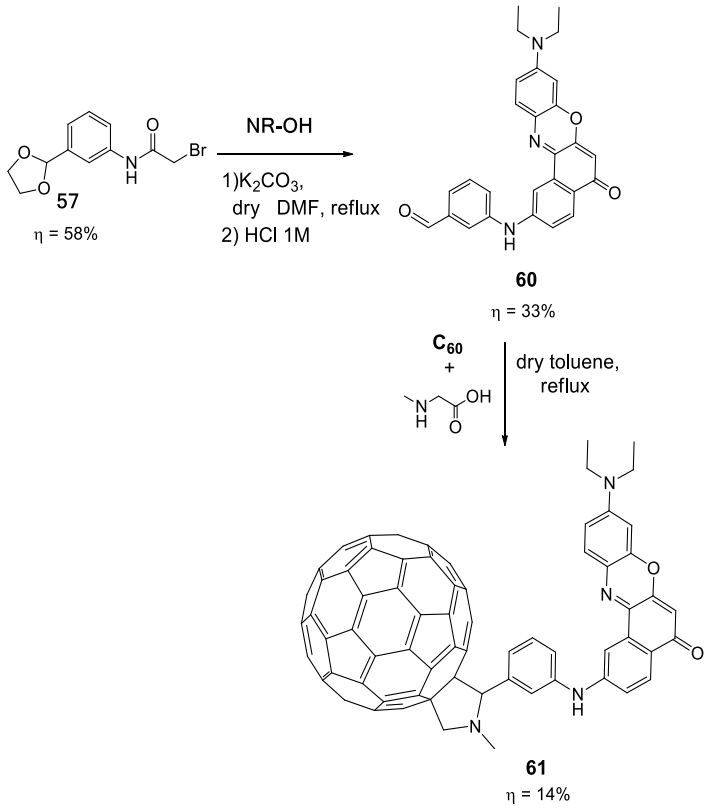

Scheme 4. *Synthesis of bichromophoric derivative **61**.*

Compound **60** was then reacted with fullerene C_{60} via Prato reaction.[25] The Prato reaction is a 1,3-dipolar cycloaddition of azomethine ylides to olefins. When heated in toluene, the formyl group is activated by sarcosine, forming an imine. The following decarboxylation of the sarcosine carboxylic group generates, in situ, an unstable ylide that immediately reacts with a fullerene double bond on a 6,6

ring position, via a 1,3-dipolar cycloaddition, to yield a N-methylpyrrolidine derivative.

The reaction afforded the new bichromophoric system **61** in 14% yield after preparative TLC purification.

The compound was studied by absorption and fluorescence spectroscopy to evaluate the occurrence of intramolecular electron transfer.

4.3.2 Nile red-Fullerene C_{60} calix[4]arene, 69

Nile red-fullerene C_{60} calix[4]arene was initially planned to be synthesized according to the same pathway adopted for reference compound **59** (Scheme 5).

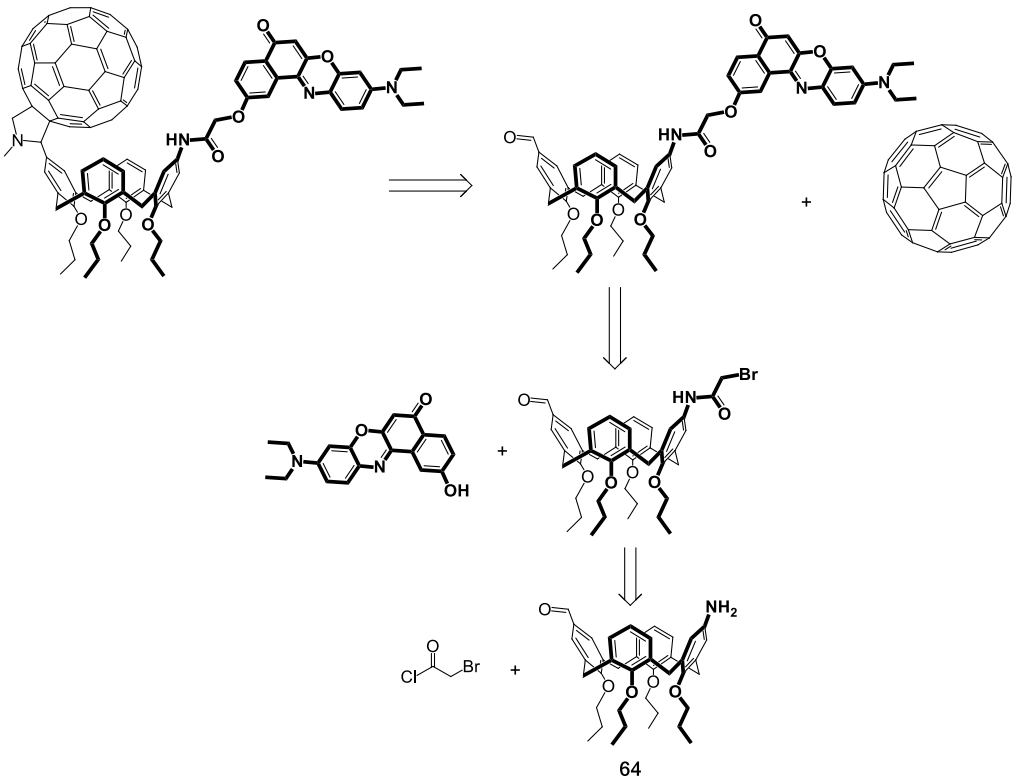

Scheme 5. *Retrosynthetic analysis for Nile red-Fullerene C_{60} calix[4]arene.*

A tetrapropoxy calix[4]arene functionalized on the upper rim 1,3-distal position with a formyl and an amino group (compound **64**) was designed to be the starting reagent of the synthetic scheme, in analogy with 3-aminobenzaldehyde (see Scheme 1 and Scheme 5). The synthesis of calixarene **64** was carried out according to Scheme 6.

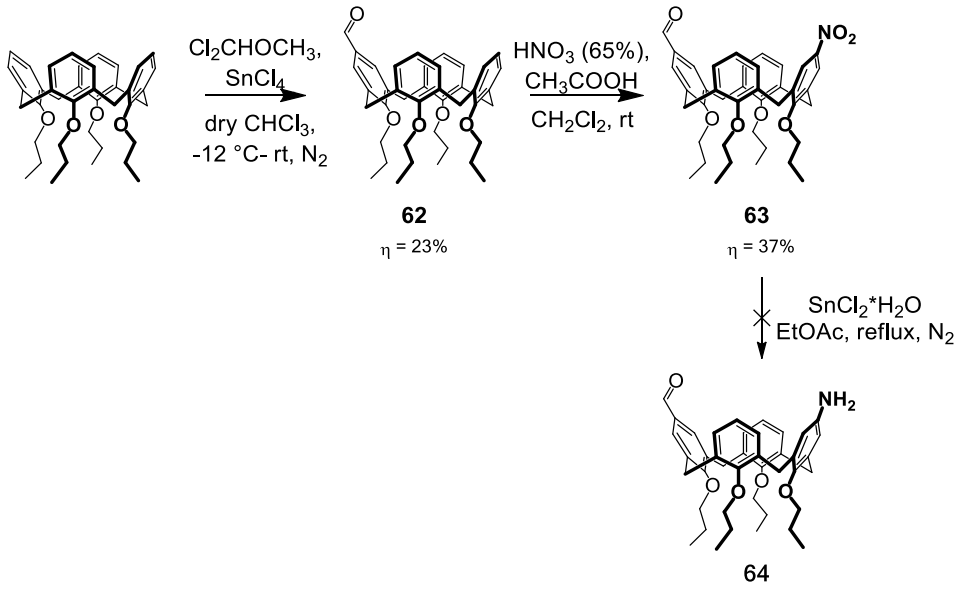

Scheme 6. *Designed synthesis for 1,3-distal amino-formyl calix[4]arene **64**.*

Intermediate compound **63** was synthesized according to a literature procedure[26] by subsequent formylation and nitration of tetrapropoxy calix[4]arene.

Selective reduction of the nitro group of **63** was performed by stannous chloride dihydrate as reducing agent. TLC monitoring during the course of the reaction indicated the initial formation of two new products. The reaction was carried out until the complete consumption of the starting material, when TLC monitoring also revealed that the product with lower retention factor had disappeared. ESI mass spectrometry showed, as most intense signals, two peaks (m/z 1235.9 and 1258.9) that did not correspond to the m/z values calculated for the desired compound (m/z calculated for [**64**+H^+]: 635.4 and m/z calculated for [**64**+Na^+]:

658.4). These peaks, instead, suggested a dimerization of two calixarene units (Scheme 7), through two intermolecular imine bonds. The presence of a singlet at 6.77 ppm in the ^{1}H-NMR spectrum (Figure 10) confirmed the presence of the imine protons. The signals of the protons *ortho* to the imine groups, moreover, are upfield shifted (6.47 and 5.74 ppm), indicating a *"closed" flattened cone* conformation of the calixarene scaffold.[27]

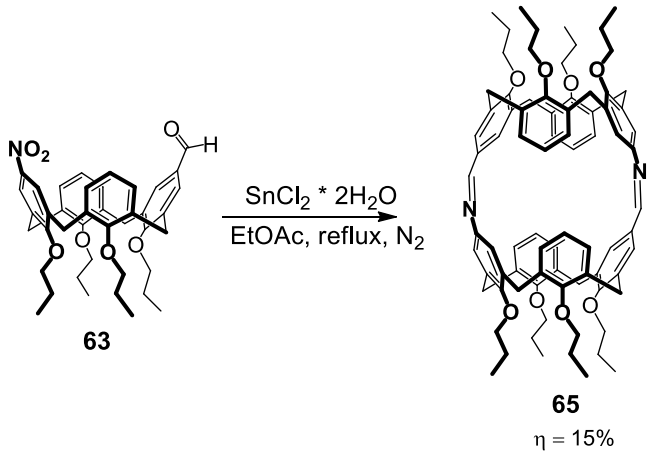

Scheme 7. *Formation of compound **65**.*

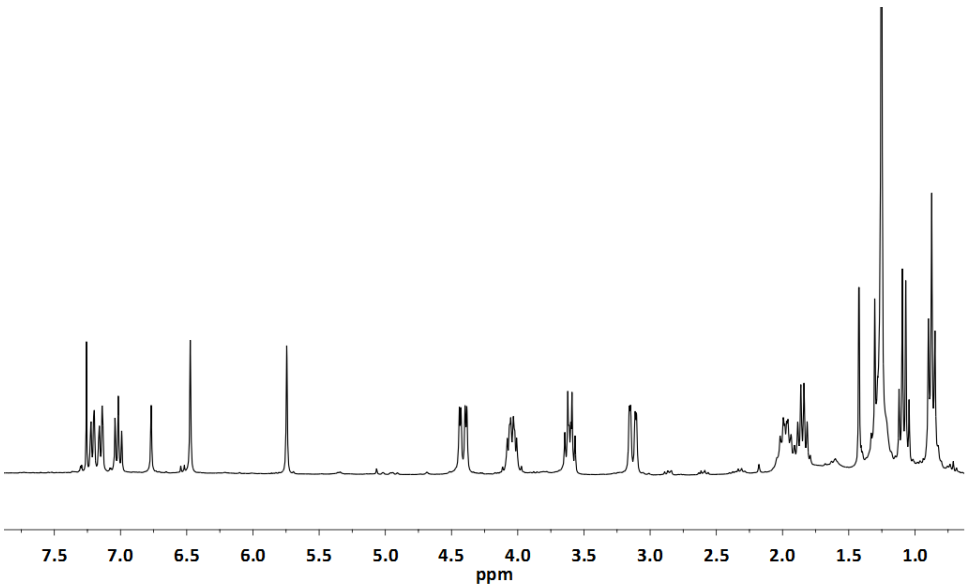

Figure 9. *^{1}H-NMR ($CDCl_3$, 300 MHz) spectrum of compound **65**.*

The unambiguous proof of the structure of this product was furnished by X-Ray diffraction analysis on a crystal of **65**, obtained by slow evaporation of a CH_2Cl_2/hexane solution. Even if the low quality of the collected data did not allow a complete refinement, the molecular structure has been ascertained (Figure 10) and consists of two *closed flattened cone* calix[4]arenes linked by imine bonds in trans configuration.

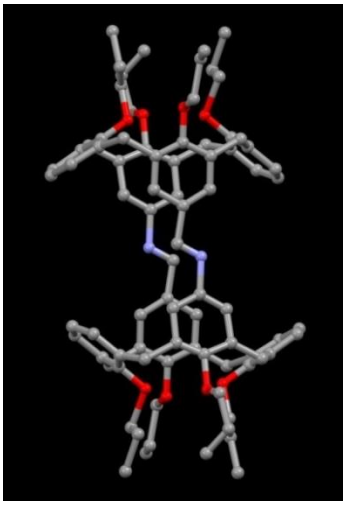

Figure 10. *Crystal structure of compound **65**.*

In light of these results, it can be hypothesized that the intermediate compound observed at earlier time of reaction, giving the spot with the lower retention factor, could correspond to the monomeric imine (**66**, Scheme 8).

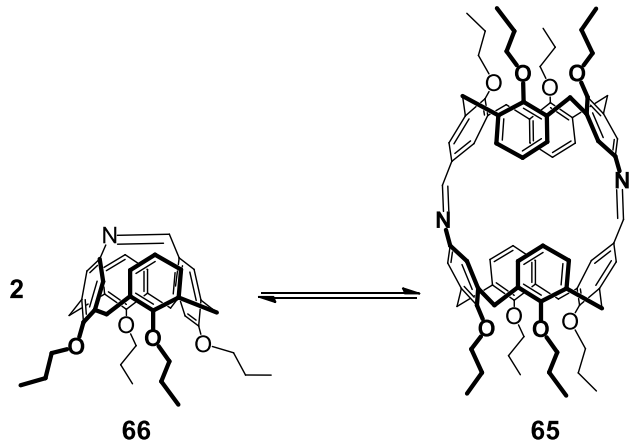

Scheme 8. *Proposed equilibrium between monomeric imine **66** and dimeric compound **65**.*

Compound **66**, whose formation is favored by the close distance between the formyl and the amino groups, has been supposed to be the kinetic product. Thanks to the reversible nature of imine bonds, long reaction times promoted its conversion to the dimeric and thermodynamically favored compound **65**. The formation of compound **65** was not expected, since none of literature work describing the selective reduction of 4-nitrobenzaldehyde to 4-aminobenzaldehyde[28] reports a polymerization of the desired product.

Many attempts were performed to hydrolyze the intramolecular imine **65** in acidic conditions, but none of which was successful.

Due to this problem and to the observation of the Smiles rearrangement in the synthesis of reference compound **61** (see par. 4.3.1, this synthetic strategy was discarded and, once again, to asymmetrically functionalize the upper rim of a calix[4]arene, the *statistical approach* was adopted (Scheme 9).

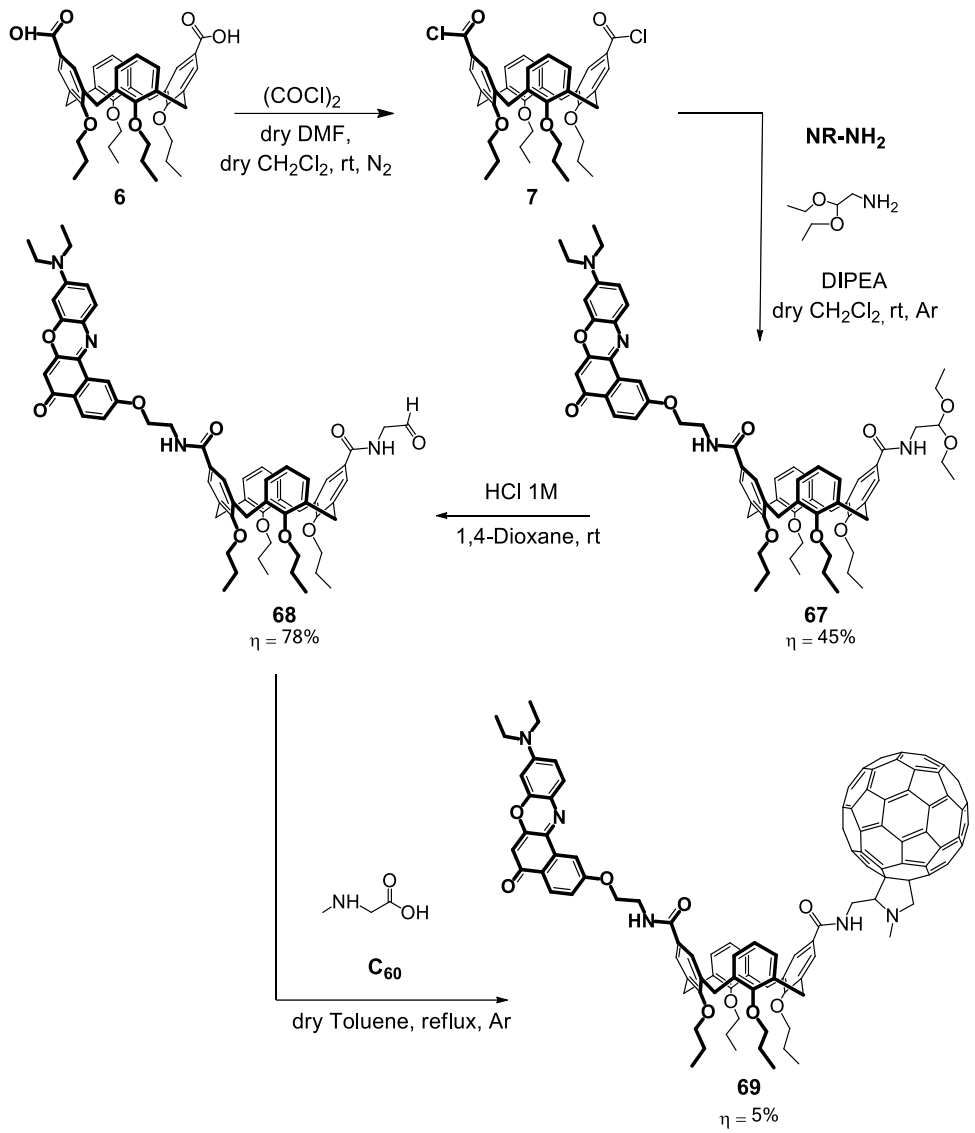

Scheme 9. *Synthesis of compound **69** by statistical approach followed by Prato reaction.*

Diacid calixarene **6**[29] was activated as acyl chloride and reacted with a mixture of **NR-NH$_2$** (see Chapter 2) and 2,2-diethoxyethanamine, affording the desired product **67** in 45% yield after column chromatography followed by preparative TLC. The acetal protecting group was then removed in acidic condition obtaining the corresponding aldehyde **68**, which, after purification by preparative TLC, was isolated in 78% yield.

The last step consisted in the condensation of fullerene C_{60} to the formyl group of **68** through the Prato reaction.[25] The reaction was performed in refluxing toluene in Argon atmosphere and it was quenched before the complete consumption of the starting material, to avoid multifunctionalizations on $\mathbf{C_{60}}$. Compound **69** was isolated in 5% yield after preparative TLC, but it was not sufficiently pure for spectroscopic characterization and electron transfer studies.

4.4 Spectroscopic studies

Compounds **60** and **61**, as well as fullerene C_{60} were studied by absorption and steady-state fluorescence spectroscopy to evaluate the occurrence of photoinduced electron transfer from Nile red to fullerene C_{60} in different solvents. The concentration of the samples was about 10^{-5} M and 10^{-6} M for absorption and fluorescence spectra, respectively.

Absorption and fluoresce spectra of compounds **60** were collected in different organic solvents with increasing polarity: toluene, chloroform and dimethyl sulfoxide. Figure 11 depicts the absorption and fluorescence bathochromic effects, which occur for **60** with the solvent polarity increase.

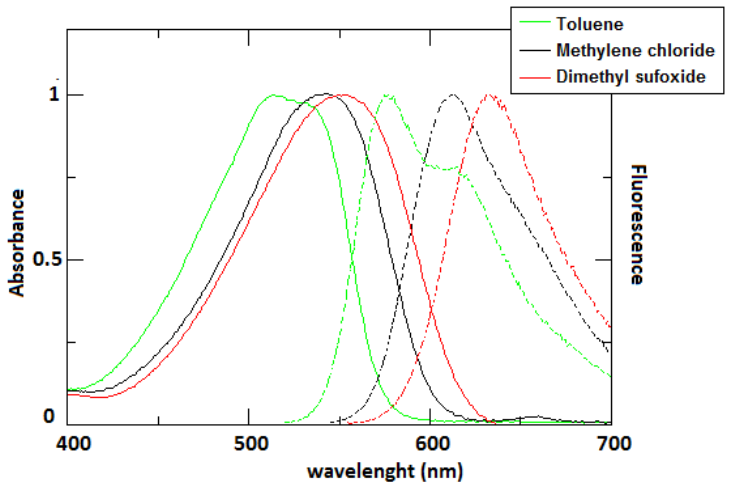

Figure 11 *Normalized absorption (full line) and emission spectra (dashed line) of compound **60** in toluene (green), methylene chloride (dark) and dimethyl sulfoxide (red.)*

The data collected for compound **60** confirmed that the presence of the aromatic bridge does not affect the Nile red spectroscopic properties.

Compound **61** was then studied only in two solvents, due to the low solubility of fullerene.

Absorption and fluorescence spectra (Figure 12) in methylene chloride and in toluene reported the presence in **61** (green line) of the spectroscopic features of **60** (red line) and **C_{60}** (blue line) spectra, confirming the covalent linkage of both the chromophoric units on the scaffold in **61**. As an example, the absorption spectrum revealed the presence of two bands, corresponding to Nile red (λ_{max}^{abs} = 542 nm in methylene chloride and λ_{max}^{abs} = 514 nm in toluene) and to fullerene C_{60} (λ_{max}^{abs} = 330 nm in methylene chloride and λ_{max}^{abs} =335 nm in toluene).

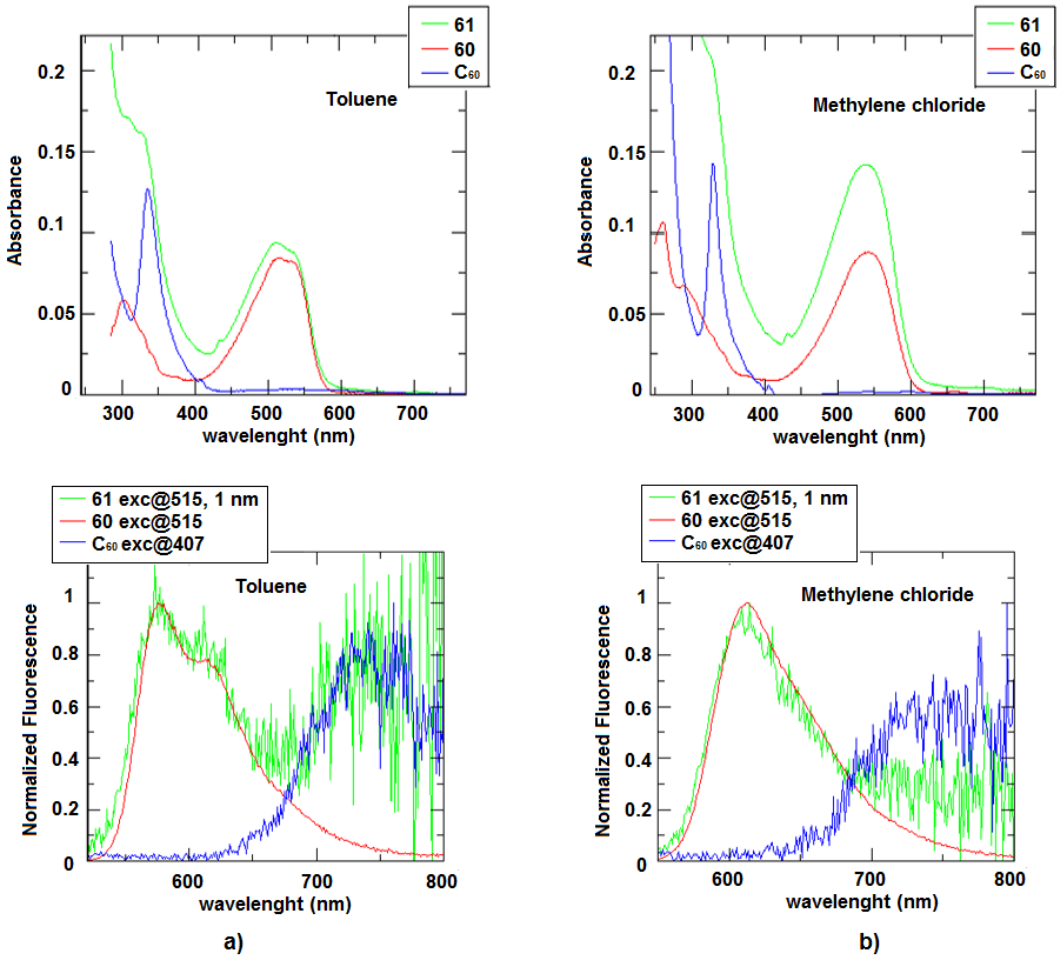

Figure 12. *Normalized absorption (top) and fluorescence (bottom) spectra a) in toluene and b) in methylene chloride of compounds **61**, **60** and **C_{60}**.*

Fluorescence spectra (Figure 12) also indicate a highly efficient photoinduced charge transfer from Nile red to fullerene C_{60}. In fact, as reported in Table 2, the fluorescence quantum yield of **61** decreases by two orders of magnitude with respect to **60**, demonstrating the radiationless quenching of photoexcited Nile red, via electron transfer. An energy transfer mechanism can be ruled out since we do not observe an increase in the emission of $\mathbf{C_{60}}$.

	60	**61**
Toluene	0.39	0.004
Methylene chloride	0.42	0.003
Dimethyl sulfoxide	0.08	-

Table 2. *Fluorescence quantum yields of compounds **60** and **61**.*

We can thus conclude that the covalent Nile red-fullerene C_{60} couple represents an efficient system for photoinduced electron transfer. Future transient studies to be performed on the dyad and on the charged species (D^+ and A^-) could give information about their lifetimes, leading to evaluate their potential application in devices for sunlight conversion.

The analogous bichromophoric calix[4]arene **69** has not been studied yet by absorption and fluorescence spectroscopies due to the insufficient purity of the isolated compound.

4.5 Concluding remarks

Nile red and Fullerene C_{60} dyes, chosen on the basis of their HOMOs and LUMOs energies, were anchored to the upper rim of a calix[4]arene blocked in the cone conformation. Since the calixarene spacer between Nile red and Fullerene C_{60} may affect the efficiency of charge transfer and/or actively assist the process, a simple linear tri-component model **61** was synthesized as a reference compound.

The synthetic pathway initially planned, however, did not lead to the formation of the desired compound **59** because of the occurrence of a one-pot three-step reaction involving a Smiles rearrangements, that yielded the secondary amine **60** instead. ^{1}H-NMR, ESI mass spectrometry and XRD analysis allowed a correct attribution of the molecular structure of **60**, while UV-vis spectroscopy indicated that the spectral properties of **60** were not different from the ones of Nile red. Fullerene C_{60} was then condensed via the Prato reaction to **60**, isolating the bichromophoric derivative **61**.

Fluorescence measurements on compound **61** showed an almost quantitative quenching of the fluorescence of Nile red, indicating an extremely efficient electron transfer from Nile red to fullerene C_{60}, as expected.

Based on these positive results, the bichromophoric calixarene-based analogue was synthesized. The first attempt was performed following a sequential approach to link in different steps the chromophoric units at the upper rim of the macrocycle. Because of the synthetic difficulties met during the preparation of the scaffold **65**, however, a statistical approach was preferred.

The synthesis of the calixarene-based analogue was performed in four steps starting from the diacid derivative **6**. This compound was first activated as acyl chloride and subsequently reacted with a mixture of Nile red functionalized with an ethylenamine spacer and amino acetaldehyde protected as acetal. After

deprotection, Prato reaction afforded compound **69** in 5% yield. Because compound **69** was not isolated sufficiently pure, a complete spectroscopic characterization was not performed. In addition, with the aim to increase both the synthetic yield and the purity, an optimized synthesis and purification of bichromophoric calixarene **69** is in progress. The desired product will be studied by absorption and fluorescence spectroscopies to evaluate the electron transfer efficiency. The dynamics of the electron transfer process and the lifetimes of the oxidized and reduced species will be measured to complete the investigations for a possible application of this chromophoric couple in artificial photovoltaic devices.

4.6 Experimental section

General methods

All moisture sensitive reactions were carried out under Nitrogen or Argon atmosphere, using previously oven-dried glassware. Dry solvents were prepared according to standard procedures, distilled before use and stored over 3 or 4 Å molecular sieves. Most of the solvents and reagents were obtained from commercial sources and used without further purification. Analytical TLC were performed using prepared plates of silica gel (Merck 60 F-254 on aluminium) and then, according to the functional groups present on the molecules, revealed with UV light. Merck silica gel 60 (70-230 mesh) was used for flash chromatography and for preparative TLC plates. ^{1}H NMR and ^{13}C spectra were recorded on Bruker AV300 and Bruker AV400 spectrometers (observation of ^{1}H nucleus at 300 MHz and 400 MHz respectively, and of ^{13}C nucleus at 75 MHz and 100 MHz respectively). All chemical shifts are reported in part per million (ppm) using the residual peak of the deuterated solvent, whose values are referred to tetramethylsilane (TMS, $\delta_{TMS}= 0$), as internal standard. All ^{13}C NMR spectra were performed with proton decoupling. Mass spectra were recorded in ESI mode on a single quadrupole instrument SQ Detector, Waters (capillary voltage 3.7 kV, cone voltage 30-160 eV, extractor voltage 3 eV, source block temperature 80 °C, desolvation temperature 150 °C, cone and desolvation gas (N_2) flow rates 1.6 and 8 L/min, respectively). High resolution mass spectra were recorded on a LTQ Orbitrap XL instrument in positive mode using CH_3CN or CH_3OH as solvents. Melting points were determined on an Electrothermal apparatus in closed capillaries.

UV-vis absorption spectra were recorded on a Perkin Elmer Lambda 650 spectrometer. Steady-state fluorescence spectra and fluorescence decays were carried out on a Fluoromax-3 Horiba Jobin Yvon spectrofluorometer Fluorescence decays were measured in a TCSPC (time-correlated single-photon counting) configuration, under excitation from selected nanoLED or laser-diode sources; fluorescence lifetimes were obtained from the reconvolution fit analysis of the decay profiles; the quality of the fits was judged by the reduced χ^2 value (fits are retained for $\chi^2 < 1.1$).

5,17-di-hydroxycarbonyl-25,26,27,28-tetrapropoxycalix[4]arene **6**,[29] 5-formyl-17-nitro-25,26,27,28-tetrapropoxycalix[4]arene **63**,[26] and **NR-OH**[30,31] were synthesized according to literature procedure.
For the synthesis of **NR-NH$_2$** see Chapter 2.

Compound 57

To a stirred solution of 3-aminobenzaldehyde ethylene acetale (250 mg, 1.51 mmol) and TEA (0.51 mL, 3.65 mmol) in dry CH_2Cl_2 (9 mL), 2-bromoacetyl chloride (0.23 mL, 2.75 mmol) was added and the reaction was carried out for 24 h, when the monitoring by TLC (CH_2Cl_2/ethyl acetate 8/2) revealed the complete consumption of the starting material. The reaction was quenched by the addition of saturated aq. $NaHCO_3$ (10 mL). The two layers were separated, the aqueous layer was extracted with CH_2Cl_2 (2x10 mL) and the combined organic layers were washed with water till neutral pH and concentrated under reduced pressure. The brown crude oil **57** (0.86 mmol, 58% yield) was quickly used in the following step without further purification.
^{1}H NMR (300 MHz, CD_3OD): δ (ppm) 7.84 (s, 1H, ArH), 7.72 (d, J = 7.8 Hz, 1H, ArH), 7.47 (t, J = 7.8 Hz, 1H, ArH), 7.36 (d, J = 7.8 Hz, 1H, ArH), 5.86 (s, 1H, ArCHO), 4.31 (s, 2H, CH_2Br), 4.23-4.20 (m, 2H, OC*H$_2$*CH_2O), 4.15-4.12 (m, 2H, OCH_2C*H$_2$*O).
A complete characterization of the compound was not performed due to the instability of the product.

Compound 60

NR-OH (118 mg, 0.35 mmol) and K_2CO_3 (146 mg, 1.06 mmol) were dissolved in dry DMF (10 mL) and compound **57** (132 mg, 0.46 mmol) was added. The solution was refluxed for 3 h, then the reaction was quenched by the addition of 1M HCl (10 mL). The aqueous layer was extracted with CH_2Cl_2 (10 mL), basified with saturated aq. $NaHCO_3$ (20 mL) and extracted with CH_2Cl_2 (20 mL). The combined organic layers were washed with H_2O, dried over anhydrous Na_2SO_4 and concentrated under reduced pressure. The violet crude oil was purified by flash column chromatography (CH_2Cl_2/CH_3OH 97/3), and pure **60** was isolated as a violet solid in 33% yield (57 mg, 0.13 mmol).

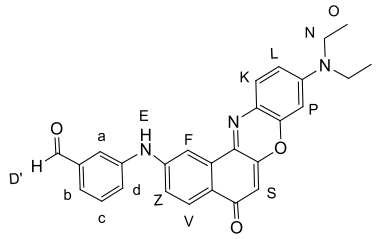

60

^{1}H NMR (300 MHz, CDCl3): δ (ppm) 10.01 (s, 1H, CHO), 8.24-8.21 (m, 2H, H_F, H_V), 7.69 (s, 1H, H_a), 7.56-7.50 (m, 4H, H_b, H_c, H_d, H_K), 7.32 (dd, J = 7.8Hz, J = 2.3Hz, 1H, H_Z), 6.64 (dd, J = 9.1Hz, J = 2.6Hz, 1H, H_L), 6.47 (d, J = 2.6Hz, 1H, H_P), 6.31 (s, 1H, H_S), 6.29 (s, 1H, H_E), 6.47 (q, J = 7.1Hz, 2H, H_N), 1.26 (t, J = 7.1Hz, 3H, H_O). ^{13}C NMR (75 MHz, $CDCl_3$): δ (ppm) 192.1; 183.0; 161.4; 151.9; 150.7; 146.8; 145.6; 142.7; 137.7; 133.9; 131.1; 130.2; 129.7; 127.6; 124.6; 123.7; 121.1; 119.0; 118.3; 109.9; 109.5; 105.4; 45.1; 12.63. ESI-MS: m/z calcd for $C_{27}H_{23}N_3O_3$+H^+438.2, found 438.3 (48%); m/z calcd for $C_{27}H_{23}N_3O_3$+Na^+ 460.2, found 460.3 (100%).

Compound 61

Compound **60** (19 mg, 0.045 mmol), N-methylglycine (7 mg, 0.079 mmol) and fullerene C_{60} (28 mg, 0.039 mmol) were dissolved in dry toluene (20 mL). The purple solution was refluxed for 20 h, until most of fullerene was converted, then the solvent was removed under reduced pressure. The violet crude was dissolved in CH_2Cl_2 (10 mL) and washed with H_2O (10 mL). The aqueous layer was extracted with CH_2Cl_2 (2x20mL) and the combined organic layers were washed with H_2O till neutral pH and concentrated under reduced pressure. Pure compound **61** was isolated by preparative TLC (CH_2Cl_2/CH_3OH 96/4) as a violet-brown solid in 14% yield (7 mg, 0.005 mmol).

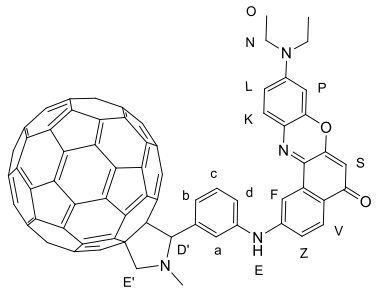

61

^{1}H NMR (300 MHz, $CDCl_3$): δ (ppm) 8.16 (s, 1H, H_F); 8.14 (d, J = 6.6Hz, 1H, H_V); 7.54 (d, J = 9.1Hz, 1H, H_K); 7.41 (t, J = 7.4Hz, 1H, H_c); 7.22-7.15 (m, 4H, H_a, H_b, H_d and

H_Z); 6.64 (dd, J_1 = 9.1Hz, J_2 = 2.7Hz, 1H, H_L); 6.46 (d, J = 2.7 Hz, 1H, H_P); 6.28 (s, 1H, H_S); 6.24 (s, 1H, H_E); 4.97 (d, J = 9.5 Hz, 1H, (HH)$_{E'}$); 4.93 (s, 1H, $H_{D'}$); 4.26 (d, J = 9.5 Hz, 1H, (HH)$_{E'}$); 3.48 (q, J = 7.2 Hz, 2H, H_N); 2.88 (s, 1H, NCH_3); 0.85 (t, J = 7.2Hz, 3H, H_O). ^{13}C-NMR was not recorded due to the insolubility of the product. ESI-MS: m/z calcd for $C_{89}H_{28}N_4O_2$+H^+ 1185.2, found 1185.5 (13%).

Compound 65

To stirred solution of 5-formyl-17-nitro-25,26,27,28-tetrapropoxycalix[4]arene **63** (100 mg, 0.150 mmol) in ethyl acetate (5 mL) under N_2 atmosphere, Tin (II) chloride dihydrate (103 mg, 0.75 mmol) was added. The solution became immediately dark orange and it was refluxed (77°C) for 24 h, when TLC monitoring (hexane/ethyl acetate 60/40) indicated the complete consumption of the starting material. The solution was cooled to room temperature and the pH was made basic (pH 7-8) by addition of sat. aqueous $NaHCO_3$, before being extracted with CH_2Cl_2 (2x20 mL). The collected organic layers were washed with H_2O (2x20 mL) and evaporated to dryness. Pure compound **65** was isolated by preparative TLC (hexane/ethyl acetate 82/18) as a yellow solid in 15% yield (26 mg, 0.021 mmol).
^{1}H NMR (300 MHz, $CDCl_3$): δ 7.21 (d, J =7.3 Hz, 4H, ArH); 7.15 (d, J = 6.18 Hz, 4H, ArH); 7.01 (t, J = 7.3, Hz, 4H, ArH); 6.77 (s, 2H, ArCH=N-Ar); 6.47 (s, 4H, ArH); 5.74 (s, 4H, ArH); 4.42 (d, J = 13.0 Hz, 8H, ArCHHAr); 4.08-4.05 (m, 8H, OCH_2CH$_2$CH$_3$), 3.64-3.56 (m, 8H, OCH_2CH$_2$CH$_3$); 3.13 (d, J = 13.0 Hz, 8H, ArCHHAr); 2.01-1.93 (m, 8H,OCH$_2$CH_2CH$_3$); 1.91-1.81 (m, 8H, OCH$_2$CH_2CH$_3$); 1.08 (t, J = 7.3 Hz, 12H, OCH$_2$CH$_2$CH_3); 0.87 (t, J = 7.3 Hz, 12H, OCH$_2$CH$_2$CH_3). ESI-MS: m/z calcd for $C_{66}H_{72}N_4O_{10}$+H^+ 1235.7, found 1235.9 (100%); m/z calcd for $C_{66}H_{72}N_4O_{10}$+Na^+ 1257.7,found 1258.9 (40%).

Compound 67

Compound **6** (0.105 g, 0.15 mmol) was suspended in dry CH_2Cl_2 (8 mL) and oxalyl chloride (0.410 mL, 4.64 mmol) and dry DMF (10 µL) were slowly added. The reaction mixture was stirred at rt for 18 h, then it was concentrated under reduced pressure. The yellow solid **7** was employed immediately in the following step without further purification.
To a stirred solution of **NR-NH$_2$** (64 mg, 0.17 mmol), 2,2-diethoxyethanamine (25 µL, 0.17 mmol) and DIPEA (0.362 mL, 2.08 mmol) in dry CH_2Cl_2 (15 mL), compound **7** (0.110 g, 0.15 mmol) was added. The reaction was carried out at rt for 20 h, when the TLC monitoring (CH_2Cl_2/CH_3OH 9:1) indicated the complete consumption of the calixarene. Then, the reaction was quenched adding H_2O (40

mL) and the two layers were separated. The aqueous layer was extracted with CH_2Cl_2 (4x40 mL) and the combined organic layers were washed with H_2O till neutral pH, concentrated under reduced pressure and the crude was purified by flash column chromatography (CH_2Cl_2/CH_3OH 95/5). The fraction containing the desired product was further purified by preparative TLC (CH_2Cl_2/CH_3OH 92/8) affording the desired product **67** in 45% yield (0.08 g, 0.07 mmol).

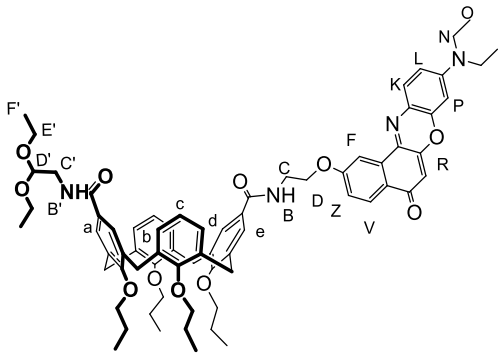

67

^{1}H NMR (400 MHz, $CDCl_3$): δ(ppm) 8.25 (d, J = 8.7 Hz, 1H, H_V); 8.11 (d, J = 2.2 Hz, 1H, H_F); 7.61 (d, J = 9.1 Hz, 1H, H_K); 7.21 (dd, J_1 = 8.7 Hz, J_2 = 2.2 Hz, 1H, H_Z);6.76-6.62 (m, 5H, H_b, H_d, H_L); 6.55-6.50 (m, 6H, H_a, H_e, H_c); 6.46 (d, J = 2.2 Hz, 1H, H_P); 6.39 (t, J = 5.5 Hz, 1H, $H_{B'}$); 6.31 (s, 1H, H_S); 6.10 (t, J = 5.8 Hz, 1H, H_B); 4.59 (t, J = 5.5 Hz, 1H, $H_{D'}$); 4.45 (d, J = 13.2 Hz, 2H, ArC*H*HAr); 4.43 (d, J = 13.2 Hz, 2H, ArC*H*HAr) 4.33 (t, J = 4.8 Hz, 2H, H_D); 3.97-3.68 (m, 10H, OC*H*$_2$CH$_2$CH$_3$, $H_{E'}$ and H_C); 3.63-3.41 (m, 8H, OC*H*$_2$CH$_2$CH$_3$ e H_N); 3.19 (d, J = 13.2 Hz, 2H, ArH*H*Ar); 3.17 (d, J = 13.2 Hz, 2H, ArH*H*Ar); 1.93-1.85 (m, 8H, OCH$_2$C*H*$_2$CH$_3$); 1.30-1.18 (m, 12H, H_O and $H_{F'}$); 1.10-0.94 (m, 12H, OCH$_2$CH$_2$C*H*$_3$). ^{13}C NMR (100 MHz, $CDCl_3$): δ(ppm) 190.7; 183.2; 167.9; 161.3; 159.7; 156.1; 150.78; 146.9; 140.1; 135.7;, 134.3;, 134.2; 131.2;, 128.7; 128.4; 128.3; 128.1;, 127.9;, 127.7; 127.2;, 127.0;, 126.9; 124.8; 122.6; 122.4; 118.2; 109.6; 106.9; 105.3; 100.9; 100.78; 96.3; 76.7; 72.4; 67.3; 62.8; 55.2; 45.1; 42.2; 39.4; 32.2; 30.9; 29.7; 29.34; 23.1; 22.7; 15.5; 14.1; 12.6; 10.3; 10.24; 10.15. ESI-MS: m/z calcd for $C_{70}H_{82}N_4O_{11}$+K^+ 1193.6, found 1193.27 (25%).

Compound 68

Compound **67** (80 mg, 0.07 mmol) was dissolved in 1,4-dioxane (8 mL) and aqueous HCl (1M, 8mL) was added. The reaction was monitored by TLC. After 4 h, the reaction was quenched adding CH_2Cl_2 (20 mL) and H_2O (20 mL). The aqueous

layer was further extracted with CH_2Cl_2 (2x20 mL) and the combined organic layers washed with H_2O till neutral pH. After evaporating the solvent under reduced pressure, the crude material was purified by preparative TLC (CH_2Cl_2/methanol 95/5), affording the desired product **68** as a violet solid in 78% yield (59 mg, 0.055 mmol).

^{1}H NMR (400 MHz, $CDCl_3$): δ(ppm) 9.65 (s, 1H, $H_{D'}$); 8.24 (d, J = 8.7 Hz, 1H, H_V); 8.08 (d, J = 2.5 Hz, 1H, H_F); 7.61 (d, J = 9.1 Hz, 1H, H_K); 7.19 (dd, J_1 = 8.7 Hz, J_2 = 2.5 Hz, 1H, H_Z); 7.01 (s, 2H, H_e); 6.90 (s, 2H, H_a); 6.73-6.52 (m, 8H, H_b, H_c, H_d, H_L and $H_{B'}$); 6.46 (d, J = 2.6 Hz, 1H, H_P); 6.34 (t, J = 4.0 Hz, H_B); 6.30 (s, 1H, H_S), 4.46 (d, J = 13.3 Hz, 2H, ArC*H*HAr); 4.43 (d, J = 13.3 Hz, 2H, ArC*H*HAr); 4.29 (t, J = 4.8 Hz, 2H, H_D); 4.20 (d, J = 4.9 Hz, 2H, H_D); 3.89-3.66 (m, 8H, O*CH*$_2$$CH_2CH_3$, H_C); 3.48-3.38 (m, 4H, O*CH*$_2$$CH_2CH_3$); 3.20 (d, J = 13.3 Hz, 2H, ArCH*H*Ar); 3.17 (d, J = 13.3 Hz, 2H, ArCH*H*Ar); 2.04-1.85 (m, 8H, OCH_2*CH*$_2$$CH_3$); 1.30-1.22 (m, 6H, H_O); 1.02-0.93 (m, 12H, OCH_2CH_2*CH*$_3$). ^{13}C NMR (100 MHz, $CDCl_3$): δ (ppm) 197.7; 183.2; 168.2; 168.0; 161.3; 159.6; 159.5; 156.5; 152.1; 150.8; 146.9; 139.8; 135.3; 134.8; 134.1; 131.2; 128.6; 127.97; 127.86; 127.6; 127.1; 126.9; 125.9; 124.8; 122.6; 118.2; 109.6; 106.8; 105.3; 96.3; 67.3; 50.5; 45.1; 39.3; 31.9; 30.9; 29.7; 29.4; 23.3; 23.2; 22.7; 14.1; 12.6; 10.4; 10.2. ESI-MS: m/z calcd for $C_{66}H_{72}N_4O_{10}$+Na^+ 1103.5 (30%), found 1103.5; m/z calcd for $C_{66}H_{72}N_4O_{10}$ + K^+ 1119.5, found 1120.9 (10%).

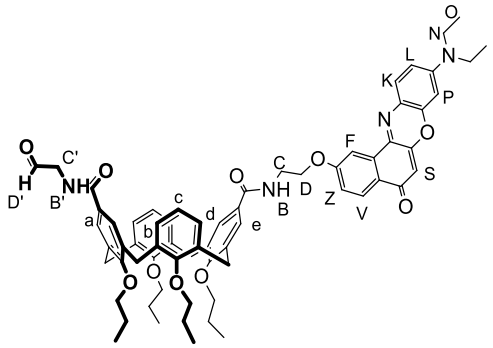

68

Compound 69

To a stirred solution of compound **68** (59 mg, 0.055 mmol) in dry toluene (10 mL), N-methylglycine (10 mg, 0.11 mmol) and fullerene C_{60} (39 mg, 0.055 mmol) were added. The reaction mixture was refluxed (110 °C) for 2 h, when TLC (CH_2Cl_2/CH_3OH 96/4) revealed the consumption of most of reagent **68**. The solvent was removed under reduced pressure and the crude was dissolved in

CH_2Cl_2 (20 mL). H_2O (20 mL) was added and the two phases separated. The aqueous layer was extracted with CH_2Cl_2 (3x20 mL) and the combined organic layers were washed with H_2O (3x50 mL). After being concentrated under reduce pressure, the crude was purified by preparative TLC (CH_2Cl_2/CH_3OH 94/6). Pure compound **69** was isolated in 5% yield (0.006 g, 0.003 mmol).

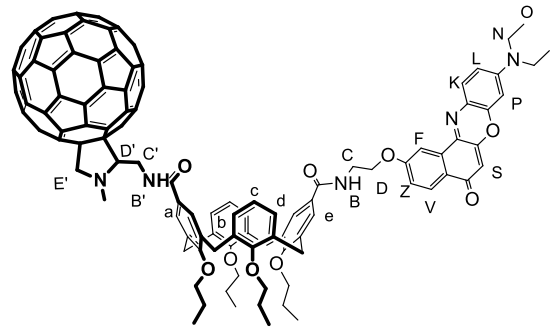

69

^{1}H-NMR (300 MHz, $CDCl_3$): δ(ppm) 8.26 (d, J = 8.7 Hz, 1H, H_V); 8.11 (d, J = 2.5 Hz, 1H, H_F); 7.51 (d, J = 9.1 Hz, 1H, H_K); 7.10 (s, 2H, H_e); 6.97 (s, 2H, H_a); 6.90 (dd, J_1 = 8.7 Hz, J_2 = 2.5 Hz, 1H, H_Z); 6.67-6.63 (m, 6H, H_b, H_c, H_d); 6.54 (d, J = 7.5 , 1H, H_L); 6.45 (s, 1H, H_P); 6.31 (s, 1H, H_s); 5.35-5.30 (m, 1H, $H_{D'}$); 4.89 (d, J = 9.5 Hz, 1H, (*H*H)$_{E'}$); 4.43-4.39 (m, 4H, ArC*H*HAr);4.34-4.28 (m, 2H, $H_{C'}$); 4.18 (d, J = 9.5, 1H, (H*H*)$_{E'}$); 4.04 (s, 2H, H_D); 3.85–3.77 (m, 6H, H_c and OC*H*$_2$CH$_2$CH$_3$); 3.65–6.58 (m, 4H, OC*H*$_2$CH$_2$CH$_3$); 3.46 (q, J = 7.1, 4H, H_N); 3.25-3.12 (m, 4H, ArCH*H*Ar); 2.95 (s, 3H, NCH_3); 2.1-1.95 (m, 4H, $OCH_2CH_2CH_3$); 1.95-1.80 (m 4H, $OCH_2CH_2CH_3$); 1.38-1.16 (m, 6H, H_o); 0.92-0.78 (m, 12H, $OCH_2CH_2CH_3$).

X-ray diffraction

The crystal structure of compound **61** was determined by X-ray diffraction methods. Crystal data and experimental details for data collection and structure refinement are reported in Table 3.

Intensity data and cell parameters were recorded at 190(2) K on a Bruker APEX II equipped with a CCD area detector and a graphite monochromator (MoKα radiation λ = 0.71073 Å). The raw frame data were processed using SAINT and SADABS to yield the reflection data file.[32]

The structure was solved by Direct Methods using the SIR97 program[33] and refined on F_o^2 by full-matrix least-squares procedures, using the SHELXL-97 program[34] in the WinGX suite v.1.80.05.[35]

All non-hydrogen atoms were refined with anisotropic atomic displacements. The hydrogen atoms were included in the refinement at idealized geometry (C-H 0.95 Å) and refined "riding" on the corresponding parent atoms, with the exception of the hydrogen atom of the amine which was found in the difference Fourier map. The weighting scheme used in the last cycle of refinement was $w = 1/ [\sigma^2 F_o^2 + (0.0595P)^2]$, where $P = (F_o^2 + 2F_c^2)/3$. Geometric calculations were performed with the PARST97 program.[36]

Formula	$C_{27}H_{23}N_3O_3$
Fw	437.48
Crystal system	Monoclinic
Space group	*P21/c*
a (Å)	10.806(2)
b (Å)	14.583(3)
c (Å)	14.471(3)
β (º)	111.643(3)
V (Å^3)	2119.6(7)
Z	4
ρ (g cm^{-3})	1.371
μ (mm^{-1})	0.091
F(000)	920
Total reflections	15683
Unique reflections (R_{int})	2371 (0.1557)
Observed reflections [$F_o>4\sigma(F_o)$]	1127
GOF on F^{2a}	1.008
R indices [$F_o>4\sigma(F_o)$]^b R_1, wR_2	0.0557, 0.1110
Largest diff. peak and hole (eÅ^{-3})	0.258, -0.162

Table 3. *Crystal data and structure refinement information for compound **61**.[a]Goodness-of-fit S = $[\Sigma w(Fo^2-Fc^2)2/(n-p)]^{1/2}$, where n is the number of reflections and p the number of parameters.* [b]*$R1 = \Sigma \| Fo|-|Fc| / \Sigma |Fo|$, $wR2 = [\Sigma[w(Fo^2-Fc^2)2]/\Sigma[w(Fo^2)^2]]^{1/2}$.*

4.7 References

1. P. F. Barbara, T. J. Meyer, M. A. Ratner, *J. Phys. Chem.*, **1996**, 100, 13148-13168;
2. S. Gunes, H. Neugebauer, N. S. Sariciftci, *Chem. Rev.*, **2007**, 107, 1324–1338;
3. H. Borchert, *Energy Environ. Sci.*, **2010**, 3, 1682–1694;
4. H. Spanggaard, F.C. Krebs, *Sol. Energy Mater. Sol. Cells*, **2004**, 83, 125–146;
5. C. Winder, N. S. Sariciftci, *J. Mater. Chem.*, **2004**, 14, 1077–1086;
6. R. Kroon, M. Lenes,J. C. Hummelen, P. W. M. Blom, B. de Boer, *Polym. Rev.*, **2008**, 48, 531–582;
7. O. V. Mikhnenko, H. Azimi, M. Scharber, M. Morana, P. V. M. Blom, M. A. Loi, *Energy Environ. Sci.*, **2012**, 5, 6960–6965;
8. C. Im, E. V. Emelianova, H. Bassler, H. Spreitzer, H. Becker, *J. Chem. Phys.*, **2002**, 117, 2961–2967;
9. B. A. Gregg, M. C. Hanna, *J. Appl. Phys.*, **2003**, 93, 3605–3614;
10. G. Yu, A. J. Heeger, *J. Appl. Phys.*, **1995**, 78, 4510–4515;
11. R. A. Marcus, N. Sutin, *Biochimica et Biophysica Acta*, **1985**, 811, 265-322;
12. M. Gilbert B. Albinsson, *Chem. Soc. Rev.*, Advance article, DOI: 10.1039/C4CS00221K, Tutorial Review;
13. V. May, O. Kuhn, *Charge and Energy Transfer Dynamics in Molecular Systems*, Wiley, **2004**;
14. O. Ito, F. D'Souza, *Molecules*, **2012**, 17, 5816-5835;
15. F. D'Souza, O. Ito, *Multiporphyrins-Fullerenes and Multiporphyrins-SWCNTs Mimicking Photosynthetic Antenna-Reaction Center, Multiporphyrin Arrays,* Ed. D. Kim, Pan Stanford Publishing: Singapore, **2012,** Chapter 8, 389–438;

16. H. Imahori, N. V. Tkachenko, V. Vehmanen, K. Tamaki, H. Lemmetyinen, Y. Sakata, S. Fukuzumi, *J. Phys. Chem. A*, **2001**, 105, 1750-1756;
17. T. Umeyama, H. Imahori, *Energy Environ. Sci.*, **2008**, 1, 120–133;
18. F. D'Souza, K. M. Kadish, *Eds. Handbook of Carbon Nano Materials, World Scientific: Singapore*, **2011**; Volumes 1 and 2;
19. S. Fukuzumi, H. Imahori, *Biomimetic Electron-Transfer Chemistry of Porphyrins and Metalloporphyrins, Electron Transfer in Chemistry*, Ed. V. Balzani, Wiley-VCH: Weinheim,Germany, **2000**; 2, 927–975;
20. D. M. Guldi, *Chem. Soc. Rev.*, **2002**, 31, 22–36;
21. Y.-X. Liu, M. A. Summers, S. R. Scully, M. D. McGeheea, *J. of App. Phys.*, **2006**, 99, 093521 (1-4);
22. S. Anandan, M. Yoon, *Spectrochimica Acta Part A*, **2004**, 60, 885–888;
23. J. J. Lee, Y. H. Kim and M. Yoon, *Journal of Photoscience*, **2001**, 8(1), 27−32;
24. Y.-S. Xie, B.V.D. Vijaykumar, K. Jang, K.-M. Choi, H. Zuo, Y.-J. Yoon, D.-S. Shin, *Bull. Korean Chem. Soc.*, **2013**, *34*, 3881–3884;
25. M. Maggini, G. Scorrano, M. Prato, *J. Am. Chem. Soc.*, **1993**, 115, 9798-9799;
26. L. Baldini, F. Sansone, G. Faimani, C. Massera, A. Casnati, R. Ungaro, *Eur.J.Org.Chem*., **2008**, 869-886;
27. O. Struck, L. A. J. Chrisstoffels, R. J. W. Lugtenberg, W. Verboom, G. J. van Hummel, S. Harkema, D. N. Reinhoudt, *J. Org. Chem.*, **1997**, *62,* 2487-2493;
28. Gokulnath, V. Prabhuraja, J. Sankar, T. K. Chandrashekar, *Eur. J. Chem.*, **2007**, 191-200;
29. F. Sansone, S. Barboso, A. Casnati, M. Fabbi, A. Pochini, F. Ugozzoli, R. Ungaro, *Eur. J. Org. Chem.*, **1998**, 897-905;
30. E. F. Elslager, D. Worth, *J. Med. Chem.*, **1970**, 13 (3), 370-376;

31. H. Lee, M.G. Choi, H.-Y. Yu, S. Ahn, S.-K. Chang, *Bull. Korean Chem. Soc.*, **2010**, 31 (12), 3539-3542;
32. SADABS Bruker AXS; Madison, Wisconsin, USA **2004**; SAINT, *Software Users Guide*, *Version 6.0*; Bruker Analytical X-ray Systems, Madison, WI **1999**. G. M. Sheldrick, SADABS v2.03: *Area-Detector Absorption Correction*. University of Göttingen, Germany **1999**;
33. A. Altomare *et al.*, *J. Appl. Cryst*., **1999**, 32, 115-119;
34. G. M. Sheldrick, *SHELXL-97.Program for Crystal Structure Refinement*. University of Göttingen, Germany **1997**, and *ActaCrystallogr*. **2008**, *A64*, 112 -122;
35. L. J. Farrugia, *J.Appl. Crystallogr*., **1999**, 32, 837-838;
36. M. Nardelli, *J. Appl. Crystallogr.*, **1996**, 29, 296-300.

Appendix

List of abbreviations

The following table describes the significance of various abbreviations and acronyms used throughout the thesis. Nonstandard acronyms that are used in some places to abbreviate the names of certain white matter structures are not in this list.

Ar	Aromatic
Boc	t-Butyloxycarbonyl ($CO^tC_4H_9$)
BODIPY	DIPYrromethene BOron Difluoride
DEAD	Diethylazodicarboxylate
DIPEA	Diisopropylethylamine
DMF	Dimethylformamide
DMSO	Dimethyl Sulfoxide
ESI-MS	Electron Spray Ionization Mass Spectrometry
J	Coupling constant (NMR)
NMR	Nuclear Magnetic Resonance
NOESY	NUclear Overhauser Effect/Enhancement Spectroscopy (NMR)
Pht	Phthalimido
ROESY	Rotating frame Nuclear Overhauser Spectroscopy (NMR)
TEA	Triethylamine
TES	Triethylsilane
TFA	Trifluoroacetic
THF	Tetrahydrofuran
TLC	Thin Layer Chromatography
UV-VIS	Ultraviolet-visible spectroscopy

Nomenclature of Calix[4]arenes

In this thesis the simplified nomenclature proposed by Gütsche is used to name calix[4]arene compounds. The position on the macrocycle are numbered as indicated in the following figure. The hydroxyl substituent defines the ipso position: subsequently the *ortho*, *meta* and *para* positions on the aromatic rings are identified without ambiguity.

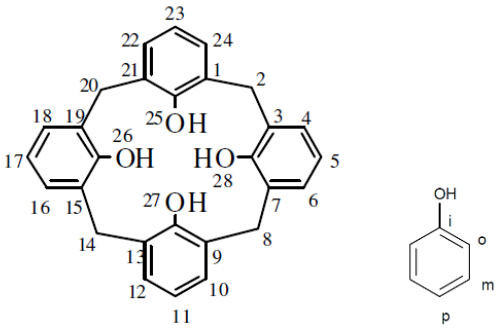

Conventional nomenclature devised by Gütsche.

Acknowledgments

It would not have been possible to write this doctoral thesis without the help and support of all the people around me. Unfortunately to only some of them it is possible to give particular mention here.

First, I would like to thank my supervisors, Dr. Laura Baldini and Dr. Francesca Terenziani, for leading me in the project during these three years. Thanks also for all the efforts you put in the correction of this thesis!

Thanks Laura for giving me useful advices and ideas, and for freedom to work in an independent way within the Ph.D. project; for your confidence and trust on me. Thank you for being for me an example (of life and as chemist).

Thanks to Dr. Mariangela Di Donato, who led the general project this Ph.D. is part of and carried out the transient absorption studies at LENS (European Laboratory for Non-Linear Spectroscopy) in Florence.

Thanks to Dr. Elisa Campioli and Dr. Cristina Sissa, who performed absorption and fluorescence measurements, and who disclosed to me to the fascinating world of photochemistry, and to Dr. Chiara Massera for X-Ray diffraction studies.

A big thanks to Prof. Alessandro Casnati and Prof. Francesco Sansone, who gave me the possibility to join their research group since my Bachelor thesis and made me love the research fields of supramolecular chemistry and organic synthesis! Thanks for all your scientific advices and knowledge.

Michela and Paola…thanks for being my moms!

My time in Lab. 192 was made enjoyable by the many friends that during these years became a part of my life: Ilaria, Marta and Stefano, Dario, Elisabetta, Federica and Gabriele, and the bachelors and master students I tutored: Alessandro, Aurora, Beatrice, Mattia, Riccardo and Stefania. I am grateful for the

time spent together, for the laughs and the arguments, for the exchanges of views, for all the advices…simply thank you, guys!
Special thanks to my family: for all their love and encouragement, for supporting me in all my pursuits. And most of all for my loving, supportive, encouraging, and patient boyfriend Gianluca, whose faithful support during this Ph.D. (but not only) is so appreciated.
Dear Friends, I am grateful to you for enriching my life and me.

Finally, I acknowledge MIUR (Ministero dell'Istruzione, Università e Ricerca), FIRB project RBFR10Y5VW, for the financial support.